UNITED KINGDOM · CHINA · MALAYSIA

Compressed Air Energy storage for large-scale renewable energy systems for a case study of Egyptian grid

Omar Ramadan

BSc, MSc

Thesis submitted to the University of Nottingham for the degree of Doctor of Philosophy

Abstract

All across the world, attention is turning to renewable energies to serve at least as a partial substitute to fossil fuels in the global energy mix, braking the latter's depletion and providing a greener solution for a more sustainable future. However, the intermittent nature of most renewable energy sources, wind and solar in particular, raises major concerns over the integration of these technologies, on a large scale, to grid systems. This thesis focuses on large-scale renewable energy storage systems, primarily compressed air energy storage (CAES) systems, which are particularly well suited for renewable energy applications. CAES can play a major role in shaping the future of renewable energy systems for not only can it bring load levelling to the system, but it can also add substantial value by providing ancillary services to the grid. The main focus of this research is adiabatic CAES which endeavours to minimize the use of natural gas by using recuperators and thermal energy storage systems, where the heat from the air during the compression stages is absorbed by a heat transfer fluid, stored, and then supplied back during the expansion process.

This project aimed to explore the potential of CAES systems as an energy storage technology for large-scale grid integrated renewable energy system. A computer model was developed to size the different components in the CAES system and also to predict the operational performance of the CAES system for different conditions using MATLAB programming. The thermal energy storage of an adiabatic CAES system was optimized using CFD analysis and experimental testing of the thermal energy storage system was carried out to validate the models. Also, an economic study was performed to assess the feasibility of the CAES system based on a case study of the Egyptian grid. The dynamic simulation of a novel configuration of an adiabatic CAES system showed that the system can achieve improved performance compared to existing CAES plants, while the economic study showed that CAES can

improve the economics of a wind farm, at least by the standards of our chosen case study location.

Acknowledgement

The path to completing my PhD experience has been filled with support from a variety of individuals and institutions to whom I am eternally grateful to. To begin with I would like to thank my supervisors Dr. Siddig Omer and Prof. Saffa Riffat for their continued help, scientific insights as well as their invaluable guidance over the past years. I remain truly grateful for all their efforts and investment in my journey to completion. I would also like to thank my internal assessor Dr. Yuehong Su for his insightful perspectives in improving my research.

It is also important to recognize the continuous support that I was fortunate to receive from the Faculty of Engineering, both in terms of financial funding- the Dean of Engineering Scholarship for international excellence-, as well as providing administrative ease during my stay in the U.K. Their help during the experimental work of my research has been important especially in securing safety procedures. In general, being at the University of Nottingham has been a particularly enlightening experience and has provided me with an easy transition to living abroad as an international student and feeling at home.

Lastly, I would of course like to thank my family who has been the source of my inspiration to embark on my PhD experience. My friends and family also represent a significant part of my support network and their unconditional support has never waned over the past few years. I especially dedicate the completion of my endeavors to my father, mother and sister; with whom I share the joy of life.

Acronyms and Abbreviations

SMES	**Super Conducting Magnetic Energy Storage**
CAES	**Compressed Air Energy Storage**
AA-CAES	**Advance Adiabatic CAES system**
A_{cav}	**Surface area of the cavern** (m^2)
$c_{p_{air}}$	**Specific heat of air** (J/kgK)
c_{pfluid}	**Specific heat of heat transfer fluid** (J/kgK)
h_{eff}	**Effective heat transfer coefficient**
H_c	**Mole specific enthalpy of air to cavern (J/K)**
K_c	**Thermal conductivity of concrete** (W/mK)
M_{total}	**Mass of air in the cavern** (kg)
$\dot{m}_c$	**Mass flow rate of air to cavern** (kg/s)
$\dot{m}_{cav}$	**Mass flow rate of air to turbines** (kg/s)
P_{cav}	**pressure of air in the cavern** $(bars)$
$Q_{Combustion}$	**heat added by combustion chamber** (J)
R	**gas constant** $(J/mol\ K)$
V_{cav}	**volume of the cavern** (m^3)
T_{cav}	**temperature of air in the cavern** (K)
T_{wall}	**temperature of the surroundings** (K)
ρ	**density of air** (kg/m^3)
ε	**effectiveness of heat exchangers**
η_c	**polytropic efficiency of compressors**

$\boldsymbol{\eta_p}$	**polytropic efficiency of the turbine**
NPV	**Net Present Value**
ROI	**Return on interest**
DCF	**Discounted Cash Flow**

Table of Contents

List of Figures

Chapter 1 Introduction

Without sufficient and sustainable energy supply solutions, the world's long-term growth potential will undoubtedly be capped, if not jeopardized. This has come to the attention of developed and developing countries alike, where the rise of large-scale renewable energy projects has become a necessity, no longer a luxury. This research aims to remove two major barriers to the growth of renewables, namely intermittency and high cost, by proposing viable energy storage solutions. A case study of the Egyptian grid was undertaken in this research to evaluate the impact of integrating a Compressed Air Energy Storage (CAES) system. With renewable energy installations set to grow tremendously in Egypt over the next decade, the option of energy storage warrants further study that underpins successful, evidence-based policymaking. That said, the research herein examines CAES extensively, with a special focus on its potential value addition to the Egyptian grid.

1.1 Load demand growth and the prospects of renewable energy

Energy demand continues to extend year-on-year gains, almost doubling in the last 30 years and projected to grow an additional 37% by 2040 (EIA International energy outlook, 2014). This is largely fueled by an unwavering growth in world population and the rapid industrialization of the developing world, both of which are expected to continue at least in the medium term. Such demand escalation must be paralleled with an equivalent rise in energy production, if the required supply of different loads at different locations is to be met. This means more power plants must be established, consuming either fossil fuels or renewable energies. While fossil fuels offer more competitive prices, higher energy densities and more reliable outputs, the rapid depletion of these resources, together with the environmental hazards associated with them and the growing concerns over climate change (Haines et al, 2006) have instigated a paradigm shift toward their more sustainable counterparts— renewable energies.

An endless untapped potential lies with renewable energies, both in terms of energy capacities and in terms of possible greenhouse effect mitigation. By definition, renewable energies are the forms of energy that are replenished by the natural processes of the Earth, and are thus environmentally-friendly. The main types of renewable energy are solar, wind, hydropower, biomass, bio-fuel, tidal, wave and geothermal energy (Jacobson et al, 2009). Much like any other infant industry, renewable energy technologies are still relatively expensive and inefficient compared to traditional energy sources; but as the industry evolves and establishes itself on larger scales overtime, it is expected to achieve efficiency gains and see improved cost effectiveness (Shedroff, 2009). In 2013, the share contribution of primary renewable energy systems (solar, wind, bio mass, and geothermal) to global energy consumption recorded a mere 1.3%, as shown in Figure 1-1(Renewables 2015 global state report, 2015), which leaves ample room for a growing contribution leading into a more balanced mix.

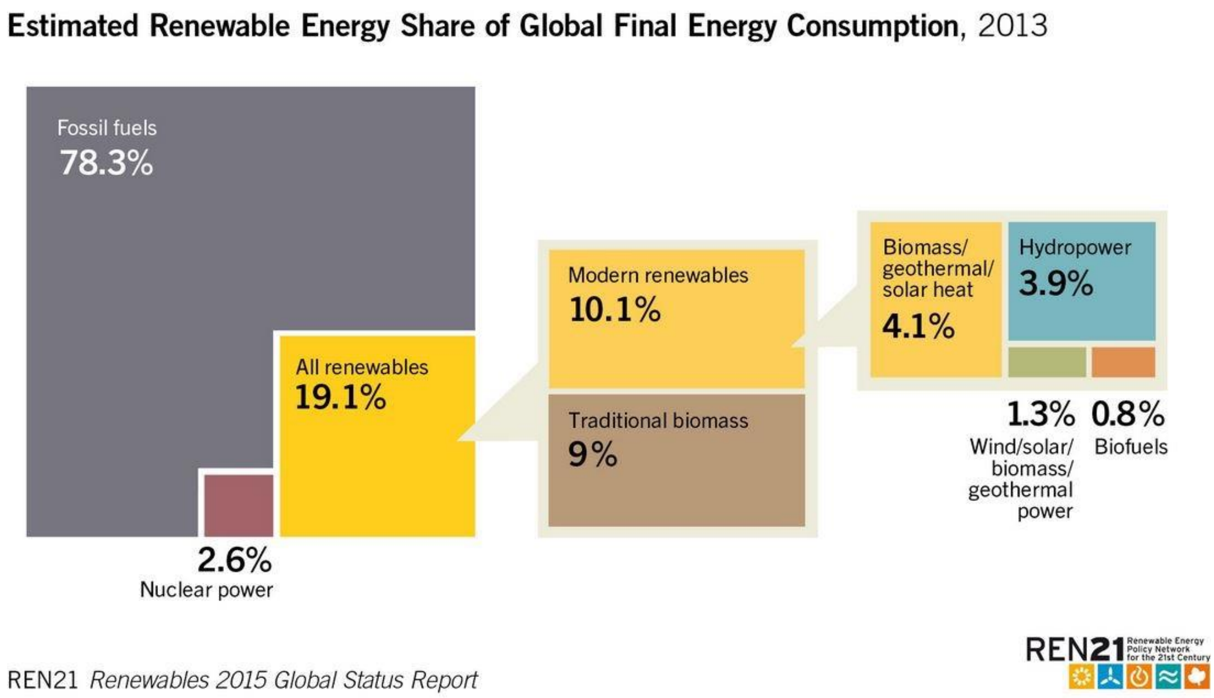

Figure 1-1 Renewable energy global consumption share (Ren21, 2015)

1.2 Renewable energy dilemmas and solutions

Global debates involving renewable energy touch on a variety of issues that hamper the exclusive dependence on these sources. Among those, a highly recurrent theme relates to their intermittency, which ends in considerable variation in the power produced. This poses technical as well as economic challenges when renewable sources are integrated on a large scale to the grid, unlike the case with fossil fuels with stable and therefore reliable output patterns. Sun and wind energy sources, for instance, cannot be controlled so as to have them provide continuous base-load power or peak-load power when required (McGraw-Hill 1984). Nonetheless, renewable energy systems have made leaps of progress in terms of operational efficiency from where they kicked off. The paragraphs that follow give a brief overview of the major renewable energy systems, with a special focus on wind and solar systems.

1.2.1 Wind energy systems

Currently, wind energy systems are confined to wind farms, where, principally, a wind plant converts the energy inherent in wind streams to electricity by converting the kinetic energy of the wind into rotational energy, which is used to drive generators. Wind turbines are made of aerodynamically designed blades which capture the power from the wind and convert it into rotating mechanical power (Blaabjerg et al, 2004). The power output of the wind turbine is dependent on the wind speed at the relevant location. As such, every wind turbine has a characteristic power performance curve which depicts the electrical power output as a function of the wind speed at the tower height. This power curve allows making predictions on the output power of a wind turbine without the need to consider the technical details characterizing the different components in the turbine (Manwell et al, 2002). The amount of wind power generation is usually governed by three key aspects related to the wind speed: a) cut-in speed: the minimum speed at which the wind turbine will start producing useful power, b) rated wind speed: the speed at which the wind turbine produces maximum power, c) cut-out wind speed: the speed after which the wind plant is shut down and stops producing power based on the control mechanism.

Wind energy has evolved as a very attractive technology as it currently represents one of the least expensive ways to produce electricity free of CO_2 emissions, thus playing a major role in the future growth of green energy (Ackerman et al, 2002). Nonetheless, it does pose other, but less severe, environmental hazards related to the noise from the wind turbines, the visual impact, the harmful interaction with birds and the electromagnetic interference—but these are not generally perceived as a brake on the growth of the technology (Manwell et al, 2002). Equally importantly, wind turbines capital costs have dropped significantly from the 1980s' levels, reaching its lowest value in the period from 2001 to 2004. It has since increased again, especially so during the period from 2004 to 2010, but remains below the earlier levels, with the forecast being a downtrend in capital costs that is to kick in the near future (IEA Wind task 26, 2012).

Bottom line is: more than 50 GW of wind power capacity was installed in 2014 alone, for a total of 370 GW of global wind production, and counting (Renewables 2015 global state report, 2015).

1.2.2 Photovoltaic systems

Another widespread form of renewable systems is solar photovoltaic (PV) modules. These convert solar energy directly into electricity (DC), again with no emissions, but better yet without noise or vibrations (Panwar et al, 2011). The DC power is then converted to AC power using a converter to supply power to the grid or to provide household use. The power produced in PV systems is dependent on the solar radiation present at the location of the PV system.

Likewise, the efficiency of PV systems has improved considerably in the past decade, and is expected to advance further going forward, which should help improve the economic viability of these systems (Goswami et al, 2004). The main types of PV systems are the amorphous, the mono-crystalline and the poly-crystalline systems. While the lifetime of most PV systems are fairly long, ranging between 20 and 30 years, according to Sherwani (2010), their main weakness lies in their low energy density. This implies a large surface area is needed to produce a fairly low sum of energy, which in turn also increases the cost of energy produced through PV systems (Panwar et al, 2011).

On the upside, again, the investment cost of PV systems is forecasted to drop by as much as 40% in the coming years, supported by rapid technological advancements and massive investments in new PV systems. The drop is conceivable by the many, given that the main factors affecting the capital costs of PV systems are the size of the manufacturing plant, the module efficiency and the cost of purified silicon. Depending on the site-specific solar radiation level, generation costs are expected to range from USD81/MWh to USD162/MWh for utility-scale systems, from USD107/MWh to USD214/MWh for commercial systems, and from USD116/MWh to USD232/MWh for residential systems by 2020 (IEA Solar Energy Perspectives, 2011). In 2014 alone, some 40 GW of PV power capacity was installed, taking the total outstanding PV capacities by the end of that year to 177 GW (Renewables 2015 global state report, 2015).

1.2.3 Possible solutions for renewable energy systems

Several different technologies are currently being researched in an attempt to contain the intermittency problem of renewable energy sources and the mismatch between their output's supply and demand. One proposition was to simply build more power generation stations, e.g. more wind turbines, than is actually required. However, because, on a large scale, building excess capacity is largely uneconomical, the suggestion renders impractical. Another proposition involves the application of smart grids, which is a very interesting direction and could have a large bearing in the future, supporting a virtually exponential growth in renewable energy technologies. A third and very viable solution lies with energy storage, which is the main focus of this thesis. The main rationale behind this option is to best utilize future production, where high levels of wind penetration to the grid may bring about intervals of excess supply, particularly on windy nights. It would be an undue waste of resources to simply turn off the generators during these times, whereas the energy could be stored for use during periods of supply shortage. Energy storage applications for electricity systems are discussed in more detail in Chapter 2.

1.3 Case Study: Egypt's Suez area

In an endeavor to demonstrate the dilemmas as well as the underlying potential associated with energy storage, a case study involving Egypt is undertaken in this report. In particular, Egypt's Suez area, which includes the Suez Gulf, Zaafarana and Hurghada, was chosen as it enjoys the highest wind energy potential in Egypt. Relevant data on this area and on Egypt, at large, is mined from the annual reports of the New and Renewable Energy Authority (NREA) and the Ministry of Electricity and Energy [NREA (2011), NREA (2012), MOEE (2011), MOEE (2012)].

Egypt's recent history shows an annual 7.9% increase in electrical energy demand, which presents a major challenge to authorities, who are in a continuous strife to ensure meeting that demand. The wind resource in Egypt's Suez area is huge and largely untapped. But plans are underway to increase the area's wind generation capacity from 0.5 GW to nearly 7.5 GW by 2020; which necessitates extensive research in order to work out solutions for adequate grid integration of the said projects. Currently, the Suez grid runs a medium voltage of 220KV and is interconnected to a high voltage of 500KV, which is considered fairly reliable. That said, the impending surge in wind farm capacities renders the addition of storage systems a very viable option, if not a must. More details on the area's wind resources, the grid, future wind farm plans and load variation in Egypt are discussed in Chapter 4 (MATLAB Modelling).

1.4Aims and Objectives

The main aim of this research is to explore the potential of energy storage systems, mainly compressed air energy storage (CAES), and how these systems can be used to improve the performance of large-scale grid integrated renewable energy systems.

To achieve these goals, these main objectives were set:

1. Critical review of the current energy storage technologies
2. Develop a computer model to size the different components of the compressed air energy storage system and predict the performance of this system under different conditions
3. Optimise the thermal energy storage system in an adiabatic CAES system using CFD analysis
4. Carry out experimental testing to validate the models
5. Perform an economic study to evaluate the feasibility of a compressed air energy storage system

1.5 Novelty of the research

The research conducted introduced novel modelling of the compressed air energy storage system for large-scale renewable energy systems. First of all, the MATLAB simulation implemented transient modelling of the adiabatic CAES system including the simulation of the performance of the thermal energy storage (TES) component on a second by second basis showing the variation of temperature at different points of the TES which is then compared with TES simulation using ANSYS CFD for validation of the results which was lacking in current research carried out for CAES systems. The MATLAB modelling also simulated the performance of a CAES system for a case study of the Egyptian grid based on future plans of wind farms installation in Egypt by 2020. A novel configuration of parallel compressors and expanders was carried out in the simulation of the CAES system to improve the efficiency of operation of the compressors and turbine expanders at different loads. In addition, an economic study was conducted on the Egyptian grid with newly issued tariffs law by the government which follows a path which is very different than the spot market prices procedure followed in different grid system including the European one. Hence, the simulation of CAES operation to maximize economic benefit was different than the operation of CAES for load-levelling which was optimized to increase the profits from the CAES system.

1.6 Thesis layout

The following describes the general structure of the thesis and the main concepts discussed. Following this introduction chapter, Chapter 2 presents a literature review of energy storage technologies currently implemented in the industry. Smaller scale energy storage systems, such as batteries as well as larger scale energy storage systems are discussed, followed by a more in-depth review of the particular system under study, namely Compressed Air Energy Storage (CAES). A historical trajectory of CAES systems is briefed, followed by a preview of existing CAES plants and the different components forming the holistic system. After that, some of the recent research that has been carried out on CAES is examined.

Chapter 3 follows with a discussion of the methodology applied in the CAES dynamic simulation using MATLAB programming. A concise illustration of the equations governing the operation of CAES is presented, along with the assumptions underlying the simulation of CAES systems under different configurations.

Chapter 4 presents a simulation of a particular thermal energy storage system that makes a component of the adiabatic CAES system (AA-CAES). In this simulation, ANSYS CFD is used to optimize the design of the thermal energy storage and test the effect of different parameters on the performance of the thermal energy storage.

Subsequently, Chapter 5 presents the results of the MATLAB modelling, where the Suez grid case study is utilized for the simulation of CAES. This comprises the sizing of the system as fit for the inputs relevant to the studied location, including wind speeds, load demand and the operational mode of the system. Afterwards, an in-depth sensitivity analysis is carried out to explore how different parameters bear on the appropriate sizing and/or operation of the CAES system.

Chapter 6 carries on with a discussion of the experimental work done for a small-scale thermal energy storage system that uses a sensible heat storage medium. The results are shown to validate both the CFD and MATLAB modelling, and enable the testing of how different parameters affect the performance of the small-scale thermal storage system.

Chapter 7 continues with an evaluation of the economic feasibility of implementing a grid-integrated CAES system in Egypt. In the same vein, Chapter 7 starts off with the equations underlying the simulation of the economic study, followed by the modelling results pertaining to the case study. After that, a study of the sensitivity of the economic feasibility of both a standalone wind system and a Wind+CAES system (for the studied location) to different parameters is carried out.

Finally, Chapter 8 ends with a concluding afterword that summarizes the main takeaways from this study together with suggested directions for future research that can build on this thesis

Chapter 2 Literature Review on Energy storage systems and their applications

2.1 Scope of the chapter

This chapter present the literature review carried out on energy storage systems and their applications, with a special emphasis on compressed air energy storage systems (CAES), which is the focal point of this thesis.

The chapter discusses the different applications of energy storage systems to limit the effect of the intermittency of renewable energies. The different types of energy storage systems are explored, along with the pros and cons of each technology. A conclusion is then drawn of the most suitable energy storage technology for use with large-scale renewable energy systems. Also, an overview of compressed air energy storage is presented, including the current operational plants and the different components used in CAES systems. Moreover, a number of key potential CAES applications are discussed in more detail. The chapter concludes with some thoughts and inferences.

2.2 Energy storage applications for renewable energy systems

In this section, the applications of energy storage systems are discussed starting from the power generation level and up to the end user level. Energy storage systems have numerous applications that can vastly improve the operation of renewable energy systems as well as the transmission and distribution processes. Energy storage can also optimize energy management at the consumer level (EPRI White paper , 2010).

2.2.1 Generation level applications

This section discusses the generation level applications that cover all of the relevant processes, from implementing renewable energy systems to the ancillary services provided, as well as the time-shifting applications.

2.2.1.1 Time shifting

Time shifting is, simply, buying electricity when the market prices are low, normally during off-peak times, storing it, and supplying the power back during peak times when the market prices are higher. From an economic standpoint, therefore, time shifting can prove profitable, depending on the O&M costs of the energy storage and the operational efficiency of the energy storage systems. Time shifting is particularly beneficial for renewable energy applications, primarily solar and wind energies, due to the intermittent nature of these sources. The given scale of energy storage dictates the type of storage technology where, for instance, small-scale energy storage system, like batteries, suit small PV systems and small wind farms, and larger scale energy storage systems, like pumped hydro and compressed air energy storage systems, suit large scale renewable energy systems(Akhil et al (EPRI), 2013).

2.2.1.2 Load levelling

This application is especially crucial when dealing with increased penetration of renewable energy systems to the grid. The energy storage systems could be used for load levelling by absorbing power from the renewable energy systems when the supply from these systems are higher than the load demand and, conversely, discharging the stored power back to the grid at peak times or when the load demand exceeds the available power at the grid. Energy storage systems are exceptionally suitable for this application due their relatively fast response. The scale of energy storage systems candidate for load levelling varies according to the scale of renewable energy systems, as mentioned earlier, with CAES and pumped hydro normally more suited for larger, grid-connected scale systems.

2.2.1.3 Ancillary services

Energy storage systems can provide some applications which can maintain the grid stability which include regulation, spinning reserves, voltage and frequency support as well as black starts.

2.2.1.3.1 Regulation

Regulation aims at maintaining the grid frequency, which is essential given the load fluctuation resulting from the supply/demand mismatch. Energy storage systems are suitable for this purpose due to their fast response time, and quick reaction to counterbalance the effect of those fluctuations. The systems provide “up regulation” by increasing discharge of electricity into the gird, and “down regulation” by absorbing electricity from the grid or reducing discharge to the grid (Akhil et al (EPRI), 2013)..

2.2.1.3.2 Spinning Reserves

In this application, energy storage systems are required to provide power to the grid whenever a portion of the normal supply suffers from an outage. The spinning reserves should be able to supply power within 10 minutes of any such outage, which makes them suitable for the application. The reserve systems are usually built as big as the largest single power supply system, so as to be able to substitute all the deficiency in power if the system becomes unavailable. There are also frequency spinning reserves, which are required to react within 10 seconds to maintain the frequency of the grid in case of an outage(Akhil et al (EPRI), 2013).

2.2.1.3.3 Voltage support

Voltage support merely requires the supply of reactive power from the energy storage systems, which maintains grid stability when there is a glut or deficiency in power supply to the grid, as well as improves power quality and reduces line losses. Voltage support requires energy storage systems to react within 30 minutes (Akhil et al (EPRI), 2013).

2.2.1.3.4 Black Start

Energy storage systems can provide start-up power to power plants that have suffered failure, and bring them back online and in operation (Akhil et al (EPRI), 2013).

2.2.1.3.5 Frequency control

This application is very similar to regulation services, with the only difference being the required response having to be much faster— in the order of seconds (Akhil et al (EPRI), 2013).

2.2.2 Transmission and distribution level applications

Energy storage systems can also have an added benefit to the grid system at a transmission and distribution levels including relieving transmission congestion and extending the operational life of the transmission and distribution equipment.

2.2.2.1 Transmission Congestion

Transmission congestion typically happens when transmission capacities cannot keep up with peak load demands, resulting in the transmission systems not being able to deliver power to service the loads, even when low-cost energy is available. Energy storage systems could reduce the additional costs associated with transmission congestion by storing the energy when there is no congestion, and discharging the stored power when congestion occurs during peak times, thus reducing the transmission capacity needed. Congested transmission lines can result in a violation of network security limits, such as thermal, voltage stability or angular stability and reliability margins (Del Rosso et al, 2014). Normally, congestion issues happen only a few times a year, at which time the energy storage system is required to release the stored power. To serve this purpose, the energy storage systems are commonly placed where parts of the transmission systems are expected to experience congestion (Akhil et al (EPRI), 2013).

Energy storage systems can also provide stability to the transmission system by enhancing its performance in cases of unstable voltage.

2.2.2.2 Distribution upgrade delay and voltage support

Occasionally, some of the electrical components of the distribution systems, the transformer for instance, are upgraded in order to be able to handle a future increase in loads, in which case the upgraded component becomes underutilized until the growth in loads occurs. Energy storage systems can be used to delay the need for installing component upgrades by supplying, itself, electricity during peak demand times and hence reducing the peak demand to be served by the distribution systems, hence buying time before new components need be added.

Also, energy storage systems can extend the operational life of the transmission and distribution equipment, as it provides power during peak times, reducing power demand encumbering the equipment, and hence alleviating the wear and tear on them.

2.2.3 End user applications

Energy storage can be utilized for end user applications which include enhancing power quality and time shifting.

2.2.3.1 Power quality and reliability

Energy storage can improve the power quality by protecting end user loads from short-duration occurrences that disturb the quality of power delivered to the users in the form of service interruptions as well as voltage surges or sags.

Energy storage systems can improve power reliability by providing power in case of a loss thereof from a power source, until it is restored.

2.2.3.2 Retail Time shifting

This corresponds to the generation level time shifting on an end-user scale. In this case, energy can be stored during off peak times when retail prices are low, and then utilized during peak times when retail prices are high, hence reducing electricity cost.

2.3 Types of energy storage

There are many different types of energy storage systems for electricity, which vary in scale and storage time. Some of these storage systems are explored next, along with the relative benefits, disadvantages, estimated costs and performance of each. Storage devices are frequently categorized by their performance characteristics, and the applications they serve (Drury et al 2011). The ideal energy storage technology should be relatively cheap, as well as with exhibit high efficiency, high energy and power density, and a long lifetime. Clearly, no one type of energy storage will have all of these attributes combined, but instead, each will be more suitable for a specific range of applications (Taylor et al, 2013). While the main focus of this thesis is energy storage for large-scale renewable energy systems, it is worth taking a look at the different energy storage systems available.

The energy storage systems reviewed in this section can be divided into

1. Electro-chemical storage
2. Electromagnetic

   a. Super conducting magnetic energy storage (SMES)
   b. Super capacitors
3. Thermal storage
4. Mechanical
   a. Pumped hydro storage
   b. Flywheel storage
   c. Pressurized air storage: Compressed air energy storage

2.3.1 Electro-chemical storage

A number of examples are discussed to illustrate this type of storage, including batteries: lead-acid batteries, nickel cadmium batteries, sodium sulphur batteries, as well as fuel cells and flow batteries. The available energy storage plants, and their costs and possible applications are reviewed as well.

2.3.1.1 Batteries

There are many different types of batteries commercially used at the moment. These include

a) Lead-acid batteries
b) Nickel-cadmium
c) Sodium-sulphur
d) Flow batteries

Lead-acid batteries are one of the oldest and most commonly used electrochemical rechargeable devices. During the charge state it contains electrodes of lead metal and lead oxide in an electrolyte of about 37% sulphuric acid, while in the discharged state both electrodes transform into lead sulphate and the electrolyte becomes primarily water (Chen et al, 2009). They cover a variety of applications, including vehicles and communications. One of their biggest utilizers is China, which represented 5% of the lead-acid batteries market in

2007, mostly for use in solar photovoltaic systems (Beaudin et al, 2010). However, the largest facility for lead-acid storage is in Chino, California; a 40 MW unit used for load levelling, and valued at USD18.2m (Moore et al, 2006). These batteries have their pros and cons. On the bright side, they have high efficiency (70-90%) and are relatively cheap (USD120/kWh) (Albright et al, 2012). However, they suffer from a short life span of around 500-1000 cycles before the start of a performance decline, and they have low energy density, though that can be compensated for by their strong surge capabilities, uninterruptible power supply and high reliability. Lead-acid batteries also require routine maintenance and have a tremendous negative environmental impact due to their explosive gas and acid fumes emissions (Chen et al, 2009). The batteries are suitable for high power quality and reserve spinning applications.

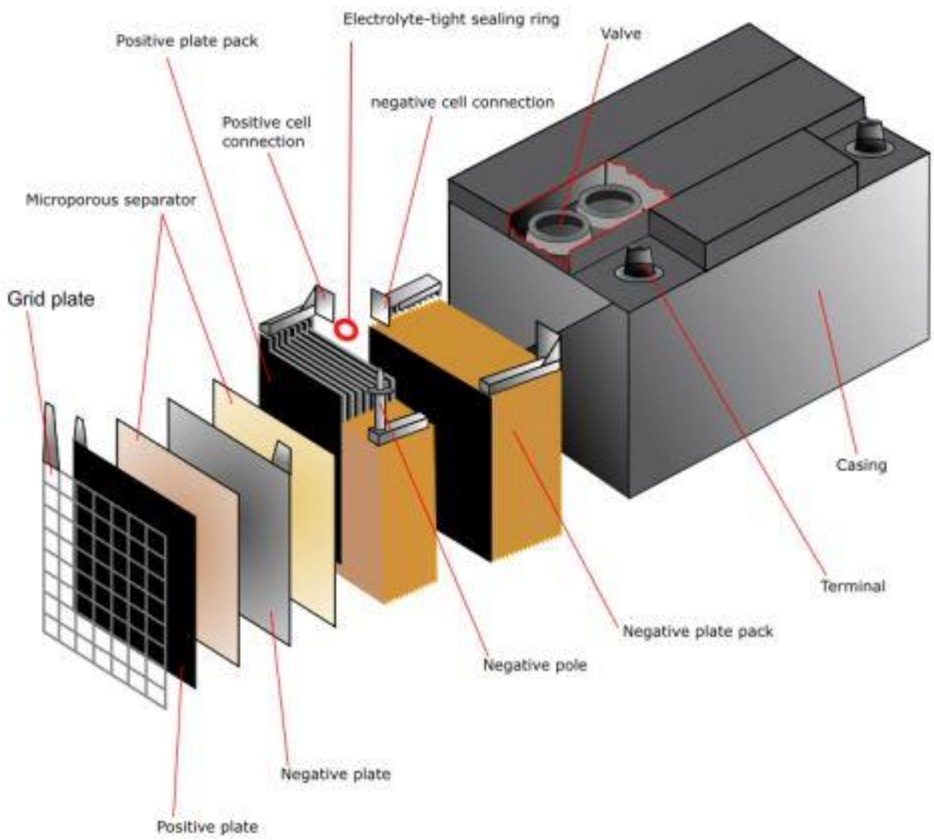

Figure 2-1 Lead Acid Batteries (University of Cambridge 2007)

Nickel-Cadmium batteries electrodes are formed of Nickel (Ni) and Cadmium (Cd), in different forms and compositions. Usually the +ve electrode is made of Nickel and the -ve electrode is composed of Cadmium hydroxide, while electrolyte is formed of Potassium hydroxide (Chen et al, 2009). Compared to lead-acid batteries, nickel-cadmium (NiCd) batteries have additional advantages. They have both higher energy density and longer life cycles (2000-2500), provide continuous power supply, and can be applied to generator-starting processes albeit with very high cost (USD1000/kWh) (Chang et al., 2009) (EUP, 2006). As such, a NiCd battery at 27 MW, powers the currently most powerful battery unit, providing 40 MW for 7 minutes. It is located in Arkansas in the United States and is used for reserves spinning and grid stabilization (McDowall, 2004).

Recently, another type, the sodium-sulphur (NaS) battery, has been gaining ground in applications. The +ve electrode is typically is molten sulphur while the –ve electrode is molten sodium with the electrolyte consisting of sodium alumina (Energy storage association). These batteries have unique characteristics that make them adequate for application in renewable energy systems. For example, they have life cycles of up to 2500 cycles, a high power density, and high efficiency (up to 90%). However, their capital cost is relatively high (USD400/kWh) (Kemet Corporation, 2013; Chen et al, 2009). The sodium-sulphur batteries are available at more than 30 sites in Japan, storing more than 20 MW of power, and used for peak load shaving (Chen et al, 2009).

On the other hand, Flow batteries have been on the rise since their development in the 1970s by Exxon (Beaudin et al, 2010). They consist of two-electrolyte system, where the chemical compounds used for energy storage are in liquid state, in solution with the electrolyte (Ibrahim et al 2008). Flow batteries have very attractive attributes including their scalability, independent sizing of power and energy, high round-trip efficiency. The response time of flow batteries is in the order of ms. Tests conducted on flow batteries showed their ability to respond in less than 0.5 ms for 100% load increase which could provide great value for grid stability applications and ancillary services (Alotto et al, 20140). Flow batteries also can store energy longer than conventional batteries. However, flow batteries have lower power density and energy density compared to other technologies, making them unsuitable for mobile applications at the moment. The efficiency of flow batteries is around 85% with over 2000 charge cycles with capital cost around $900/kWh (Alotto et al, 2014). The largest flow battery installed at the moment is a 4 MW/6 MWh plant installed by SEI for J-Power in 2005 and its main application is to smooth the power output fluctuations at Subaru Wind Villa Power Plant (Alotto et al, 2014).

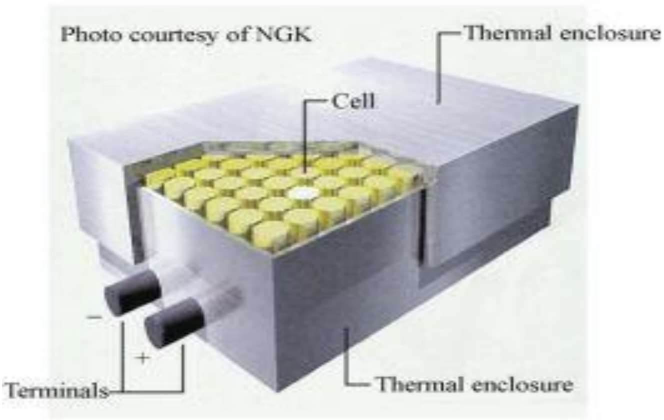

Figure 2-2 Sodium Sulphur batteries (Chen et al, 2009)

2.3.1.2 Fuel cells

Fuel cells produce electricity using electro-chemical energy conversion. The fuel cells are composed of an anode and a cathode, separated by an electrolyte. Hydrogen is passed through the anode, while oxygen is passed through the cathode, resulting in the formation of hydrogen ions and electrons at the anode. These hydrogen ions move to the cathode by virtue of the electrolyte and the electrons move to the cathode via an external circuit. Water is formed at the cathode from the combination of hydrogen and oxygen. Electricity is produced by the flow of electrons through the external circuit. Fuel cells are different from batteries because they require a continuous supply of fuel and oxygen (or air) to sustain the chemical reaction.

A hydrogen cell uses hydrogen as a fuel and oxygen as an oxidant (Chen et al, 2009). There are different types of fuel cells that vary by changing the electrolyte used.

Fuel cells have many advantages, including a relatively high energy density, a flexible scale of operation that can vary from KW to MW, and fittingness for modular construction. However, they have a relatively high cost (USD425-USD475/ kW) (Beaudin et al 2010).

2.3.2 Electromagnetic energy storage

2.3.2.1 Super conducting magnetic energy storage (SMES)

SMES works by storing inductive energy from the flow of DC through the super-conducting coil, where the energy content is determined by the current, through the number of turns in the coil. SMES is the only technology that stores electrical energy directly in electrical current form. The energy stored in any given moment is equal to half the product of inductance and square the current (Beaudin et al 2010). The temperature of the coil must be kept at a temperature close to absolute zero in the superconducting state—done by immersing it in liquid helium contained in a vacuum-insulated cryostat (Connolly, 2007).

This system consists of four main components: a conductor coil, power electronics to control the flow of the current, a refrigeration system to make sure the coil is kept at a controlled low temperature, and vacuum (Zhao et al, 2015). The losses in the system are primarily concentrated in the refrigeration equipment, reducing the system efficiency. Inverters are connected to the power electronics to transform the DC current output from the SMES to AC current, along with a transformer to adjust the power to the AC system (e.g. a grid). The power electronics system does not expend much energy loss because of its very high efficiency. Theoretically, the SMES system has a very high efficiency (97%) with a very fast response, and can be implemented on a large scale though only for a short period of time (Chen et al, 2009). However, for the system to be implemented on a large scale, the coils must be of a very wide diameter, which can be very costly. Other major disadvantages of SMES include the short-range energy storage (in the order of seconds) and the high initial cost.

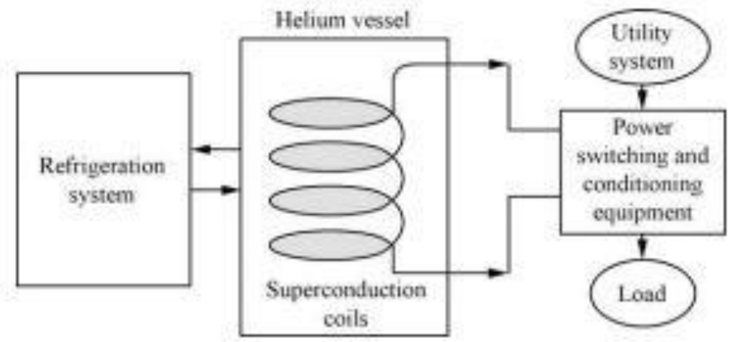

Figure 2-3 SMES (Chen et al, 2009)

The typical rating of a SMES system is 1-10MW with seconds of storage time, but effort is being made to establish larger systems with power capacities of 10-100MW (Gonzalez et al, 2004). The largest installation includes six or seven units, located in upper Wisconsin, and developed by American Superconductor in 2000. In year 2000, installations of SMES were added in Wisconsin consisting of 3 MW/ 0.83 kWh. The units serve in power quality applications and reactive power support, among other uses (Beaudin et al, 2010).

2.3.2.2 Super Capacitors

Super capacitors store energy using an electrolyte solution enclosed by 2 solid conductors. They are similar to conventional capacitors but with a much higher power density (Chen et al, 2009). Super capacitors’ efficiency stands at around 90%, and their storage timeframe ranges from seconds to hours. However, they have a high capital cost that goes up to USD20,000/kWh (Hadjipaschalis et al, 2009). Super capacitors are normally used for power factor correction, and grid voltage and/or frequency support.

2.3.3 Mechanical Energy storage

There are different commercial mechanical energy storage systems which include

a) Flywheel Storage

b) Pumped Hydro Storage

c) Compressed Air Energy storage

2.3.3.1 Flywheel storage

Flywheels operate by means of a rotational motion to store energy. A motor is used to spin a rotor during charging mode. During discharging, the same motor acts as a generator to produce electricity using the rotational energy of the flywheel. The energy stored in flywheels is directly proportional to the angular velocity and the moment of inertia of the flywheel (Ribeiro, 2001). However, the finite strength of materials used in a flywheel limits the maximum amount of energy that can be stored. Power electronics are used to manage the output's frequency and voltage. The efficiency of flywheels can reach as high as 95% as no thermodynamic processes are involved (Chen et al, 2009). The reported flywheel capital cost varies considerably in the literature from USD100-USD800/KW (Lipman et al, 2005) to USD1000-USD5000/kW (Chen et al, 2009). Flywheels store power in the order of KW (e.g. 100’s KW/10’s of seconds) so their uses are mostly limited to high power/short duration applications. Larger scale flywheels (in order of MW) can serve in reactive power support, spinning reserve and voltage regulation (Chen et al, 2009). An example of commercial flywheels systems is a 5 kW h, 200 kW flywheel system is used to stabilize the local grid in Utsira, Norway (Beaudin et al, 2010)

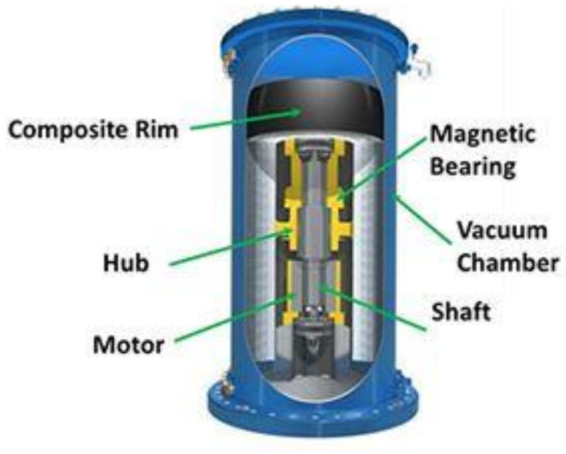

Figure 2-4 Flywheel system (Beacon Power, LLC)

2.3.3.2 Pumped Hydro Storage

Pumped hydro storage is the most widely used type of energy storage, with a worldwide energy storage capacity of more than 90 GW (Denholm et al, 2004). The process of operation of pumped hydro storage is quite simple. During periods of low load demand, these stations use the surplus electricity to pump water from a lower situated reservoir to an upper reservoir. When demand is greater than the supply, the water flows out of the higher reservoir and drives the turbines to generate electricity during peak hours (Ibrahim et al, 2008). A height difference between two natural bodies of water or artificial reservoirs is a prerequisite. Also, the volume of water is directly proportional to the stored energy, so higher volumes of water can always be used to maximize energy storage

Hydro storage systems have efficiencies of around 80% (Ter-Gazarian, 1994), which is relatively high compared to other storage systems. Another major advantage is their ability to act rapidly owing to the brief start-up time for hydro turbines (as short as 3 minutes from shutdown) and their minor energy loss over time (only through evaporation) (Sorensen, 2007). In addition, the lifecycle of pumped hydro can reach as much as 50 years (Schoenung, 2001). However, the cost of pumped storage system is relatively high, reported at around USD600-USD2000/KW (Beaudin et al, 2010). The major disadvantages of pumped hydro storage include the height difference required for the system to work effectively, the very high capital cost for building a hydro storage system, and the environmental concerns associated with building hydro power plants. Pumped hydro systems are typically used for energy management, frequency control and provision of reserve, since they have the highest rating among the available energy storage systems.

2.3.3.3 Compressed Air Energy storage (CAES)

Compressed air energy storage (CAES) is essentially the main focus of this thesis. An overview is hence warranted in this section, with more detailed descriptions to follow in upcoming sections. CAES is a bulk electrical energy storage technology that is suitable for both long duration storage (tens of hours) and large scale (thousands of MW) applications (Van der linden, 2006). This makes it a very suitable option for large-scale wind farm-integrated grids (Succar et al, 2008); more so compared to other energy storage facilities with lower capacities and lower output periods like batteries, flywheels and magnetic storage systems, which are discussed earlier. The basic principle of operation of a CAES system is during the times when the supply is higher than the demand, charging mode starts where the surplus power operates the compressors, producing air under high pressure which is stored in an underground cavern with minimal heat and pressure loss. Intercooling is implemented between the compression stages to ensure the air going into the underground cavern is within safety operation in term of inlet air temperature and also to reduce the compressors work. When the demand is higher than the supply, the discharge mode starts where the air under high pressure powers the turbines to generate power which is then supplied to the grid. Combustion chambers are implemented between turbine stages to increase the temperature of air to the desired inlet temperature of the turbines. CAES can store power in the order of MWs and for hours long. It also has a relatively higher power capacity and a short start up time (emergency start up takes only 9 minutes) (Chen et al, 2009). CAES systems are, therefore, particularly well-suited for load-levelling and time-shifting applications (Cavallo, 2007). Again, the capital cost cited in literature varies, as will be discussed in greater details in the subsequent chapters. The main disadvantage of CAES systems, at least for the already existent plants, is their use of natural gas during discharge time, making CAES not an entirely green source of storage (Zafirakis et al, 2010). The efficiency of CAES depends on its type; for instance, the efficiency of a diabatic CAES system stands at around 40%, while the theoretical efficiency of an adiabatic CAES system could be as high as 70% (Kere et al, 2015).

2.4 Concluding remarks on energy storage systems

Each of the discussed technologies has its unique advantages and disadvantages. Across the board, however, a number of factors determine the suitability of each storage technology to a specific purpose. For large-scale grid-integrated wind turbines, these factors are the capacity of the system, the cost of the system (whether initial capital cost or continuous costs as maintenance for instance), the reliability and the efficiency of the system under different conditions.

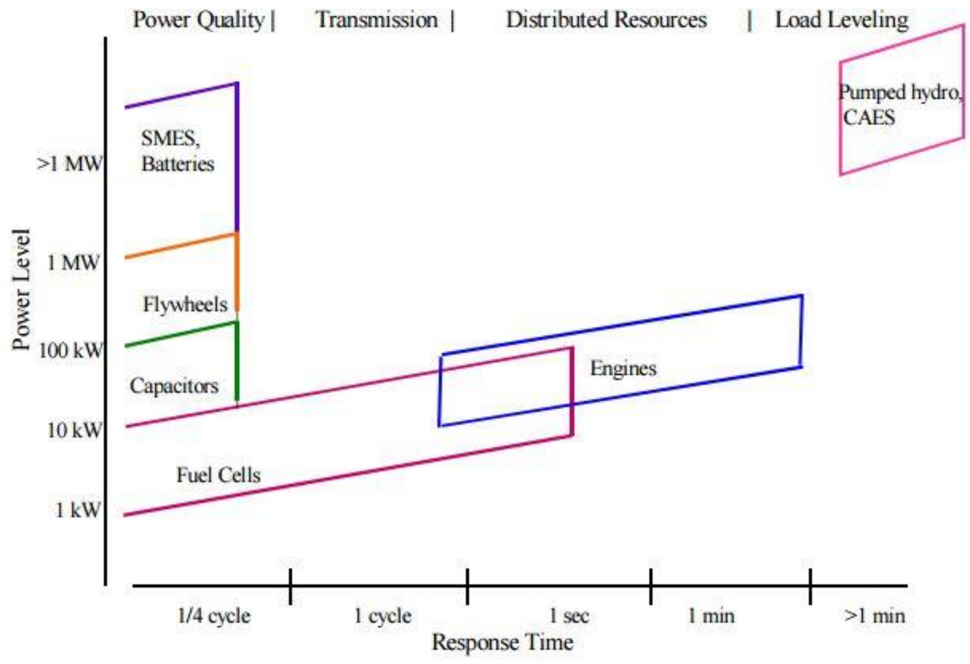

Figure 2-5 Comparison of different energy storage systems power level vs Response time (Schoenung 2001)

Flywheels are not considered a suitable option for the large scale of the grid-integrated turbines because of their relatively small storage capacity. As for batteries, many different types of the technology can be used. However, the high capital cost associated with large-scale storage batteries is an economic setback, besides the disadvantage of a short lifetime for the majority of battery technologies.

Pumped-hydro storage is a well-established technology, commissioned with many systems all over the world. It has a high storage capacity, which is critical for large-scale applications. However, its main disadvantages include a high capital cost, and the logistical nuisance associated with establishing a setup that provides for a difference in heights between two reservoirs.

Table 2-1 Comparison of potential large scale energy storage systems in terms of maturity, application and site limitations (Pieper et al, 2010).

	Maturity	Main Applications	Site limitations
CAES	Mature	Large scale renewable energy integration	Specific geology requirements
Hydrogen Storage	Not yet demonstrated on a large scale	Suitable for decentralized applications	No specific geologies
Batteries	Mature only on a small scale	Flexible and well suited for decentralized applications	No specific geologies
Pumped Hydro	Mature	Well-suited for centralized applications	Needs difference in heights between reservoirs

Surveying the available energy storage systems, CAES appears to be most suited for use with large-scale grid-integrated turbines owing to its large storage capacity, adequate start up time, and relatively low capital cost.

2.5 Overview of Compressed Air Energy Storage (CAES)

This section discusses compressed air energy storage systems –this thesis's focal point. The overview herein starts with a brief history of CAES, followed by a survey of suitable locations for building an underground air reservoir for the CAES operation. After that, different types of CAES system are discussed with special attention to adiabatic compressed air energy storage. The main components of CAES are then examined. Finally, the recent research that has been carried out on the topic is reviewed.

2.5.1 History of CAES systems

The CAES has been known and used in industrial applications since the 19th century (White paper, 2011). CAES emerged as a new technology in the 1970s, but interest in CAES decreased in the decade that followed due to the emergence of lower-cost gas turbines. Lately, however, that interest has been renewed owing to the growth of wind power and the suitability of CAES to that technology (Wang et al, 2012).

The process by which the system operates entails compressing the air, storing it in a large underground cavern, and later used to power turbines (Swider et al, 2007). The system allows for several hours, or days of energy storage, which allows power providers to deliver electricity during peak hours when the demand for electricity and price are at the highest level.

2.5.2 Suitable Locations for CAES systems

Salt, hard rock and porous rock are three suitable geologies for CAES caverns. The two currently operating CAES systems use salt domes as storage reservoirs. The hard rock geology involves higher cost of mining a new reservoir, which makes it less financially appealing compared to salt reservoirs (Taylor et al, 1999). The main requirements for CAES using rock caverns are stability, air tightness and an acceptable surface subsidence (Lux, 2010). Kim et al (2012) conducted a study on the losses incurred when operating the CAES in rock caverns, and concluded that using rock caverns is feasible, from an air leakage perspective, if the temperature of the inlet air is close to the temperature of the rock. Additionally, the cost of development can be relatively low in the case of using existing mines. Depleted natural gas caverns are another option that can prove economically attractive, as they are already existent and can handle the pressure. However, they are mostly originally designed to slow pressure variations, and so may not be readily operational

(Arizona Research Institute, 2010). Porous rock presents the lowest cost option for development as a reservoir, though this cost varies depending on the characteristics of the storage layers. Another advantage of using porous rocks is the lower costs associated with incremental additions to the storage capacity, compared to other geologies [Ter-Gazarian (1994)].

2.5.3 Types of CAES systems

A number of different processes can be employed in a CAES system. The first is the conventional or "diabatic" CAES. This type involves burning natural gas in an expansion turbine, in a similar way to that of a combustion plant. Two energy inputs characterize the diabatic CAES system: compressed air, and natural gas fuel. As a result, instead of a single round-trip efficiency, the efficiency of a conventional CAES is characterized by the amount of natural gas energy used to generate each kilowatt-hour of electricity, and the amount of electrical energy input per unit of electrical energy output (Ibrahim et al, 2015). In the diabatic CAES, however, more energy is generated than stored, because natural gas is used during the power generation process (Ter-Gazarian, 1994).

Two other major types of technologies have been approached, namely the adiabatic and the isothermal CAES. In the adiabatic system, the compressed air is cooled down and the heat generated from compressing the air is stored and used to re-heat the expanding air during the generation cycle. In an adiabatic compressed air energy storage system, the heat generated from the compression is stored in a thermal energy store, instead of being vented (Rogers et al, 2014). This stored thermal energy is later used to heat up the air passing from the store into the expander turbine, so that no fuel need be burned, with the result being lower cost, higher efficiency and less harmful emissions and less environmental impact. However, implementing an adiabatic CAES system requires the additional capital costs of a thermal energy store and heat exchangers. Thermo-dynamical calculations predict that adiabatic systems would have higher efficiencies than diabatic systems, though no adiabatic CAES systems exist thus far. Figure 2-6 shows the system configuration of both a diabatic and an adiabatic system.

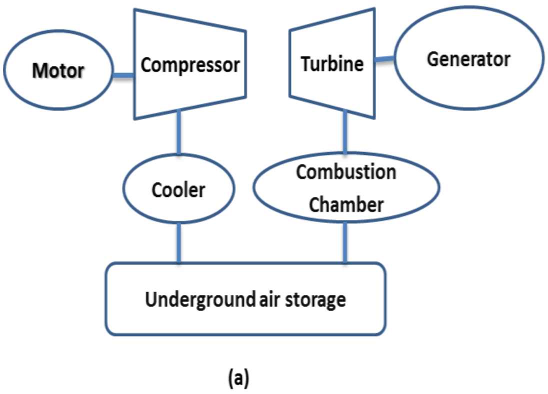

Figure 2-6 (a) showing a diabatic system and (b) showing an adiabatic system [Doetsch et al (2009)]

There are also isothermal CAES systems, which compress and expand the air at a constant temperature without using fuel during the expansion cycle. Isothermal CAES, however, is still in the early stages of development, and as such its performance is yet to be assessed on a practical level. Sustain X, which is a leading global provider of grid-scale energy storage, has completed the construction and begun the start-up of the first isothermal CAES system (Sustain X, 2013). The plant has a 1.5MW capacity and is based in New Hampshire, U.S.A. The isothermal CAES has a low capital cost, a long lifetime, and high efficiency (McBride et al 2013). It is also capable of scalability and can hence run applications across the electricity market chain, from generation through to transmission and distribution.

Dr Nakhamkin (2007, 2009) introduced several new configurations that can be applied to reduce the cost and the delivery time using off-the-shelf components compared to a conventional diabatic system. An overview of the best performing among those configurations is presented next. Figure 2-7 shows the CAES-AI with a bottoming cycle air expander. In this configuration, a conventional CAES system with an add-on recuperator (similar to a McIntosh plant) is employed, with the addition of a gas turbine being introduced. The exhaust of the high pressure expander is injected into the compressor discharge of the added gas turbine, hence increasing the power output from the gas turbine. The total net power of the system, in that case, includes the power from the HP and LP expanders as well as the gas turbine.

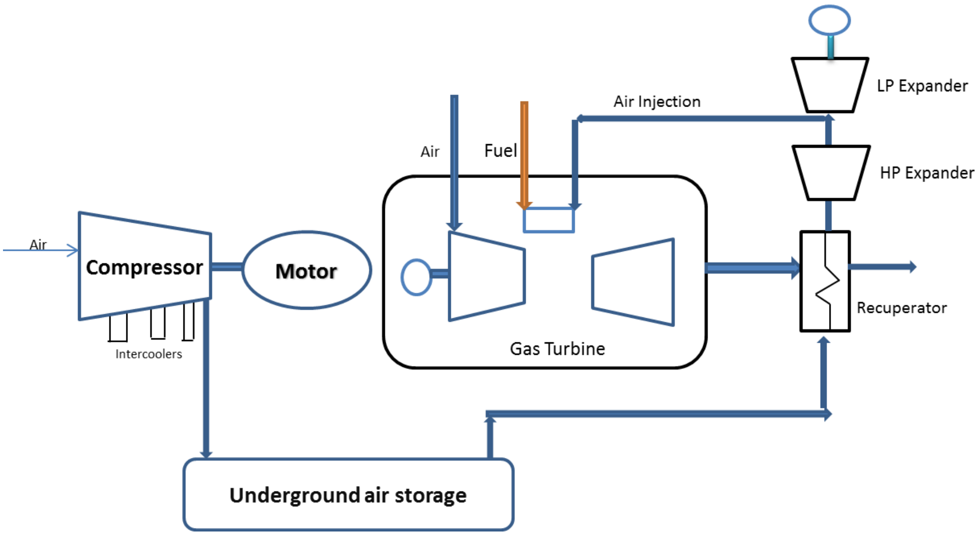

Figure 2-7 CAES air injection concept with a bottoming cycle air expander

Figure 2-8 shows the concept of CAES with a bottoming cycle and inlet chilling. In this setup, only 1 expander exists. The exhaust of this expander is injected into the compressor inlet of the gas turbine. The expander is optimized to have the exhaust flow rate equal that of the gas turbine compressor inlet. The total power of the system, in this case, is the sum of the expander power and the gas turbine power.

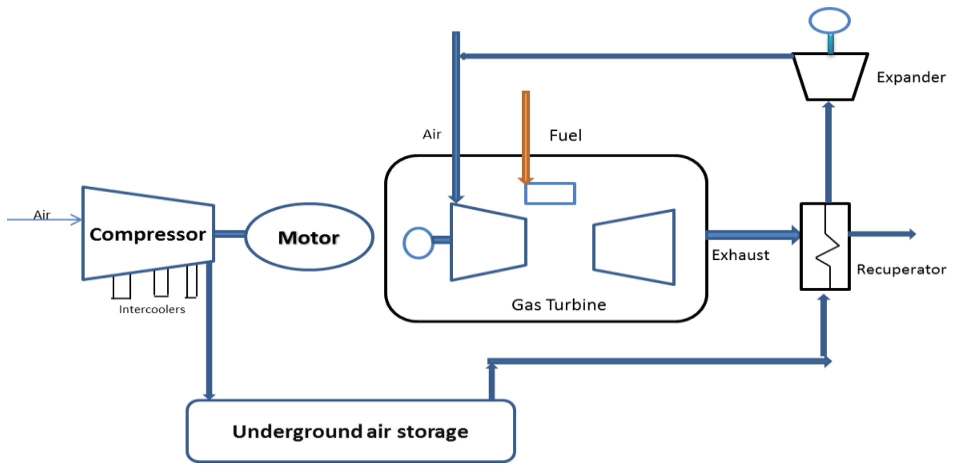

Figure 2-8 CAES concept with bottoming cycle air expander and inlet chilling

Figure 2-9 shows the concept of CAES with a bottoming cycle air expander, where the expander power is the CAES power. The expander does not have to meet the flow rate of the compressor in the gas turbine and hence enjoys more sizing flexibility.

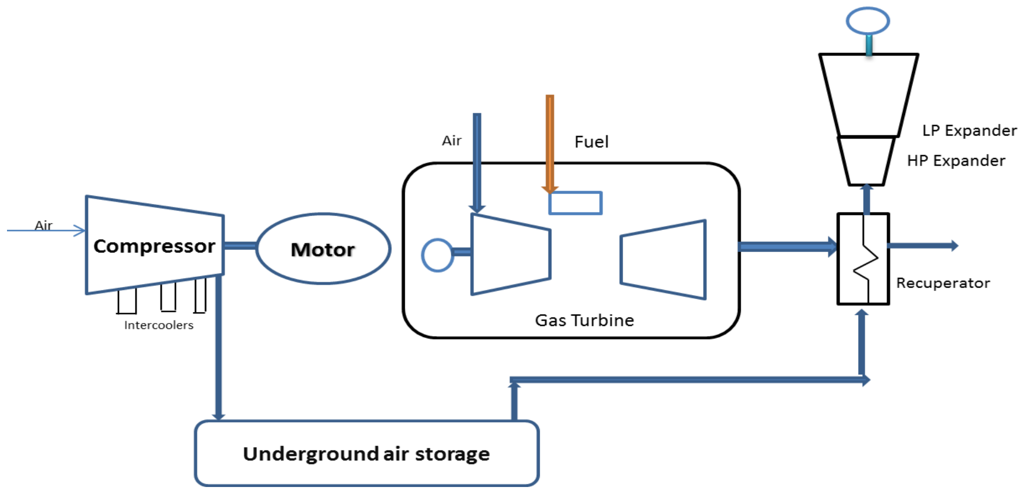

Figure 2-9 CAES concept with a bottoming cycle air expander

In conclusion, the most efficient type is the air injection with a bottoming cycle air expander, with a heat rate of 4009kJ/kWh.

Succar et al (2008) introduced the new concept of a constant cavern pressure CAES system. The cavern volume in this system is smaller than that of a conventional CAES system. The system works by using water from a surface reservoir to displace the compressed air in the cavern (Kondoh et al, 2000). Very deep air storage is needed to produce the pressure difference, which increases the cost of the system. A hydraulic pump can be used to enable the construction of the cavern with a shallower depth, but the pump would consume around 15% of the total power produced (Kim et al, 2011). Kim et al (2010) proposed a constant pressure cavern CAES system combined with a pumped hydro system, and performed a study which concluded that the hydraulic part consumes 37% of the total power and around 23% of the total power during the discharging stage. The round-trip efficiency of the hydraulic part can even worsen due to the irreversibility resultant from deficient heat transfer between the two media (air, water) and the cavern.

2.5.4 Current and Proposed CAES

Only 2 operational CAES plants exist worldwide; one in Germany and another in the U.S.A, both of which are discussed next. Among those currently under construction, the largest CAES plant is in Ohio, U.S.A, called Norton, with a capacity of 2,700MW (Arizona, 2010). However, the plant’s construction works have been postponed (Funk J, 2013). Another project, the Iowa Energy storage facility, was started in Dallas, U.S.A in 2006 for a capacity of 270MW, built on porous rock geology, but was terminated later in 2011 for geological reasons (Schulte et al, 2012).

2.5.4.1 Huntorf CAES system

This facility was built in Bremen, Germany, in 1978 with a capacity of 290MW, and was designed by ABB Automation company for E.N Kraftwerke. The Huntorf plant is the first compressed air storage/gas turbine power station in the world and has been operating successfully for over 22 years (Crotogino et al, 2001). The facility was originally designed for a 2-hour output, but has been modified to allow for a 3-hour power output. At full charge, the cavern is pressurized to 70 bars and is discharged down to 50 bars. The facility utilizes salt cavern storage geology. In 2006, its capacity was increased to 321MWwhich can be reached within 6 minutes. E.N Kraftwerke's CAES plant was built in response to the growing capacity of wind power in Germany and the growing importance of the 'minute reserve. From the time when it was commissioned, the plant has been expanded from 150,000 m^3 to 310,000 m3 of storage volume. The plant has a 90% availability and a 99% starting reliability (Schainker, 2004). Huntorf is a diabatic CAES system, which uses natural gas to heat the air entering the turbines, hence its relatively high heat rate (Meyer, 2007).

Figure 2-10 Huntorf Plant in Germany (Crotogino et al, 2001)

2.5.4.2 McIntosh

This CAES system was built by Alabama Electric Cooperative in Alabama, U.S.A., in the 1990s. It has a capacity of 110MW and utilizes a salt geology as well. The facility is designed for 26 hours of power output. At full charge, the cavern is pressurized to 76 bars and is discharged down to 45 bars. During discharge, 155 kg of air flows out of the cavern every second. This facility has a starting reliability of around 92%; and has a running reliability of 97% for power generation, and an approximately 99.5% running reliability for compression. The plant efficiency stands at around 55%. The higher efficiency of the McIntosh plant is due to its use of a recuperator to extract heat from the turbine exhaust gases, which is reused to heat the compressed air before entering the turbine. Benefits of using a recuperator is discussed further in CAES components section. Table 2-2 (Meyer, 2007) summarizes the key facts pertaining to the two existing CAES plants.

Figure 2-11 McIntosh CAES plant in US (Clean energy Action Project)

Table 2-2 Specifications of Huntorf and McIntosh CAES plants (Meyer, 2007)

	Huntorf	**McIntosh**
Date of commissioning	1978	1991
Specifications of the caverns	Two cylindrical salt caverns with a combined volume of 310,000m^3	One salt cavern with a volume of 538,000m^3
System electrical output	290MW for 2 hours	110MW for 26 hours
Energy required for 1 kWh electricity	0.8kWh electricity 1.6 kWh gas	0.69 electricity 1.17 kWh gas
Pressure range(bars)	50-70	45-76
Miscellaneous	First CAES plant	First CAES plant with recuperator

2.5.5 Issues with and challenges of CAES systems

Compressed air energy storage has some issues pertaining to installation and performance. The main issue with CAES is finding a suitable geology for installation. The location where CAES will be installed must have one of the geologies discussed in section 2.5.2. CAES is therefore, location-dependent. Diabatic systems are the only systems currently implemented in both Huntorf and McIntosh (with recuperator), with the Iowa plant implementing isothermal CAES, albeit system not operational yet. This is another issue with CAES, as these diabatic systems are not completely green because they burn natural gas in order to heat the air entering the turbine, which also increases the heat rate of the system and lowering their efficiency. Therefore, the implementation of a complete adiabatic system is currently very attractive, with plenty of research being carried out on it. Another issue that pertains to the safety of operation is that the pressure inside the system goes up to 80 bars on a daily basis. Thus, the design of the cavern, and all system components, must be sized so as to withstand this pressure. Selected thermal storages for adiabatic systems must be able to endure very high temperatures as well. Therefore, the strength levels of these storage systems must be carefully studied to ensure they meet the operation condition. Similarly, choosing the heat transfer fluid should be made carefully, allowing it for instance to operate below its flash point.

2.5.6 CAES applications for renewable energy systems

Compressed air energy storage can be used in multiple applications with integration into the grid, and even with isolated grid networks. One common application for grid and isolated systems is load levelling, which is the main benefit of CAES from a technical point of view, capitalizing on its ability to store energy when supply is higher than demand and release the energy when demand is higher than supply. For normal grid networks, CAES can provide many services. These include time shifting, which is buying electricity when prices are low, storing it, and then releasing it at higher market prices—an economic purpose primarily (Greenblatt et al, 2007). CAES can also provide ancillary services, like voltage control by providing VARS, which is applied in both Huntorf and McIntosh systems(EPRI Handbook, 2003). Also, CAES can be used as a supplementary spinning reserve, providing power in case of a grid power outage, as it has a short start-up time (9 minutes for emergency). Additionally, CAES can be used for frequency regulation to reduce the effect of imbalances in the grid system resulting from fluctuations in supply and demand levels.

2.5.7 Research carried out on CAES systems

Research on CAES has covered diverse topics, including performance of the system's various components, different uses and applications of CAES, economic feasibility of CAES systems, and wholly new concepts pertinent to CAES systems. The research carried out started in the 1990s and has since increased tremendously, especially in the past 5 years. This section will present some of the research carried out on CAES systems, ordered by topic, starting with those covering the operation of the system, on to the novel concepts and finally the economic performance studies.

2.5.7.1 New concepts

As was mentioned in section 2.5.3, Dr Nakhamkin et al (2007, 2009) have introduced novel concepts, which include off-the-shelf components that could reduce the capital cost of a CAES system. They presented CAES with steam injection and bottoming cycle with inlet chilling, among other concepts. The products that embody the realization of these concepts vary significantly, in terms of performance, with the air injection with a bottoming cycle air expander proving to have the lowest heat rate. Jubeh et al (2012) simulated two of the concepts suggested by Dr Nakhamkin (2007, 2009): compressed air energy storage with air injection and compressed air energy storage with inlet chilling (discussed under section 2.5.4 Types of CAES systems), and concluded that compressed air energy storage with inlet chilling performs better in terms of generated power and primary efficiency, but with a lower energy ratio compared to compressed air with air injection. Kim et al (2011) introduced a new concept involving constant pressure CAES systems, with the aim of reducing the volume of the underground cavern. For this purpose, they recommended the use of water together with air in the cavern, noting however that the hydraulic pump would have to consume a significant portion of the power in both the charging and the discharging cycle. Meanwhile, Sustain X is endeavouring to implement an isothermal system in Iowa but the project has not been completed yet. On another front, adiabatic systems as well are being explored, with Wolf et al (2014) proposing a low temperature TES, which could help with the construction and improve the economic feasibility of a thermal storage system, as well as reduce start-up time, with the downside however being the lower round-trip efficiency achieved. Yang et al (2014) has introduced a system, HTCAES that simply uses a conventional adiabatic CAES with heat added to the TES via an electrical resistance heater that uses reluctant wind power. Their research concluded that using this system would increase the power produced whilst maintaining the same scale of compressors, turbines and operating pressures of the system.

2.5.7.2 CAES performance analysis

Jubeh et al (2012) explored how varying each of several parameters, including mass flow rate of discharge, ambient temperature and pressure ratio of compressors and turbines, can affect the performance of the system. They concluded that the operational efficiency decreases with higher pressure ratios, while higher ambient temperatures improve performance. Zhao et al (2014) tested the combination of an adiabatic CAES system with a flywheel energy storage system, and provided a parametric analysis for the combined system. Grazzini et al (2008) studied the effect of varying the assembly of the compressors and the turbine during the operation of the CAES system, specifically, by changing the connections between the compressors (series or parallel) during charging, and the turbine during discharging. They concluded that the performance of the system could be enhanced if this changeable configuration setup is implemented properly. Barbour et al (2015) studied replacing the indirect contact heat exchangers and the thermal storage used in the CAES system with direct contact (packed bed) heat exchangers, arguing that using a packed bed heat exchanger would improve the heat transfer rate and hence increase the efficiency of the system. Hartmann et al (2012) investigated the optimal number of series compressor modules, concluding that a 2-stage compressor module is best in terms of performance enhancement, with less equipment required. They also argued that the maximum efficiency of a CAES plant is actually around 62%, which is lower than its theoretical efficiency of 70%. As mentioned earlier under the discussion of lined rock caverns, Kim et al (2012) and Rutqvist et al (2012) explored the operation of underground lined rock caverns at shallow depths (100m). Kim et al concluded that the loss in the system does not exceed 1%, particularly when the temperature of the air entering the cavern is not considerably higher than the ambient temperature. Rutqvist et al (2012) found that number to be even less, asserting that only 0.16% of the injected air mass is leaked daily. Raju et al (2012) modelled the variations in the temperature and pressure of the air in the cavern using a value estimate of the heat transfer coefficient. They validated their simulation by a comparison to the Huntorf CAES plant, demonstrating that the thermodynamic variations in the cavern are neither isothermal nor adiabatic but rather someplace in between. Zhang et al (2013) paid special attention to the TES part of the adiabatic CAES system. Using thermodynamic calculations, they concluded that— even at maximum power efficiencies—TES systems leave untapped energy, and that the utilization of energy in TES systems can be optimized with proper pressure ranges. Dr Garvey (2012) examined the prospect of using a multi-stage thermal storage with a multi-stage expansion, together with the possibility of adding solar heat to increase the total output of the said system. His findings entailed a turnaround efficiency of 85% and confirmed that the integration of a solar thermal system could enhance the operation by a substantial margin. Li et al (2012) introduced a tri-generation system that utilizes compressed air energy storage and thermal storage for generating power, heating and cooling— albeit on a smaller scale. They concluded that this setup could improve performance, compared to a conventional tri-generation system. Zhang et al (2014) considered the integration of CAES with wind, and studied the effect of wind speed fluctuations on the performance of the system. They found that the wind turbine and compression processes are affected by the wind speed fluctuation. They also found that changing the wind speeds changes the compression power used compared to the rated power of compressors, considering how that could affect the compressors' efficiency. Yang et al (2014) focused on the heat exchangers in the adiabatic CAES system, and ascertained that the higher the heat exchangers' effectiveness, the better the performance of the CAES system (higher efficiency), and that any pressure losses in the heat exchangers reduces the heat energy stored in the TES, hurting in turn the efficiency of the system.

2.5.7.3 Cost of CAES systems

Amid increased wind penetration to the grid, several studies have been conducted on the competitiveness of the CAES system economically. Pehnt et al (2008) implemented a stochastic electricity market model to measure the effect of significant wind power generation on the operation of the system, and the economic value of investments in CAES systems in Germany. Denholm et al (2009) evaluated the economic benefit that accrues from reducing transmission costs when co-locating the wind energy and the energy storage system. Mauch et al (2012) assessed the attempt to reduce dispatch uncertainties by trading the wind power in day-ahead markets, ignoring the income from ancillary services, and concluded that without tax incentives, wind-CAES systems are unlikely to be profitable in day-ahead markets. Madlener et al (2011) compared the economics of three variants of the CAES system, namely, wind farms without CAES, independent CAES systems, and CAES systems integrated with wind. The study found that the feasibility of each is contingent upon the relevant spot and minute reserve markets. Zafirakis et al (2009) hypothesized a CAES system integrated with wind in the island of Crete and explored the economic feasibility of its implementation. Safaei et al (2014) compared a conventional CAES plant with a decentralized CAES (DCAES) plant where compressors were coupled with the wind farms and distributed near the heat loads to use the heat of compression for district heating. The study took into consideration the extra cost of the pipelines connecting the compressors, and the storage reservoir supplementing the DCAES system. Lund et al (2009) used energy plan programming to determine the optimal strategy for CAES to trade electricity to the grid using the spot market prices of Denmark’s Nord Pool market. Marano et al (2012) explored the combination of a wind and a solar system coupled with compressed air energy storage, concluding that CAES can increase annual profits, improving the economic appeal of renewable energy systems. Wang et al (2012) assessed the economic feasibility of 19 bus power systems accompanying 8 wind farms integrated with CAES in China, and tested the sensitivity of their findings to natural gas prices and the discount rate. They found that CAES can exploit arbitrage opportunities and recover wind curtailment. De Boer et al (2014) studied the effect of assimilating a power-to-gas system, a pumped hydro storage and compressed air energy storage in an electricity system, at different wind power penetration levels in the Netherlands. They concluded that the pumped hydro system accrues the highest economic benefit, followed by the CAES system, and then the power-to-gas system. Abbaspour et al (2013) carried out an economic analysis of CAES integrated with wind to evaluate its aptitude in serving 2 distinct purposes in turn. The first purpose entailed maximizing total profit, which they assessed with and without CAES, and concluded that CAES can increase annual profits. The second entailed providing power to the grid at minimal cost, with the conclusion being that CAES reduces the total cost of power. Mason et al (2012) compared, from an economic viewpoint, the integration of CAES to wind with the addition of a natural gas combined cycle. They concluded that at current natural gas prices in the U.S., the latter is more feasible, but that on the longer-term, if the natural gas price increases, wind with CAES can become more economically appealing

2.6 Description of CAES systems

In this section, the components of a CAES system are discussed in more details, along with the importance of each to the system. The CAES system comprises of:

1. Compressors
2. Heat Extraction
    a. Intercoolers
    b. Regenerators/Recuperators
    c. Heat exchangers
3. Air Storage
    a. Cavern (suitable geologies mentioned earlier)
4. Heat Addition
    a. Combustors chambers
    b. Heat exchangers/Recuperators
5. Turbine

2.6.1 Compressors

This section discusses the types of compressors, their popularity and suitability for a CAES system. Since the compressors industry is fairly mature, this thesis will not discuss details about the compressors' operation nor that of the turbine expanders.

There are two main types of compressors:

1) Axial flow compressors
2) Centrifugal flow compressors

Both types can be used for various purposes, which are primarily classified as industrial, aerospace or research purposes. This report is primarily concerned with industrial compressors. In a CAES system, the compressors are coupled in series, and are expected to produce air in very high pressures (70 bars in the case of Huntorf and 76 bars in the case of McIntosh). For each single compressor, however, having very high pressure ratios has a main disadvantage, namely, the reduction of the operating range of the compressors. This creates a tendency in the compressors industry toward lower per-stage pressure ratios. The main benefit of increasing the pressure ratio per stage, on the other hand, is the reduction in the number of stages, which lowers cost (Boyce, 2012).

More on the thermodynamics of both isothermal and adiabatic compression are explained in this section for a better understanding of the process involved. According to the ideal gas law, the pressure is related to volume and temperature as follows:

$$P = \frac{nRT}{V} \tag{2-1}$$

Where V is the volume of the gas, n is the amount of substance in moles, R is the universal gas constant, and T is the absolute temperature.

For an isothermal process, the temperature is constant, and since n and R_o are constants, then

$$PV = \text{constant} \tag{2-2}$$

This means that pressure and volume are inversely proportional in this case. Therefore, the work done from volume V_A at pressure P_A to volume V_B at pressure P_B can be given by the following equation:

$$W_{A\to B} = \int_{V_A}^{v_B} PdV = \int_{V_A}^{V_B} \frac{nRT}{V} dV = nRT\int_{V_A}^{V_B} \frac{1}{V} dV = nRT \ln \frac{V_B}{V_A} = P_A V_A \ln \frac{P_A}{P_B} \tag{2-3}$$

A purely adiabatic process can only occur if the system is thermally insulated from the surroundings and no energy enters or leaves the system, in which case:

$$PV^{\gamma} = \text{constant} \tag{2-4}$$

where γ is the adiabatic index and is given by

$$\gamma = \frac{C_p}{C_v} \tag{2-5}$$

C_P being the specific heat for constant pressure process and C_V being the specific heat for constant volume process. The volume of air, as a function of pressure, is

$$V = V_A \left(\frac{P_A}{P}\right)^{\frac{1}{\gamma}} \tag{2-6}$$

Therefore, the net work done in an adiabatic process is given by:

$$W_{A\to B} = \int_{P_A}^{P_B} VdP = \int_{p_a}^{P_b} V_A \left(\frac{P_A}{P}\right)^{\frac{1}{\gamma}} dP = P_A^{\frac{1}{\gamma}} V_A \left(P_B^{\frac{\gamma-1}{\gamma}} - P_A^{\frac{\gamma-1}{\gamma}}\right)\left(\frac{\gamma}{\gamma-1}\right) = P_A V_A \left(\left(\frac{P_B}{P_A}\right)^{\frac{\gamma-1}{\gamma}} - 1\right)\left(\frac{\gamma}{\gamma-1}\right)$$

The absolute temperature in an adiabatic process is given by:

$$T_B = T_A \left(\frac{P_B}{P_A}\right)^{\frac{\gamma-1}{\gamma}} \tag{2-7}$$

It is important, however, to realize that the above-described equations depict isothermal and adiabatic processes only in theory, which cannot be fully met in reality, since there is no perfect conductor or insulator. Thus, the processes can be close to either system; and for industrial compressors, the operation normally lies between both processes

Axial flow compressors are high-flow, low-pressure compressors. They are the main type of compressors used for high power applications. An example is shown in Figure 2-12 (Boyce et al, 2012). Most of the gas turbines with an output power in excess of 5 MW use this type of compressor.

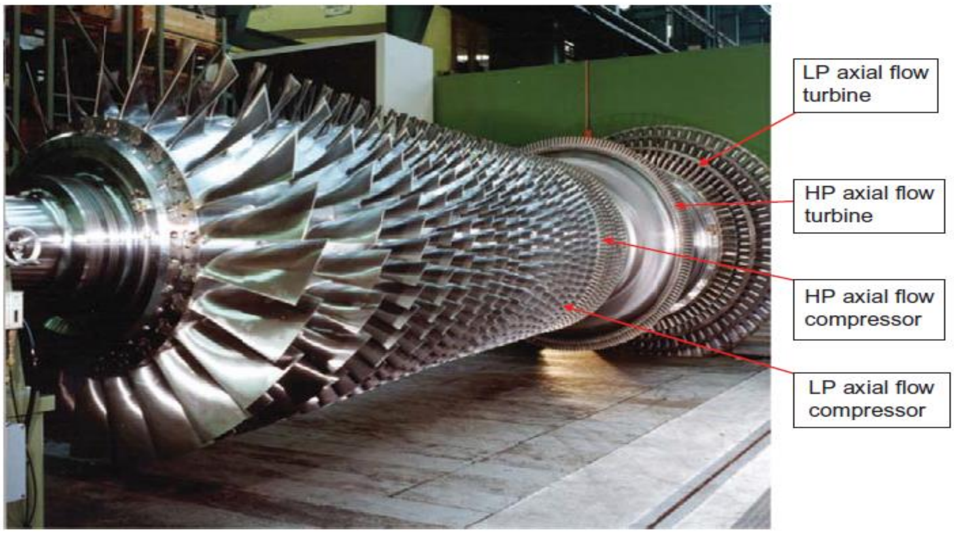

Figure 2-12 Axial flow compressor [Boyce (2012)]

On the other hand, centrifugal compressors are mostly used in small gas turbines. Their benefits to the axial flow include higher stability and a larger operating range. Their main disadvantage, on the other hand, is their low efficiency compared to the axial flow. Figure 2-13 shows a single-shaft industrial centrifugal compressor (Zunft et al 2006).

Figure 2-13 Single-shaft industrial centrifugal compressor [Zunft et al (2006)]

In the CAES setup, multiple compressors are connected in series in order to provide the high air pressure required for the CAES operation. After each compressor stage, an intercooler is placed to reduce the outlet temperature from each stage, as will be discussed in more detail in section 2.3.3.4. This should result in reducing the temperature of the inlet air going into the following stage of compression, which will eventually affect the performance of the compression stage. Most of the previous researches carried out for CAES used a 3-stage (series) compression to provide the required pressure, with intercoolers after each stage.

2.6.2 Turbines

The turbine’s role is to convert the energy of the pressurised air into mechanical energy that drives a generator for the production of electricity. Before discussing the types of turbine expanders, a number of issues associated with turbines are underlined. The main factors affecting the turbine’s efficiency are the mass of air inflowing to the turbine and the inlet air temperature and pressure (Barnes et al 2011). To improve the turbine’s efficiency, some type of adaptation to the inflowing mass and pressure should be incorporated. The mass flow is a major concern, because pressure varies with the load during operation. To solve this issue, a rather complicated method is currently being used, namely throttling, which causes losses and reduction of efficiency (Ter-Gazarian, 1994). Therefore, some adaptive stages are being introduced into the operation, such as the sliding-pressure air turbine, which yet faces the problem of the high temperature and pressure requirement.

The efficiency of the turbine can be derived using the following equation (Hartman et al, 2012):

$$\eta_{turbine} = \frac{dH}{vdP} \tag{2-8}$$

Normally the turbines efficiency is in the range of 90-95% (Boyce, 2012). The temperature variation across the turbine is given by

$$T_2 = T_1 \left(\frac{P_2}{P_1}\right)^{\frac{\eta}{\eta-1}} \tag{2-9}$$

Where n represents the polytropic index, the subscript 1 refers to the inlet and the subscript 2 refers to the outlet.

The two main types of turbines used are the axial flow turbines and the radial inflow turbines. The axial flow is considerably more popular— used in more than 95% of turbine applications [Boyce (2012)]. Axial flow turbines are either the impulse type or the reaction flow turbines. Impulse type axial flow turbines maybe used for power generation applications, aerospace and other high-power density system applications. The main applications of reaction flow axial turbines include expanding hydrocarbon gases and fluorinated refrigerants. Figure 2-14 shows a schematic of an axial flow turbine.

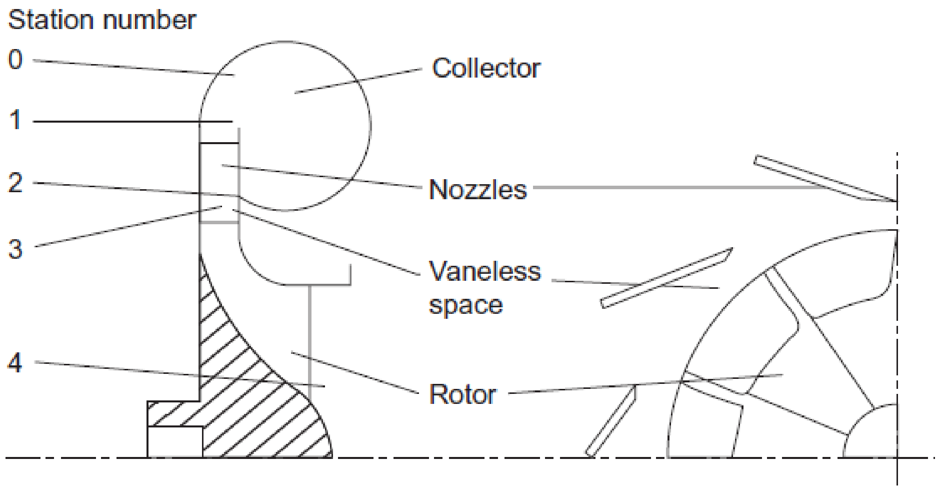

Figure 2-14 Axial flow turbine [Boyce (2012)]

On the other hand, radial inflow turbines are nearly identical to centrifugal compressors with a reversed flow. They come in two main types: the cantilever and the mixed-flow, though the former is rather unpopular because of its complexity. The most common application of the radial inflow turbine is the exhaust-driven turbocharger used in internal combustion engines. Millions of these units are used in car, truck, aircraft, and industrial engines. Other applications include smaller gas turbines, organic Rankine-cycle turbine generators, and air and natural gas separation plant turbo-expanders.

2.6.3 Heat extractors and heat addition

2.6 3.1 Gas Combustor

In the endeavour to improve the performance of a CAES plant, the main target is to reduce the consumption of fuel as much as possible, or eliminate it altogether when possible, which is in theory an operational achievement of the adiabatic CAES system. In a complete adiabatic system, therefore, no combustor would be used. The job of the combustor is to increase the inlet temperature going into the turbine, so as to improve its performance. This is done by burning fuel in the combustor, and converting the resultant heat into compressed air coming out of the cavern. A number of different factors affect the combustor's performance, and hence the amount of fuel required. These include the efficiency of the combustor and the pressure drop of the air leaving the combustor. The amount of energy required from the combustion chambers depends on the inlet temperature of the air entering the chambers. The heat rate of a CAES system is a measure of its efficiency, based on the amount of power actually consumed in the combustion chambers. The lower the heat rate of the system, the better the performance.

2.6.3.2 Regenerators/Recuperators

Regenerators/recuperators simply serve as heat exchangers, heating the air coming out of the cavern using the heat of the air leaving the turbine. This has the effect of reducing the amount of fuel burnt in the combustor stage, possibly eliminating the need for that stage altogether, lowering thus the heat rate of the system. The regenerator of a 25 MW turbine heats around 4.5 million Kgs of air each day (Boyce 2012).

Inside the regenerators, the heat is transferred between two bodies through the exposure to a third medium. The heat flows from and to that third medium. Recuperators, on the other hand, prevent the mediums from mixing. The heat is transferred by arranging the gas flows in such a way to allow for optimizing the temperature distribution in recovering the exhaust heat back to the compressor output. The advantage of a regenerator over a recuperator is its smaller volume, which translates into lower cost of materials, making it more advisable financially (Boyce 2012). The problem with regenerators, on the other hand, ensues from the mechanism of mixing with a third medium, which can cause lower efficiency. In heating, ventilation and air-conditioning systems, recuperators are commonly utilized to re-use waste heat from the exhaust air that is normally expelled into the atmosphere. They can also be used to preheat combustion air going into a furnace. Regenerators and recuperators may also be attached to thermal oxidizers that preheat the (ultimately) exhaust air from industrial processes [ESC (2012)].

2.6.4 Thermal Energy Storage (TES) (Adiabatic System)

This component is only used in adiabatic CAES systems. During the charging phase, the heat transfer fluid absorbs heat from the compressed air between the compression stages. The subsequently hot heat transfer fluid flows through a thermal storage, which in turn absorbs the heat from the heat transfer fluid. During the discharging operation, air flows from the cavern and across the thermal energy storage, where it absorbs the heat, and its temperature increases to meet the turbine inlet temperature, and then expands through the turbine to produce electricity in the generator. The basic idea of the TES is to store the heat and minimize the temperature losses during charging and discharging so as to achieve high process efficiency levels. Using thermal energy storage should lessen the need to use combustion chambers, lowering hence the heat rate and improving the efficiency of the system. In addition, reducing the use of fuel in the operation of CAES enhances it appeal as a clean energy storage option. The thermal energy storage could be sensible heat storage (eg. concrete), latent heat storage or chemical storage. 5.2 Literature on thermal storage systems

2.6.4.1 Types of thermal energy systems

Thermal energy storage can be categorized into three types: sensible heat storage, latent heat storage and thermo-chemical energy storage. For sensible heat, no phase change will be involved while it is applied in storage within a required temperature range (Kuravi et al, 2013)(Glatzmaier, 2011).The thermal energy stored in the sensible storage is given by equation (5-1):

$$Q = mc_p\Delta T \qquad (2\text{-}10)$$

Whereas the main basis of the latent heat storage is the usage of the heat absorbed and released during the phase change of a material. Among the thermal storage methods, latent heat storage has been regarded as the most promising, with the high energy density storage and hence lowering the required volume of thermal storage (Kenisarin,2010). As for thermo-chemical storage, the main advantage is the higher energy storage density compared to other types of energy storage materials, due to the reversible chemical reaction instead of the specific heat.

Sensible heat storage is very mature and a relatively less complicated technology, which makes it favourable for large-scale systems. On the downside, however, large or even oversized volumes or quantities of sensible heat materials have to be applied to satisfy the system needs which adds to the cost of the system (Wu et al, 2014). This is due to the relatively lower energy storage density compared to latent heat systems.

As such, proper choice of storage medium material is essential to the performance of thermal energy storage system as a whole. There are many other factors governing the performance of TES materials which include: density, specific heat capacity, thermal conductivity, coefficient of thermal expansion, stability, cost and availability (Kuravi et al, 2013). The following describes the processes associated with sensible, latent and chemical heat storage.

a) Sensible Heat Storage

- No change in phase occurs as storage is achieved by increasing the temperatures of a medium, which is mainly solid or liquid
- The rate of heat transfer mainly depends on specific heat capacity which governs the energy density and thermal diffusivity.
- The currently installed utility scale TES in solar thermal plants use sensible heat stores
- Materials for sensible heat stores include concrete, rock sand and metal, depending on the temperature range
- Concerning concrete , research shows that the high temperature concrete is suitable for use as a sensible heat storage material up to 500 ˚C (Laing et al,

2011); and its advantages are that it has been tested extensively and proved successful and stable under high temperatures. It is also low in cost, high in strength and reliable (Laing et al, 2006). Also, concrete has high specific heat, good mechanical properties (e.g. compressive strength) (Gil et al, 2010). The concrete has relatively low thermal conductivity, however thermal conductivity of concrete is significantly affected by the type and percentage of coarse aggregate, and moisture content. Therefore varying any of these could improve the thermal conductivity (Shin et al, 2012) .

- Very mature technology with ease of heat transfer and simplicity of the storage system

Table 2-3 looks at a comparison of thermal properties of some of the available sensible storage mediums (Herman et al, 2002)

Table 2-3 Thermal properties of sensible storage materials

Material	Thermal Conductivity (W/m.K)	Density (kg/m^3)	Specific heat capacity(kJ/kg.K)	Temperature range (°C)
Sand-Rock	1	1700	1.3	200-300
Concrete	1.5	2200	0.85	200-500
Cast iron	37	7200	0.0.56	200-400
Cast steel	40	7800	0.6	200-700

b) Latent heat storage

As for latent heat storage, the following describes some of its characteristics-

- Materials are used which change the phase at a certain temperature, hence the enthalpy during the phase change is exploited (Kuravi et al, 2013).
- The most crucial parameters which guide the selection of the materials include the melting Point, heat of fusion, density, heat capacity, thermal conductivity, and cost of production (Bhatt et al, 2010)
- The solid-liquid latent storage is the process mainly used due to the better volumetric expansion compared to liquid-gas; and higher latent heat compared to solid-solid.
- For low thermal conductivity materials, materials with high thermal conductivity could be added to increase the overall thermal conductivity. The materials that could be added include graphite, metal fibres and ceramics (Pomianowski et al, 2013). Microencapsulation of PCMs can also increase heat transfer rate and hence improve the performance of latent heat storage materials (Jegadheeswaran et al, 2009).

Table 2-4 shows properties of some of the organic substances used as PCMs (Zalba et al, 2003)

Table 2-4 Properties of latent heat materials

Material	**Melting Temperature(˚C)**	**Latent heat of Fusion(J/g)**	**Thermal conductivity(W/mK)**	**Density (kg/m^3)**
$NaNO_3$	307	172	0.5	2260
KNO_3	333	226	0.5	2100
KOH	380	149.7	0.5	2120

c) Thermochemical storage

Finally, for thermochemical storage, the following provides some insight into its usage-

- The process depends on heat for reversible chemical reactions. The amount of heat stored depends on the heat of reaction (Glatzmaier,2011).
- Its advantage is that it could reduce thermal losses when compared to sensible heat stores.
- It enables high storage densities at a temperature level up to 1000°C (Schaube et al, 2011)
- Yet, some of the limitations include lower stability and high cost

Figure 2-15 (Kuravi et al, 2013) shows the level of maturity of the technology compared to the energy density involved. The sensible storage mediums have been extensively tested in various projects and proved very successful. This is why they have high maturity level, while they possess lower energy density compared to the other storage mediums, which have not been tested as much as the sensible stores.

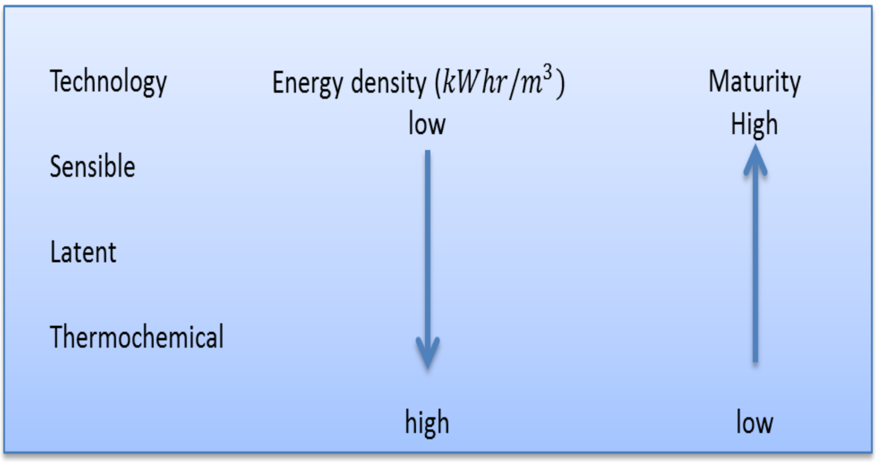

Figure 2-15 Comparison of different energy storage systems

Passive storage uses a solid material, as its storage medium and the heat transfer fluid passes through the thermal energy storage during charging and discharging only. The storage mediums could be inexpensive solids like concrete, sand or rocks for sensible storage, or they could be PCM materials for latent storage. There are thus different types for passive storage systems which are mainly:

1) Systems with embedded or enhanced heat transfer
2) Packed bed systems

    1) Systems with embedded or enhanced heat transfer

        - This entails integrating tubes within a solid storage to improve heat transfer.
        - As for the high thermal conductivity material, the compatibility with the storage material and the heat transfer fluid is essential.
        - In the case of concrete for example, during charging the heat transfer fluid passes through the pipes embedded in the concrete to heat it. While during discharging the heat transfer fluid, now the colder fluid, flows through the pipes in the concrete in the reverse direction to be heated by the concrete

    2) Packed bed systems

        - In this case, heat transfer fluid flows between the storage material for heat transfer where there is direct contact between the heat transfer fluid and the storage medium.
        - Also, most packed bed systems are based on one tank system, hence reducing the cost of the system.
        - Many studies were carried out on different storage materials used as beds such as sand, concrete and iron pellets; as well as with different heat transfer fluid flowing through them, whether they are liquid or gas

2.6.5 Intercooling

In order to improve the output of the system, either the turbine output should be increased or the input to the compressor reduced. Because work is directly proportional to temperature difference, as given by $h(t) = nC_p \delta tT$, without intercooling at each stage, the system would have an increased inlet temperature, increasing in turn the work done by compression. Intercooling, therefore, decreases the required compression work. Also, the spared heat from the intercoolers can instead be delivered to the TES to be used later in the expansion stage—which is the basic strategy of adiabatic CAES. However, intercooling too needs some power, as well as some water requirements. The same goes for reheating inside the turbine expander. Adding heaters between the stages of the turbine expander increases the work output of the turbine, while keeping unchanged the work output from the compressors, hence increasing the total work output of the system.

Intercooling techniques can be divided into inlet cooling and injection cooling techniques. Inlet cooling has a number of different types including evaporative methods, refrigerated systems, combinations of both, and thermal energy storage systems. Injection systems, on the other hand, comprise injection of water, steam or compressed air (Boyce 2012).

Evaporative cooling is a considerably low-cost method (costs around GBP30/KW) and can be easily installed. Water is sprayed on media blocks, and the air flowing through these blocks evaporates the water and consumes some latent heat, hence cooling down the compressors airflow. This method is very effective in low-humidity areas. Refrigerated systems are much more effective comparatively, but are much more expensive. Combinations of both systems can be optimal, depending on the requirements of the system, its location and the climate conditions (Boyce 2012).

2.7 Literature review conclusions and outlook

This chapter surveyed the literature covering energy storage systems with a special focus on compressed air energy storage (CAES). First off, the chapter discussed the applications that energy storage systems, of different scales, can bring to both isolated networks and the grid. Then, the different types of energy storage were discussed; starting with smaller scale storage systems, like batteries, and on to larger scale systems, like pumped hydro and CAES. After that, the compressed air energy storage system was discussed in more detail, touching on its history, its types, and its detailed components. Afterwards, the applications of CAES to the grid were discussed; and finally the research and studies recently carried out on CAES were discoursed.

Chapter 3 Mathematical Modelling of CAES systems

3.1 Introduction

This chapter discusses the MATLAB modelling of the CAES. The MATLAB modelling is used to simulate the design sizing and the operation of the compressed air energy storage (CAES).The MATLAB modelling process is discussed in detail, starting from the assumption required for modelling followed by the input parameters to the sizing process and finally the operation methodology of the CAES modelling. The mathematical formulation for the different components forming the CAES system is discussed in details.

3.2 Methodology of the MATLAB modelling

The sizing and operation models of the CAES are developed and implemented using an advanced high-level technical computing language and against the interactive environment of MATLAB R2012. Mathematical formulations presented in this chapter are used to develop of a transient model to predict the CAES system's thermal and electrical performance with various input and output parameters. First, an analytical model was developed to specify the wind speeds at the location and the load variation of the case under study. Using these inputs, the number of hours of surplus power and system deficiency is estimated, and then the time for charging and discharging of the CAES is deduced. In addition, the available surplus power and the deficiency in power supply are calculated. This information is used to size the components of the energy supply system, including the compressors rating (flow rates handled, maximum pressure ratios and the number of parallel and series chains used to supply the required power), turbines rating, cavern volume size, thermal energy storage volume (in case of addition of thermal energy storage) and size of the heat exchangers. After the sizing stage is completed, the operation stage starts using a transient simulation. For each time step, the governing equations are solved in MATLAB and the values of the varying parameters of the system are calculated. These parameters include temperature variation of the charging and discharging modes, pressure of air in the cavern, mass flow rates of air in both modes, temperature of heat transfer fluid, temperature of the thermal energy storage, and power output of the CAES and the efficiency of the system. Figure 3-1 presents the flowchart of the MATLAB program.

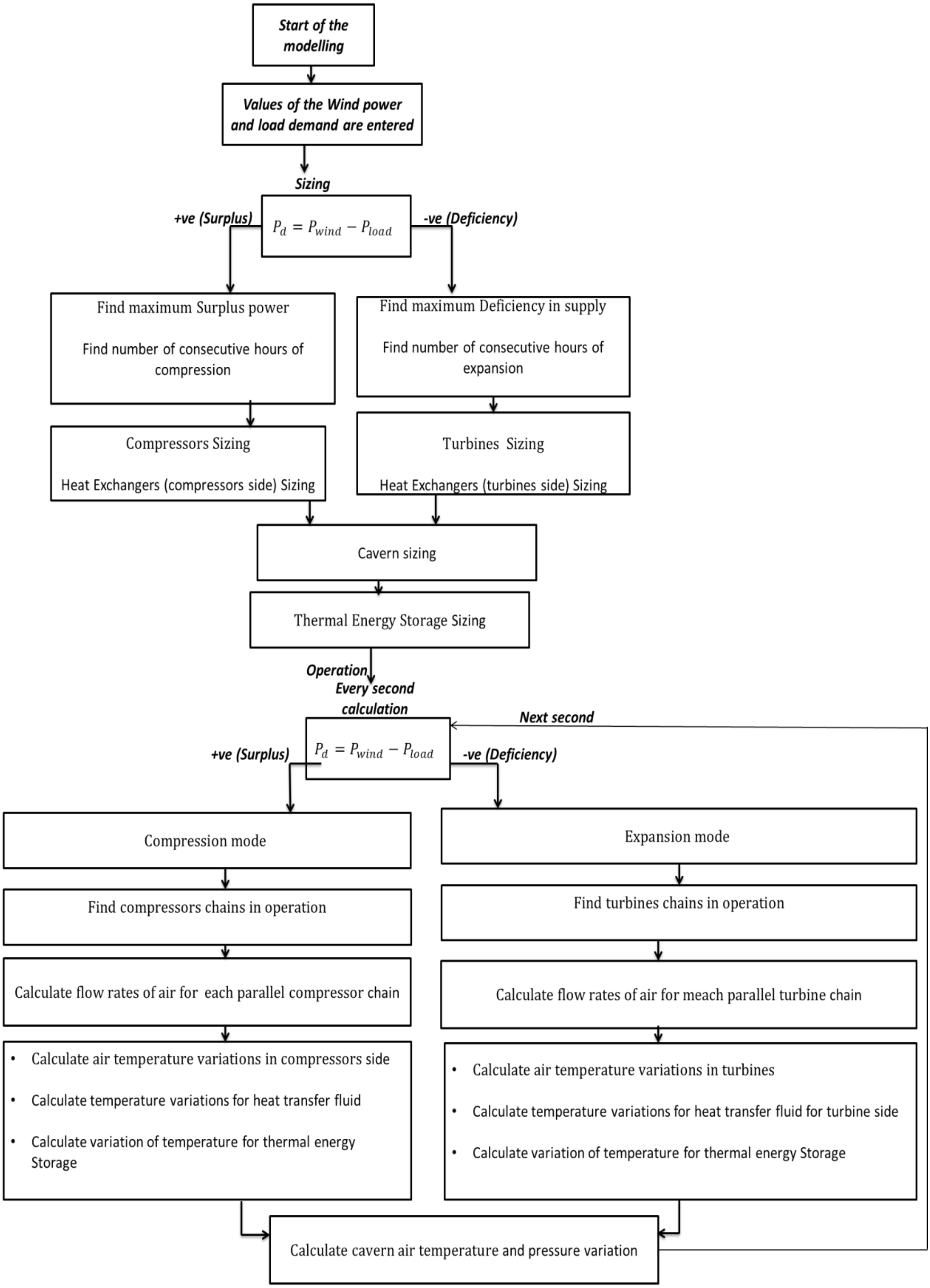

Figure 3-1 Flowchart of the simulation model

There are 3 different designs developed in the MATLAB model:

1. Diabatic System
2. Diabatic System with recuperator
3. Adiabatic system (with recuperator and thermal energy storage)

Figure 3-2, Figure 3-3 and Figure 3-4 show the 3 different designs. The system sizing and the operational model of the system methodology explained in the next section are for the full case of an adiabatic system with recuperators and thermal energy storage.

3.2.1 Inputs to the model

Before the simulation of the CAES can start, some assumptions are made and are incorporated into the model in order to be able to size and then simulate operation of the system. These assumptions include:

a) Wind speed data at the case study location
b) Electrical load of the case study
c) Type of the system (Diabatic, diabatic with recuperator, Adiabatic with Recuperator and TES exhibited in Figure 3-2, Figure 3-3 and Figure 3-4)
d) Maximum operating pressure and temperature in the cavern
e) Minimum operating pressure in the cavern (based on turbine inlet pressure)
f) Technical information of both the compressors and the turbines
g) Properties of the thermal storage (thermal conductivity, specific heat capacity)
h) Properties of the heat transfer fluid including operating temperature range
i) Effectiveness of the heat exchangers

3.2.2 System Sizing (common for 3 designs)

Having incorporated the assumptions into the model, the system is now able to size the different components of the CAES system, which include the compressors, the air storage cavern, the turbines and the thermal energy storage.

a) Available Power to CAES

The power output (P_{wind}) from each wind turbine can be estimated using equation (3-1) (Maton, et al, 2012) :

$$P_{wind} = \frac{1}{2}\rho A C_p U^3 \tag{3-1}$$

where,

ρ is the density of air,

A is the area swept by the rotors

C_p is the power coefficient of the turbines

U is the wind speed

The difference between the supply and the demand is calculated by equation (2)

$$Surplus = P_{wind} - P_{load} \tag{3-2}$$

The number of consecutive hours of both compression and expansion is calculated so as to be used in sizing the volume of the cavern. Also, the peak compression and expansion powers are recorded for use in sizing the compressors and the expanders in the system.

b) Size and arrangement of the compressors

The compressors are sized using multiple parallel chains with compressors arranged in series to cater for high incoming powers in a more realistic setup. In order to cater for the entire range, the power ratio of each parallel chain is split such that the power halves each time. For example, the ratio is set at 2:1 for a set of 2 parallel chains, 4:2:1 for 3 parallel chains, 8:4:2:1 for 4 parallel chains, etc. This means that for the 2 parallel chains that the compressors could cater for 1/3 times the maximum power input. For 3 parallel chains, the figure is 1/7 times of the maximum output, and for the 4 parallel chains, it is down to 1/15 times of the maximum output. Similarly, in the MATLAB simulation presented in Chapter 5, the 4 parallel chains configuration is used, allowing for the lowest compressor power, catering 1/15 of the maximum power input to the compressors. From a performance viewpoint, the higher the number of chains, the better the performance, because different compressors will be catering for higher ranges of power, and hence be working close to their rated values, resulting in higher efficiency. However, from an economic point of view, a higher number of parallel chains means an increase in the number of compressors, and therefore a higher cost. The number of chains is determined by the desired lowest output. This method also ensures that the mass flow rate entering each parallel chain is limited. A number of turbines are used in parallel at different stages of expansion in order to supply high power outputs in the same manner as that of the compressors. Figure 3-4 shows the arrangement of the simulated system where multiple parallel chains are used for both the compressor and turbine side for an adiabatic system.

c) Sizing of the Underground Air Storage (cavern)

The sizing of the cavern in the MATLAB simulation is implemented such to enable use of most of the surplus power available to the CAES system. This suggests that the volume of the cavern is sized sufficiently large so as to prevent the air pressure or temperature in the cavern from reaching the maximum operating limits. Sizing optimization also entails limiting any oversizing of the cavern in order to reduce the cost of the system. The sizing of the cavern is set by the following equation:

$$Vcav = \frac{\max\left((m_t \times CHE),(m_c \times CHC)\right) \times R \times T_{max}}{P_{max} - P_{min}} \tag{3-3}$$

Where,

$Vcav$ is the volume of the cavern

m_t *and* m_c are the mass flow rate from the compressors to the cavern and the mass flow rate from the cavern to the turbines respectively

CHE and CHC are the number of consecutive hours of expansion and compression respectively

R is the universal gas constant

T_{max} is the maximum operating temperature of air in the cavern

P_{max} and P_{min} are the maximum and minimum limits of the pressure of air in the cavern, determined by the geology of the location and specification of the turbines.

d) Sizing of the turbines

The sizing of the turbines is implemented in a similar manner to that of compressors. The turbines are arranged in multiple parallel chains to cater for high powers in a more realistic setup, with 2 turbines in series for different pressure ranges. Again, the higher the number of chains, the better the performance, because different turbines will be available to produce power for the higher ranges, and hence be working close to their rated values, achieving a higher efficiency for the system. The number of chains is determined by the lowest desired output.

e) Design of the thermal energy storage (for adiabatic CAES system)

The proposed design for the thermal energy storage medium entails using sensible heat storage in the form of a concrete block. Embedded copper pipes are installed in the concrete storage. The number of embedded pipes is determined by the size of the thermal energy storage so as to provide uniform temperature distribution. Concrete is chosen on basis of its availability and low relative cost. The thermal energy storage is sized such that it is capable of taking in most of the heat from the compression stage and reusing it for the air discharged from the cavern before entering the turbine. The thermal energy storage capacity (C_{cap}) is calculated as:

$$C_{cap}(Joules) = m_f \times Cp_f \times (TX12 - Tf_{min}) \times Compression\ time \tag{3-4}$$

Where,

m_f is the flow rate of the heat transfer fluid (kg/sec)

Cp_f is the specific heat capacity of the heat transfer fluid (J/KgK)

$TX12$ is the temperature of the heat transfer fluid entering the thermal storage (shown in Figure 3-4)

Tf_{min} is the minimum temperature of the heat transfer fluid (set at 300K)

$Compression\ time$ is the maximum consecutive compression time (s)

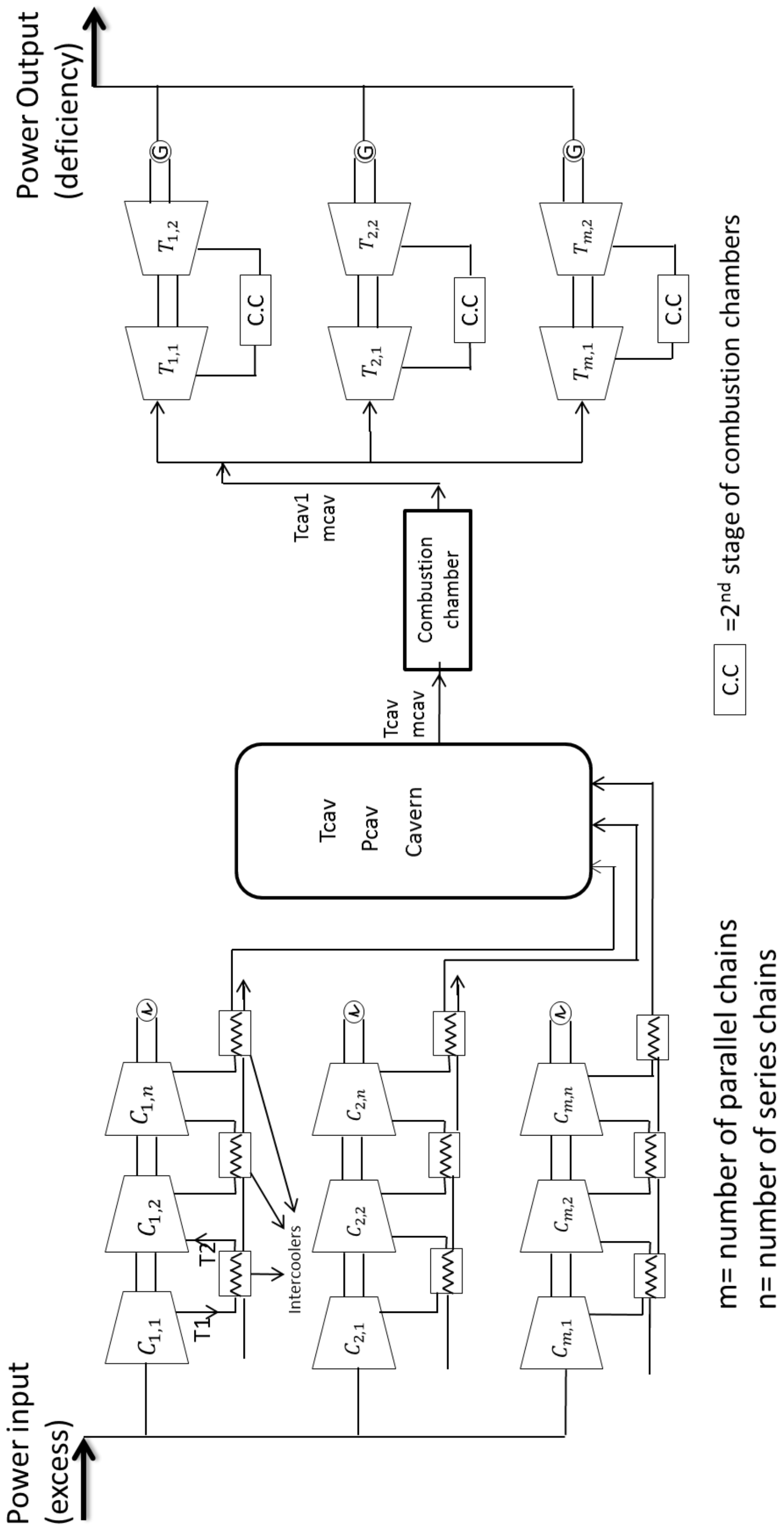

Figure 3-2 Full diabatic system design

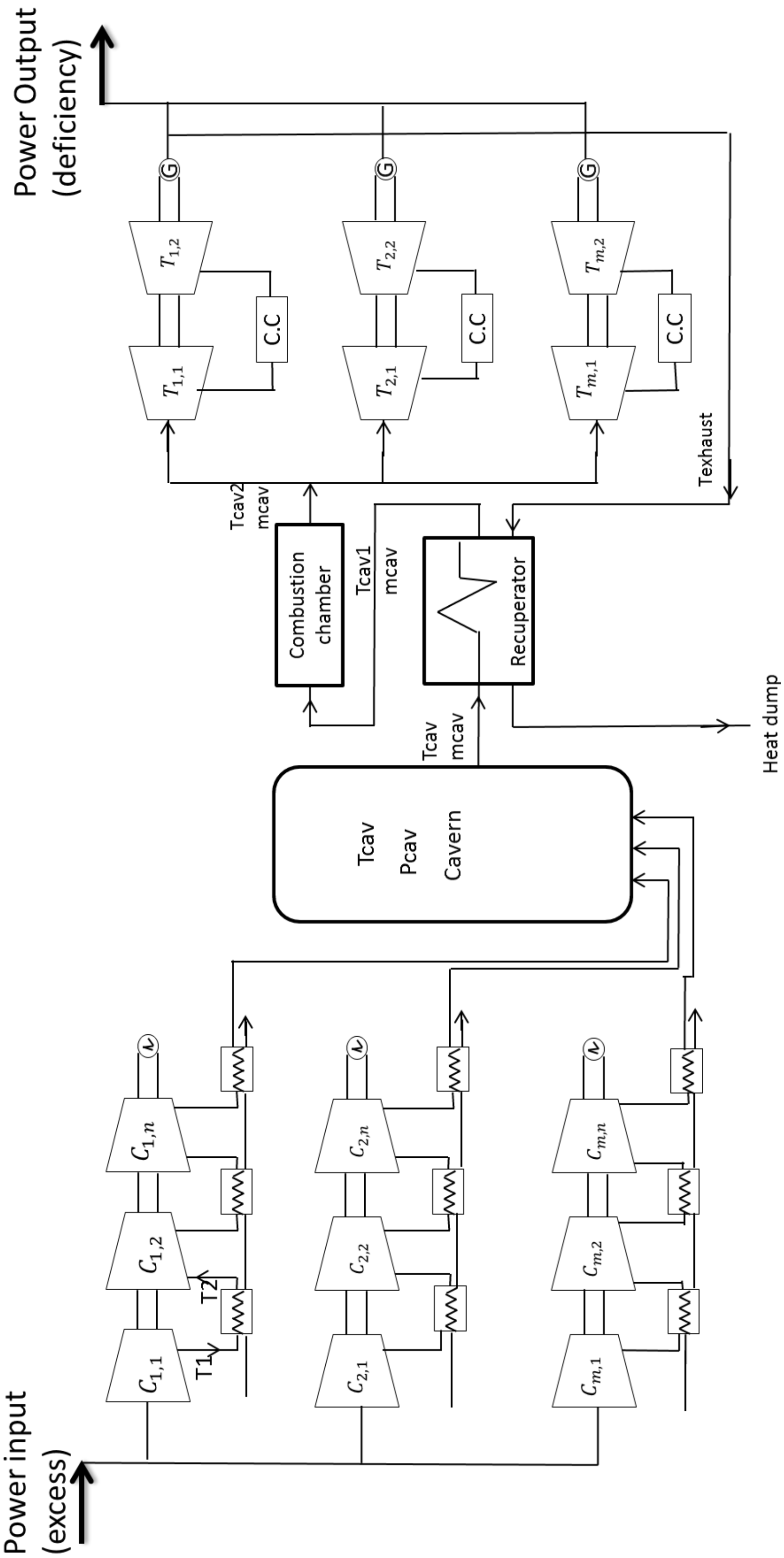

Figure 3-3 Full system design with added recuperator

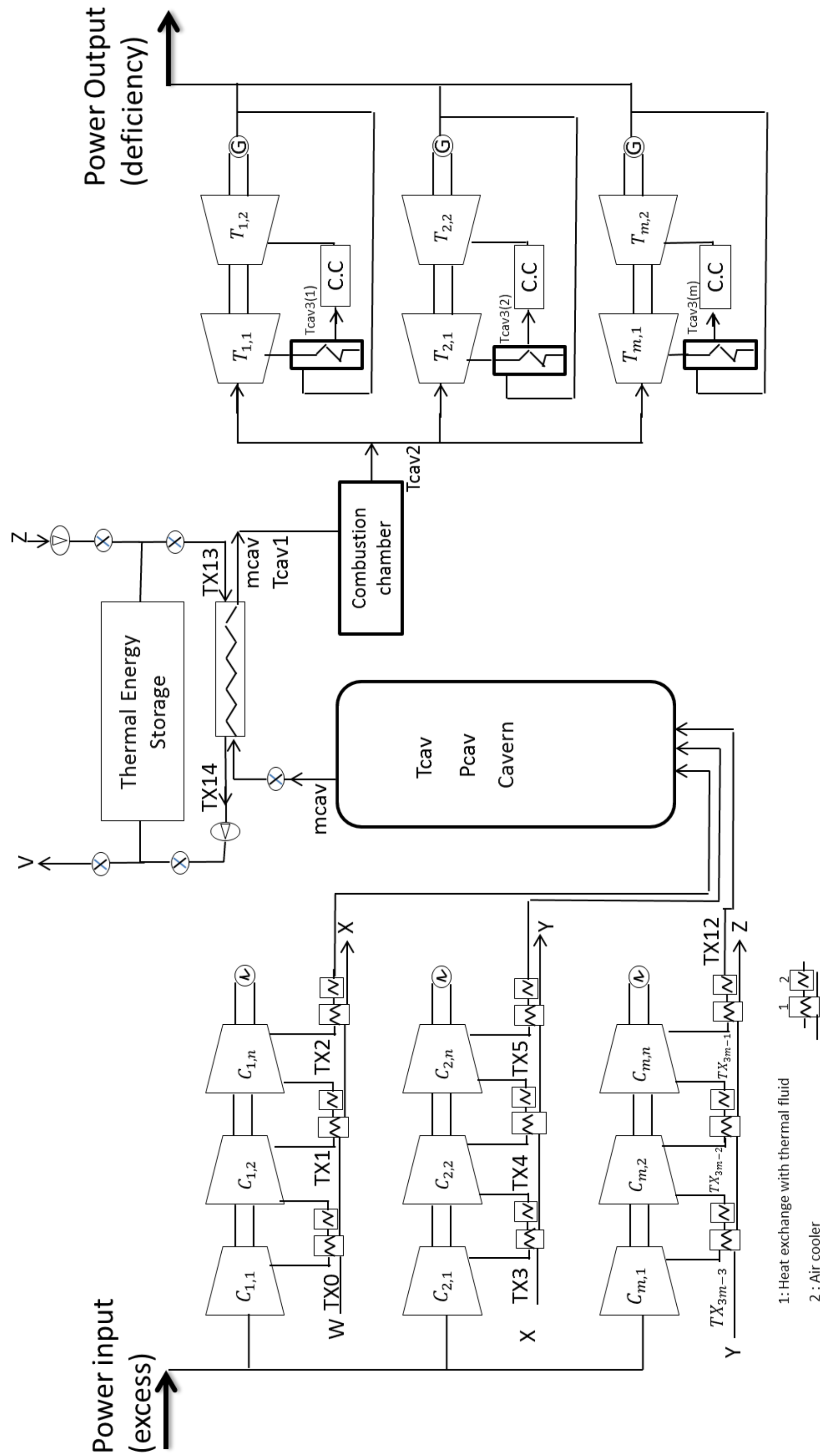

Figure 3-4 Full system design with added recuperator and thermal energy storage

3.2.3 Operation of CAES (common operation for all designs)

Once the size of the different components of the system is determined, the model will be able to simulate the transient operation of the CAES system. The results of the simulation include the temperature and pressure of air in the cavern, the temperature of the thermal energy storage, the compressor powers for each chain, the turbines power for each chain, the combustion power required and the heat rate of the system.

a) Available Power to CAES

The surplus/deficiency of power from wind to CAES follows the wind power output and electrical load governed by equations (3-1) and (3-2)

b) Compressors operation

When there is excess wind power supply, the surplus power is used to operate the compressors. The equations governing each compression stage are given by (Hartmann et al, 2012):

$$\left(\frac{P_2}{P_1}\right)^{\left(\frac{\gamma-1}{\eta_C\times\gamma}\right)} = \frac{T_2}{T_1} \qquad (3\text{-}5)$$

$where\ \eta_c$ is the polytropic efficiency of the compressors

$\gamma = 1.4$ is the specific heat ratio

$P_1 and\ T_1$ are the pressure and temperature of air at the compression inlet, respectively

$P_2 and\ T_2$ are the pressure and temperature of air at the compression outlet, respectively

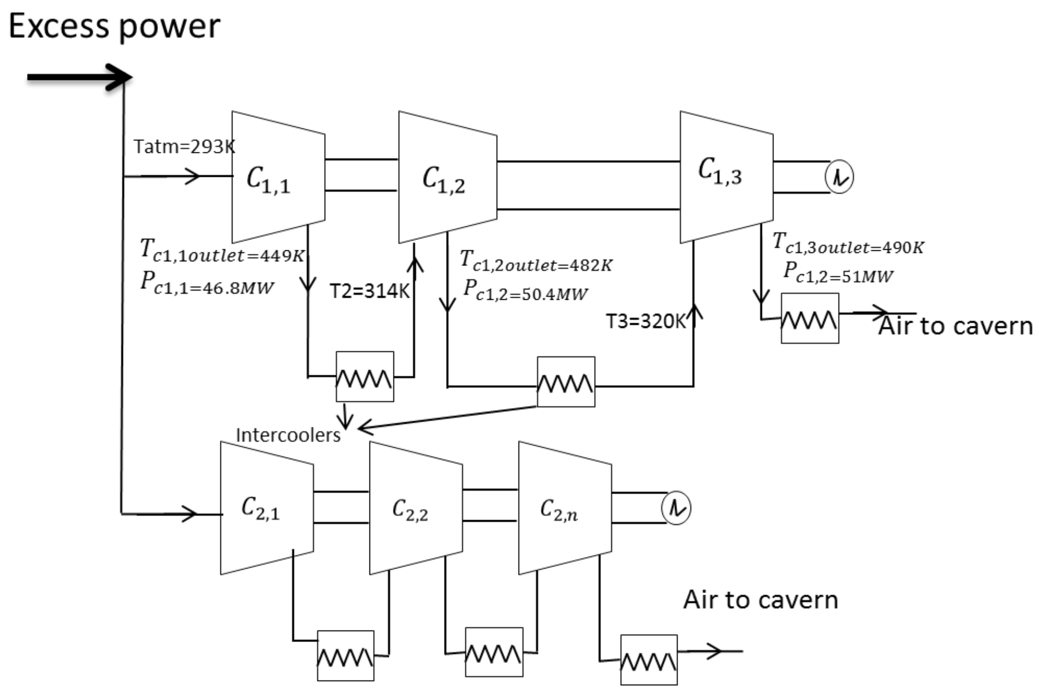

Figure 3-5 Schematic of compression stage of a diabatic CAES system at a compression time instant

c) Heat exchangers on Compression side

In the heat exchanger, air flows from the compressors to the underground air storage while the heat transfer fluid flows from the thermal energy storage, absorbing the heat from the air, and back into the thermal energy storage. For a single stage of heat exchangers on the compressor sides, equations (3-6) and (3-7) provide the respective air and heat transfer fluid streams outlet temperatures:

$$T_2 = T_1 - \varepsilon \times (T_1 - T_{x0}) \tag{3-6}$$

$$T_{x1} = T_{x0} + \frac{\varepsilon \times \dot{m}_c \times C_{p_{air}} \times (T_1 - T_{x0})}{\dot{m}_f \times C_{p_{fluid}}} \tag{3-7}$$

$where\ T_1 and\ T_{x0}$ are the inlet temperatures of the air stream and the heat transfer fluid stream, respectively.

T_2 and T_{x1} are the outlet temperatures of the air stream and the heat transfer fluid stream, respectively

ε is the effectiveness of heat exchangers

In the cases of adiabatic system and the design with added recuperators, the compressed air is intercooled after each compression stage and the heat extracted from compression is dumped, whereas in the case of the design with added thermal energy storage, the compressed air is intercooled in each compression stage after the heat exchange with the heat transfer fluid by a smaller amount than the diabatic designs. For the adiabatic system, the heat exchange operates in a close loop where the TX0 is the return temperature of the heat transfer fluid after exchanging the heat with the thermal storage. Therefore, in the case of the added thermal energy storage, the TX0 is expected to increase with time (as the temperature of the thermal storage rises), resulting in less heat exchange with air after compression. The idea of having the heat transfer fluid connected in series for the different chains of compression is for the heat transfer fluid to extract as much heat as possible, bearing in mind that during the charging period, rarely does all the parallel chains operate at the same time due to the varying nature of the surplus power. It is worth to note that at the time when the thermal energy storage temperature increase up to a point when there is minimal heat transfer with the compressed air after each compression stage, the intercoolers placed after each heat exchanger as well as the aftercooler extract the heat from the compressed air, albeit less than that designed for diabatic cases. The intercoolers and aftercooler for the diabatic cases are designed to extract the heat from the compressed air to limit the injected temperature of air flow to the cavern to a specific maximum. On the other hand, the intercooler and aftercooler for the adiabatic case are modelled to decrease the temperature of compressed air by a certain level for 2 modes: the first of which is low-level cooling if the TES temperature and hence the temperature of the heat transfer fluid is relatively low so more heat can be extracted from the compressed air, and the second of which is high-level cooling if the TES temperature and so the heat transfer fluid temperature become closer to that of the compressed air which limits the heat transfer between them to prevent the temperature of the injected flow of air to the cavern from getting too high.

d) Operation of the underground air storage cavern

In the underground air storage (cavern), when air under high pressure is added, the internal energy of the cavern increases, and vice versa when the air is taken out during the expansion stage. The rate of change of the internal energy in the cavern is given by (Raju et at, 2012):

$$d\left(\frac{M_{total}(t)U}{dt}\right) = \dot{m}_c h_c - \dot{m}_T h_T - hA_{cav}(T_{cav} - T_{wall}) \tag{3-8}$$

Terms 1 and 2 on the right hand side are the change in enthalpy due to the flow in and out of the cavern. $M_{total}(t)$ is the instantaneous total mass of air in the cavern at a given time, which varies with the incoming air flow from the compressors or outgoing air flow to the turbines. The last term is the heat losses to the surroundings, where h is the heat transfer coefficient between the cavern wall and the air.

Solving equation (3-8) (Raju et al, 2012) will result in:

$$\rho(t)C_p\frac{dT}{dt} + \frac{\dot{m}_c C_p(T_{cav} - T_{inlet})}{V_{cav}} - \frac{dP}{dt} + h_c(T_{cav} - T_{wall}) = 0 \tag{3-9}$$

Equation (3-9) describes the overall heat transfer balance based on the volume of the cavern. h_{eff} is the effective heat transfer coefficient and is expressed as a function of air flow rates in and out of the cavern. $\frac{dP}{dt}$ represents the variation of pressure with time during system operation. $\rho(t)$ is the compressed air density as a function of time; the density of air changes with time as the mass of air in the cavern changes.

M_{total} changes according to the rate of air inflow into the cavern. T_{cav} also changes during the course of system operation, and denotes the overall cavern temperature. Therefore, the pressure variation during the operation of the cavern is calculated using the instantaneous values of the temperature and mass of air in the cavern. Assuming a molecular weight of air of 0.029 kg:

$$P_{cav} = \left(\frac{M_{total} \times R \times T_{cav}}{0.029 \times V_{cav}}\right) \quad (3\text{-}10)$$

M_{total} is the mass of the air in the cavern

R is the universal gas constant

T_{cav} is the air temperature in the cavern

V_{cav} is the volume of the cavern(constant)

e) Operation of the turbines (power generation part)

The output from the system is due to the work done in the turbines, which is dependent on the enthalpy flow of the air stream through the turbine and is given by:

$$\dot{H} = \dot{m}_T c_{p\_air} T_{air} \quad (3\text{-}11)$$

Where c_{p_air} is assumed to be constant at 1005 $J/kg.K.$

The polytropic equation for the expansion process is given by:

$$\left(\frac{P_3}{P_4}\right)^{\left(\frac{\eta_p(\gamma-1)}{\gamma}\right)} = \frac{T_3}{T_4} \quad (3\text{-}12)$$

$where\ \eta_p = 0.85$ (Wu, 2012) is assumed to be constant, and represents the polytropic efficiency of the turbine

$\gamma = 1.4$, and represents the specific heat ratios

$P_3\ and\ T_3$ are the pressure and temperature before the expansion in the turbine, respectively

$P_4\ and\ T_4$ are the pressure and temperature after the expansion in the turbine, respectively

Besides power generation, the operation of the system differs across the 3 different designs of the MATLAB model. For each model, the operation process is explained next.

i. Diabatic design (Expander part)

In this design setup, the temperature of air coming out of the cavern equals the temperature of air going into the 1st stage of the combustion chamber. The energy requirement for 1st stage of combustion in this case is:

$$Q_{Combustion1} = \frac{\dot{m}_{cav} \times C_{p_{air}} \times (T_{turbine\_1a\_Inlet} - T_{cav})}{\eta_{c.c.}} \quad (3\text{-}13)$$

The energy requirement for the 2nd stage of combustion is the summation of the combustion powers used by the parallel chains of expansion:

$$Q_{Combustion2} = \sum_1^n \frac{\dot{m}_{cav\_n} \times C_{p_{air}} \times (T_{turbine\_b\_Inlet} - T_{turbine\_a\_outlet})}{\eta_{c.c.}} \quad (3\text{-}14)$$

$where\ \eta_{c.c.}$ is the combustion chambers' efficiency

$T_{turbine\_1a\_inlet}$ is the high pressure expander (1st stage) inlet temperature

$T_{turbine\_1b\_outlet}$ is the high pressure expander outlet temperature

$T_{turbine\_2a\_inlet}$ is the low pressure expander (2nd stage) inlet temperature

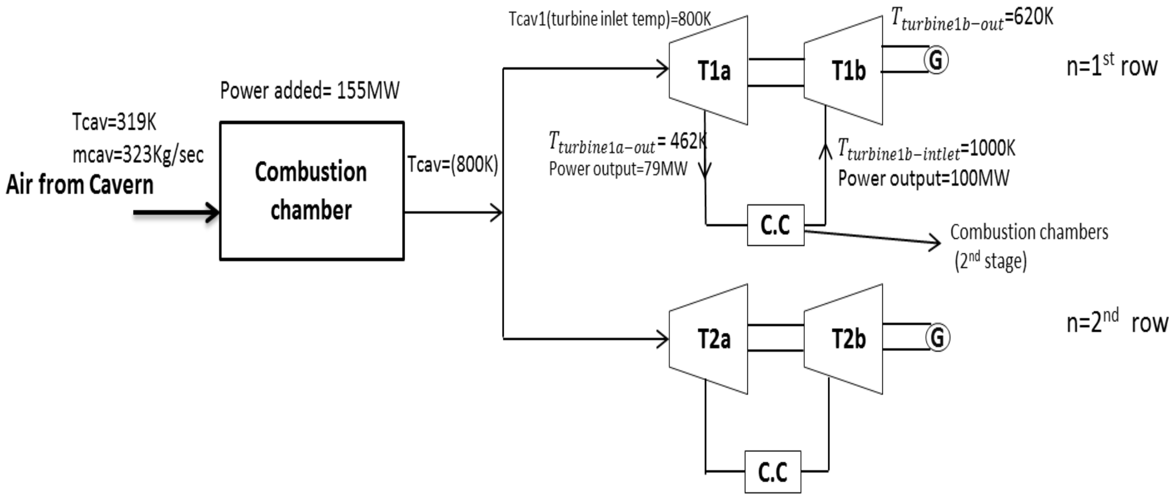

Figure 3-6 Schematic of expansion stage of a diabatic CAES system at an expansion time instant

ii. Diabatic design with added recuperator (expander)

In this setup, a recuperator is placed before the 1st stage of combustion. The air coming out of the cavern is heated in the recuperator before the combustion chamber in order to reduce the heat energy requirement of the combustion chamber before the turbine inlet. The temperature of air after the recuperation unit is given by the following equation:

$$T_{cav1} = T_{cav} - \varepsilon(recup) \times (T_{cav} - T_{exhaust}) \quad (3\text{-}15)$$

The energy requirement for the 1st stage of combustion in this case is:

$$Q_{Combustion1} = \frac{\dot{m}_{cav} \times C_{p_{air}} \times (T_{turbine\_1\_Inlet} - T_{cav1})}{\eta_{c.c.}} \tag{3-16}$$

The energy requirement for the 2nd stage of combustion is the summation of the combustion powers used by all of the parallel chains of expansion:

$$Q_{Combustion2} = \sum_1^n \frac{\dot{m}_{cav\_n} \times C_{p_{air}} \times (T_{turbine\ n,2\_Inlet} - T_{turbine\ n,1\_outlet})}{\eta_{c.c.}} \tag{3-17}$$

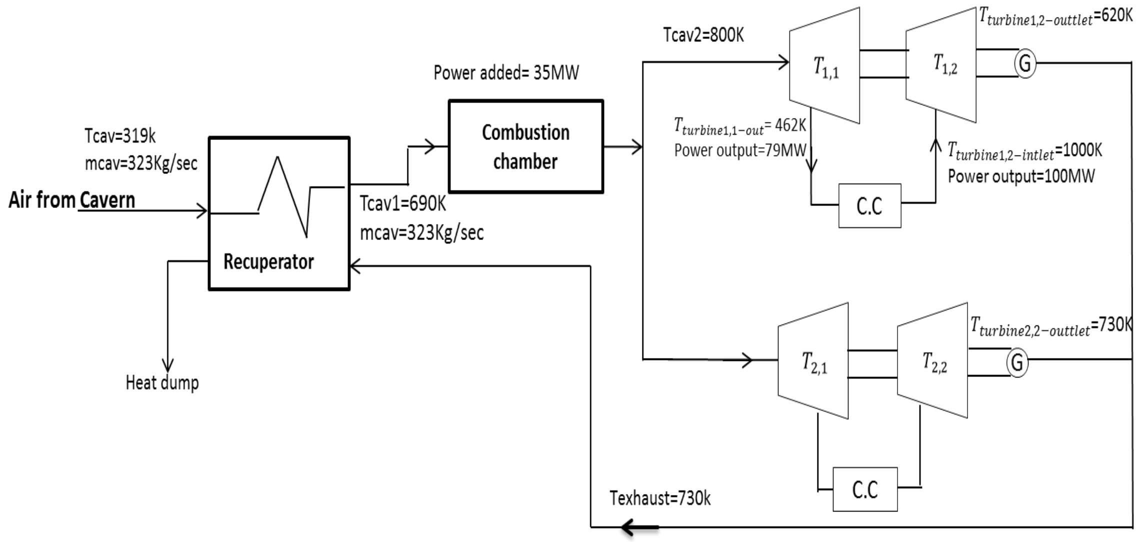

Figure 3-7 Schematic of expansion stage of a diabatic CAES system with an added recuperator at an expansion time instant

iii. Design with added thermal storage and recuperators

In this design, a thermal storage system is placed before the 1st stage of combustion and recuperators are placed in each of the parallel chains before the 2nd stage of combustion as shown in Figure 3-8.

The temperature of the air stream discharged from the cavern after the heat exchange with the heat transfer fluid is calculated using the following equation:

$$T_{cav1} = T_{cav} - \varepsilon \times (T_{cav} - T_{x13}) \tag{3-18}$$

$where\ T_{cav}\ and\ T_{x13}$ are the inlet temperatures of the air stream and the heat transfer fluid stream, respectively

The air from the cavern gains thermal energy from the thermal store, and then passes through the gas combustion chamber where its temperature is increased to the required inlet temperature of the turbines.

For this design, the equation for the energy requirement of the 1st stage of combustion chamber, $Q_{Combustion}$, is given by:

$$Q_{Combustion\_1} = \frac{\dot{m}_{cav} \times C_{p_{air}} \times (T_{turbine\_1\_inlet} - T_{cav1})}{\eta_{c.c.}} \tag{3-19}$$

After the first stage of expansion, heat is exchanged between the exhaust of the low-pressure turbine and the output of the high-pressure expander using the recuperator; after that, all air streams are heated back to the required inlet turbine temperatures, using gas burning combustion chambers. The heat exchange in the recuperator is calculated as follows:

$$T_{cav3(1)} = T_{turbine\_1\_outlet} - \varepsilon(recup) \times \left(T_{turbine\_1,2\_outlet} - T_{exhaust}\right) \tag{3-20}$$

$$Q_{Combustion2} = \sum_{1}^{n} \frac{\dot{m}_{cav\_n} \times C_{p_{air}} \times (T_{turbine\_2\_Inlet} - T_{cav3})}{\eta_{c.c.}} \tag{3-21}$$

where T_{cav3} is the temperature of air after the heat exchange with the exhaust temperature in the recuperator before the 2nd stage of combustion.

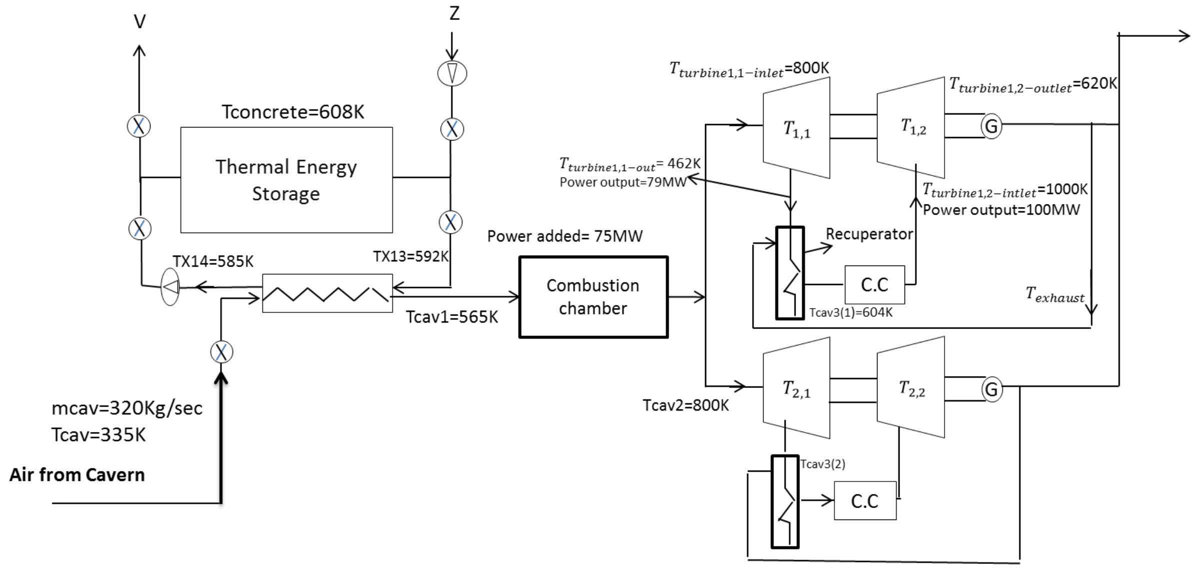

Figure 3-8 Schematic of expansion stage of an adiabatic CAES system at an expansion time instant

f) Operation of the thermal energy storage (For the design of adiabatic system only)

The thermal energy storage is divided into multiple equal sections in order to take into account the temperature gradient across the storage. The finite difference method is used to calculate the temperature profile for each section at each time step. The following equations are used for the calculation of the thermal resistance for each section for every time step of the simulation. The results of the numerical calculations of the operation of the thermal energy storage is compared in section 5.4.2.5 with the results obtained in the ANSYS CFD analysis (Chapter 4) using same size and configuration of thermal energy storage (including diameter of pipes, number of pipes and same gap distance between pipes) as well same inlet conditions and initial parameters. The conductive heat resistance through the thermal storage media (concrete for this case) for each section is given by:

$$R_{cond} = \frac{ln\left(\frac{r_o}{r_i}\right)}{k_c \times 2 \times pi \times L_p} \tag{3-22}$$

where,

r_i is the radius of the pipe

r_o is half the distance of the gap between the pipes

k_c is the thermal conductivity of the concrete

L_p is the pipe length

The Reynolds number is calculated for each time step. Since the fluid temperature changes continuously, and the fluid flow rate, density and viscosity also change with the temperature, the Re number also changes with temperature.

$$Re = \frac{D \times v_{fluid} \times \rho}{\mu} \tag{3-23}$$

where,

D is the pipe diameter

v_{fluid} is the fluid velocity

ρ is the fluid density

μ is the fluid viscosity

Using the Reynolds number, the fluid Nusselt number is calculated based on whether the fluid flow is turbulent or laminar.

For the turbulent flow and for $3000 < Re < 5 \times 10^5$

$$x = (0.79 ln\ Re - 1.64)^{-2} \tag{3-24}$$

$$Nu = \frac{\frac{x}{8}(Re-1000)Pr}{1+12.7\left(\frac{f}{8}\right)^{0.5}(Pr^{\frac{2}{3}}-1)} \tag{3-25}$$

While for Re<3000

$$x = (0.79 ln\ Re - 1.64)^{-2} \tag{3-26}$$

$$Nu = \frac{\frac{x}{8}(Re-1000)Pr}{1+12.7\left(\frac{f}{8}\right)^{0.5}\left(Pr^{\frac{2}{3}}-1\right)}\left(1+\left(\frac{D^{\frac{2}{3}}}{L}\right)\right) \tag{3-27}$$

Where L is the length of the pipes and Pr is the Prandtl number

The convective heat transfer is calculated using equation (25):

$$h(t) = \frac{Nusselt(t) \times K(t)}{Pipe\ diameter} \tag{3-28}$$

The total resistance is then calculated using:

$$R_{total} = \frac{1}{h(t) \times A_p} + \frac{ln\left(\frac{r_o}{r_i}\right)}{k_c \times 2 \times pi \times L_p} \tag{3-29}$$

$where\ h$ is the convective heat transfer of the heat transfer fluid.

Using equations 3-22 to 3-29, the heat transfer between the fluid and the thermal storage media is calculated for every section at each time step.

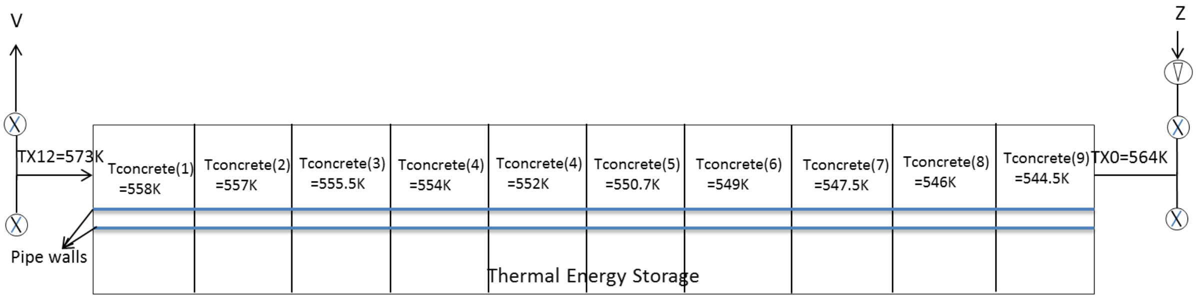

Figure 3-9 Concrete temperatures for different sections using inlet temperatures of heat transfer fluid of 573K after 4 hours of heating

g) Overall efficiency and heat rate of the system

Normally two methods of efficiency calculations are used in calculating the performance of CAES systems (Ter-Gazarian, 1994, Succar et al, 2008). The first method is the overall efficiency where the output energy of the system is the turbine energy(E_{turb}), while the input energy is the compressors energy(E_{comp}) in addition to the combustion energy (E_{comb}) required during the expansion stage. The overall efficiency (η_o) is then given by:

$$\eta_o = \frac{E_{turb}}{Ecomp+Ecomb} \tag{3-30}$$

However, it had to be mentioned that it would not always give an accurate result as there can be some energy left in the CAES system which is not tapped yet (air under high pressure in the cavern). Therefore a more accurate efficiency representation should be considered by calculating the combustion energy required for each kWh of output and also including the efficiency of the compressors (η_{comp}) and the turbines (η_{turb}).

$$\eta = \frac{E_{output}}{E_{comb}} \times \eta_{comp}\eta_{turb} \tag{3-31}$$

The other way to estimate the efficiency of the CASE system is based on the calculation of the heat rate of the system, which is the measure of how much combustion heat is added to the system to enable it to produce one kWh of energy. The heat rate is then calculated as:

$$Heat\ rate = \frac{Combustion\ Energy}{Output\ Energy} \times 3600 \tag{3-32}$$

3.2.4 Constraints to the operation of the CAES system

A number of constraints govern the operation of the system:

a) The compression mode stops if the air in the cavern reaches the maximum temperature or the maximum pressure

b) The expansion mode stops if the air in the cavern reaches the minimum pressure (minimum pressure inlet for the turbine operation)

c) For the adiabatic system, if the temperature of the heat transfer fluid reaches the maximum operating temperature, the heat exchange between the heat transfer fluid and the air (in the compression part) stops. In this case, the heat extracted only by the intercoolers after each compression stage (higher-level cooling).

3.3 Conclusions

This chapter discussed the mathematical formulation used in the Matlab program for the different system designs including the diabatic system, diabatic system with a recuperator and the adiabatic system. The mathematical modelling was discussed for the different components of the system in both the sizing part of the system and the operational part of the system. The Matlab model was developed using the equations presented in this chapter and used for the modelling of the case study of the Egyptian grid which is discussed in Chapter 5

Chapter 4 Design sizing and performance of the thermal energy storage

4.1 Scope of the work

The performance of the thermal energy storage proposed for the adiabatic CAES system is investigated in this chapter. As mentioned in Chapter 2, the Adiabatic Compressed Air Energy Storage System uses thermal energy storage to store the excess heat during the charging cycle (Compression process); and releases this heat the air coming from the cavern before entering the turbine to improve the efficiency of the whole system. The thermal energy storage reduces the amount of energy supplied by the burning of gas in the combustion chambers, thus improving the performance of the CAES system

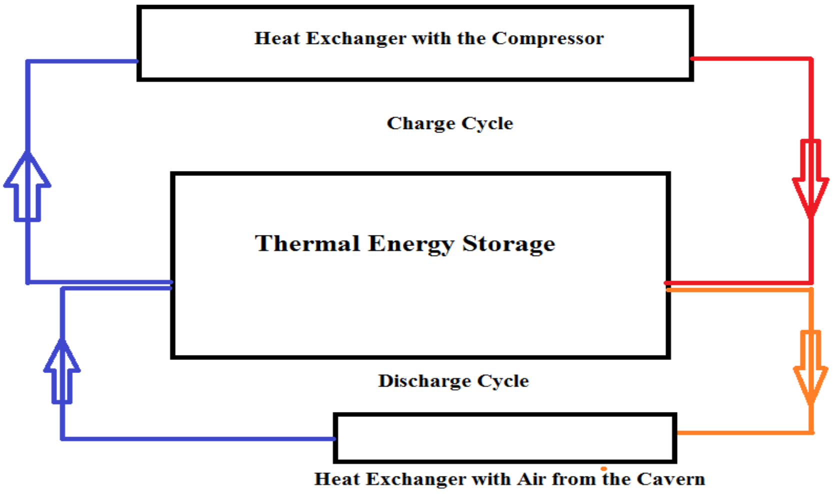

Figure 4-1 A Schematic diagram showing the working principle of TES

For the thermal energy storage to satisfy the needs of an adiabtic system; several requirements need to be met. Firstly, the thermal energy storage needs to extract the heat from the compression stage so that the temperature of air entering the underground air reservoir (cavern) is maintained under a certain range, which is usually defined by the geology of the case study's location and the turbine operating range. Secondly, the thermal energy storage should be able to give as much energy as possible during the discharge period.

Therefore, it should be able to attain high temperatures to be able to give out as much heat as possible to increase the air temperature before going to the turbine to limit the use of combustion chambers.

4.2 Aims and Objectives

The idea behind the CFD modelling is to implement a heat transfer simulation to optimize the design of the thermal energy storage,. The simulations are thus developed to optimize the design of the thermal energy storage configuration including the number of pipes, the distribution of pipes and the aspect ratio of the thermal energy storage. CFD simulations are also used to compare the results with that of the thermal energy storage part in the Matlab modelling which is discussed in Chapter 5.

Concrete is used as storage medium with embedded copper pipes. Concrete is used due to its availability and relatively low cost as well as it is a proven good performance medium in heat transfer applications. Several parameters are varied for the simulation of thermal energy storage to test their effect on the heat transfer of the system. The variable parameters include:

a. Pipe diameters
b. Thermal conductivity of the concrete block used
c. Flow rates of inlet heat transfer fluid
d. Different number of pipes
e. Aspect ratio of concrete

The cross section of the base case model of concrete is shown in Figure 4-2 (not to scale). There are 7 pipes evenly distributed in a concrete block. The gaps between each pipe are set to be the same value. The distance between the outer pipes and the model boundary is set to be a half gap, as in reality there will be other pipes transferring the heat symmetrically to the outer boundary.

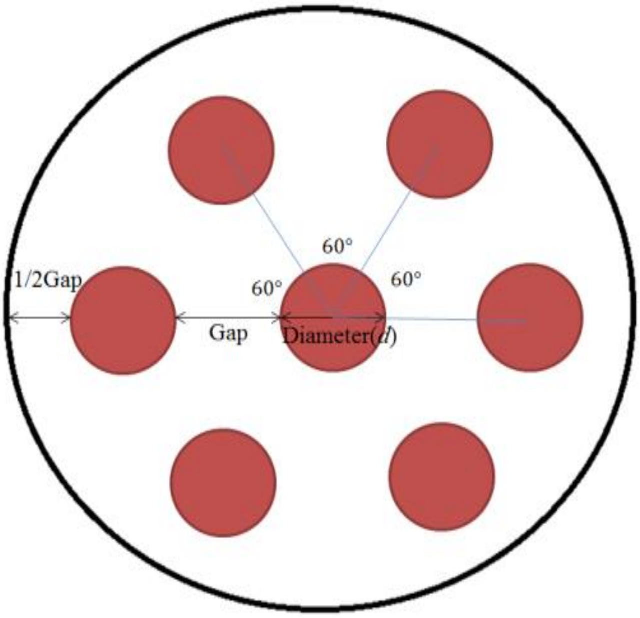

Figure 4-2 Concrete and pipes sizing

The concrete block shape implemented was a cylindrical to ensure equal heat distribution to the concrete body. The length of the design used was 700mm in length with surface diameter of 315 mm; and for initial analysis a pipe diameter of 50mm is used. The distribution of the pipes is shown in Figure 4-3.

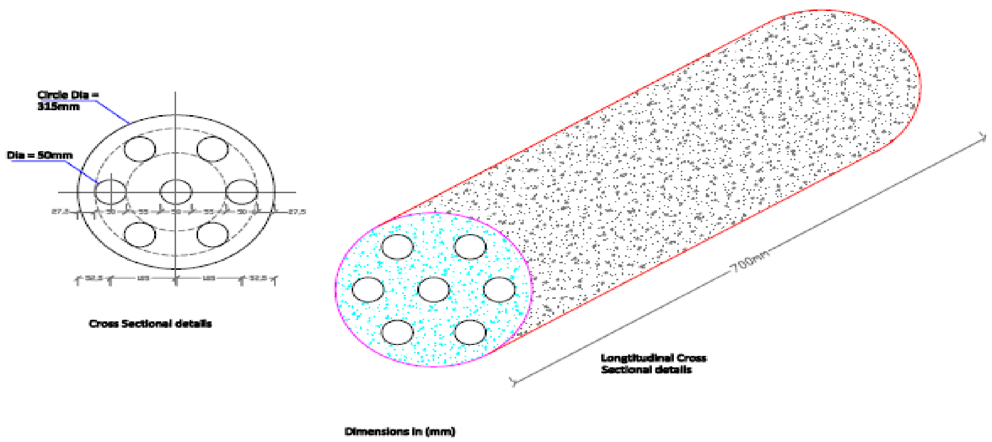

Figure 4-3 Model design

4.3 System description and working principle

There are certain steps to go through for simulation using CFD. The main steps are discussed as follows:

1. The main physical geometry
2. Meshing of the storage domain
3. Specifying the boundary conditions
4. Simulation of the model

4.3.1 Physical geometry drawing

The first step for the CFD simulation was to build the geometry of the model. For the base case, a concrete block of 315mm in diameter and a length of 700mmis used. This required 7 embedded copper pipes, 50mm in diameter each as shown in Figure 4-4

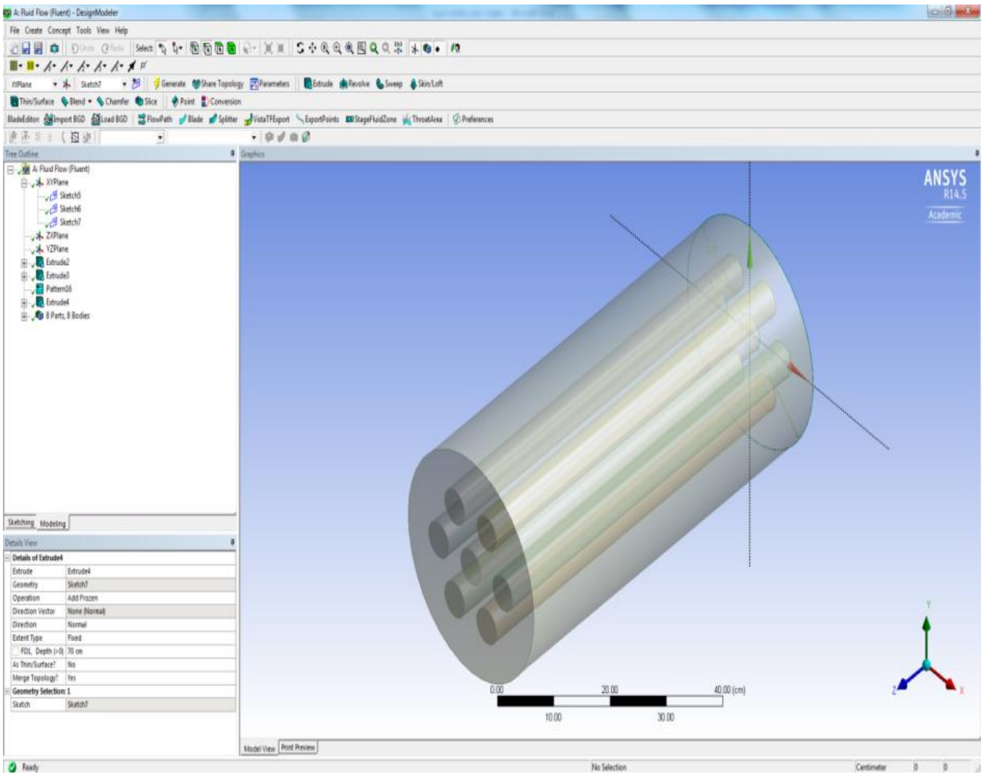

Figure 4-4 Geometry of the model

4.3.2 Meshing of the thermal energy storage

The meshing process required for the system includes the inlets, outlets, walls, and the body of the working fluid and the thermal energy storage

For example, Figure 4-5 shows the body of the thermal energy storage with the embedded pipes.

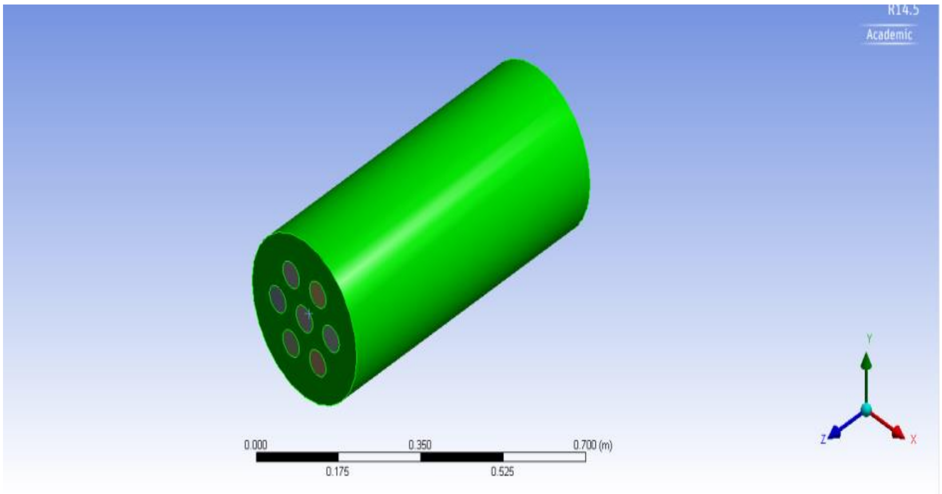

Figure 4-5 Body of the TES

The second step of this process is generating the mesh for the model. The meshing of the pipes, fluid and the concrete store are shown in Figure 4-6 and Figure 4-7 respectively.

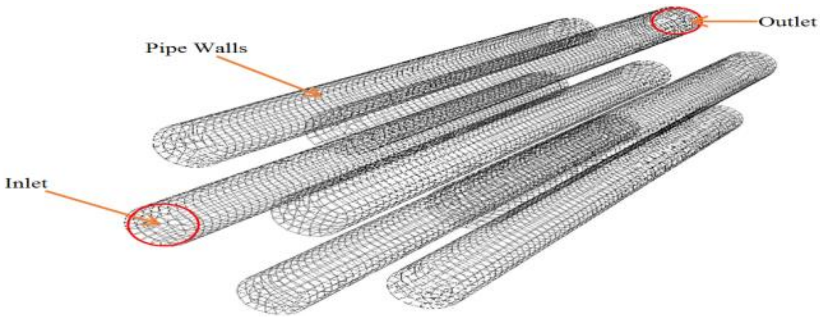

Figure 4-6 Meshing of the pipes

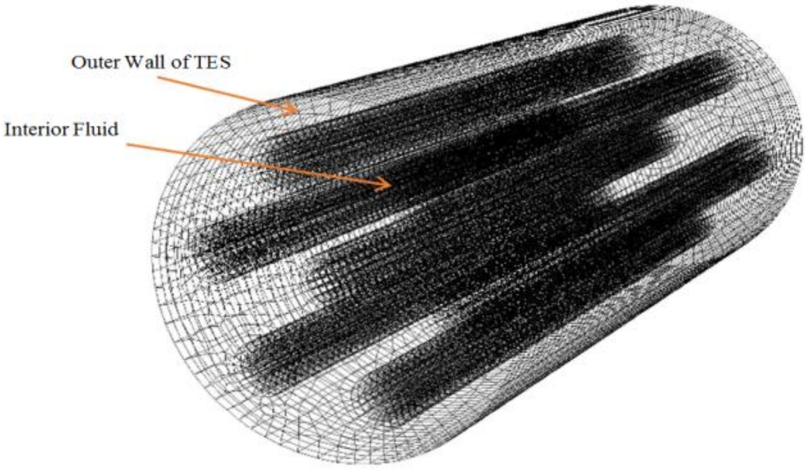

Figure 4-7 Meshing of the whole model

4.3.3 Model Setup

This stage includes defining the solver time, whether it is in a steady state or transient. It also includes:

a. Properties of the materials
b. Defining the Cell conditions (relating the mesh to the materials used)
c. Defining the boundary conditions
d. Adding monitors to the system
e. Solution initialization
f. Running the simulation

4.3.3.1 Properties of materials

The main materials used in the simulation include the following:

1. Thermal Energy storage (concrete)
2. Heat transfer fluid (mineral oil)
3. Pipes (copper pipes)

1. Thermal Energy Storage

For the sensible heat storage modelled in this study, concrete is used as the heat storage medium. The properties of the concrete used in the simulation were varied for the thermal conductivity. The specific heat capacity was set to850 $J/Kg.K$ and the density to $2200Kg/m^3$(Hermann et al, 2002).

2. Heat transfer fluid

White mineral oil is used as the heat transfer fluid for heat exchange with the TES. White mineral oil has relatively stable thermal properties under high temperature. It can handle temperatures higher than 300˚C, which makes it particularly suitable for this study. The properties for the white mineral oil used are displayed in Figure 4-8 (TT Boilers thermal Oil report).

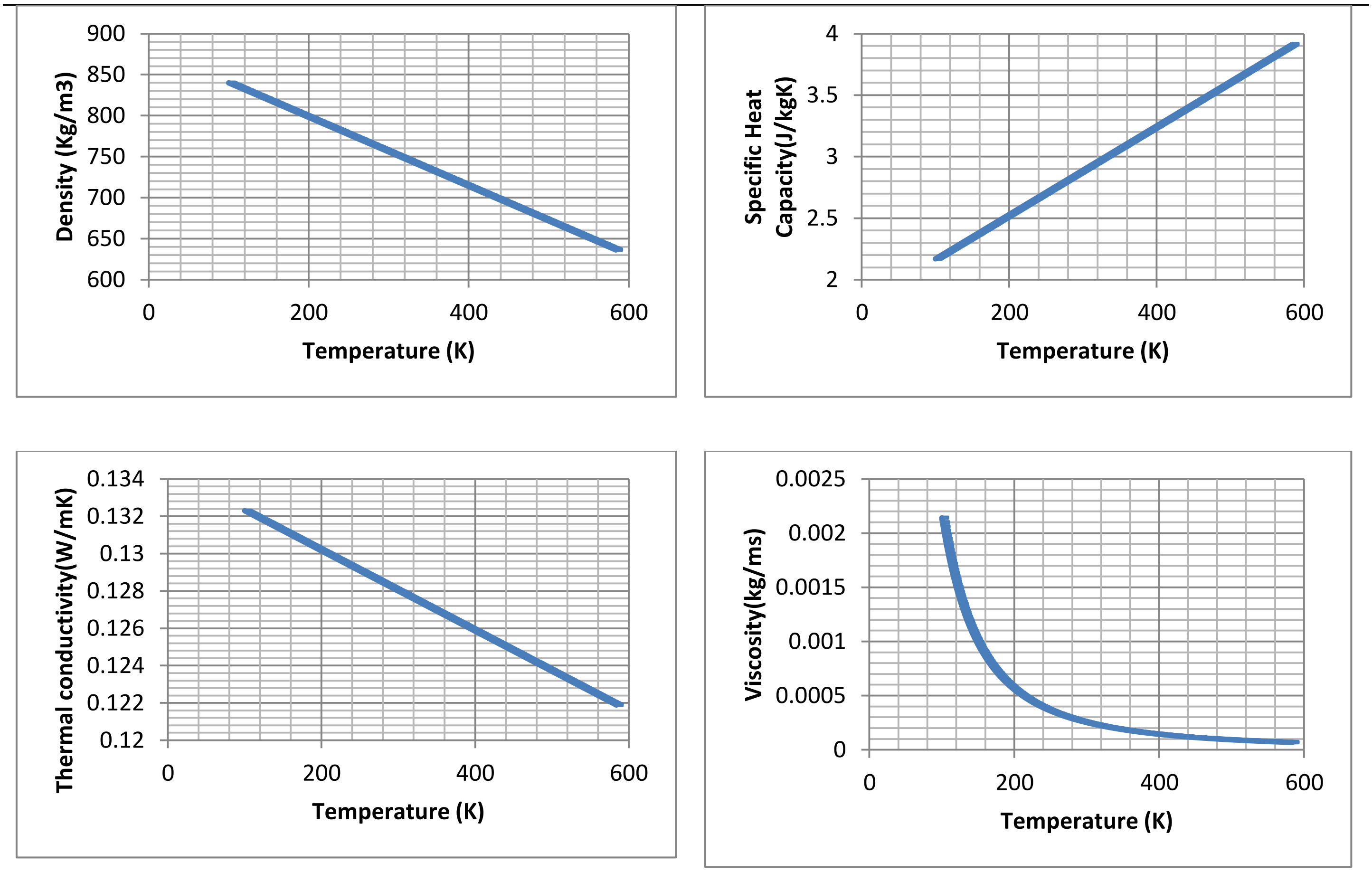

Figure 4-8 Properties of the white mineral oil

3. **Heat exchanger pipes**

Copper pipes are used in this system, mainly due to their good heat transfer characteristics with high thermal conductivity. The properties of copper are saved in the ANSYS CFD database and are directly used

4.3.3.2 Cell properties (Relating the mesh to the materials used)

This step basically links the defined materials in the mesh to that in the materials' setup. As a result, this includes linking the thermal energy storage to the properties of concrete used; as well as the heat transfer fluid to the properties of the white mineral properties that were used in the simulation.

4.3.3.3 Boundary conditions

In this stage, the heat transfer between the heat storage and the heat transfer fluid, as well as the heat transfer from the thermal energy storage to the surroundings are defined. The inlet flow properties are also setup during this step.

The boundary conditions used in the simulation are displayed in Table 4-1.

Table 4-1 Boundary conditions for ANSYS CFD

Parts	Type and Description
Inlet	Thermal: Inlet temperature set at 573.15K initially
Concrete	‘Stationary wall’, No slip
(Outer surface wall)	Thermal: No heat flux (Ensure no heat loss from TES)
Pipe	Thermal: Coupled
(Pipe walls)	Pipe thickness 1.2mm
Outlet	‘Pressure- outlet’

4.3.3.4 Temperature profile of the system

There are temperature sensors for the heat transfer fluid and concrete at three different positions in z-axis at 0.2m, 0.4m and 0.6m from the inlet. The temperature is monitored and recorded continuously for the duration of the simulation. The positions where the temperature of the heat transfer fluid and concrete are monitored are shown in Figure 4-9. In addition, the total surface heat flux through all the seven pipe walls was set to be monitored throughout the simulation.

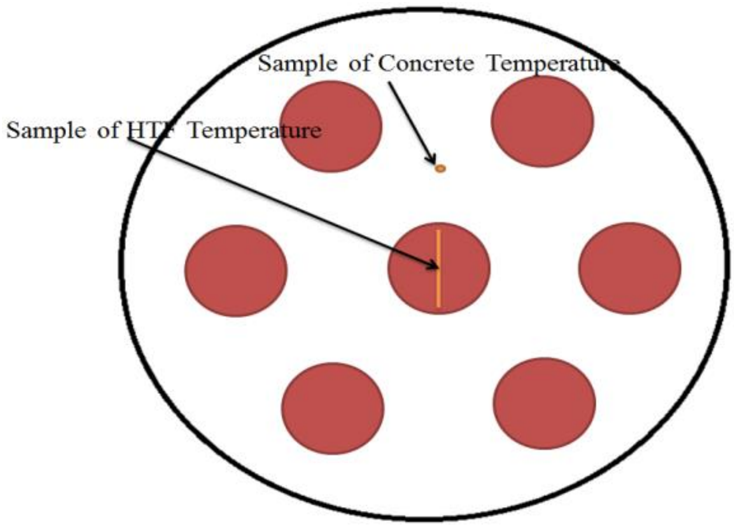

Figure 4-9 Positions where the heat transfer fluid and concrete temperature are monitored

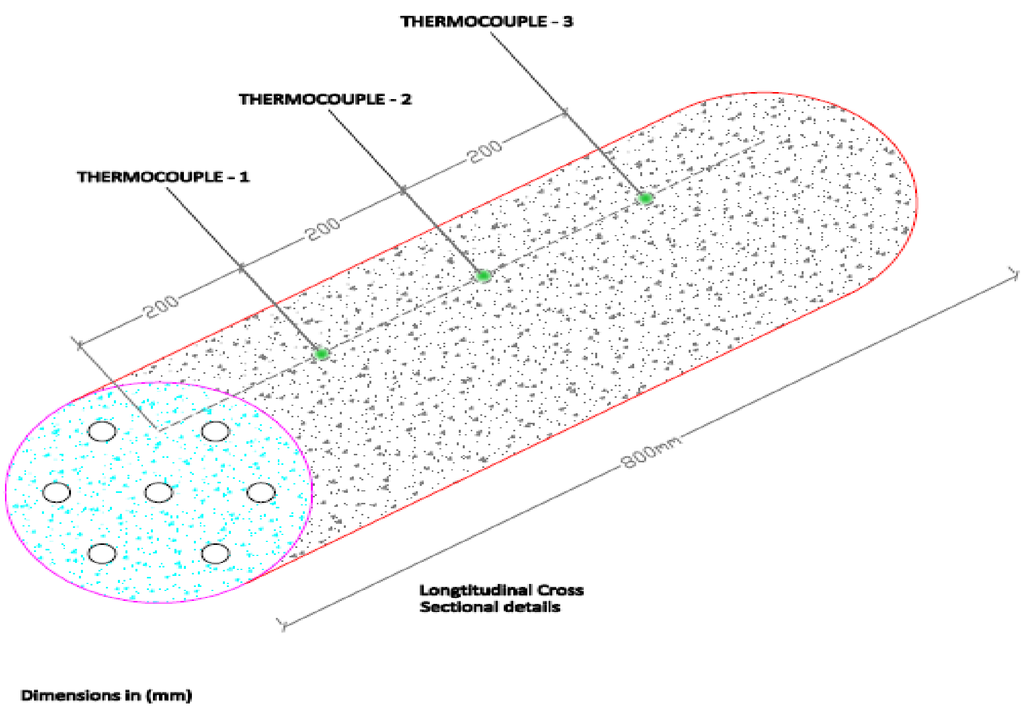

Figure 4-10 Positions of temeprature monitoring in concrete block

4.3.3.5 Simulation of the model

As for the final step, it is here where the maximum number of iterations per time step are set to ensure the conversion of the solution, as well as the total time steps for the simulation. The maximum number of iterations was chosen to be 10 Iterations/ time step which should be sufficient for convergence of solution.

4.4 Simulation Results

To determine which design of the TES would perform better, the criteria used for comparing and selecting the better design for the various parameters is:

a) Temperature difference of heat transfer fluid between the TES inlet and outlet

The temperature of working fluid is regarded as the first priority to be considered as the rate of all heat transfer in the whole cycle is determined by the temperature difference between the heat transfer fluid and the concrete volume media. It is also a significant enhancement for the heat collection from the compressor, as a lower temperature of the heat transfer fluid will lead to a larger amount of thermal energy absorbed from the compressed air.

b) Heat transfer from the heat transfer fluid to the concrete through the pipes

Heat energy from the heat transfer fluid to the concrete is a crucial criterion for a better design, which is equivalent to the amount of heat energy stored.

For the CFD simulation, analysis is done using different factors affecting the heat transfer process for thermal energy storage. The factors analysed are the pipe diameter, flow rates, thermal conductivities of the concrete, aspect ratio of concrete. The time frame was 10 hours for each simulation. This time was chosen as previous CAES installations had a compression time of nearly 10 hours, which is the time where charging mode is ‘on’ and hence the thermal energy storage is in operation.

4.4.1 Base Case (Monitoring at different positions of concrete)

In the base case, seven pipes were used as explained earlier with thermal conductivity of 2.2W/mK for concrete and an inlet flow rate of 0.1kg/sec and a concrete length of 0.8m with a diameter of 315mm. Each pipe diameter is 50mm. The concrete block has a diameter of 315mm; therefore the heat transfer fluid area constitutes 17.5% of the total area of the concrete block. The test was carried out for both charging and discharging periods.

Therefore for the first 3.3 hours- charging period- the following inputs were used

a. The heat transfer fluid inlet is 573K
b. concrete initial temperature is 300K

This means that heat will be transferred from the heat transfer fluid to the concrete due to the temperature gradient.

As such for the following 3.3 hours, discharging phase, the following inputs were added

a. Inlet to the fluid will be from the reverse side and is set to 350K
b. Concrete temperature is the same as the last time step from the charging cycle

Thus the fluid will be absorbing the heat from the concrete block in this case.

The simulation carried out monitored the concrete temperatures at different positions, the inlet and outlet of the heat transfer fluid, as well as the heat energy transferred between the concrete and the heat transfer fluid.

Monitoring temperature at different length of concrete

For this test the temperature of concrete is monitored at different positions to find out the temperature distribution in the concrete block for both the charging and discharging period.

Figure 4-11 shows the variation of temperature with time for the concrete thermal energy storage. Position 1, 2 and 3 are positioned at 0.2m, 0.4 and 0.6 m from the inlet respectively. In the first 3.3 hours- charging period- heat is transferred from the heat transfer fluid to the concrete causing the temperature to increase from the initial 300K to a range of 540K to

555K, depending on the position in the concrete. It is also seen that at the start of the operation, heat transfer is higher than later in the operation as the curves start to smooth out.

During the discharging cycle, the concrete temperature decreases as heat is transferred from the concrete to the heat transfer fluid. In this case, the heat transfer fluid inlet is set at 350K. As the operation continues, the concrete temperature gets closer to that of the inlet and the heat transfer starts to decrease.

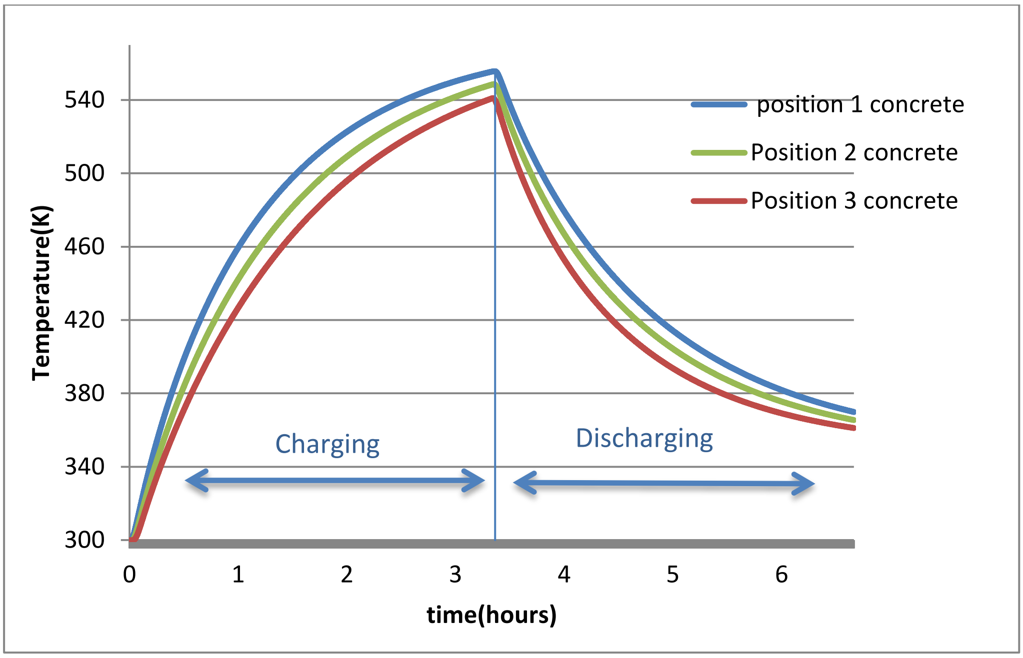

Figure 4-11 Temprature profile distribution along the concrete block

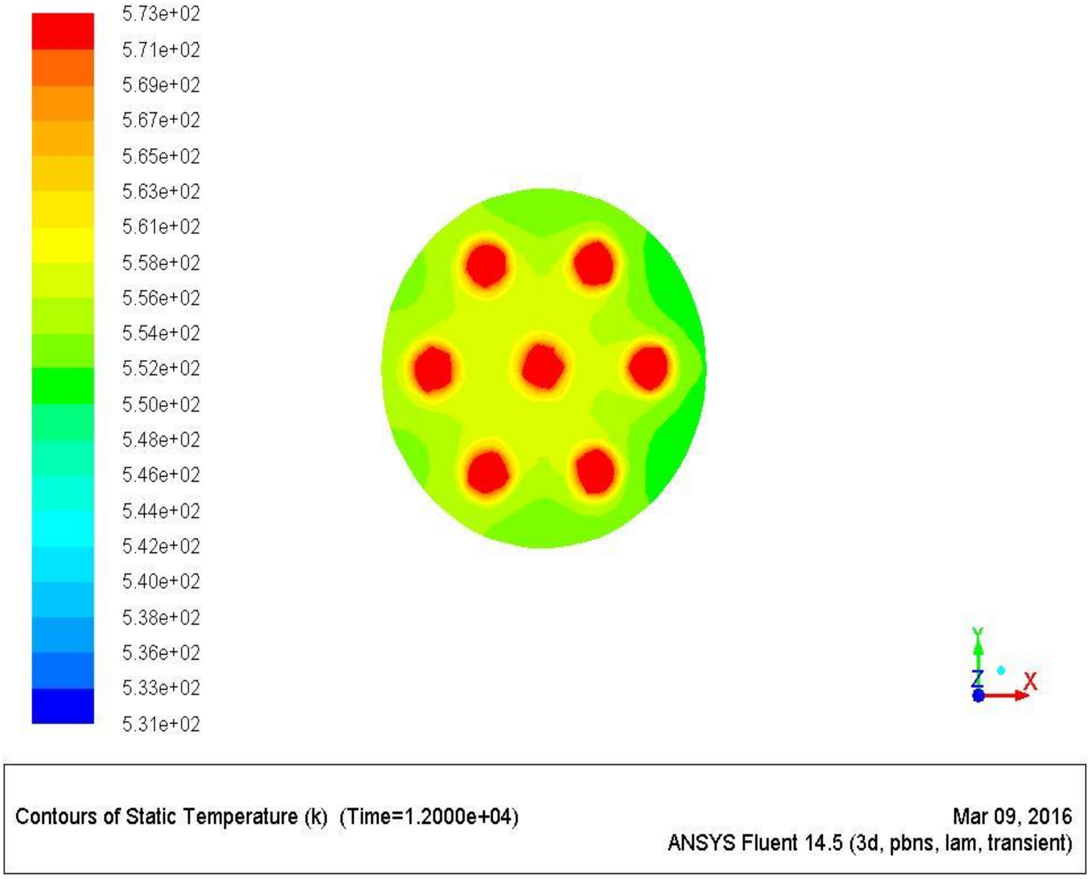

Figure 4-12 Front view of temperature contours after 3 hours of charging

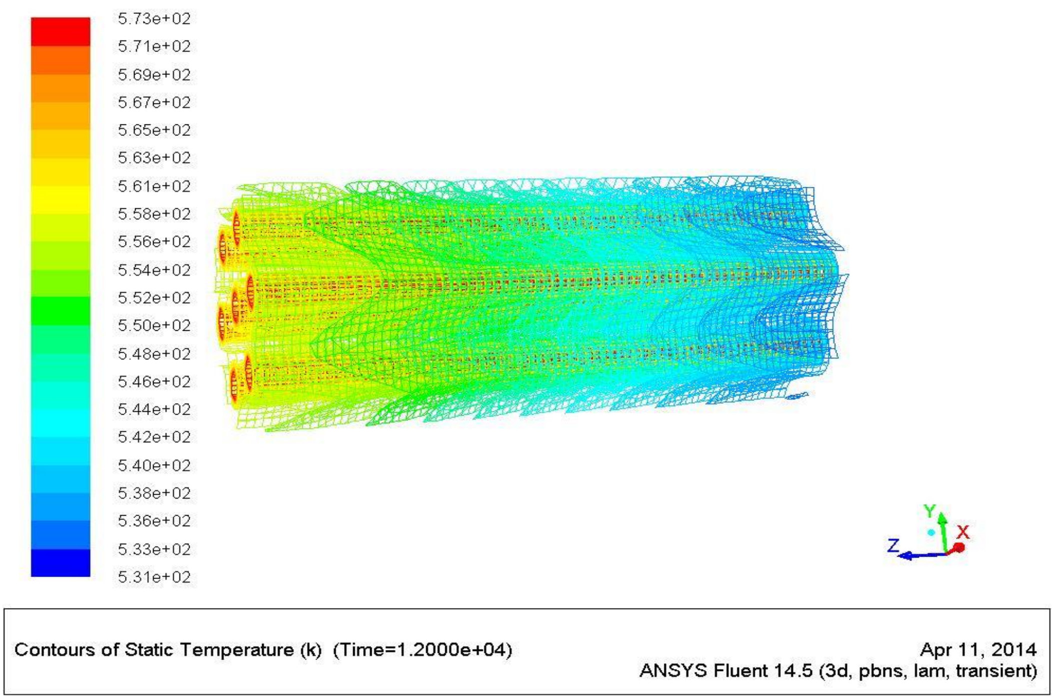

Figure 4-13 Side view of temperature contours after 3 hours of charging

Figure 4-14 shows the hourly concrete temperature for the different positions during the charging cycle. At the start of operation, the initial temperature is the same for all the positions of concrete. After 1 hour of operation, the concrete temperature is higher at position 1 followed by 2 then position 3. The same observation is recorded for the 3 hours of charging. This can be explained by the fact that since position 1 is closest to the inlet temperature, heat transfer is higher as the heat transfer fluid is at its highest temperature. When the heat transfer fluid reaches the concrete at position 2, some of the heat is already lost to the concrete, therefore the temperature of the heat transfer fluid at this position is lower than the inlet, leading to a lower temperature of concrete at position 2 compared to that of position 1. Same is true for position 3 compared to positions 1 and 2.

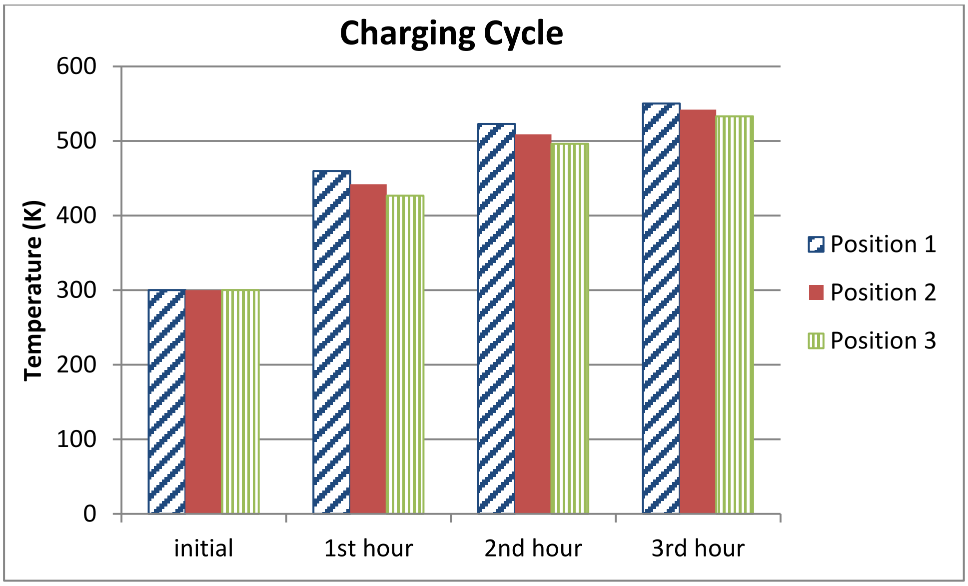

Figure 4-14 Hourly concrete block temperature

Figure 4-15 shows the hourly temperature gradient of concrete at different positions during the charging cycle. It is clear that in the first hour, the concrete temperature at position 1 is higher than that of 2, followed by position 3. However, for the following two hours, the temperature gradient is highest at position 3 followed by 2 then 1. The explanation for this is that during the first hour of charging, the heat transfer fluid temperature, as mentioned earlier, is highest at position 1, therefore highest heat transfer rate leads to the highest temperature gradient. During the next two hours of operation, the concrete temperature at position 1 is higher than that at position 2 then 3. Therefore, the temperature gradient between the concrete thermal energy storage and the heat transfer fluid is lower, leading to a lower heat transfer after the first hour of operation, making hourly concrete temperature difference lower at position 1 followed by 2 and 3. Taking the example of the temperature after two hours in the heating cycle, at the position 1 it is 523K, 509K at the second position and 496K at position 3. It can be seen that there is a large range of temperature along the length of concrete. As such the temperature gradient between the heat transfer fluid and the concrete is expected to be lower for concrete positions closer to the inlet and vice versa for those closer to the outlet.

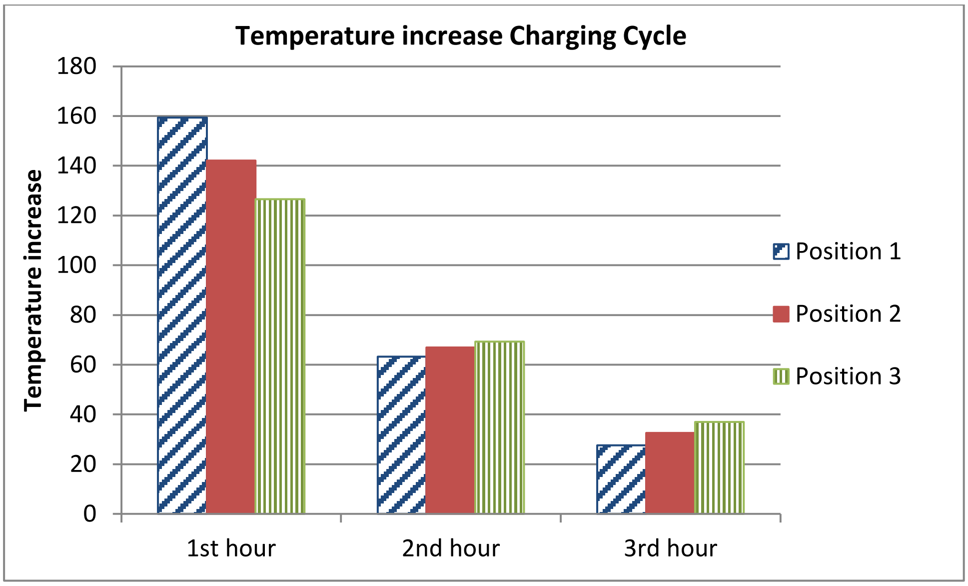

Figure 4-15 Hourly temperature increase of concrete

Figure 4-16 shows the hourly temperature of the concrete block at different positions for the discharging cycle. Similarly to the charging cycle, the temperature at position 1 is highest followed by that at position 2 and then 3.

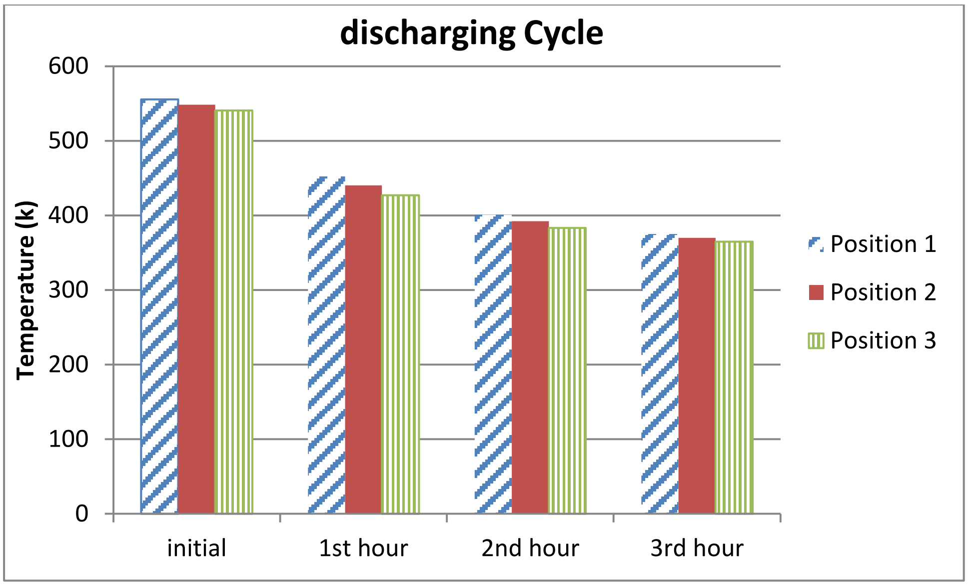

Figure 4-16 Hourly temperature of concrete for disharge cycle

Since the inlet of the cold fluid is reversed from that in the charging cycle, the now cold heat transfer fluid flows (inlet reversed) from the position closest to position 3. Therefore, initially the temperature gradient is highest at the inlet between the heat transfer fluid and the now hot concrete (close to position 3), as the fluid heats up as it moves along the length of concrete. This causes the temperature difference during the first hour of operation to be highest in position 3, followed by 2 and then 1. However, after the first hour of operation, the temperature decrease in concrete becomes lowest at position 3, then at position 2, followed by position 1. This can be explained in the same manner as the earlier discussion for the charging cycle. Simply, that after the first hour of operation, the concrete temperature at position 3 is lower than that at position 2 and therefore the temperature gradient between the cold fluid and the concrete at position 3 is lower compared to that of position 2. As such there is less heat transfer leading to a lower temperature variation of concrete, which is also true for position1 compared to that of position 2 and position 3.

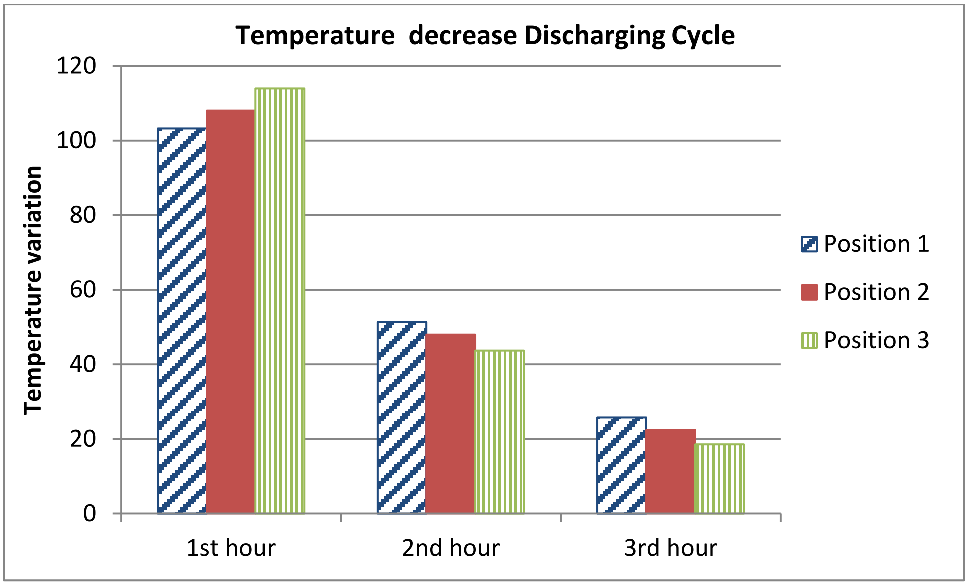

Figure 4-17 Hourly temperature variation of concrete in the discharging

a. Heat transfer fluid (mineral oil)

Figure 4-18 shows the fluid temperature at the inlet and outlet for both the charging and discharging cycles. For the charging period, the fluid inlet is set to 575K. The outlet temperature increases with time during the charging mode. This is due to the increase of the concrete's temperature as the charging continues, there is less temperature gradient between the heat transfer fluid and the concrete, and so the outlet temperature is higher. Similarly in the discharging cycle, the inlet fluid (previously the outlet position) is set at 350K and at the outlet now (previously the inlet position) the temperature decreases as the discharging mode is on. Thus as the concrete's temperature starts decreasing as the operation continues, leading to a lower temperature gradient between the cold heat transfer fluid and the hot concrete. This finally results in less heat transfer so the fluid outlet temperature becomes lower.

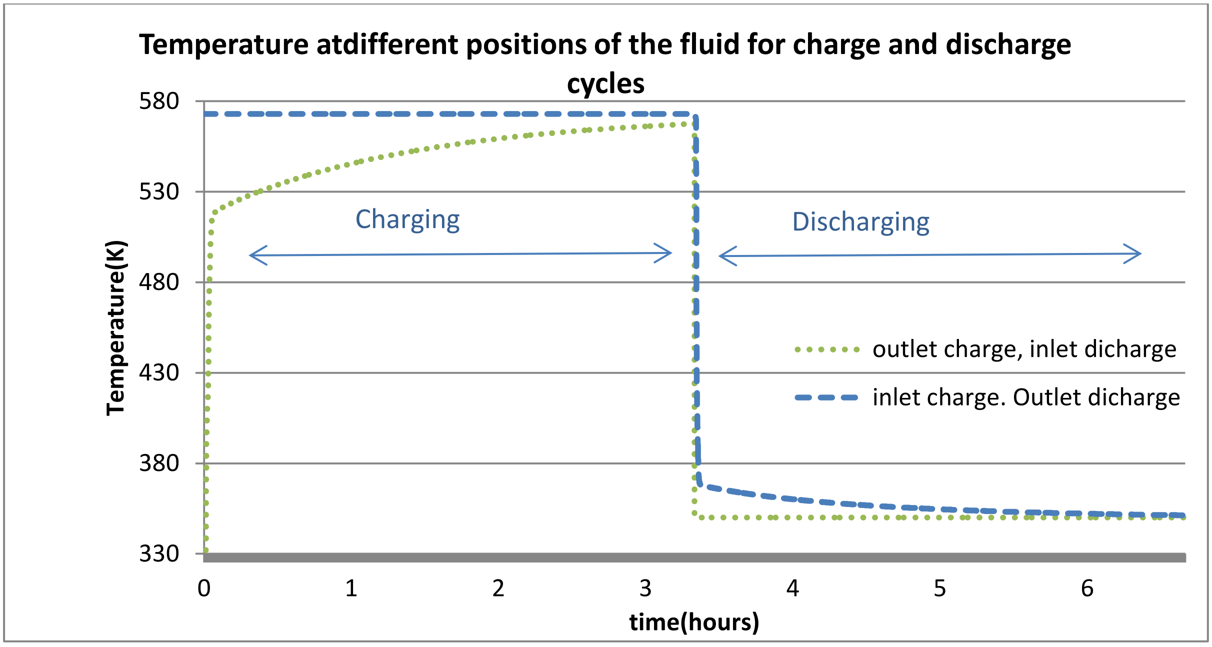

Figure 4-18 Inlet and outlet temperatures of heat transfer fluid

b. Amount of Energy Stored

The hourly energy stored is calculated using:

$$E = mC_p\Delta T$$

Where m is the mass of concrete, C_p is the specific heat capacity of concrete and ΔT is the average temperature change of the concrete. The thermal energy stored is calculated every hour.

As explained earlier, the thermal energy stored decreases every hour starting at around 4kWh in the 1st hour down to around0.9kWh in the 3rd hour, due to the increase of the concrete's temperature, which decreases the temperature gradient between the heat transfer fluid and concrete; hence causing less heat transfer

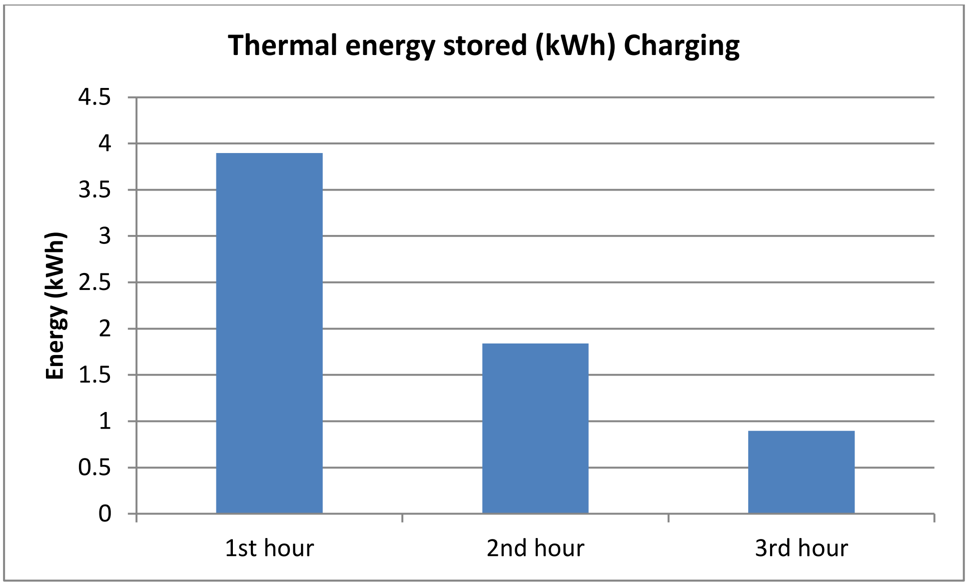

Figure 4-19 Hourly energy stored during the charging mode

Figure 4-20 shows the hourly energy extracted from the concrete, starting from around 3.5kWh in the 1st hour to 0.7kWhr in the 3rd hour of operation. This can be explained by the decrease in the concrete's temperature after the start of operation, leading to a lower temperature gradient between the cold heat transfer fluid and concrete; and resulting in less heat transfer.

In addition, the thermal energy stored is higher than that absorbed from the concrete, since the initial temperature of concrete before heating was 293K; while the initial temperature of the cold fluid before discharging was set to 350K. As a result, the temperature gradient for charging is higher than that for discharging, and thus there is a higher heat transfer for a charging cycle compared to discharging.

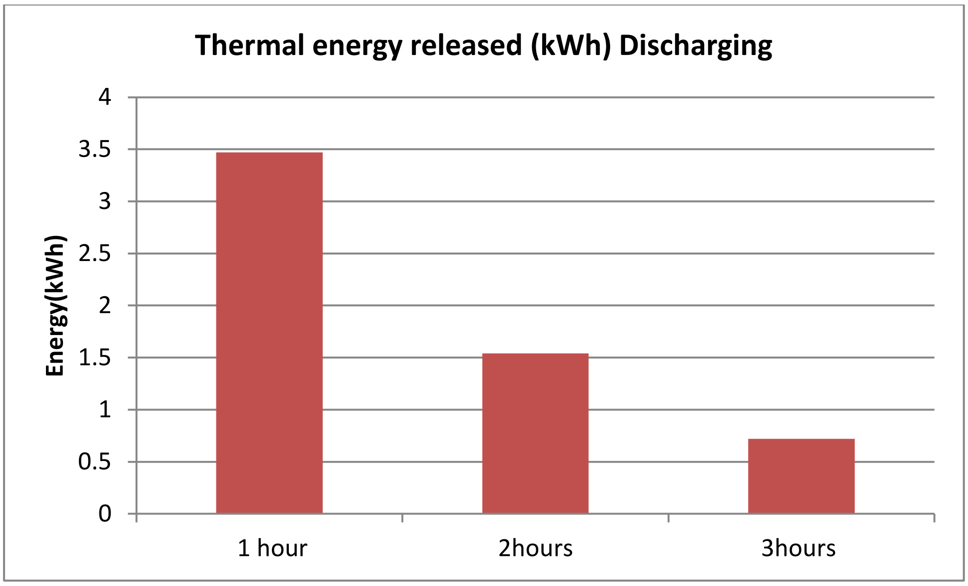

Figure 4-20 Hourly energy released during the dishcarging mode

4.4.2 Effect of pipe diameters

The first analysis that was developed is testing under different pipe diameters. The chosen pipe diameters for comparison were 22mm, 28mm and 50mm. The dimensions for each are shown in Table 4-2. The temperature outlet of the heat transfer fluid and the heat energy transferred through the pipes are the most important factors for this study, and their results will be discussed. This simulation was carried out for a period of nine hours, however the first seven hour results are discussed in detail, since the heat transfer becomes very low afterwards. This simulation considers only the charging cycle. Different inlet velocities are used in each case to simulate the same inlet flow rate of the heat transfer fluid.

Table 4-2 Dimensions for different pipe diameters

Pipe number	Diameter(mm)	Gap(mm)	length(mm)	Mass flow rate(kg/s)	Inlet velocity(m/sec)
7	22	83	700	0.1	0.05
7	28	77	700	0.1	0.031
7	50	55	700	0.1	0.01

a. Effect of pipe diameters on fluid Temperature outlet

Figure 4-21 shows the heat transfer fluid outlet temperature using different pipe diameters. It is clear that using bigger pipe diameters would result in a higher heat transfer which in turn results in the decrease of the outlet temperature of the heat transfer fluid, which is beneficial for the CAES system. For the smaller pipe diameters, since the outlet temperature is higher, this means that the temperature of the fluid going to the compression stage of the CAES system is higher. This means it can absorb less heat from the compressed air in the compression stage of the CAES system.

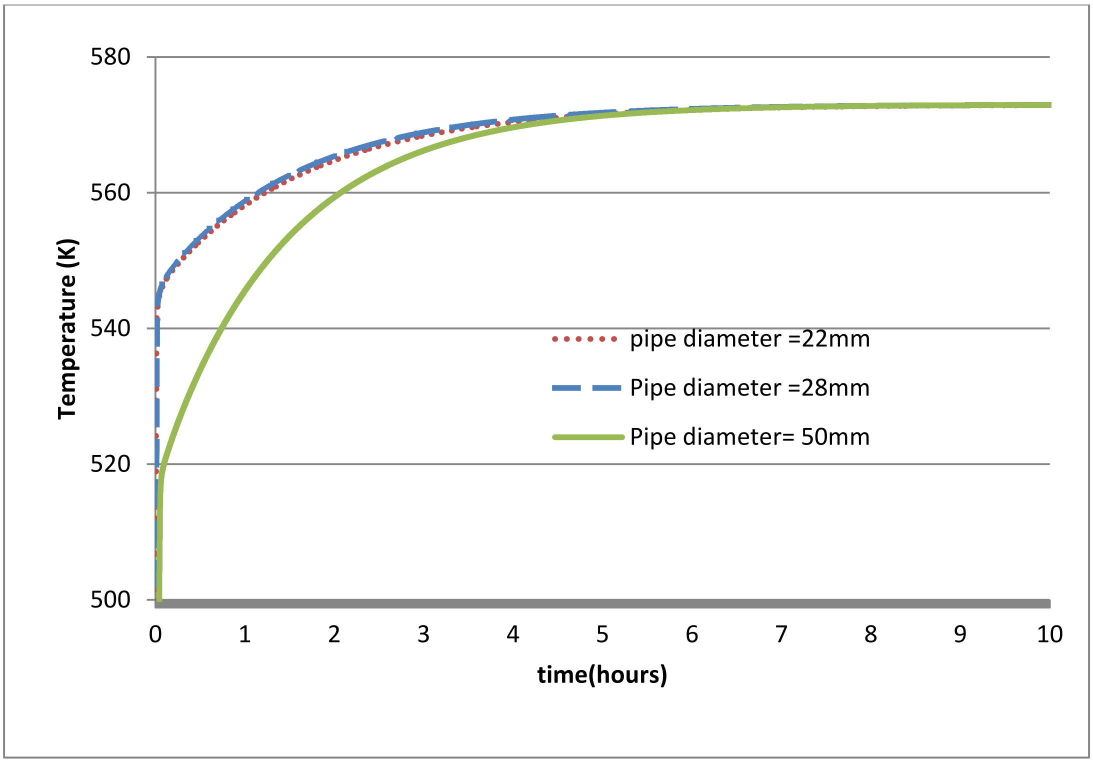

Figure 4-21 Outlet temperature of heat transfer fluid for different pipe diameters

b. Temperature of concrete

Figure 4-22 shows the increase of the concrete's temperature by time for the three diameters of pipes simulated. They all reach around 573K after around 7 hours of operation; but the 50mm diameter pipe takes a shorter time to reach this temperature. However, this is not a determining factor as to which design is better, since the highest temperature is reached by the end of the charging mode.

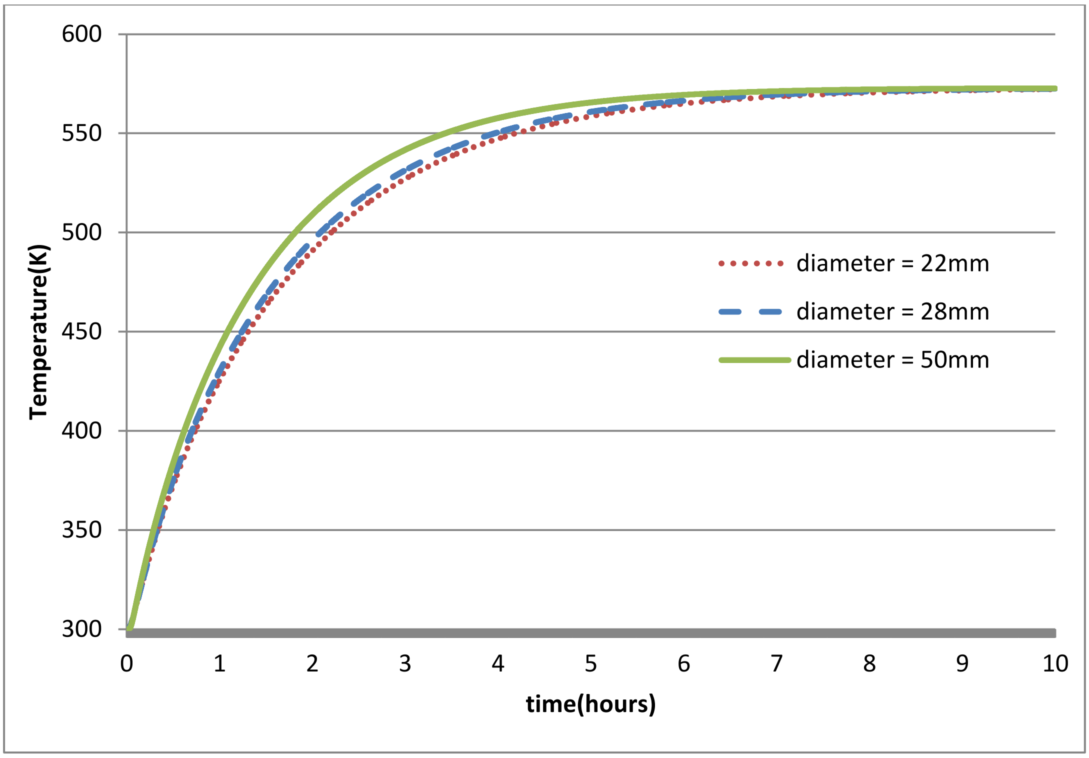

Figure 4-22 Effect of pipe diameters on temperature of concrete

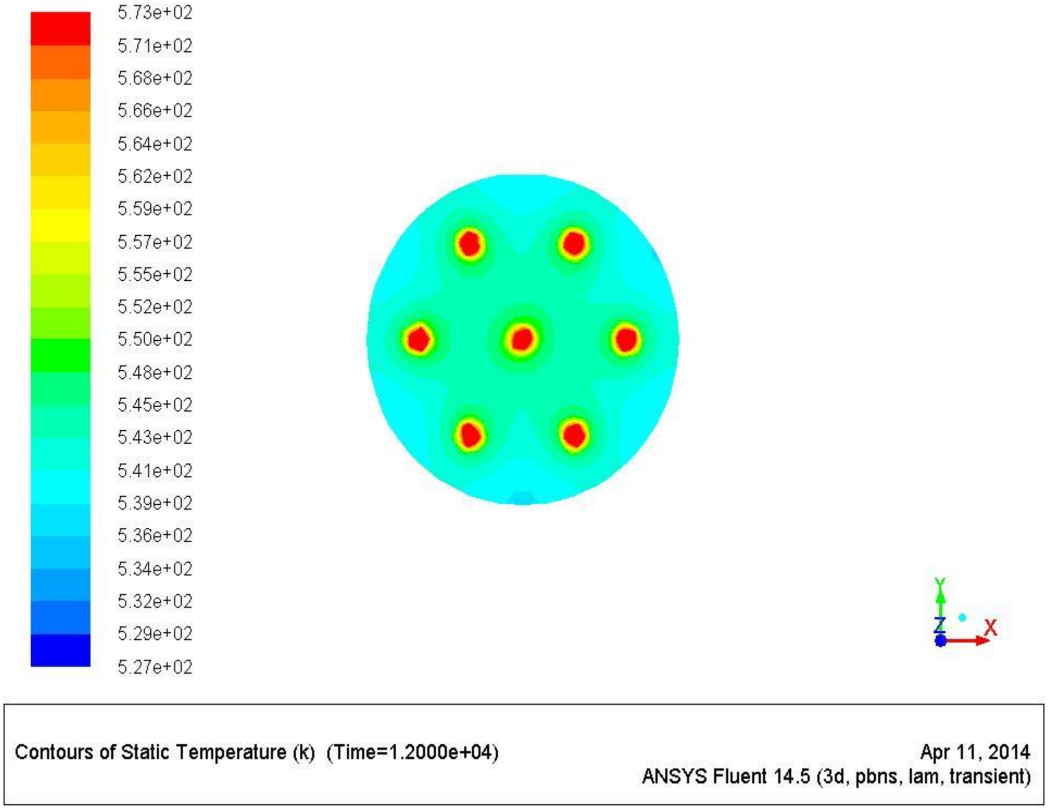

Figure 4-23 Front view of contours for TES for 28mm pipes (after 3 hours of charging)

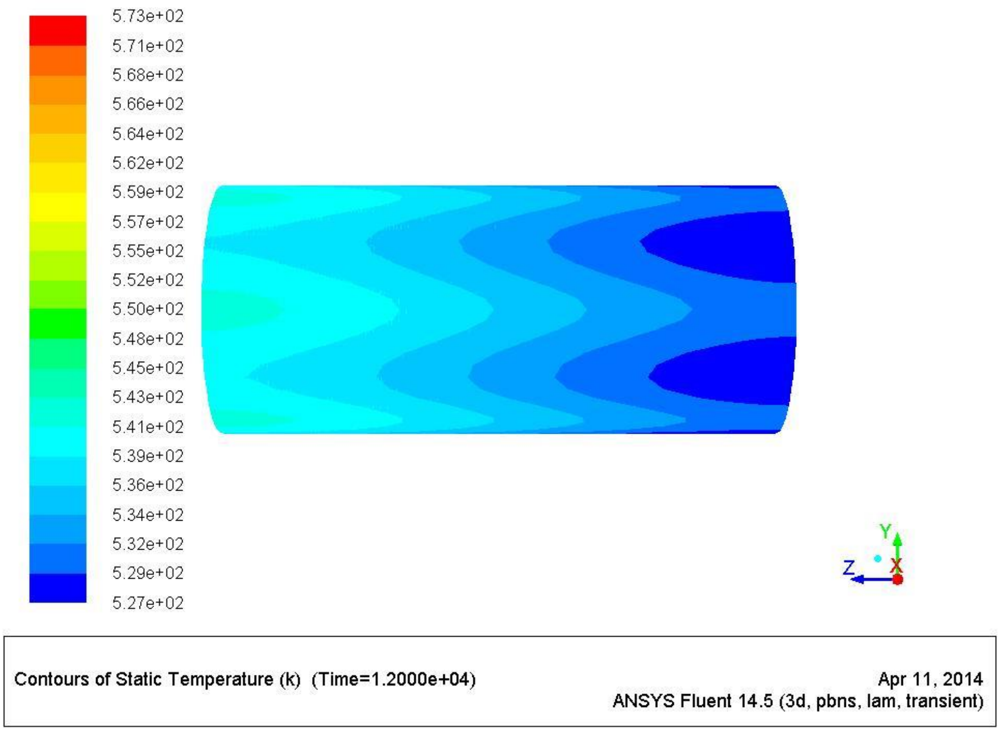

Figure 4-24 Side view of contours for TES for 28mm pipes (after 3 hours of charging)

Figure 4-25 shows the hourly increase in concrete temperature using different pipe sizes. Initially, there is higher heat transfer when using the bigger pipe diameter, however as the operation continues, the temperature increases becomes similar. This is due to the higher contact area of concrete with the pipes using a larger diameter, and so the heat transfer is higher at the start of operation. Yet as the operation continues, the concrete temperature gets higher at a faster pace using the larger diameters, and thus later in the operation, the temperature gradient between the heat transfer fluid and the concrete becomes lower. As a result, this yields lower heat transfer for larger pipe sizes and hence a lower concrete temperature increase.

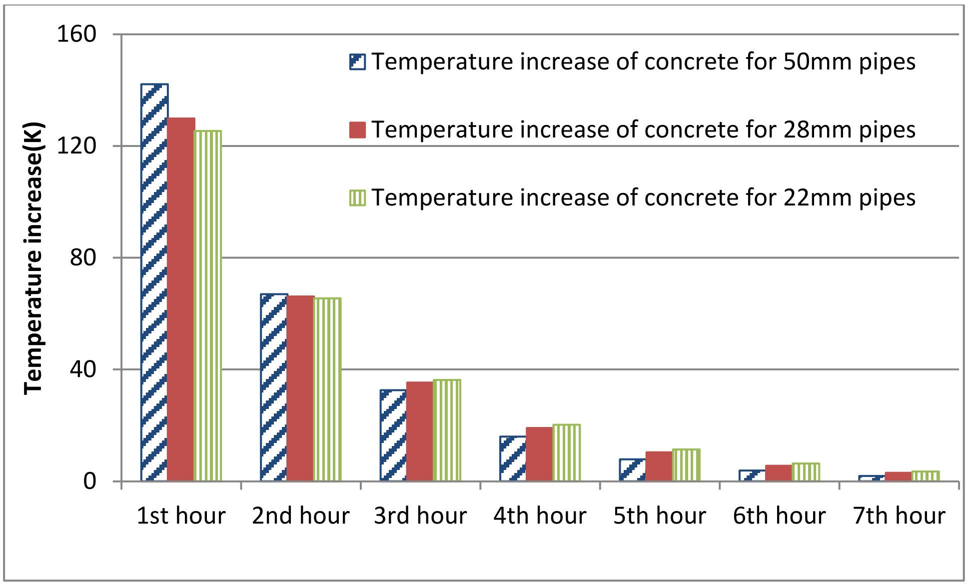

Figure 4-25 Hourly temperature increase of concrete using different pipe diameters

c. Amount of Heat Energy stored

Concerning heat energy stored, Figure 4-26 shows the hourly thermal energy stored using different pipe diameters. This figure shows different results compared to the previous diagram, as the mass of concrete increases using smaller pipe diameters due to the lower area taken by the pipes. Therefore, even at the start of operation, using 28mm and 22mm pipe diameters yields higher energy stored for the whole operation as compared to using 50mm pipe diameters.

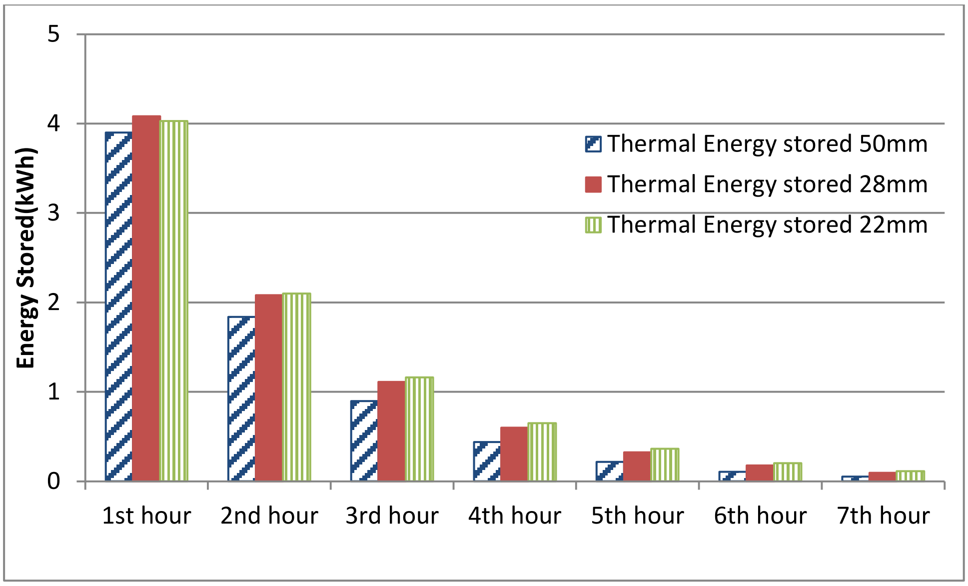

Figure 4-26 Hourly thermal energy stored for different pipe diameters

Pipe diameters' discussion

As mentioned earlier in the chapter, the main factors which critical to CAES is the heat energy transferred, as well as the outlet temperature of the heat transfer fluid.

a. Heat energy

Primarily, using smaller pipes achieves higher energy storage even at the start of operation when the temperature increase of concrete is higher using 50mm diameter pipes, due to the lower mass of concrete block in this case. Therefore, using a smaller diameter of pipes resulted in improved energy storage.

b. Fluid outlet temperature

Using a larger pipe diameter resulted in a lower temperature of the heat transfer fluid outlet, which is critical to CAES operation especially, during the first three hours of operation.

Ultimately, it is a trade-off between the heat energy stored and the outlet temperature of the heat transfer fluid. There is not much difference in both different pipe diameters. Yet better performance is achieved in terms of outlet temperature of the heat transfer fluid using 50mm.

4.4.3 Effect of thermal conductivity

In this section, the effect of thermal conductivity on heat transfer was taken into account for the 50mm diameter of pipes of the design model. Since there are different types of concrete with variable thermal conductivity, two values were chosen for thermal conductivity. The first is 0.9W/mK which is regular concrete aggregate; and secondly 2.2W/mK, which is asphalt concrete aggregate (Islam M, et al 2014).

a. Heat transfer fluid temperature outlet

Figure 4-27 shows the temperature of concrete for different thermal conductivities simulated. In this case, the heat transfer fluid temperature outlet is higher for the first hour of operation for the lower thermal conductive concrete. Afterwards, for the rest of the ten hours, the heat transfer fluid outlet temperature is almost the same using different thermal conductivities.

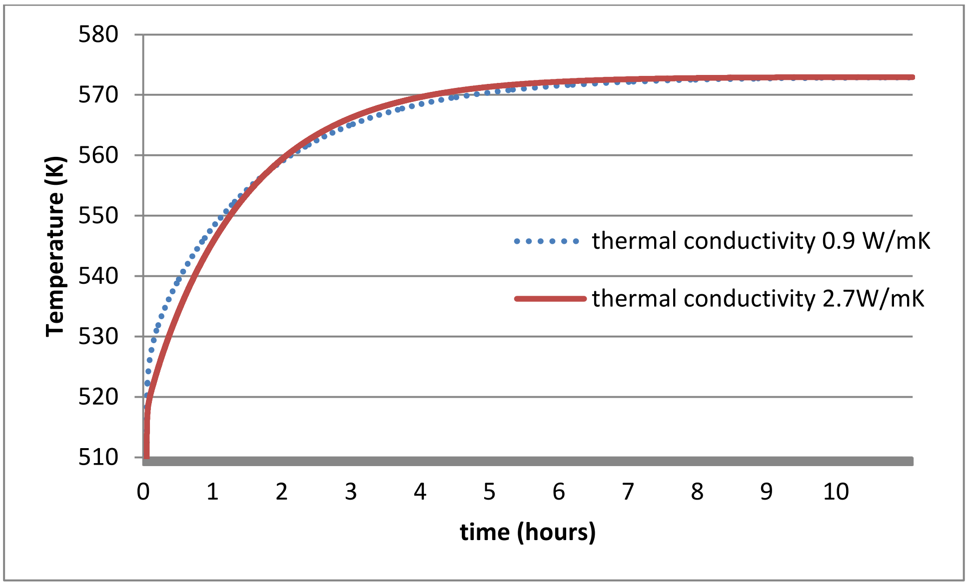

Figure 4-27 Outlet fluid temperature for different thermal conductivities

The effect of thermal conductivity is minimal in this design. So at the beginning of operation, there was more heat transfer when using concrete of higher thermal conductivity which then becomes lower after the 1st hour. So if shorter time was used then the effect would be slightly bigger but for the time frame chosen (similar to CAES), changing the thermal conductivity of concrete has no significant effect.

b. Concrete temperature

Figure 4-28 shows results which follow a similar pattern to those of Figure 4-27. It illustrates that there is more heat transfer at the beginning of the operation for the concrete with higher thermal conductivity, thus reaching a higher temperature faster than that with lower thermal conductivity. However, by the end of the ten hours of charging, both concrete blocks reach the same temperature.

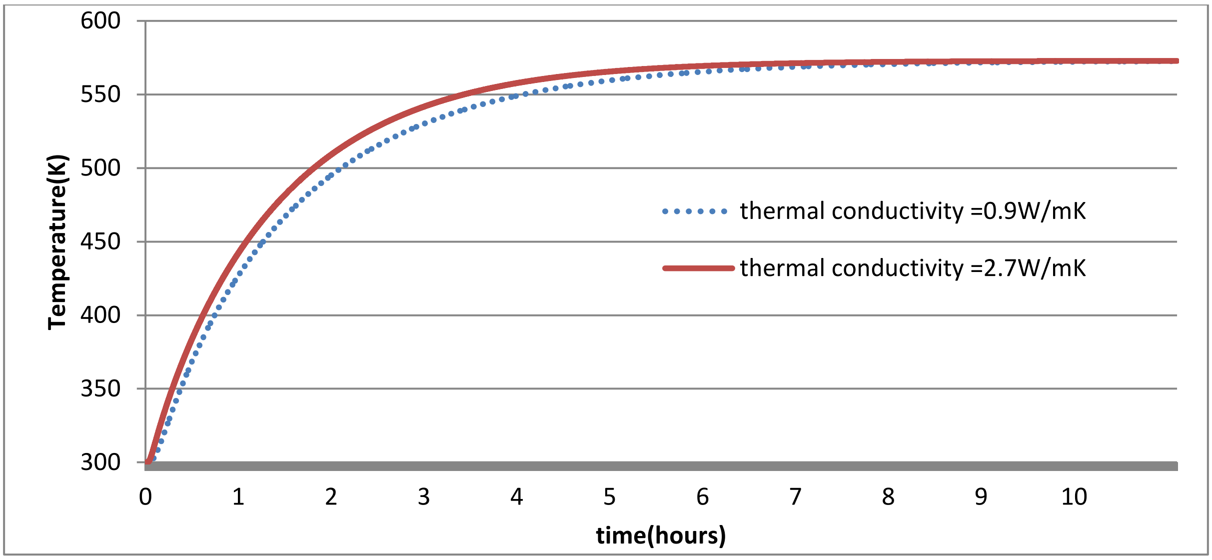

Figure 4-28 Temperature of concrete for different thermal conductivity

In addition, Figure 4-29and Figure 4-30 show the hourly temperature increase for concrete and the hourly energy stored using different thermal conductivities. These again follow the same explanation of Figure 4-28. Higher heat transfer occurs when using high thermal conductivity at the start of operation, but the concrete temperature rises faster using higher thermal conductivity. This leads to a lower temperature gradient between the heat transfer fluid and the concrete at the later stage of charging. As a result, lower energy is stored, as well as a temperature increase of the concrete.

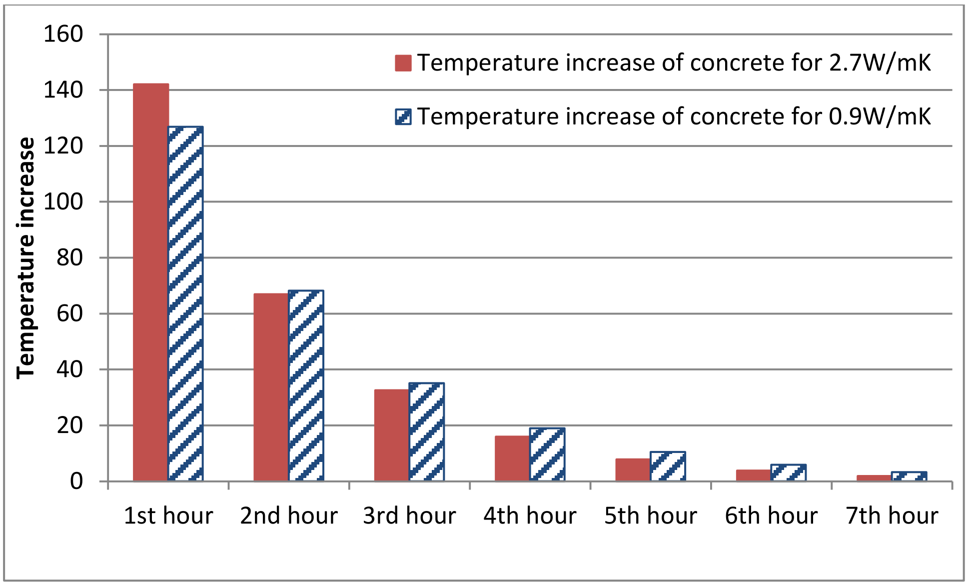

Figure 4-29 Hourly temperature increase of concrete using different thermal conductivities

c. Thermal Energy stored

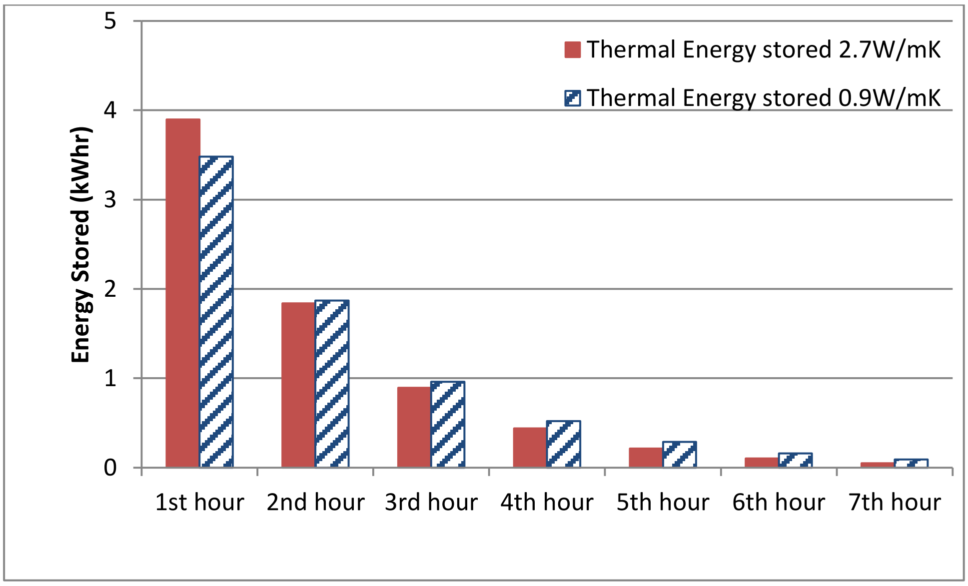

Figure 4-30 Hourly energy stored for different concrete thermal conductivities

Effect of Varying Thermal Conductivity

Changing the thermal conductivity of concrete from 0.9 to 2.7W/mK had a minimal effect both on the heat energy transferred and the outlet of the heat transfer fluid. This is true even if the charging cycle lasts for less than three hours, which is less than the minimum expected charging time for CAES.

4.4.4 Effect of mass flow rates

The flow rate was varied between 0.1kg/sec (0.01m/s) and 0.6kg/sec (0.05m/s) for each pipe. In this way, it is imperative to document the effect of changing the inlet velocity on heat transfer fluid temperature outlet and the energy stored as follows.

a. Heat transfer fluid temperature gradient

For the different inlet velocities, Figure 4-31 shows that there is an effective difference between using 0.01m/sec and 0.05m/s inlet velocities. The simulation of 0.01m/sec inlet velocity results in lower outlet temperature of the heat transfer fluid for the first six hours of operation, compared to a fluid inlet velocity of 0.05m/sec. This simulation shows that for a thermal energy storage case of the CAES system, the operation with lower inlet velocity 0.01m/sec- is better for this study. Since the outlet temperature is much lower, and then more heat can be absorbed from the air in the compression stage in the CAES system.

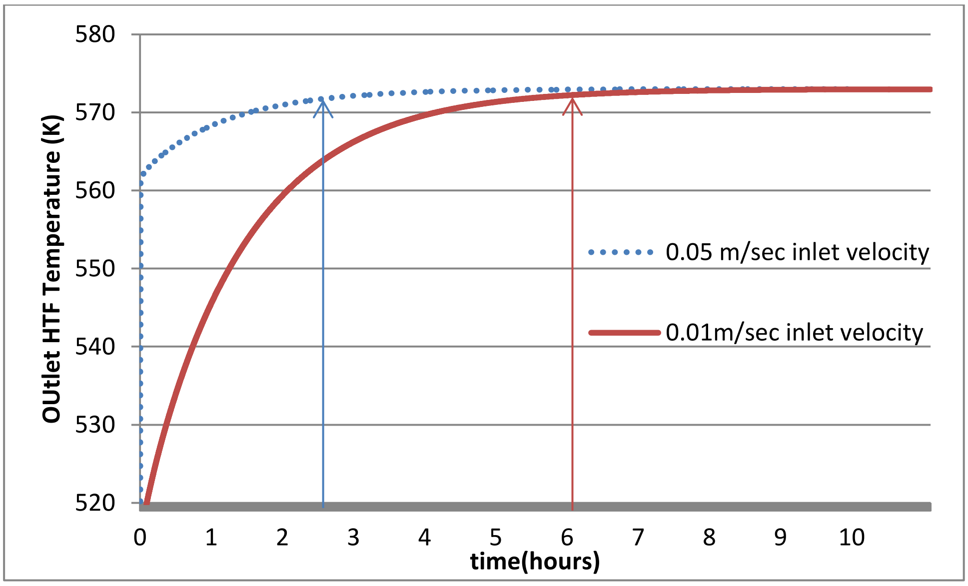

Figure 4-31 Outlet temperature of fluid for different inlet velocities

b. Concrete temperature

Figure 4-32 shows that for the two simulations with different inlet velocities, the temperature of the concrete block reaches the maximum temperature before the end of the 10 hours. However, the simulation with an inlet velocity of 0.05m/sec (higher velocity), reaches the maximum temperature faster than that of the lower velocity inlet simulation.

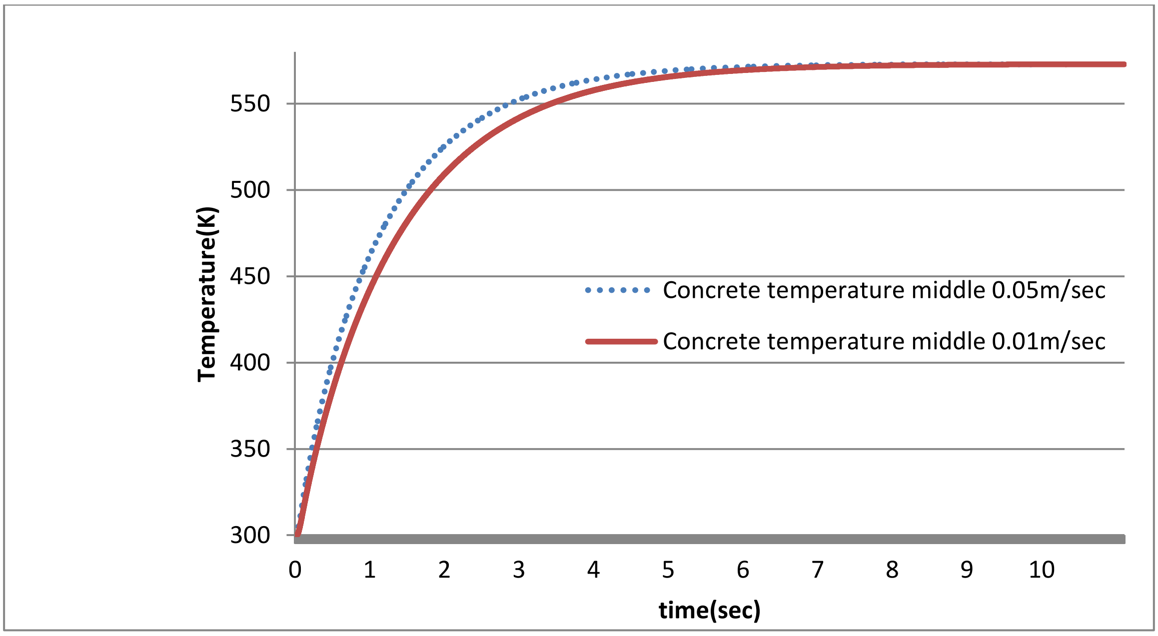

Figure 4-32 Temperature of the concrete block for different inlet velocities

Figure 4-33 and Figure 4-34 show the temperature increase of concrete and the thermal energy stored using different inlet velocities. When using a faster inlet velocity, the increased heat transfer is faster between the heat transfer fluid and the concrete. Thus earlier during the charging mode, the concrete temperature increases and thermal energy stored is higher when using a higher inlet velocity. Yet afterwards, the heat transfer decreases as the temperature gradient between the concrete and the heat transfer fluid is lowered using higher inlet velocity. This results in lower energy stored and a lower concrete temperature increase

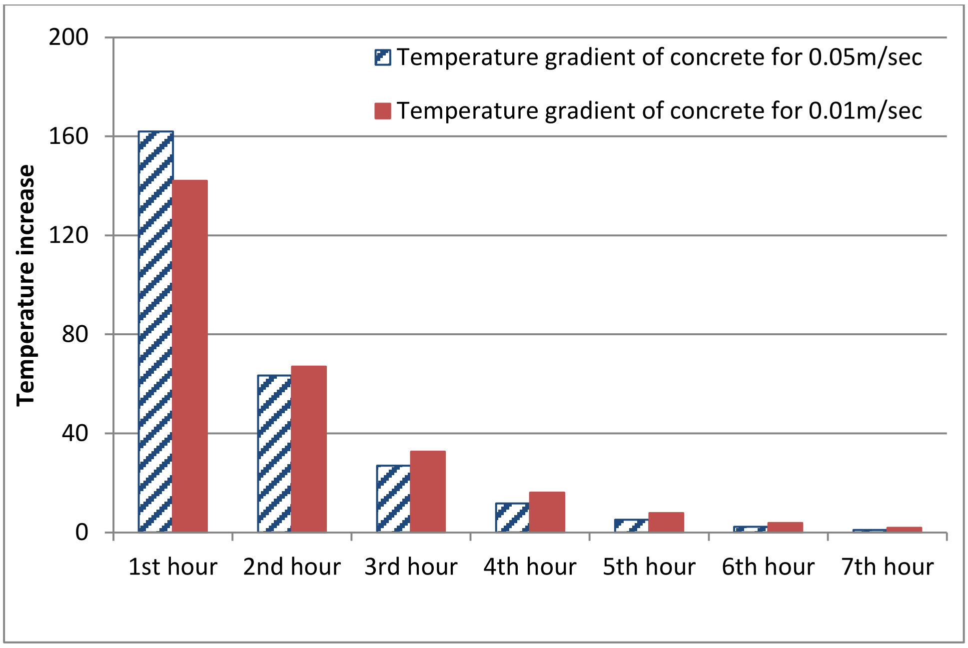

Figure 4-33 Hourly increase in concrete block temperature

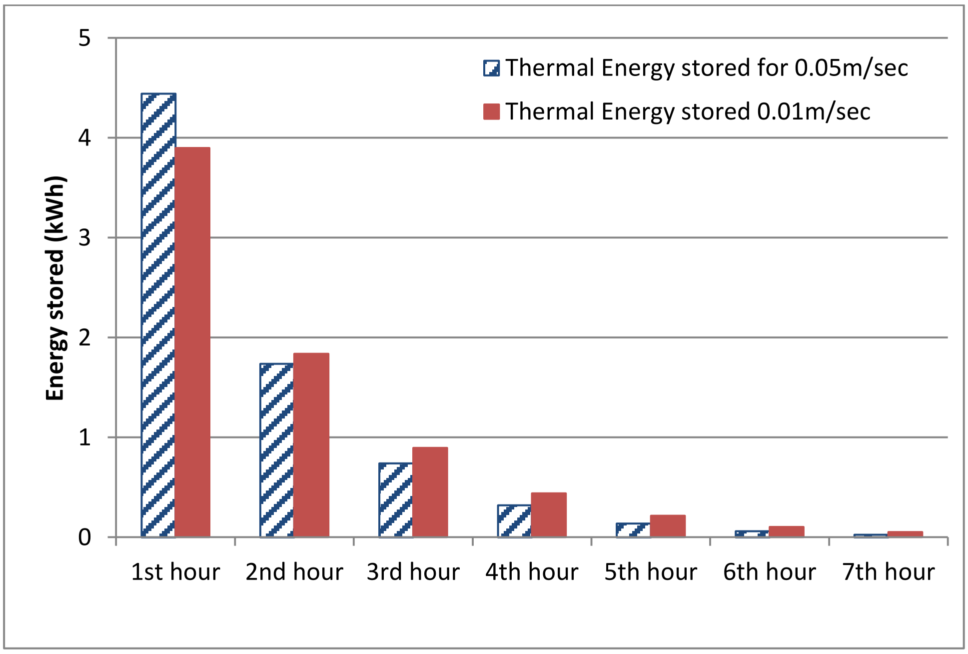

Figure 4-34 Variation of the thermal energy storage

Effect of flow rates remarks

In this case using a lower flow rate (inlet velocity of 0.01m/sec) for the thermal energy storage design used yielded better results. Regarding the thermal energy stored, the inlet velocity does not actually have a decisive effect. However, as seen in Figure 4-31, using the lower inlet velocity reduces the outlet temperature of the heat transfer fluid. This is especially true in the first 6 hours, which would have an improved effect on the operation of the CAES system. Thus for this design using a lower fluid inlet velocity seems more suitable for the desired application.

4.4.5 Impact of the inlet temperatures

For this test, different inlet temperatures of heat transfer fluid are simulated ranging from 473K to 573K (base case). The simulation was carried out for three hours

Figure 4-35 shows the outlet temperature of the heat transfer fluid using different fluid inlet temperatures. It is clear that when using higher inlet temperatures, the expected outlet fluid temperature is higher, even if there is a higher heat transfer with the concrete.

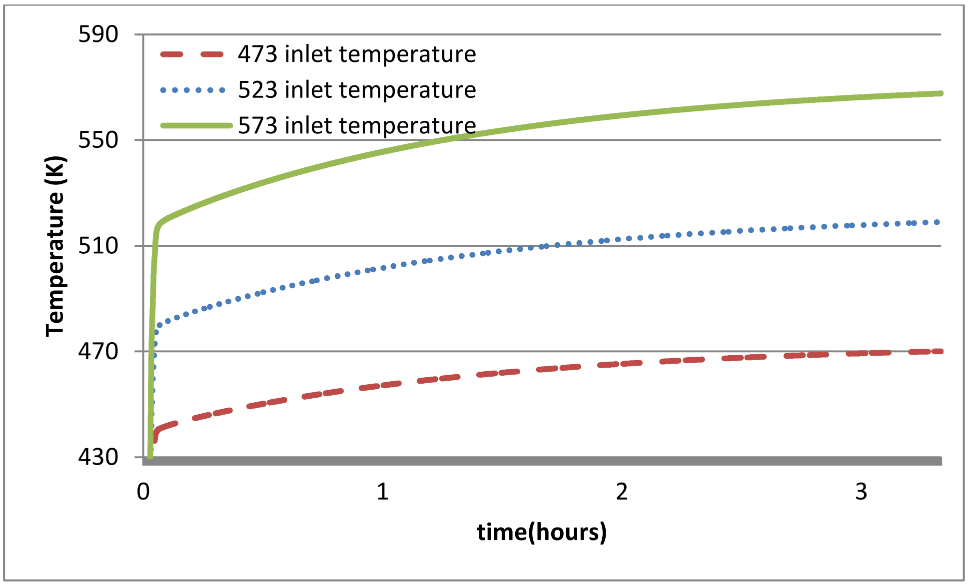

Figure 4-35 Effect of the inlet temperature on the outlet temperature of heat transfer fluid

a. Concrete temperature

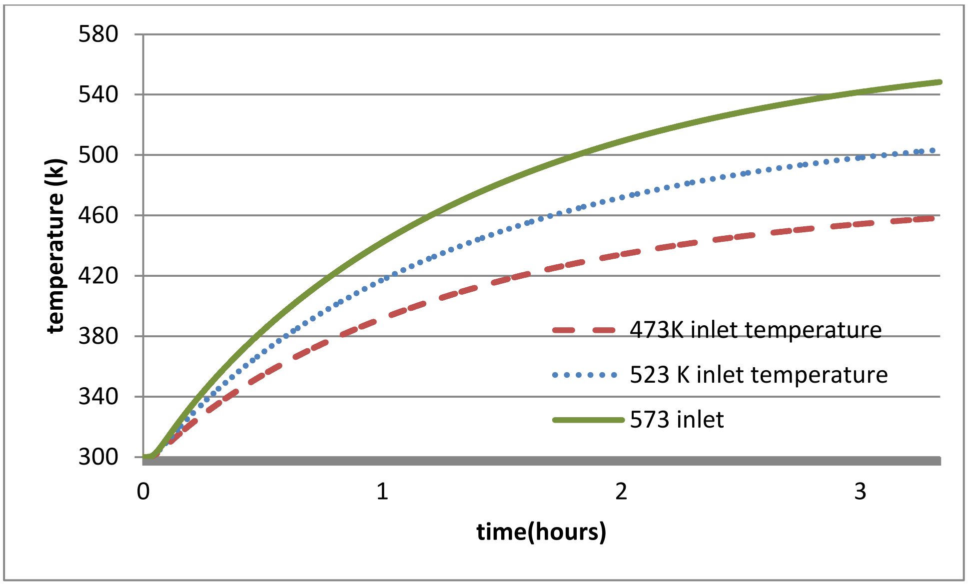

Figure 4-36 Effect of inlet temperature on concrete block profile

Figure 4-36shows the concrete temperature using different inlet temperatures. The higher the inlet temperature, the higher the heat transfer. Thus a higher temperature increase of concrete means a higher hourly thermal energy stored; as shown in Figure 4-37and Figure 4-38 respectively

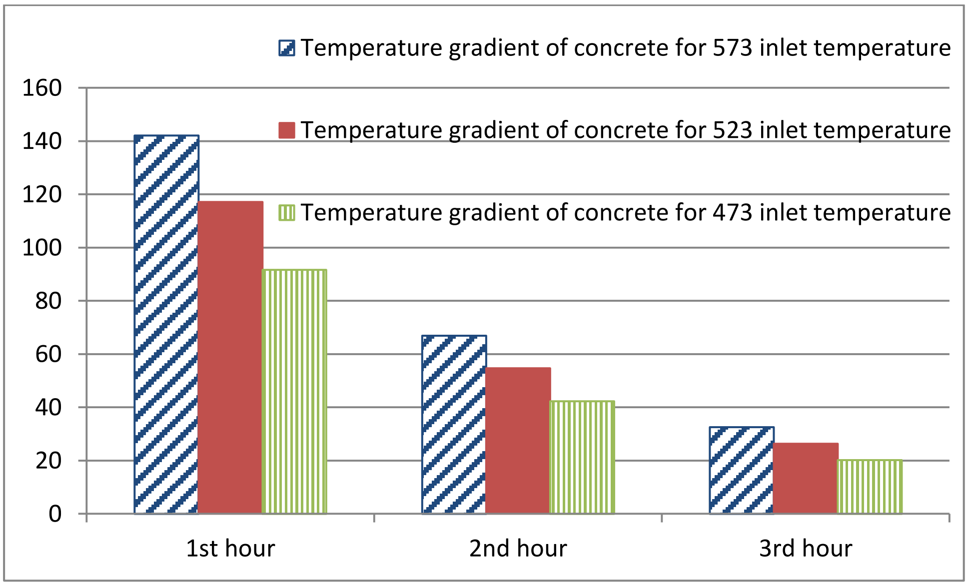

Figure 4-37 Hourly temperature increase of concrete block

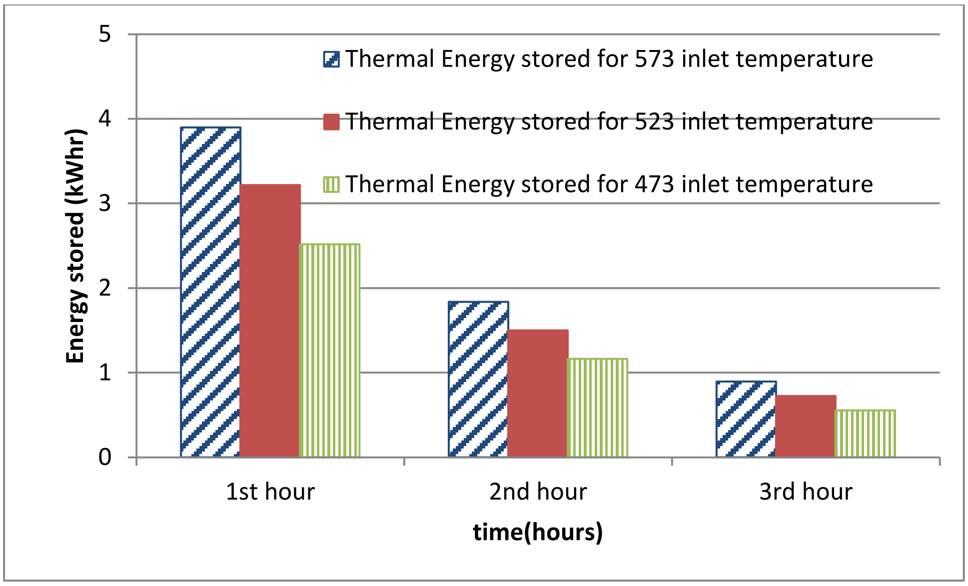

Figure 4-38 Hourly energy stored for concrete block

Effect of inlet temperatures remarks

It is clear for this section that the higher the inlet temperature of the heat transfer fluid, the higher the heat transfer; and more thermal energy is stored in the concrete block. On the other hand, the higher the inlet temperatures, the higher the outlet temperature of the heat transfer fluid. Therefore, a decision needs to be made according to what is important to the CAES system.

4.4.6 Effect of number of pipes

In this case, a varying number of pipes of heat transfer fluid is used for the same size of the concrete block. The simulations added to the basic case are nine pipes and five pipes, and the results of these simulations are compared for the same input parameters. Figure 4-39and Figure 4-40 show the geometry of both the nine and five piping configurations.

Table 4-3 Specifications for different pipe numbers

Design	Pipe diameter(mm)	Surface Area of pipes(m^2)	Mass of concrete(kg)	Mass flow rate(Kg/sec)	Inlet velocity (m/sec)
5 pipes	50mm	0.01	130.5	0.1	0.15
7 pipes	50mm	0.0137	123.5	0.1	0.01
9 pipes	50mm	0.0177	115.8	0,1	0.0082

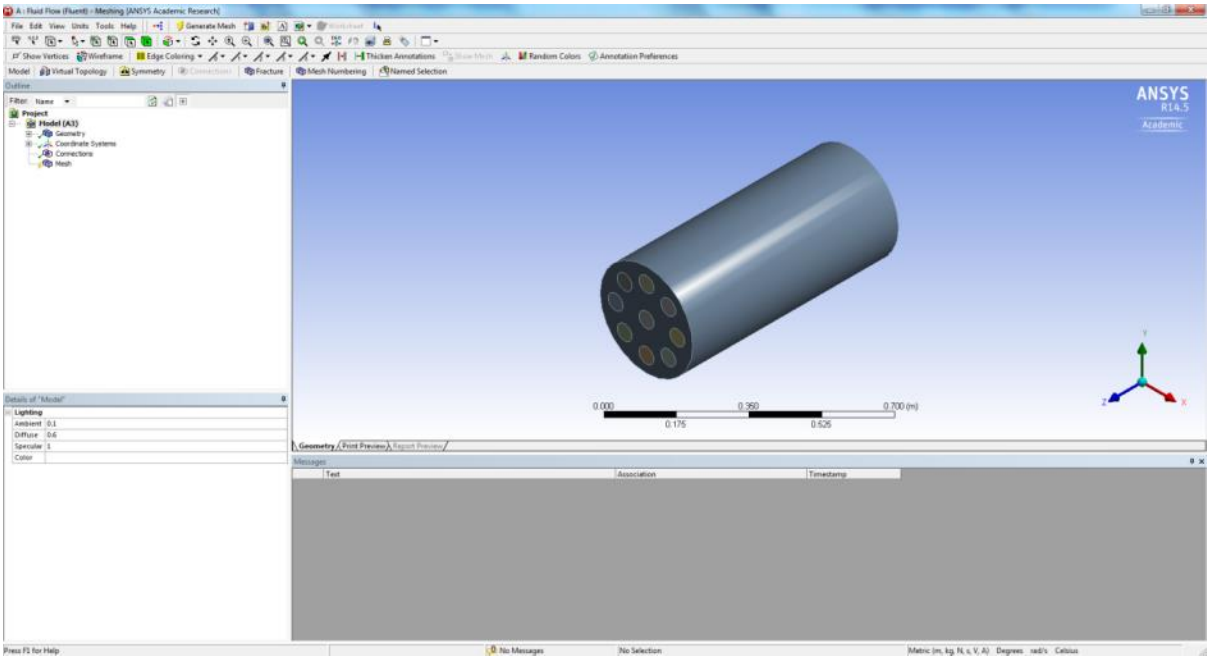

Figure 4-39 Geometry for 9 pipe arrangement

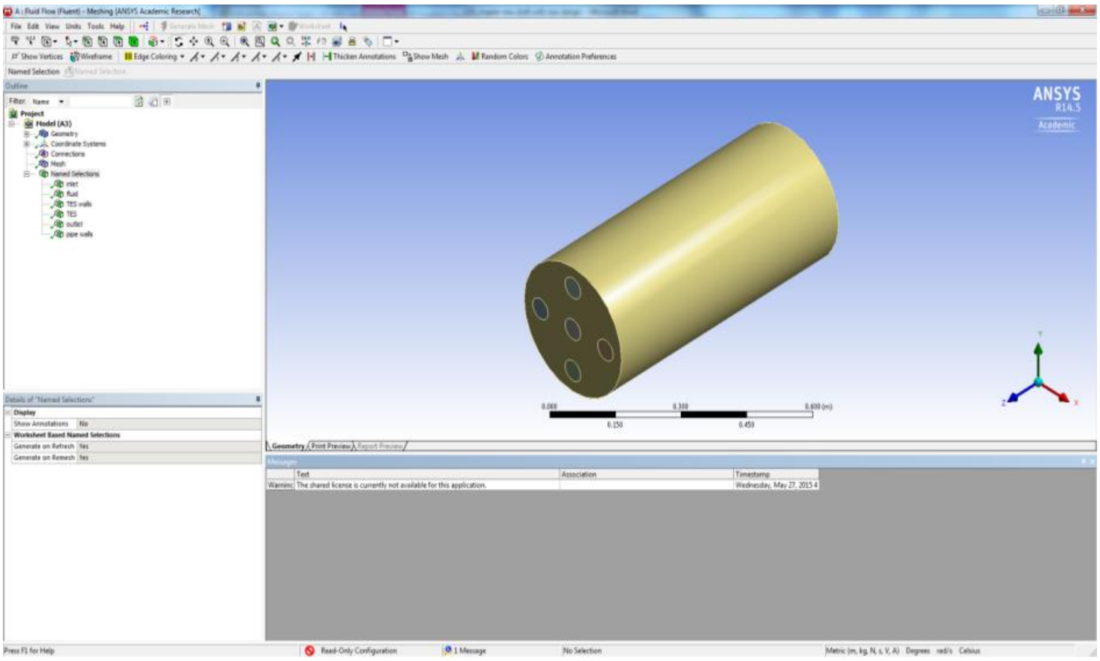

Figure 4-40 Geometry for 5 pipe arrangement

To begin with, Figure 4-41 shows the outlet temperature of the heat transfer fluid using different numbers of pipes. For the first hour of the charging period, using a higher number of pipes results in a lower temperature of the heat transfer fluid. However, as the operation continues, the outlet temperature of the fluid increases using nine pipes compared to seven and five pipes for our design.

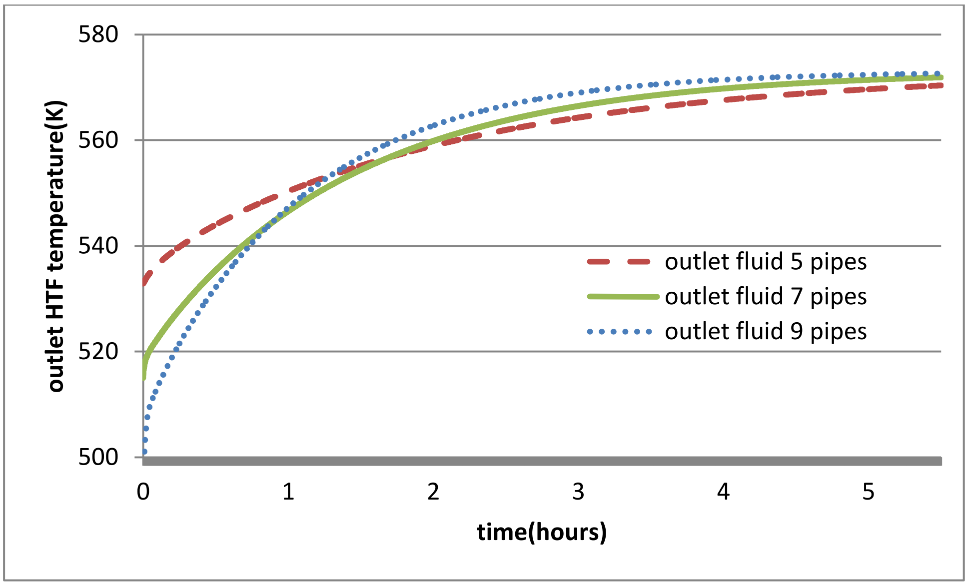

Figure 4-41 Heat transfer fluid outlet using different number of pipes

Additionally, Figure 4-42 shows the concrete block temperature using the different number of pipes. The rise in temperature when using more pipes is much higher than using fewer early in the operation. This can be explained by the fact that there is a smaller mass of concrete for bigger number of pipes as well as more contact area between the pipes and the concrete block which leads to higher rate of temperature increase and hence concrete block saturating quicker. This can be clearly seen in Figure 4-43, which shows the hourly increase in concrete temperature. In the first hour, there is a much larger increase of concrete temperature using nine pipes, which is around 35 K higher than that of seven pipes, and 60 K higher than that of five pipes. After the first hour, the impact of using more pipes on concrete temperature becomes lower than that of fewer pipes.

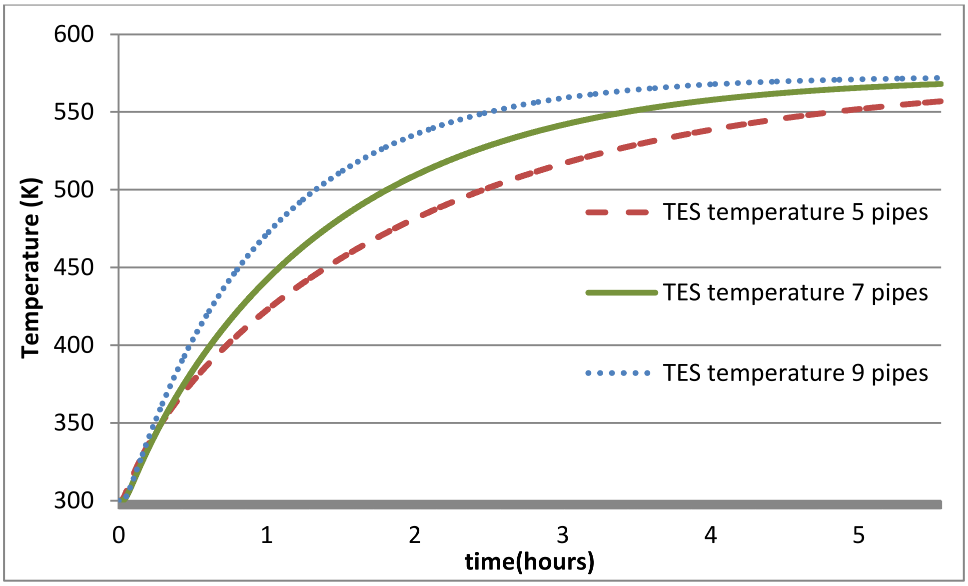

Figure 4-42 Concrete block temperature using different number of pipes

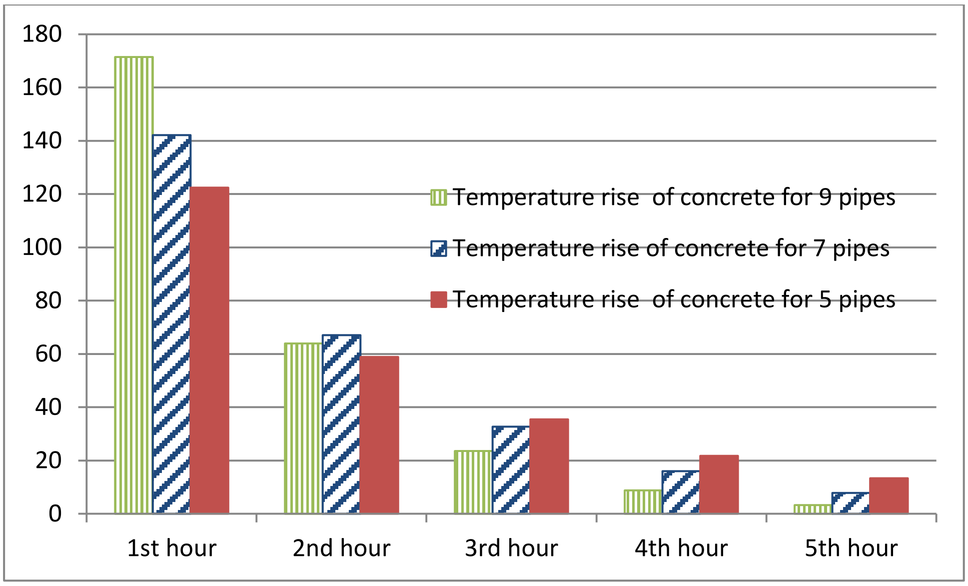

Figure 4-43 Hourly temperature rise of concrete using different number of pipes

Also, Figure 4-44 shows the hourly energy stored in the concrete block. Due to the much larger rise in temperature during the first hour, there is higher thermal energy stored using nine pipes. Afterwards, the energy stored follows the same pattern as that of the concrete hourly temperature rise.

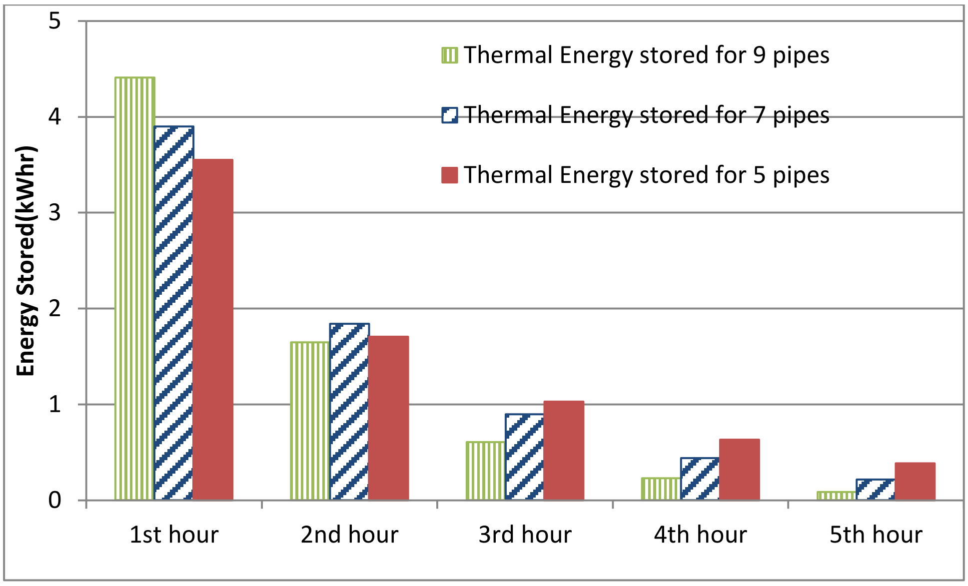

Figure 4-44 Hourly energy stored using different number of pipes

Effect of Pipe Number remarks

In the first hour of operation, using nine pipes resulted in increased heat transfer between the heat transfer fluid and the concrete block. This also resulted in a lower temperature of the heat transfer fluid. Yet, since the heat transferred in the first hour is much larger using nine pipes, the temperature gradient between the concrete block and the heat transfer fluid decrease, which results in lower heat transfer after the first hour, hence lower increase in concrete temperature and higher outlet temperature of the heat transfer fluid. Since the CAES charging mode is expected to last more than three hours, therefore using large number of pipes is not recommended in this case.

4.4.7 Effect of Aspect ratio

The TES aspect ratio, comprising of concrete and pipes, was increased from 2.5 to 15 to test the impact on the outlet temperature of the fluid, which is a significant factor in our findings.

To portray the variance in outlet temperature, Figure 4-45 shows the effect the TES aspect ratio. It seems that the bigger the system aspect ratio, the lower the outlet temperature of fluid. This is explained by the fact that the fluid keeps losing heat to the concrete along the length of the TES. Therefore, for a higher length, a higher distance is travelled by the heat transfer fluid and more energy is transferred to the concrete. Therefore, the outlet temperature is reduced, which is an important factor to the CAES operation.

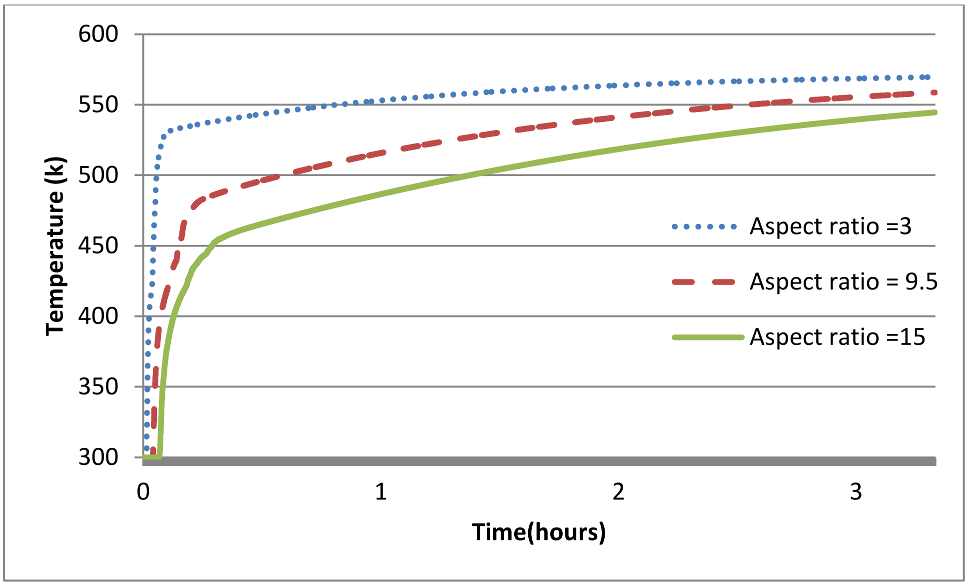

Figure 4-45 Outlet fluid temperature using different lengths of concrete

Effect of aspect ratio remarks

It is clear that the use of longer TES improves the heat dissipation to the TES. This reduces the outlet temperature of the heat transfer fluid and hence improves the CAES system performance.

4.5 Conclusions

This chapter investigated the heat transfer performance of the thermal energy storage for a CAES system using ANSYS CFD modelling. The analysis was carried out for the factors affecting the operation of the thermal energy storage configuration. Each was varied to test their effect on the heat transfer in the system to optimize the design of the thermal energy storage with the heat transfer fluid.

Some of the parameters that were investigated included the thermal conductivity of the concrete block which has shown that it does not have much effect on the heat transfer of the system. On the other hand, the diameter of pipes and the number of pipes for a certain diameter of concrete block were inter-related. For instance, using a larger diameter of pipes improved the operation of the system, as it lowered the outlet temperature of heat transfer fluid; while increasing the number of pipes had a minor effect on the operation of the TES, as there was slight different in the temperature of heat transfer fluid after the first hour of operation. This proved that increasing the contact area between the concrete block and the heat transfer fluid would improve system performance, but only up to a certain limit. This is because increasing the contact area above a certain threshold, will reduce the mass of TES and hence would cause the outlet temperature of the heat transfer fluid to increase.

Also, using a lower flow rate was found to be better for the operation of thermal energy storage, especially if the charging period is below six hours. In addition, it was shown that increasing the aspect ratio of the thermal energy storage would result in a lower outlet temperature of the heat transfer fluid, which is ultimately beneficial to the CAES operation

Chapter 5 Mathematical modelling of the CAES system for a case study of Egyptian grid

5.1 Scope of the chapter

The main aim of this chapter is to investigate a CAES system for the Egyptian grid case study. The proposed plans for installing new wind farms are tested with the expected load demand by 2020. The performance of a proposed CAES system with thermal energy storage is tested for the case study using a dynamic MATLAB simulation, developed in Chapter 3. The performance will be tested for a 3 day period in summer when the load demand is at its highest for the Egyptian grid case. The results of the performance of CAES and how it could add value to the grid are discussed in details for the Egypt case study.

5.2 Methodology of the analysis

For this chapter, the MATLAB modelling is carried out for the base case study of Suez, Egypt. Initially the simulations results for an adiabatic system, with an added recuperator and a thermal energy storage, are presented first. Afterwards the simulation results carried out under different designs of the system explained previously are compared. The designs simulated include-

a. Diabatic system with no recuperator or thermal energy storage
b. Diabatic system with an added recuperator
c. Adiabatic system (with added recuperator and thermal energy storage) which is the main focus of this chapter

There are several main parameters that are monitored in detail when comparing the results of these simulations. These include the temperature and the pressure of air inside the cavern, and the heat rate (efficiency scale) for each system. Added to these is the temperature of the thermal energy storage in the case of the adiabatic system with added thermal energy storage. The second section of this chapter focuses on the analysis of the sensitivity studies for the best design. The sensitivity study will include sizing of the volume of cavern, the thermal energy storage sizing, and the maximum operating temperature of the heat transfer fluid. The results of each study are compared with the base case simulation in order to investigate the effect of each parameter.

5.3 Egyptian Case Study

5.3.1 General Energy Situation

Electric supply in North Africa, especially in Egypt, is a major issue as the power supply systems are struggling to meet the load on a daily basis and hence regular power cuts have become a routine practice in the Egyptian grid. The electrical energy load in Egypt increases annually as shown in Figure 5-1between 2007 and 2011 [MOEE, 2010]. The peak demand has increased by 26% from 2007 to 2011 with an annual increase of 6.5%. Therefore, based on the average rate of energy increase in the recent five years, it is expected that the electrical energy load will increase by 58.5% by 2020 compared to 2011 numbers..

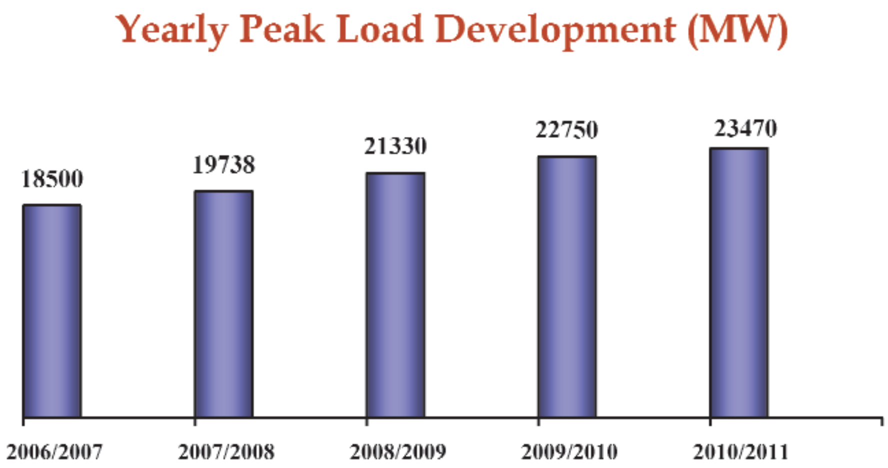

Figure 5-1 Yearly peak electrical energy load in Egypt

The variation of the energy load pattern in a summer day in Egypt is shown in Figure 5-2 [MOEE, 2010]. A very similar pattern takes place in winter but with lower load and lower peak load.

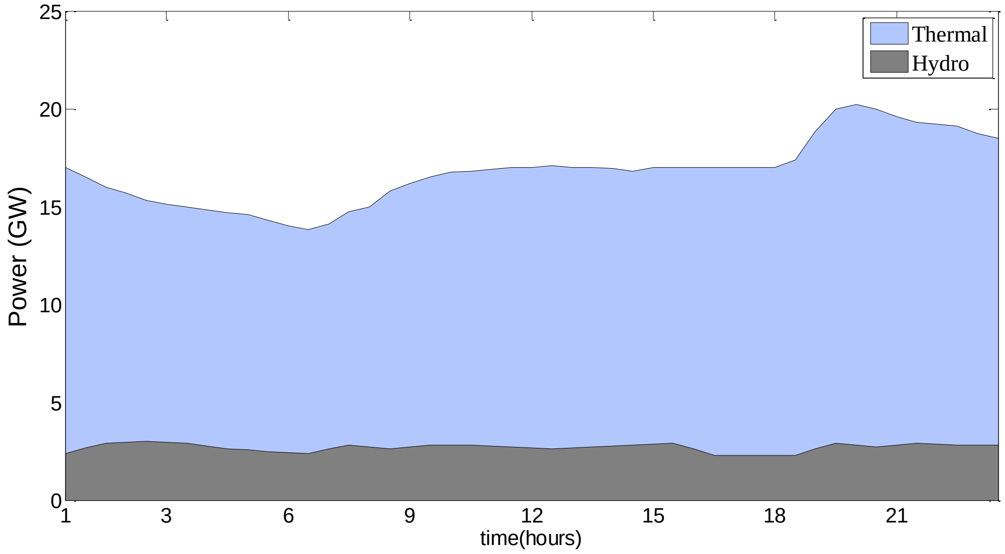

Figure 5-2 Variation of the energy load in Egypt in June 2009

The application of renewable energy technology in Egypt is very limited despite the large untapped resource for such energy sources, especially solar and wind energy. Currently, there are plans to increase the renewable energy supply in Egypt immensely in the next decade to supply 20% of the total electricity energy. Of this 20% energy share, 12% is expected to be supplied by wind energy. This assumes that the installed wind energy capacity will increase from 780 MW to 7.2 GW by 2020 [NREA, 2011]. Wind energy is to a certain extent widely available in Egypt and is particularly high in the Suez area. The wind map for Egypt is shown in Figure 5-3 showing the areas with highest wind speeds. Thus, it is expected that this massive increase in wind energy supply will cause large levels of penetration into the grid. As such, the issue of energy storage becomes essential in order to minimize the effect of wind intermittency on the stability of the fragile Egyptian grid [NREA, 2011].

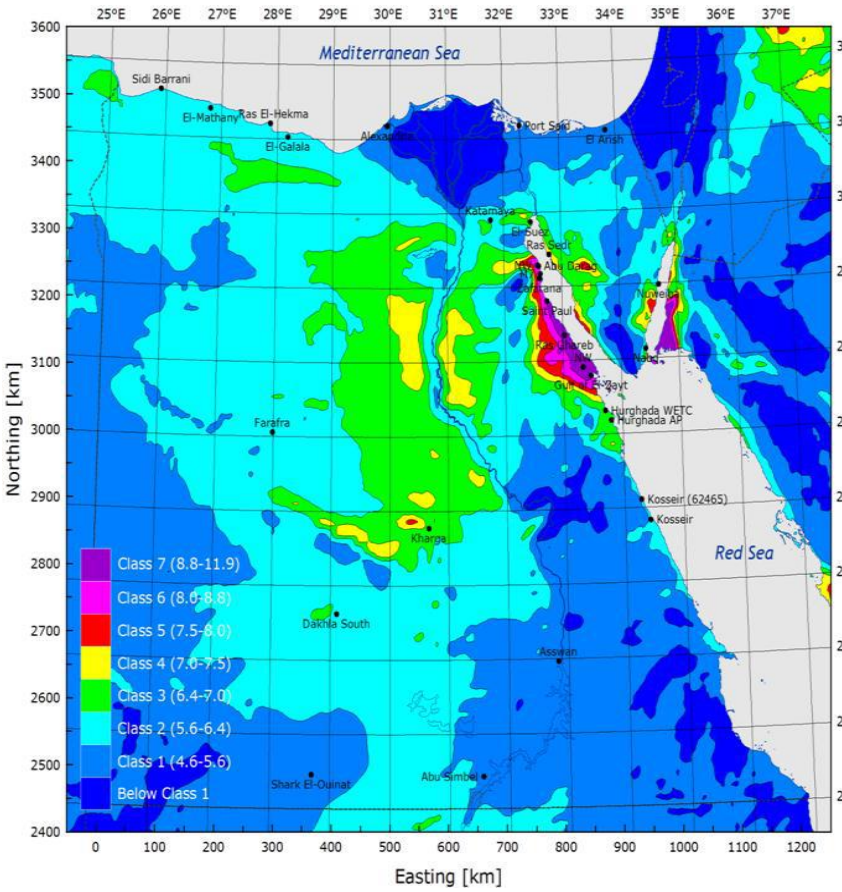

Figure 5-3 Wind Map of Egypt

5.3.2 Wind Electrical Supply in Suez Area

There are three planned projects in the Suez area totaling 580MW of installed capacity [NREA, 2011]:

a) 180 MW farm financed by the Spanish Government;

b) 200 MW farm implemented by MASDER;

c) 200 MW farm implemented in cooperation with German Development Bank (KFW), French Development Agency (AFD) and the European Investment Bank.

It is therefore important to analyze the feasibility of implementing CAES systems in Egypt in order to accommodate the proposed wind farms to be installed in the Suez Area. A model is developed using MATLAB software to simulate the effects of implementing the suggested CAES system on the overall electrical output from the wind farms planned in the Suez area. The model also looks at the implications on the overall electrical supply to the load, and how this could benefit the Egyptian grid and minimise the concerns of high levels of wind penetration.

The geology of the Suez area close to the site of wind farms is formed of basement rocks [Rabeh et al, 2003]. This geology is suitable for excavation, and thus creating an underground air reservoir (cavern) is possible. This type of geology is less favorable economically compared to molten salt for example as rock excavation could cost around $30/kWh compared to $1/kWh for salt caverns. However, several studies have been conducted on the possibility of operation of CAES in underground rock caverns in terms of air tightness and stability. Most of these have shown that this type of geology would be suitable as an underground cavern for CAES operation, with a possibility of operation under shallow depth for pressures between 45-80bars [Kim et al, 2012].

This chapter focuses mainly on the technical aspects of Compressed Air Energy Storage. Using the data from the Suez area, the next section will provide more details on the technical model.

5.4 Suez Area case study modelling

Focusing on the Suez Area in Egypt, this section discusses the modelling of the Suez CAES system including the simulation assumptions, followed by the design sizing of the different components of the system, and finally the operational results of the system.

5.4.1 Simulation Assumptions (System with added recuperator and thermal store)

Wind Power Estimation

As mentioned earlier, the planned projects in Suez, with a current installed capacity of 580 MW, is simulated as a single wind farm with 193 (V90-3MW) Vestas wind turbines of 3MW each. This wind turbine is chosen based on the compatibility of turbine characteristics with the weather data at the location. Table 5-1 shows the number of turbines and the characteristics of each. The power curve for the VESTAS wind turbines in this simulation is shown in Figure 5-4 [VETAS Manual]. Wind speeds data is collected from a location in the Suez Area upon which this model is based. The collected data for three summer days is presented in Figure 5-5. These data are used to size the various components of the CAES system.

Table 5-1 Turbine Parameters

Turbine Parameters	
No of turbines	193
Swept area (m^2) of each turbine	6362
Cut in speeds (m/s)	3
Cut out speed (m/s)	25

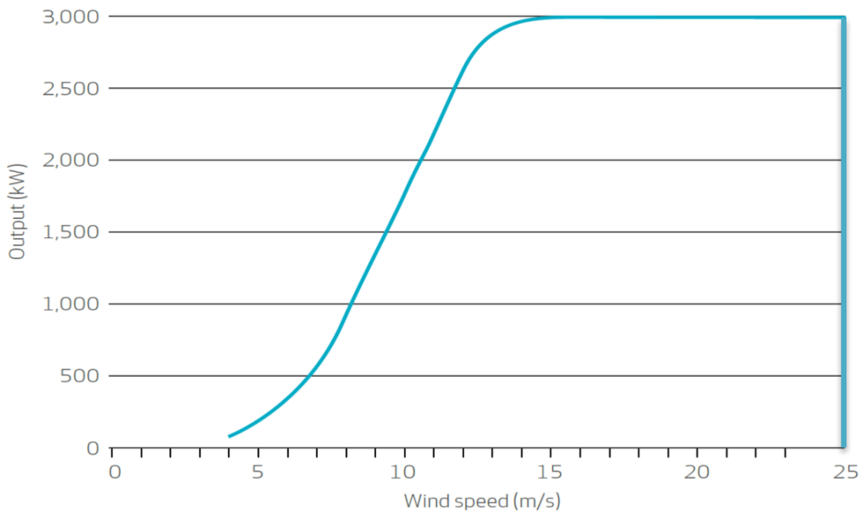

Figure 5-4 Power Curve of VESTAS V90-3MW Turbine [Vestas Manual]

As mentioned in section three, the electrical load demand in Egypt is expected to increase by 1.58 times compared to the current demand. Since the wind energy supply in Egypt is expected to reach 12% of the total electrical supply in 2020, the proposed wind farms in Suez would be 8% of the total wind supply. Therefore, the Suez wind farms will eventually represent around 1% of the total electricity supply in Egypt. An estimate of 1% of the expected 1.58 times increase in load demand in Egypt is taken as an estimate of the load supply in the modelling of the case study.

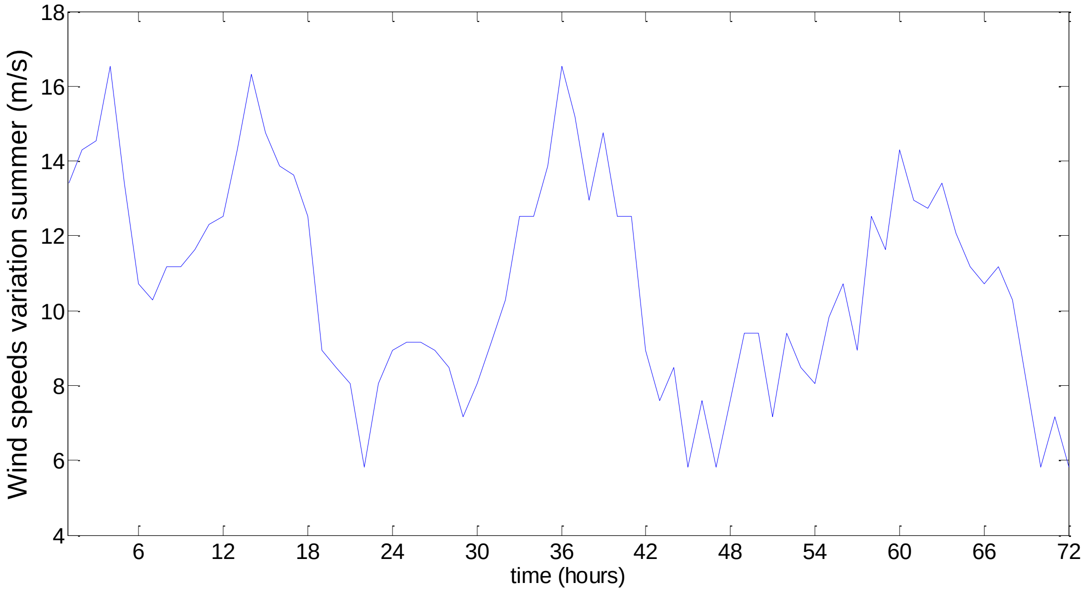

Figure 5-5 Hourly wind speed variation (summer)

Figure 5-5shows the data obtained from monitoring the Suez weather climate and wind speeds for a month in the summer. This data is used as input to the MATLAB model and is used to predict the wind energy potential at this location. Based on the obtained results, it is shown that the wind potential here is relatively high; varying between 6 m/s to 17 m/s under summer climate conditions. Another point observed is the daily variation of the wind speed over the three days period of the collected data. Also, the wind is highest at midday throughout the monitoring period.

Several other assumptions were made in order to run the simulations. For the cavern, the maximum allowable pressure and minimum allowable pressure in the cavern are based on the geology and are estimated at 75 bars and 45 bars respectively. These are based on previous studies of CAES systems for similar geologies of the Suez area [Kim et al, 2012], with a maximum operating temperature of air in the cavern figuring around 373K.

In addition, heat exchangers effectiveness is assumed at 85%; while the temperature of the cavern wall is assumed to be 303K.

For the design of the adiabatic system with an added thermal energy storage and a recuperator, the concrete used as a storage medium was of thermal conductivity 1.4 W/mK, a specific heat capacity of 971J/kg K and a density of 2400kg/m^3[Lamond et al 2006]. The heat transfer fluid chosen for this simulation is mineral oil. The mineral oil has good thermal characteristics and temperature range (up to 350˚C) which makes it a good medium of heat transfer between the air stream and the thermal energy storage.

Different cooling modes are set for the adiabatic CAES system depending on the temperature of the compressed air after the heat exchange with the thermal fluid to prevent the temperature of compressed air entering the cavern from getting too high.

Table 5-2. Cavern operation parameters

Cavern Parameters Assumptions	
Maximum pressure (bars)	75
Minimum operation pressure (bars)	45
Maximum Temperature (K)	373
Temperature of surrounding (K)	303

Table 5-3. TES Parameters(for design with added thermal energy storage)

TES Parameters	
Heat transfer fluid maximum temperature (°C)	**37**5
Thermal energy storage thermal conductivity($W/m.K$)	1.4
Thermal energy storage Density(kg/m^3)	2400
Thermal energy storage Specific Heat ($J/kg.K$)	**971**

5.4.2 Design Sizing Results

After sizing the CAES system components, the numerical simulation model was used to predict the operational behaviour of the system under real conditions. The input parameters of the load and the wind speeds data of the Suez area are used to calculate the percentage of load demand, the wind power expected from the proposed plants and the excess/deficiency in the power supply which are plotted Figure 5-6. The positive values indicate that the wind energy supply is higher than the load demand, whereas the negative values show that the wind supply is lower than the load. Thus, according to Figure 5-6, the air compression process starts when the excess/deficiency power values are positive. This lasted for around 17 hours during the first compression stage, and then the expansion started when the excess/deficiency power values are negative, which lasted for around 13 hours during the first expansion stage. The charging and discharging periods are of course diversifying due to the variation of the supply and demand.

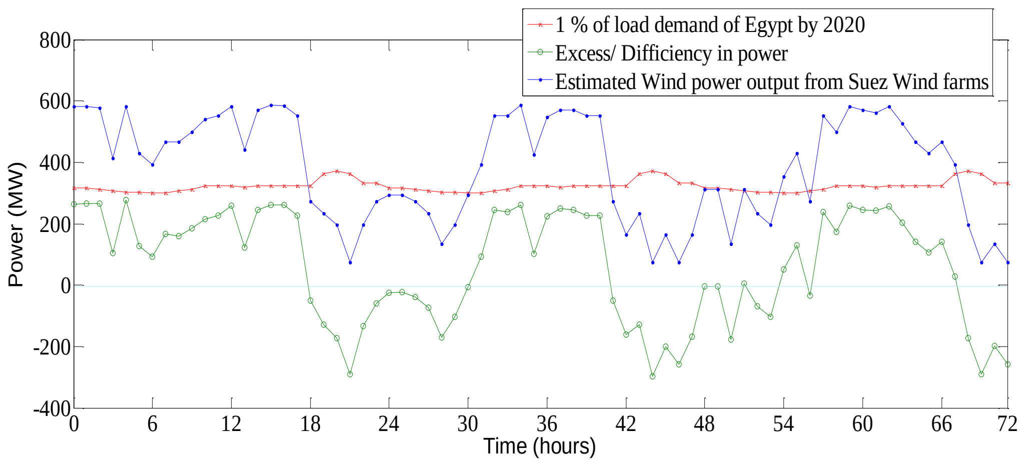

Figure 5-6 Hourly variation of the load, wind power and excess/deficiency power

5.4.2.1 Compressors Sizing

Concerning the compressors, these are divided into several parallel chains. The number of chains is determined by the desired lowest output following the parallel chains method explained in Chapter 3. In this 4 parallel chains of compressors were selected to allow catering for relatively low power, or 1/15 of the maximum power available for the compressors. During the sizing of the system using MATLAB, it was found that for the data of wind and load demand for Suez from Figure 5-7, the maximum compressor power calculated from the highest surplus power is 277.5 MW. Since this system uses parallel chains, therefore the minimum power that this design can cater for is given by the following:

$$Lowest\ rated\ chain = \frac{PSurplus_{max}}{(15)}$$

$$Lowest\ rated\ chain = \frac{277.5W}{(8+4+2+1)} = 18.5MW$$

Figure 5-7 shows the compressors chains with the maximum power in each chain. There are 4 parallel chains with the lowest rated at 18.5MW and the highest rated at 148MW, there are heat exchangers between each compressor and the following compressor for intercooling followed by an air cooler for each stage. The heat transfer fluid on the other hand flows in a series fashion.

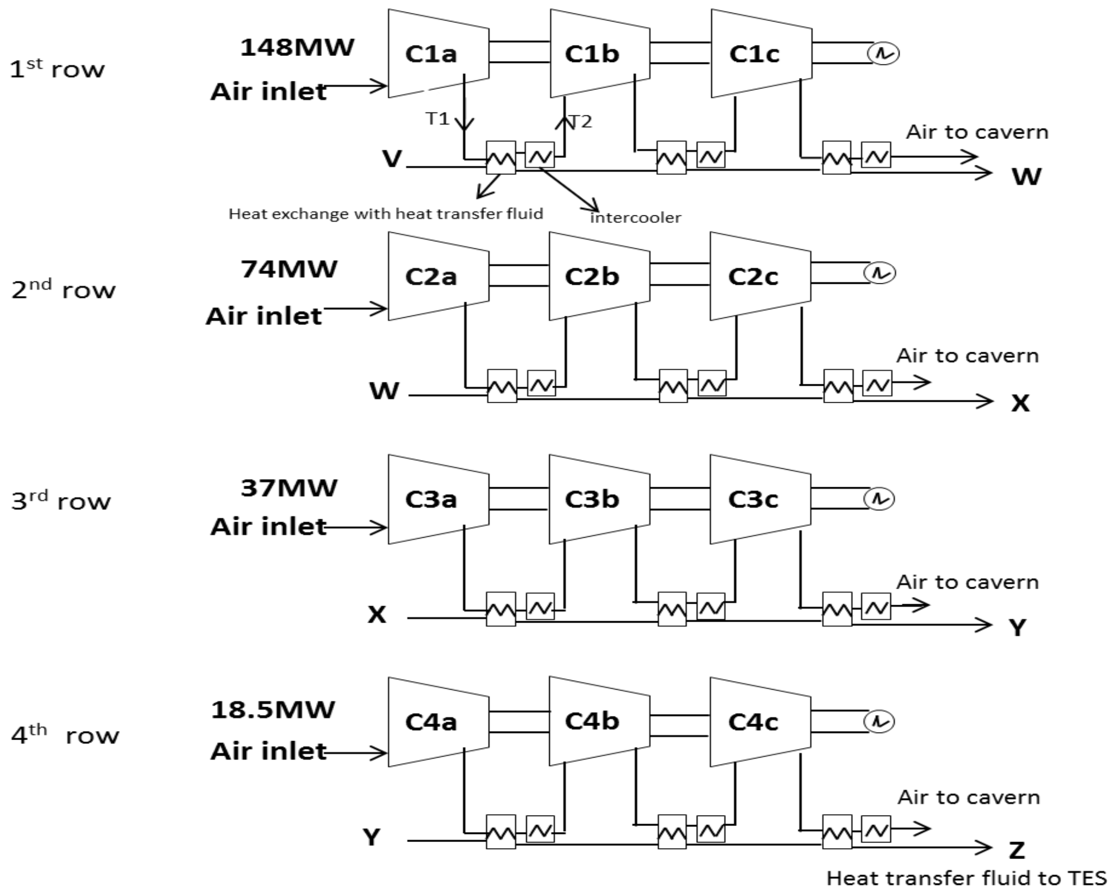

Figure 5-7 Compressors array setup

For this configuration, the four parallel chains almost always don't operate together at the same time, which is dependent on the surplus power. For example, if the surplus power is 218MW, only chain 1 and chain 2 are in operation, while if the surplus power is 100MW, chains 2 and 3 are in operation. The 4 chains can only operate simultaneously if the Surplus power is above 267MW for this configuration.

5.4.2.2 Cavern Sizing

The sizing of the volume of the cavern is performed using a method which ensures that the cavern is big enough to allow for the system to be in operation at all times. This means that for the sizing method used, the cavern should never be full nor empty. The volume of the cavern is designed based on the mass flow rate of air incoming or leaving the cavern. It also uses the number of consecutive hours in which the system is in compression mode or expansion mode, which is calculated by the program using historical data (excess and deficiency values calculated from wind and load demand data). The volume of the cavern to meet the above conditions is calculated as. 1,110,000 m^3 using equation (3-3).

5.4.2.3 Turbine Sizing

As for the turbines' sizing, this is performed using the same method of compressors' sizing. Based on the weather and electrical load data shown in Figure 5-6, the maximum power output needed from the turbines, which is the lowest value in the Excess/Deficiency curve, is around 300MW leading to 4 parallel chains with the maximum power output expected from each chain as shown in Figure 5-8, which is calculated in the same manner as that of the compressors (Max Power output/15 for the lowest rated chain). Figure 5-8 shows the turbine chains setup with the air from the cavern enters the expansion stage (after heat exchange with thermal energy storage in case of adiabatic CAES system). There is also a recuperator after the 1st stage of expansion in each of the parallel chains followed by a combustion chamber before the 2nd stage of expansion.

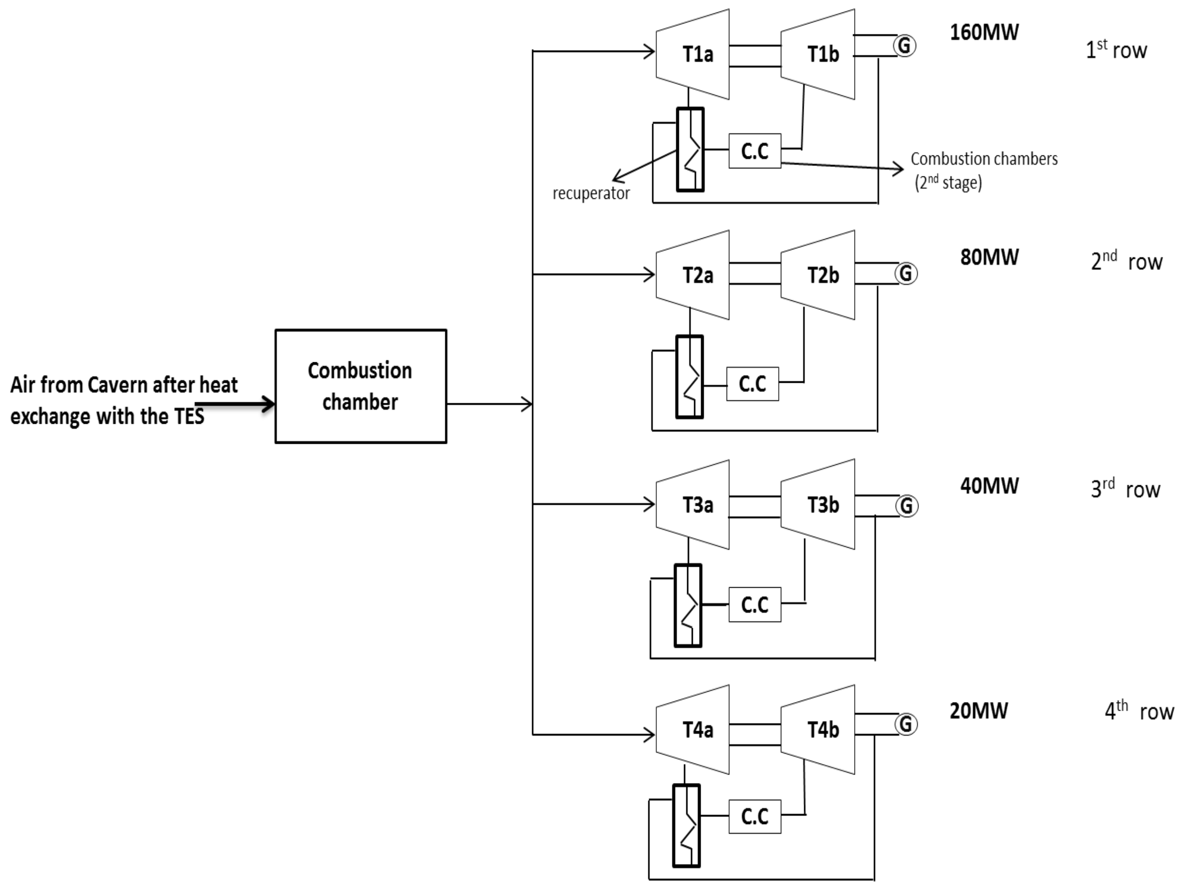

Figure 5-8 Turbines array setup

5.4.2.4 Thermal energy storage (TES) sizing (for the design with added thermal energy storage)

The TES sizing was performed by using data compiled from CFD analysis, which was discussed in Chapter 4, to find the optimum configuration of the thermal energy storage. These in particular should maximize the overall efficiency of the system, which is determined based on the amount of output power produced and the amount of heat needed from the combustion chambers. The sizing of the thermal energy storage was performed by calculating the thermal energy storage capacity needed for the number of consecutive hours the compressors are expected to operate. A total thermal energy storage volume of 11,000m^3(using equation 3-4) is required for storing the heat energy from the compressors in this study. The thermal energy storage system is divided into multiple smaller units one of which is shown in Figure 5-9. The thermal energy storage implemented the same diameter of pipes and distances of gap between pipes as the modelling used in the CFD modelling,

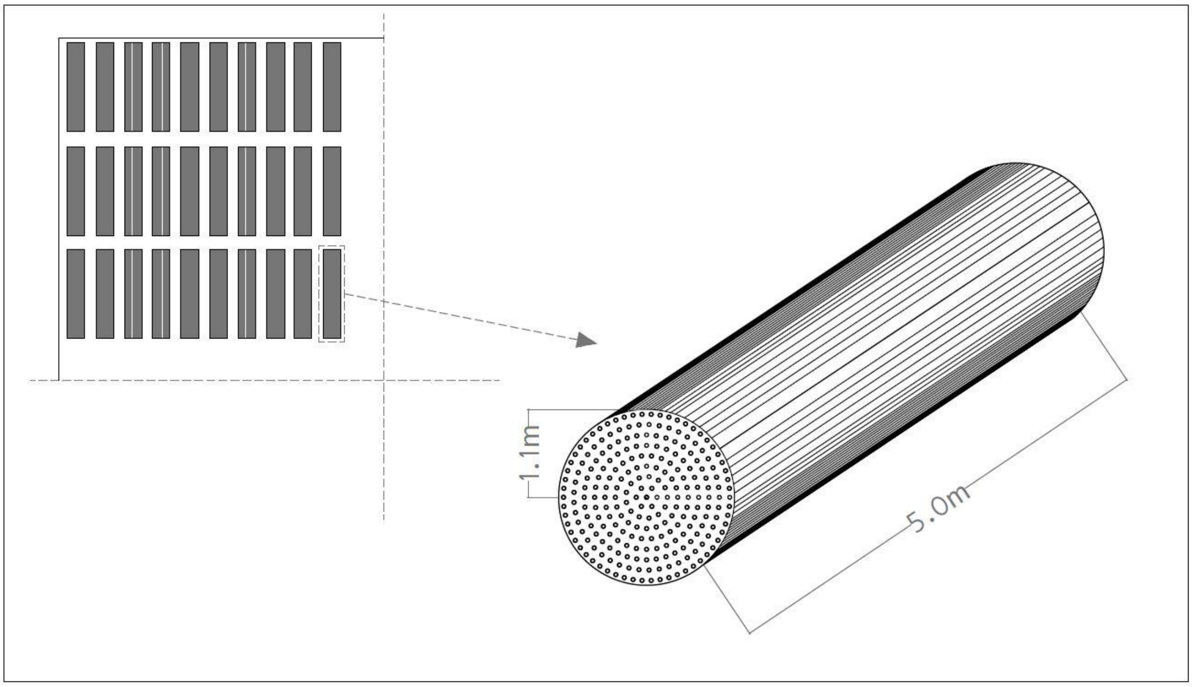

Figure 5-9 Thermal energy storage system configuration

5.4.2.5 MATLAB results comparison with CFD modelling

In this section, the CFD modelling results are compared with the MATLAB results (small scale equivalent to CFD modelling carried out in Chapter 4) for the thermal energy storage in order to test the results of thermal energy storage modelling in the MATLAB. The MATLAB program simulation in this case implemented a design of the thermal energy storage size and configuration identical to that used in the CFD modelling (smaller scale) including the diameter of pipes, the gap distance between the pipes as well as the number of pipes. The comparison was done for different speeds of inlet velocities to accommodate for both laminar and turbulent flow of the heat transfer fluid in the thermal energy storage system.

1st simulation (using an inlet velocity of 0.1 m/sec)

For this simulation, the flow is turbulent and the temperature of concrete with time at the same sensor positions for MATLAB and CFD is demonstrated in Figure 5-10.

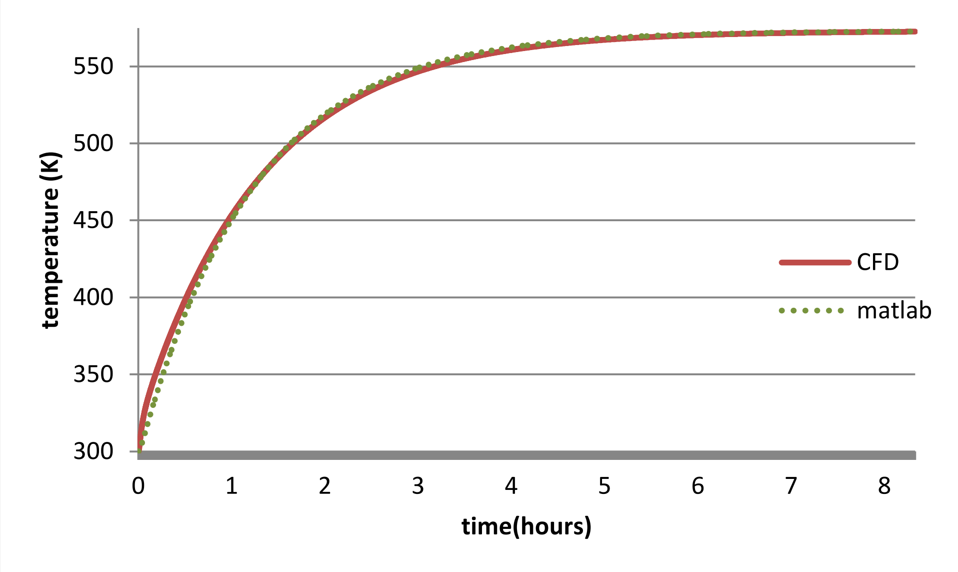

Figure 5-10 CFD and MATLAB results using an inlet velocity of 0.1m/sec

As shown in the aforementioned figure, the MATLAB curve is very close to the CFD simulation. The results for the relative discrepancy are displayed in Figure 5-11 where the discrepancy does not exceed 2% between the simulations in both.

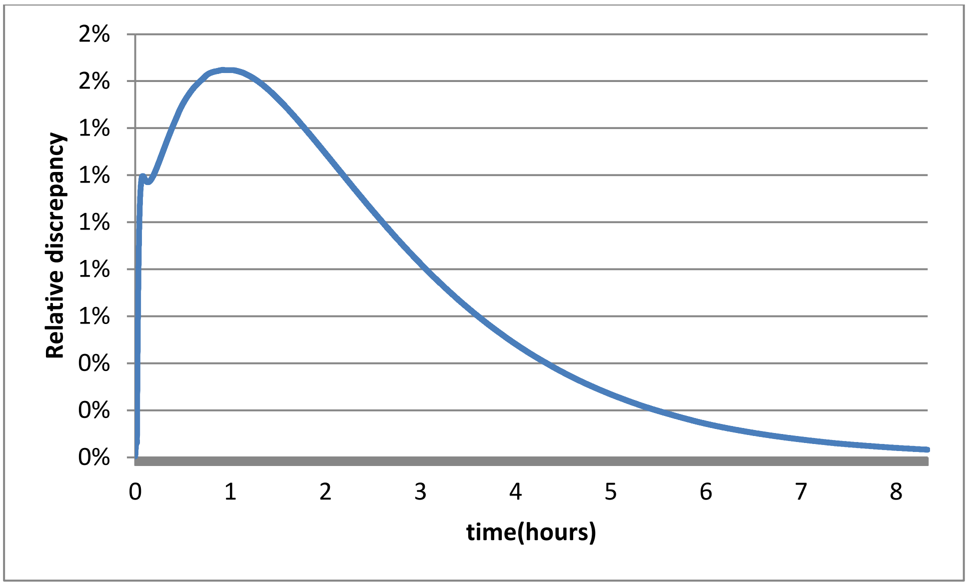

Figure 5-11 Relative discrepancy between CFD and MATLAB for an inlet velocity of 0.1m/sec

2nd simulation (using an inlet velocity of fluid of 0.01m/sec)

This simulation shows a laminar flow of the heat transfer fluid in the thermal energy storage. The results of the validation of the programs are shown in Figure 5-12 and Figure 5-13.

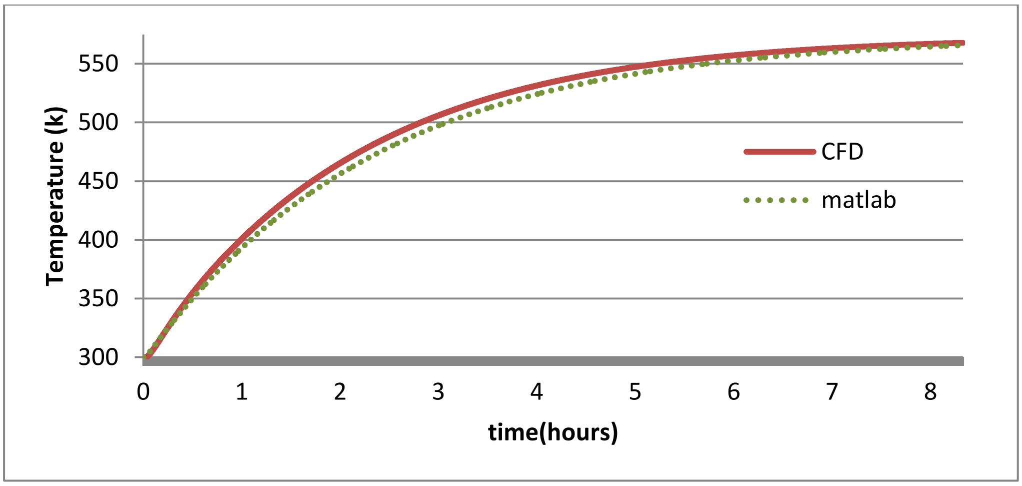

Figure 5-12 Concrete temperature for CFD and MATLAB using an inlet velocity of 0.01m/sec

Once more, the relative discrepancy is also very low, within 2% for the entire operation, between the two simulations using CFD and MATLAB for the same design of the thermal energy storage.

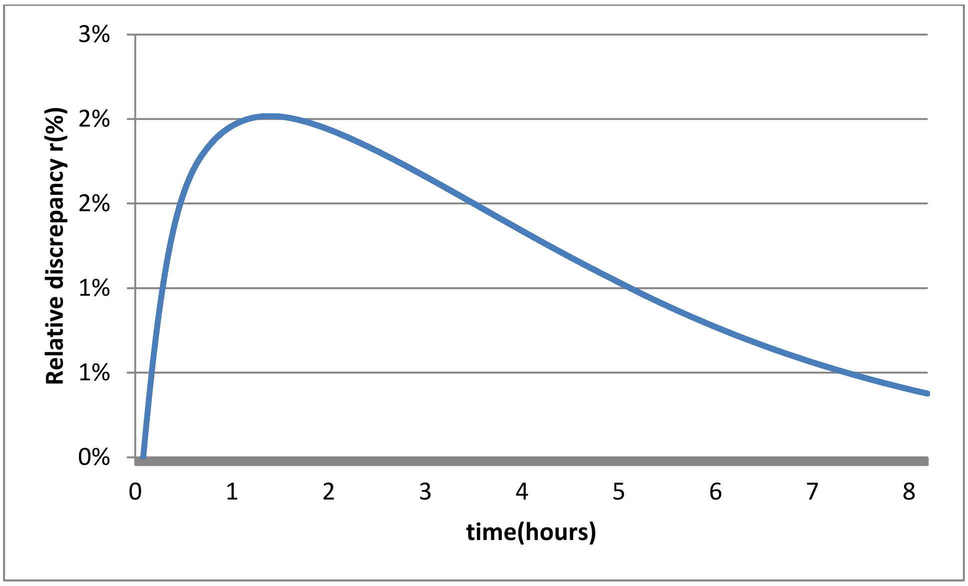

Figure 5-13 Relative discrepancy between CFD and MATLAB for inlet velocity of 0.01m/sec

5.4.3 System Operational Results

5.4.3.1 Comparison of different designs

To begin with, Figure 5-14and Figure 5-15 show the variation in the temperature of the air in the cavern and the combustion power requirement for the different configurations of the system. For the case of the adiabatic system with the added thermal energy storage, the temperature of the air in the cavern is higher than in the two cases of using a recuperator and the case of the diabatic system. For the cases of diabatic system and the system with a recuperator, an assumption is made (based on the Huntorf and the McIntosh plants) where the heat absorbed from the air using the intercoolers in the compressor stage is dumped. Therefore, the rise in air temperature in the cavern is relatively low compared to the case of an adiabatic system. In the case of the adiabatic system, the temperature variation is quite higher due to the fact that in this case, there is a closed loop cycle where the heat transfer fluid circles between the thermal energy storage and the compressors when the charging mode is ‘on’. While an air cooler is present after each heat exchanger in the compression stage, it is set to cool the air by a certain amount. Therefore, as the temperature of the thermal energy storage gets higher, the heat transfer fluid temperature coming out of the thermal energy storage is high. This then becomes the inlet temperature of the heat transfer fluid going to the heat exchange with the air coming out of the compressors. This will result in a reduction of the temperature gradient between the air after the compressors and the heat transfer fluid, which results in a reduced heat exchange causing the temperature of air to be higher compared to the other designs. Therefore, the temperature variation of the air in the cavern variation becomes higher, which is also valid for the discharge mode.

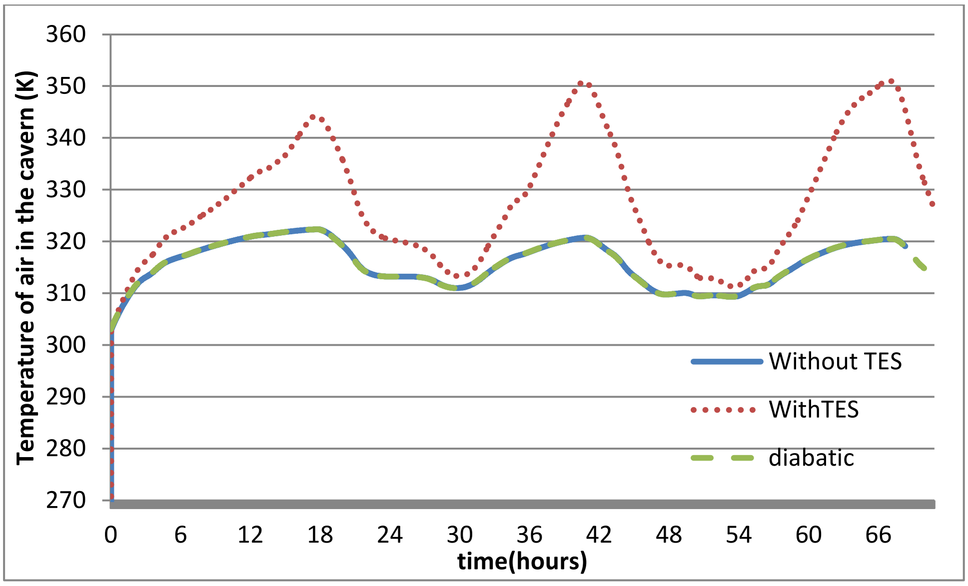

Figure 5-14 Different designs effect on air temperature in the cavern (K)

Furthermore, Figure 5-15 shows the combustion power required from the different designs of the system. In this case combustion power (positive only in the discharge mode) is lowest using the case of an added TES plus the recuperator, followed by the design of a diabatic system with an added recuperator and finally the diabatic system with no recuperator. This can be explained by the fact that when using a diabatic system, there is no heat recovered to increase the air temperature before entering the turbine. As such, the heat required becomes highest in this case. However, using an added recuperator recovers some of the heat from the turbine exhaust and hence reduces the heat required from the combustion chambers. Adding a TES to the recuperator also results in a decrease in the required power from the combustion chambers. This is because there is extra heat recovered from the thermal energy storage added to the heat recovered from the turbine exhaust, therefore less combustion power required.

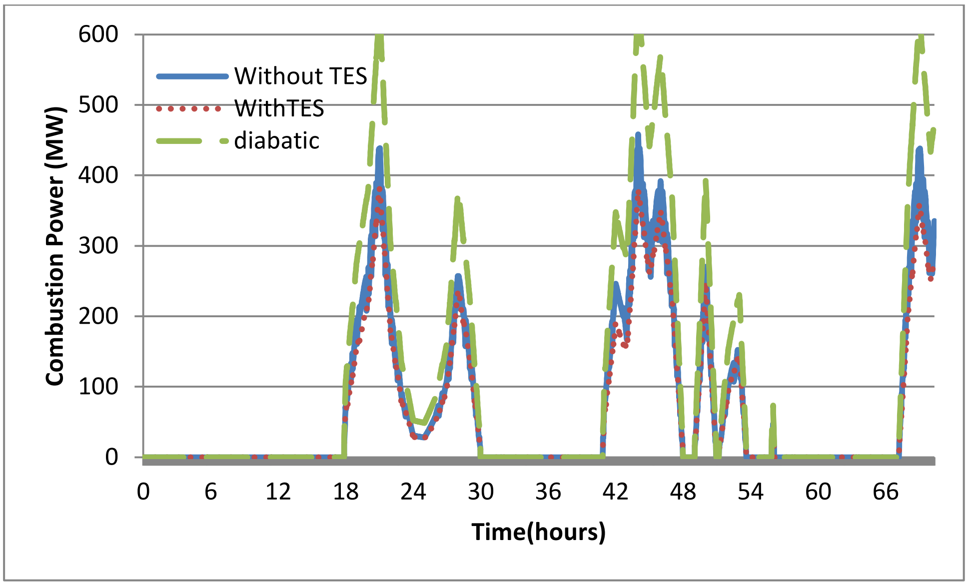

Figure 5-15 Combustion power requirement for different designs

Table 5-4 Heat rate for different designs

Design Type	**Diabatic**	**diabatic (Recuperator without TES)**	**Adiabatic (TES + Recuperator)**
Heat rate(KJ/kWh)	6000	4450	4062
Efficiency (%)	42	56.6	62

5.4.3.2 Adiabatic system with added recupertor and thermal energy storage

In this section the operational results for the main parameters in the CAES system are discussed for the best design system using an adiabatic system with an added thermal energy storage. Figure 5-16displays the pressure variation of the air in the cavern during 3 days of system operation. These are the results of the MATLAB simulation with the variation of the pressure which are calculated and plotted against the operation time. As shown, the pressure increases when there is a surplus of power reaching around 68 bars after 17 hours of operation, and then the expansion mode starts. The pressure never reaches the minimum allowable value of 45 bars, indicating that there is adequate compressed air to meet the full demand during the discharge period.

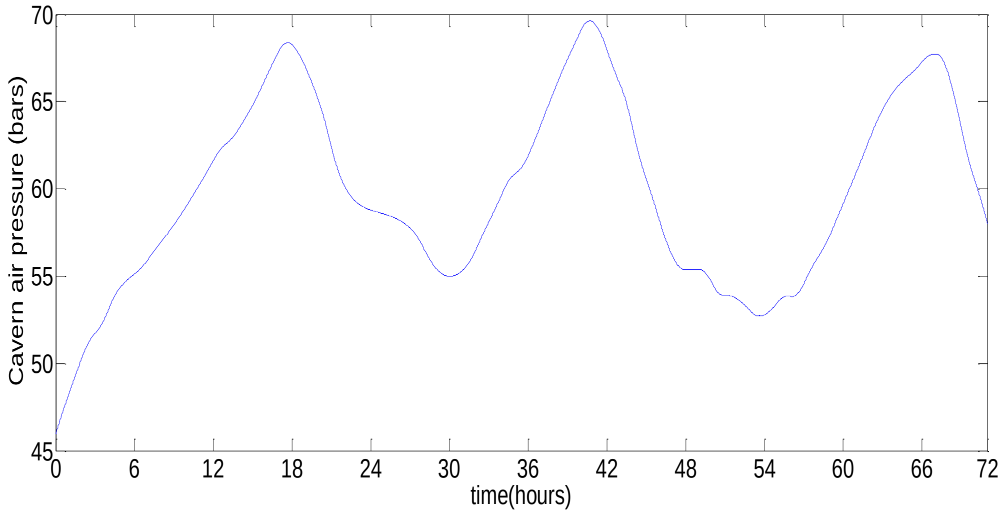

Figure 5-16 Hourly variation of the cavern air pressure (bars)

Figure 5-17 illustrates the temperature variation of the air in the cavern which follows a pattern quite similar to the pressure variation in the cavern. The temperature increases during compression stages and decreases during expansion processes as expected. Specifically, the temperature increases from around 303K to 344K after 17 hours of compression, then as expansion starts, the temperature decreases back to almost 313K after 13 hours. The rate of change of temperature is changing with time, which is dependent on the mass flow rate in and out of the cavern.

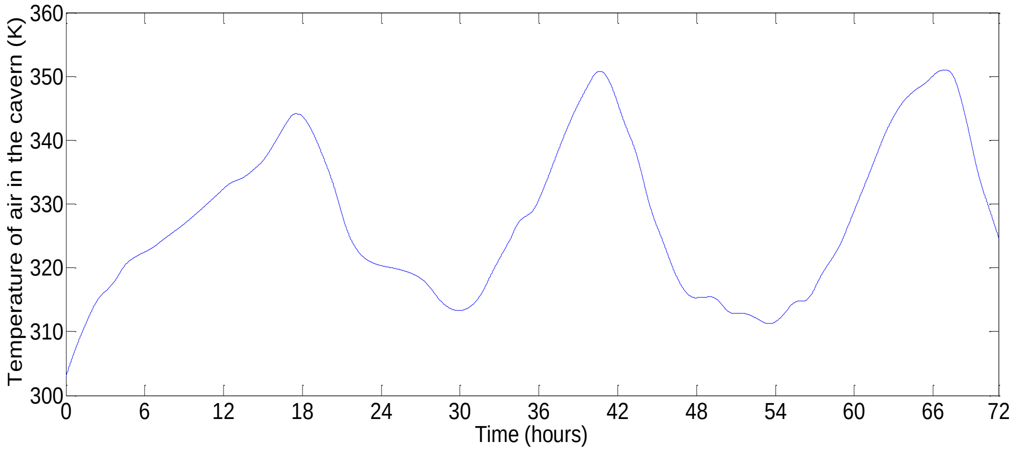

Figure 5-17 Hourly variation of cavern air temperature (K)

Figure 5-18shows the variation of temperature in the thermal energy storage during 3 days of the operation period. The energy in the TES is important to preheat the discharged air from the cavern before entering the combustion chamber for further heat addition and then expansion through the turbine.

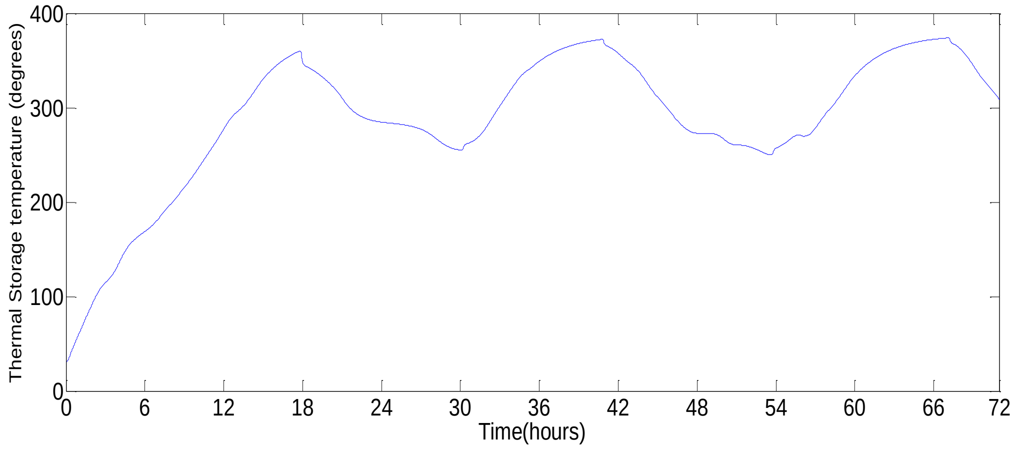

Figure 5-18 Hourly variation of thermal energy storage temperature (°C)

As shown in Figure 5-18the temperature in the concrete block increases from around 30°C (303K) to reach a maximum of 373°C (646K) for the volume of concrete chosen in this system. It can be observed that combustion chambers are used almost all the time during the discharge mode in order to supply the extra heat required for the air before entering the turbine as shown in Figure 5-19. Also, since the highest temperature reached by the concrete block during the operation is around 646K and the turbine inlet is set at 1000K; this means that at least 350K is required at the expansion stage using the combustion chamber. Additionally, Figure 5-19shows the heat added by the combustion chambers to the air during the expansion process. It is obvious that the heat added by the combustion chambers varies with time according to the heat available to the thermal energy storage of the turbine operation. Also, the required energy from the combustion chamber is always zero during the compression time.

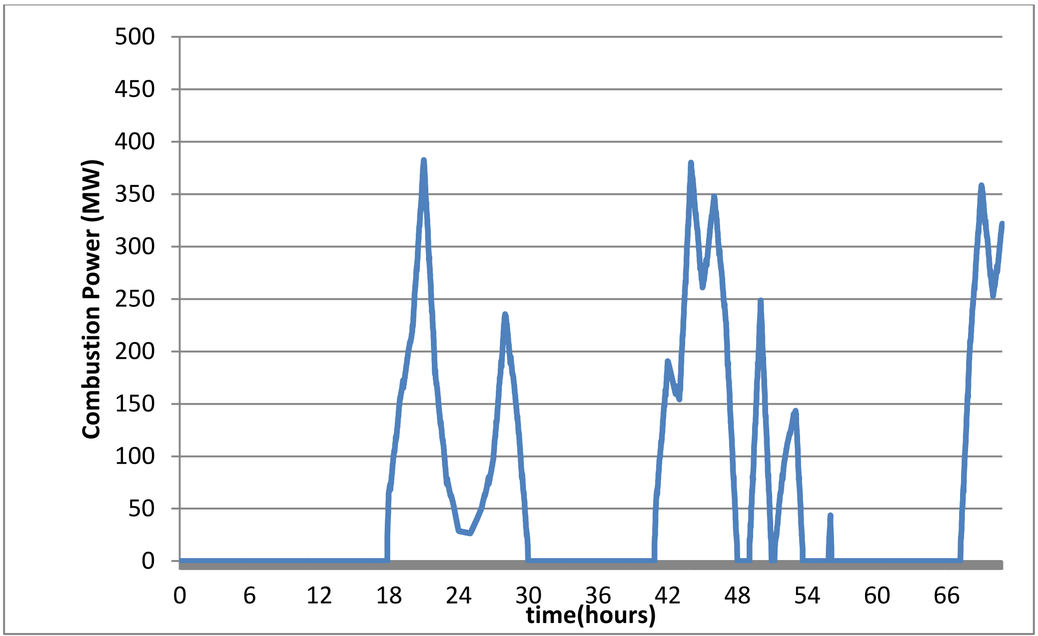

Figure 5-19 Hourly variation of the combustion chamber Power

On another note, Figure 5-19 shows the benefit of implementing a CAES system for large scale integration of wind into the grid. When there is excess power, the shaded blue area shows the power supplied to the CAES system (charging mode). The shaded grey area shows the amount of power supplied from the CAES system to the grid when the demand is higher than the supply. The CAES system delivers almost the entire power supply that is needed to cover the deficiency in power supplied by wind.

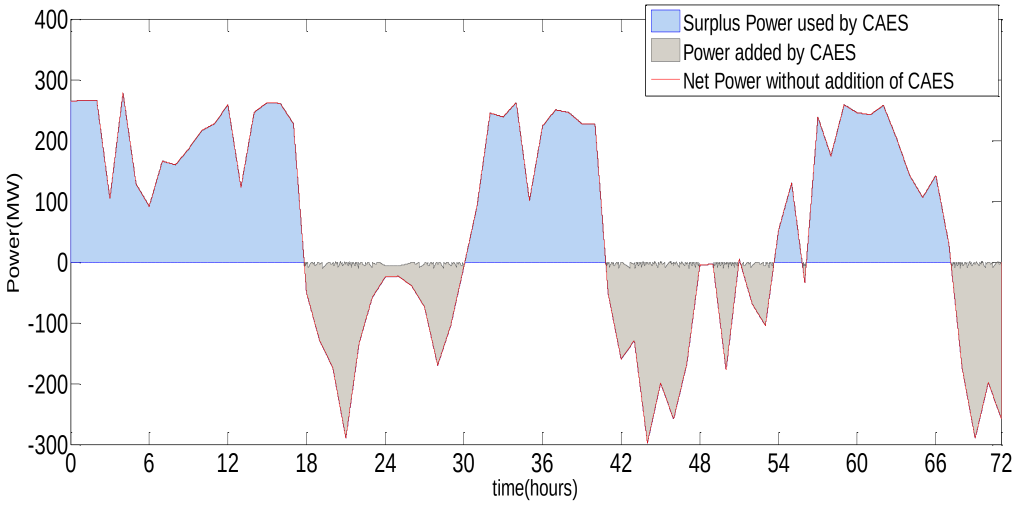

Figure 5-20 Hourly net power delivered with and without CAES

5.4.4 Sensitivity Analysis for Suez Area case study

The previous analysis has exposed some of the assumptions that were taken into account when simulating the Suez Area case study. As such, some of the variables in the system are tested for sensitivity to find out the extent of an effect on the operation of the system. In particular attention is given to the temperature and pressure of air in the cavern, the thermal energy storage temperature, and the combustion power requirement of the combustion chambers. The heat rate is also displayed for the sensitivity study. The main variables tested are-

1. Cavern Volume
2. Thermal energy storage volume
3. Operation temperature of the heat transfer fluid
4. Operational pressure range of the cavern

5.4.4.1 Volume of the cavern

As explained earlier, the cavern volume was calculated on the basis that it would be big enough to accommodate the entire operation without the need of any shut down of the cavern being full during compression or empty during expansion. The number of consecutive hours of either compression or expansion is taken into account in the design of the cavern volume. As seen in the base case study, the cavern volume had enough size for the operation of the system (the system never reached either maximum pressure or minimum pressure). Different volumes of cavern are simulated and their results are shown as follows.

The sensitivity simulations carried out for cavern volume variation from 80% to 120 % of the volume of cavern calculated earlier for the design of the operation of the system.

Figure 5-21 shows the effect of changing the volume of the cavern from 80% of base case (1.1Million m^3) to 120% of base case. Using 80% of the volume of the base case, results in an operation shutdown twice during the 3–day operation period for a total time of around 6 hours when the pressure of air in cavern reaches 75 bars (maximum pressure allowed). This means that even when there is excess power from the wind farms, the CAES system will not be able to use that power due to the cavern being over pressurized. On the other hand, using 120% of the cavern volume results in the CAES system never reaching the maximum or minimum pressure allowed, thus making the system available at all times. However, using 120% means extra costs of the system with no added advantage in energy supply. Therefore, using the base case shows better operation pressure results.

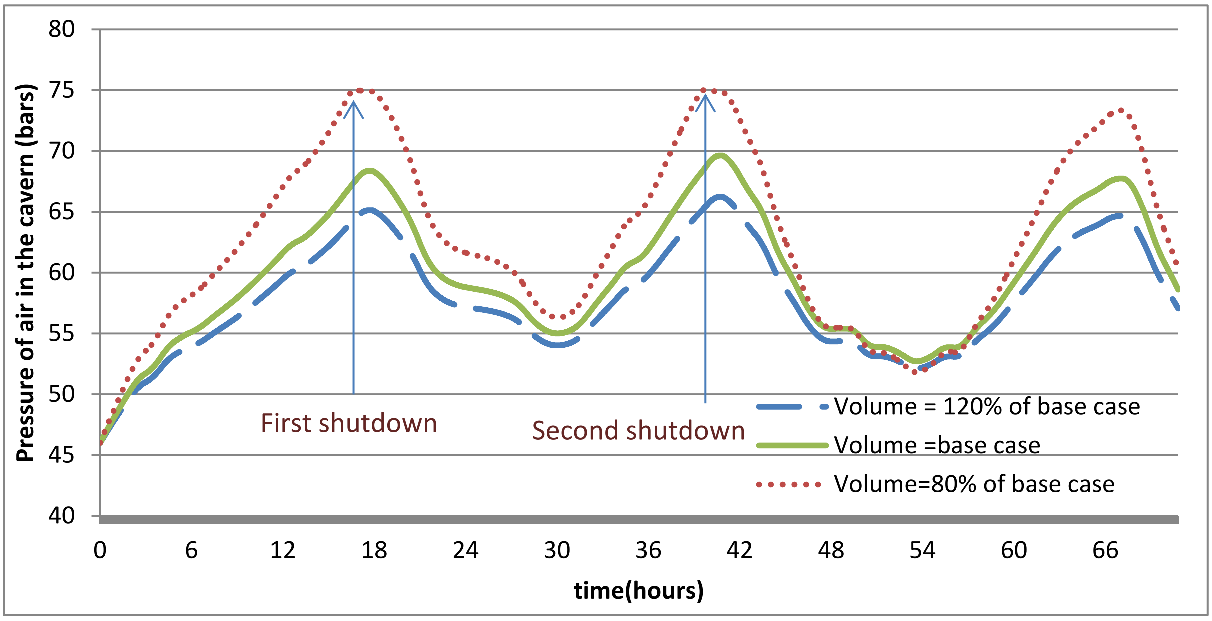

Figure 5-21 Effect of cavern volume on the pressure of air in the cavern

Primarily, Figure 5–22 shows the effect of different cavern volumes on the temperature of air in the cavern. The pattern is similar to that of the pressure of air in cavern. In the case of 120% of cavern volume, the temperature is always lower than the maximum operational temperature compared to that of the base case, which does not have any effect. This is due to the temperature of air in the cavern being lower than the maximum allowable operational temperature at all times. However, using a smaller volume of cavern results in shutting down the compressors when the system reaches maximum pressure as mentioned before. Yet in this case, it is worth mentioning that, when the CAES operation stops after around 17 hours, the temperature of air in the cavern does not stay constant. Since the wall temperature is at 323K, some heat is lost to the surrounding ground as the temperature of air is higher than that of the cavern wall. Therefore, there is a slight decrease in temperature of air in the cavern until the expansion starts and hence the temperature starts to drop further as a result of air discharge.

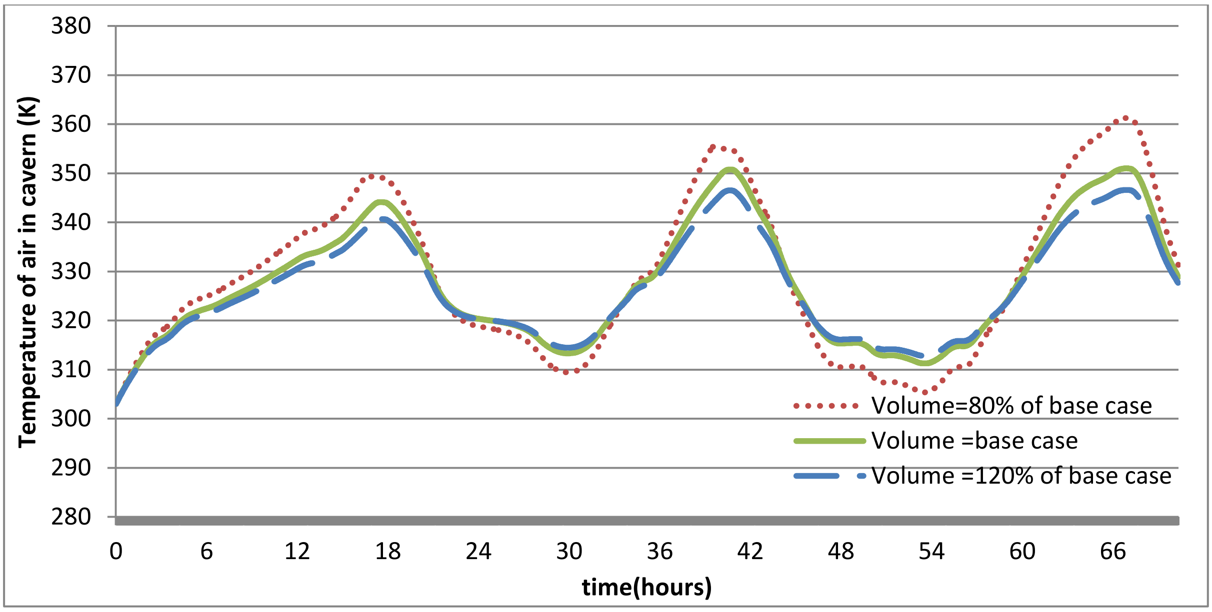

Figure 5-22 Effect of volume of cavern on the temperature of air in the cavern

Figure 5-23 shows the temperature of the thermal energy store using different volumes of cavern. It is obvious from the figure that the curves of the base case and 120% of the base case are almost identical. Since, the system is operational for the entire time with no shut-downs and the inlet temperature to the TES from the compressors is the same, hence there is a same temperature of thermal energy storage. However, using 80% of the volume of the TES yields different results. The reason for this is that there is an operation standstill after around 17 hours due to the cavern being full. Therefore, the thermal store temperature remains constant for the case of 80% of volume of cavern, while the temperature keeps increasing for the other cases. The rate of change of temperature after this is slightly higher using a smaller volume of cavern as the temperature of the thermal energy storage is lower. Hence, there is a higher temperature gradient between the inlet temperature of oil after a heat exchange with air from compressors and the temperature of the thermal energy storage.

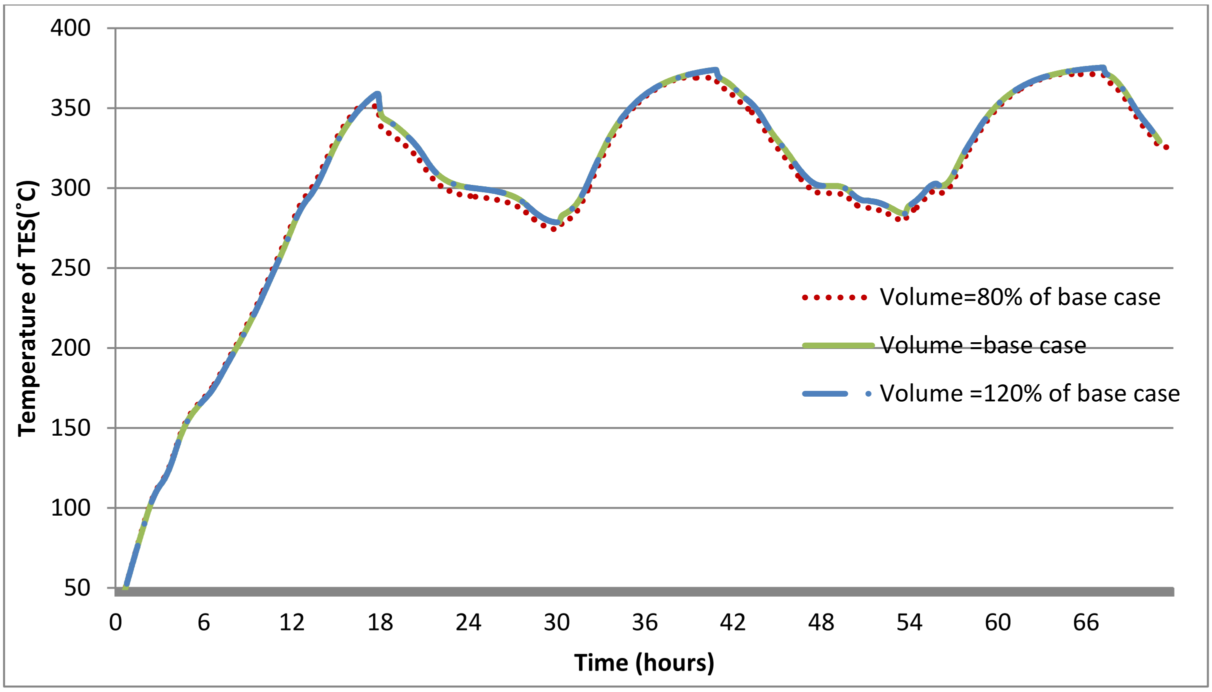

Figure 5-23 Effect of cavern volume on temperature of thermal store

Table 5-5 Heat rates for different volumes of cavern

Volume of cavern m^3	**80% of Base (888,000)**	**Base case (1,110,000)**	**120% of base case(1,332,000)**
Heat rate(MJ/kWh)	4040	4062	4080
Efficiency (%)	62.3	62	61.7
Power available for storage(MWh)	6667	7778	7778
Total Power Output (MWh)	3527	3527	3527

Also, Figure 5-24 shows the benefit of adding a CAES system to the net power of the wind turbines and the load demand for using 80% of the volume of the cavern. However in this simulation (80% of cavern volume), the power taken by CAES, represented by the blue shaded area, is not using all the surplus power available for the CAES system. This is due to the temperature of air in the cavern reaching the maximum operating pressure set at 75 bars, resulting in the system shutting down 2 times during the 3 day period of operation.

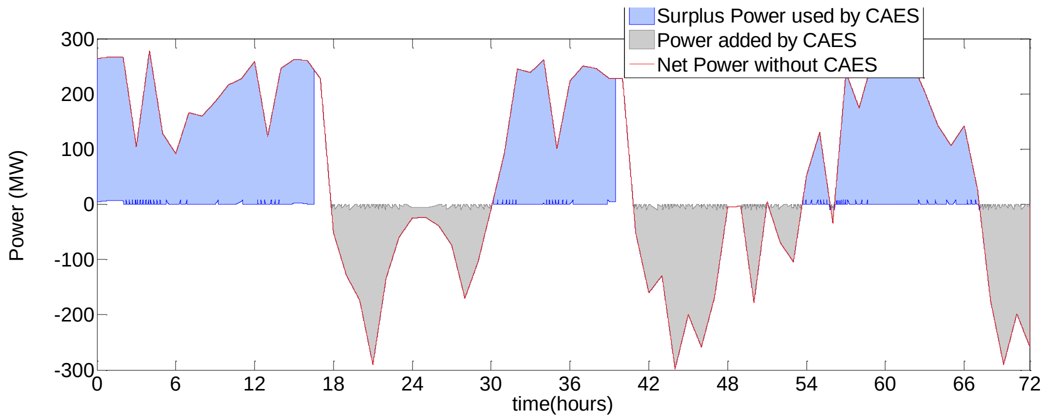

Figure 5-24 Effect of adding CAES on net power for 80% of the cavern volume

Remarks on the effect of the volume of cavern

During these tests, it was clear that the size of the volume of the cavern mainly affects the temperature and pressure variation of air in the cavern, with minimal effect on the combustion chamber power. Using a smaller volume of cavern would reduce the economic cost of building a new cavern. However using a smaller cavern would result in shutting down the compressors even when there is excess power to be used.

On the other hand, using a higher volume of cavern compared to the base design case, would result in lower temperature and pressure of air in the cavern, which is better from a safety perspective to operate at a temperature and pressure lower than maximum points. However, building a bigger cavern would result in more overall cost to the CAES system.

5.4.4.2 Size of the Thermal Energy Storage

For the second test, the size of the thermal energy storage was varied from 5000 $m^3$to 15000 m^3 to test how it affects the performance of the system.

To begin with, Figure 5-25 shows the effect of the volume of the thermal energy storage on the pressure of air in the cavern; where the base case is11000m^3 of thermal energy storage.

Using higher volume of thermal energy storage will allow for more heat extraction from the air going into the cavern leading to lower temperature of air going to cavern and that therein. This in turn leads to lower variation of pressure of air in the cavern which is shown in Figure 5-25. However using lower volume of thermal energy storage means that the rate of temperature increase of the thermal energy storage is higher and so the rate of increase of the heat transfer fluid temperature is higher which results in the heat transfer fluid reaching the maximum temperature of operation for the heat transfer fluid which was set to 377˚C. When the heat transfer fluid reaches its maximum operating temperature, no heat is extracted from the compressors stages by the heat transfer fluid, which means that air is only cooled by the air coolers present after the heat exchanger stage which is set to cool the air only by a certain amount. Therefore, the temperature of air going into the cavern is much higher, translating into a higher rate of increase of temperature of air in the cavern, as well as a higher rate of change of pressure during the operation. This results in the system shutting down once during the 3-day operation for the case study used due to the temperature of the cavern reaching the maximum temperature for an operation set at (373K). The results of this sensitivity study are shown in Figure 5-24, Figure 5-26and Figure 5-27.

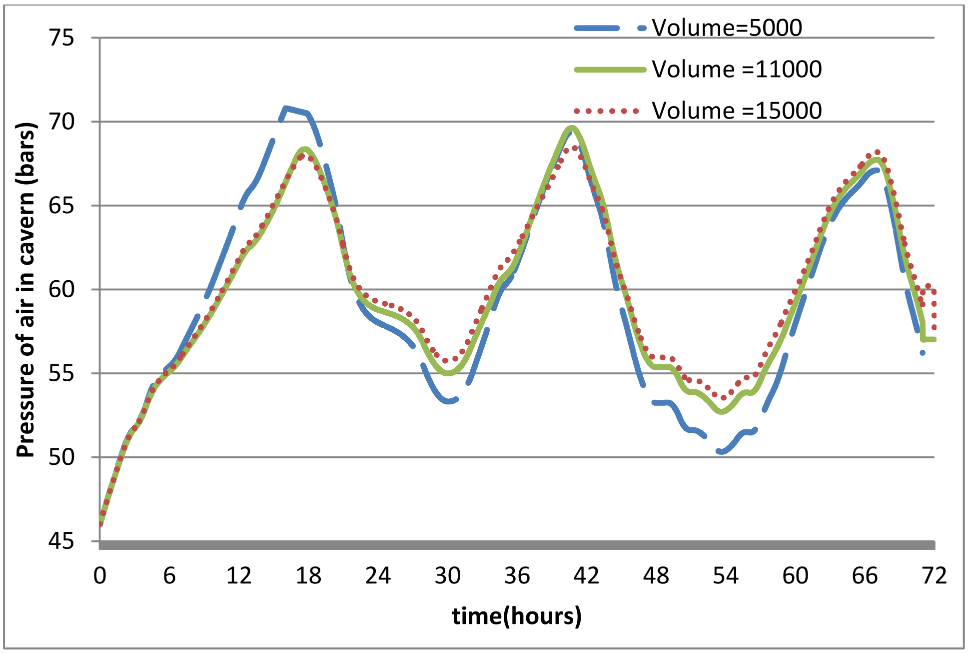

Figure 5-25 Effect of TES size on the pressure of air in cavern

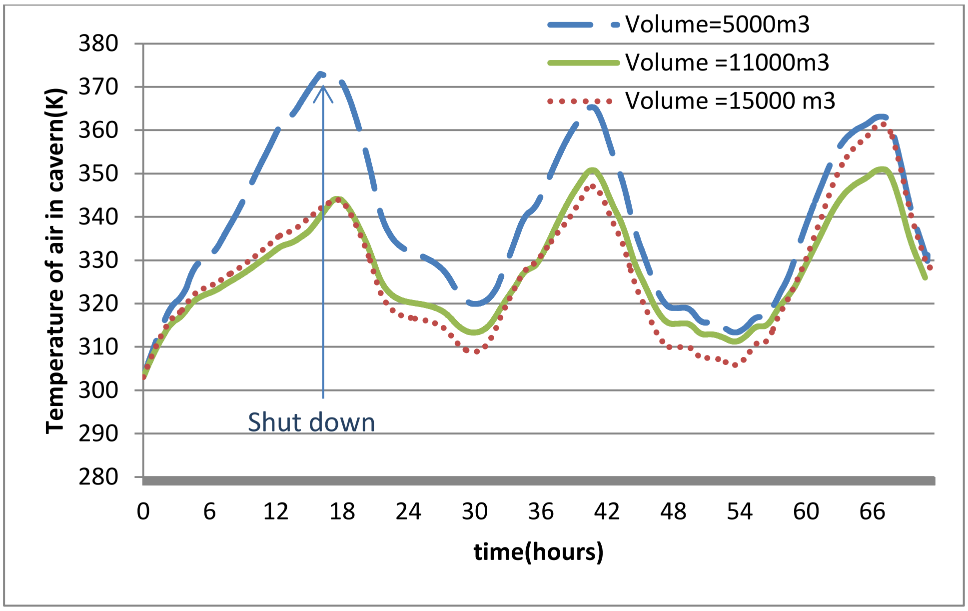

Figure 5-26 Effect of TES size on the temperature of air in the cavern

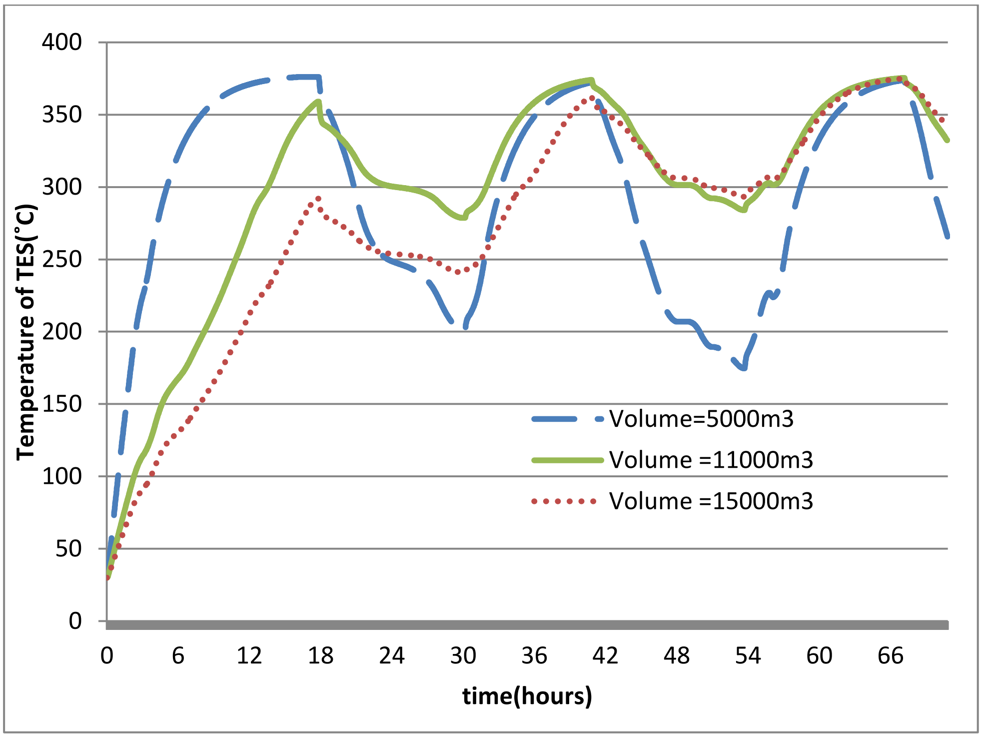

Figure 5-27 Effect of TES size on the temperature of the TES

Table 5-6 Performance for different volumes of thermal storage

Volume of TES(m^3)	**5000**	**11000(base case)**	**15000**
Heat rate(MJ/kWh)	4350	4062	4120
Efficiency (%)	58	62	61
Combustion Energy (MWh)	5000	4638	4722
Energy Available for storage(MWh)	6944	7778	7778

In addition, Figure 5-28 shows the benefit of adding CAES to the net power of the wind turbines and the load demand using a smaller volume of the thermal energy storage. However in this simulation, the power taken by CAES, shaded in blue, is not using all the surplus power available for the CAES system. This is due to the temperature of air in the cavern reaching the maximum operating temperature set at 373K, resulting in the system shutting down at least once during the 3 day period of operation. The longest of these was early on after around 14 hours of operation.

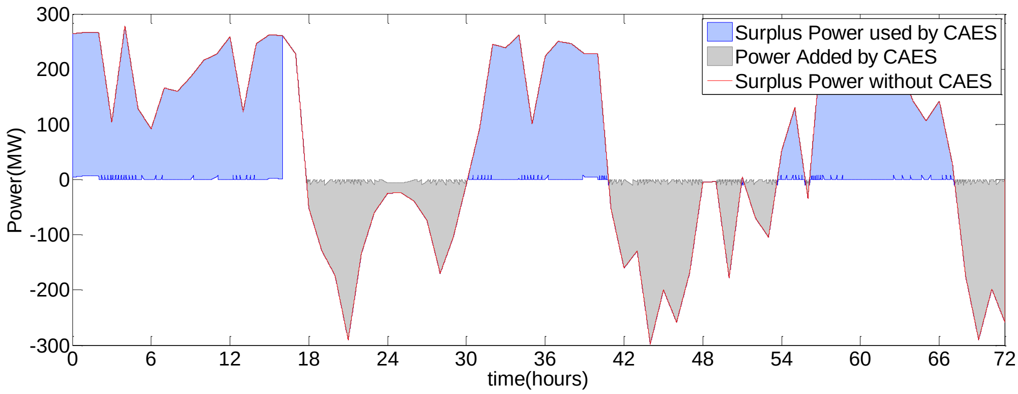

Figure 5-28 Effect of adding CAES on net power for a volume of $5000m^3$ of TES

In general, the combustion chamber power depends on the outcome of the heat exchange between the air coming out of the cavern and the temperature of heat transfer fluid out of the thermal energy storage. Therefore, in the case of using lower volume of concrete ($5000m^3$), the required combustion power is higher than that needed for the other two cases. Figure 5-29 shows the effect of different volumes of concrete effect on combustion chamber power. Yet, it is not very clear in the figure the difference in combustion power. However, it becomes more obvious after 44 hours, where the peak for the combustion chamber power for the case of 5000m^3 volume of thermal energy storage is around 414MW. While the combustion power in the case of using TES volume of 15000m^3 peak after 44 hours is around 382 MW, showing a difference of 32MW. In order to illustrate this more clearly, the combustion energy used for the 72 hour period was summed for all the 3 cases and are shown in Table 5-6.

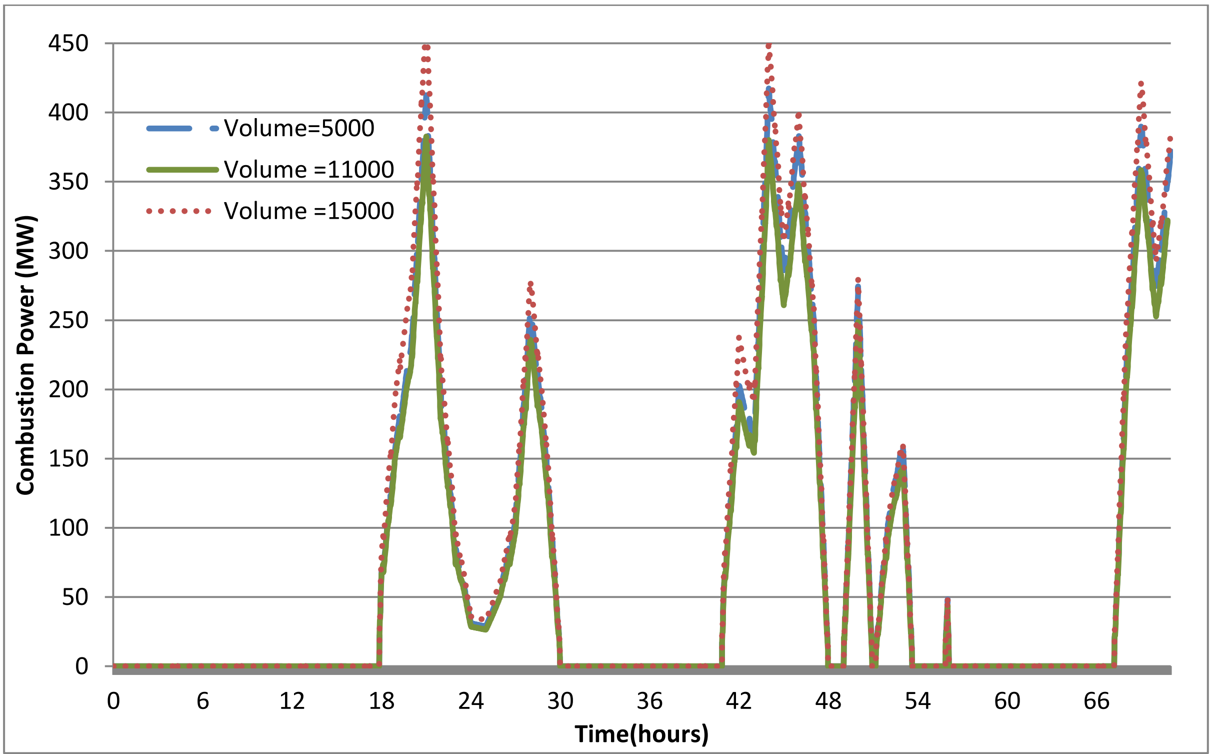

Figure 5-29 Effect of TES size on combustion power requirement

Figure 5-30 shows the accumulative combustion energy required every 12 hours of operation using different maximum operating heat transfer fluid temperature to portray a clearer result than that of Figure 5-30

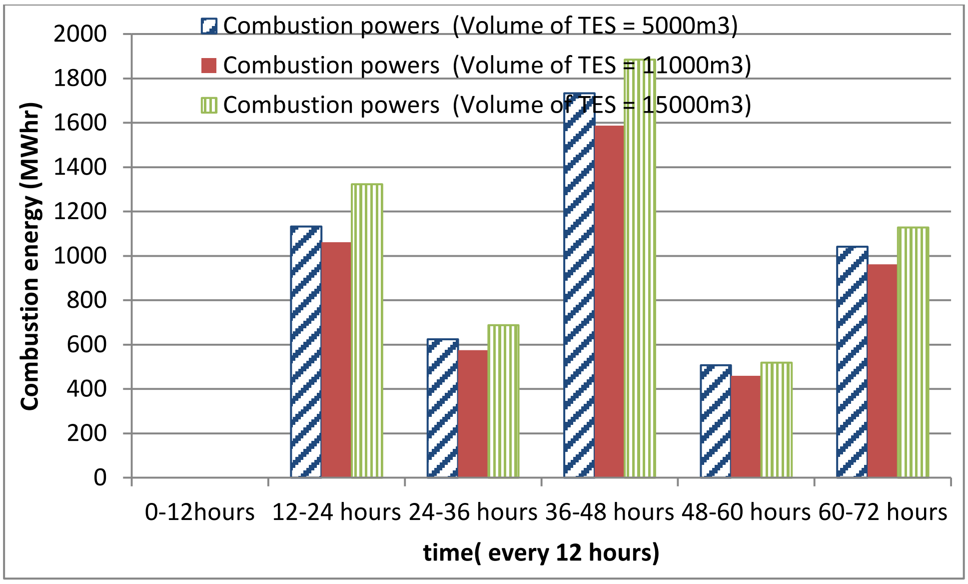

Figure 5-30 Combustion energy every 12 hours for different volumes of thermal energy storage

It is also worth mentioning why the case of using 11000m^3 (base case) required less overall combustion energy and produced lower heat rate compared to that of the 15000m^3 volume of thermal energy storage. In the latter 36 hours of operation, the combustion energy required from the simulation with a volume of thermal energy storage of 11000m^3 was slightly higher than that of 15000m^3. However in the first 36 hours of operation, the combustion power needed was less than that of the base case, which resulted in an overall reduction in combustion power required for the base case. In the first 36 hours during expansion, starting at the 18th hour, the thermal energy storage temperature for the base case was higher than that of 15000m^3case by 50 $^{\circ}$C; whilst the temperature of air in cavern in the base case was slightly higher. Therefore, this will result in a bigger temperature gradient between air flowing out of the cavern and the temperature of heat transfer fluid from the thermal energy storage. This leads to a higher air temperature after the heat exchange with heat transfer fluid, and thus lower combustion energy is needed to raise temperature to turbine inlet requirement, for the base case during a first expansion stage. This changes afterwards but on a much smaller scale resulting in an overall improved performance, using the base case of $11000m^3$

Remarks on size of the thermal energy storage

Ultimately, using a smaller design of the volume of the thermal energy storage has negative results on the operation of the CAES system. Sizing a smaller volume of TES will result in the shutdown of the system during the three compression stages during the 72hour operation period. Also, it would result in more combustion power; hence more cost of operation and less efficiency of operation.

On the other hand, using a bigger volume of thermal energy storage compared to base case sizing would result in lower temperature and pressure of air in cavern. Yet, since the simulation of the base sizing of the thermal energy storage, results in the temperature and the pressure of the air in the cavern being within the operating range, then having a higher volume of TES has a minimal improvement on the performance of the system. However, using a higher volume of thermal energy storage would result in slightly more combustion power to be added (due to lower temperature of TES) as well as the added cost of manufacturing higher volume thermal store.

5.4.4.3 Temperature of OIL

The third element to be tested within this sensitivity study concerns the oil used. The mineral oil chosen for our simulation had properties which were introduced earlier in this chapter. The maximum operational temperature of the mineral oil was set to 377˚C. This temperature was varied to test its effect on the CAES performance. The simulation was also performed for a maximum temperature of operation of the mineral oil at 600K (327˚C) and 700K (427˚C).

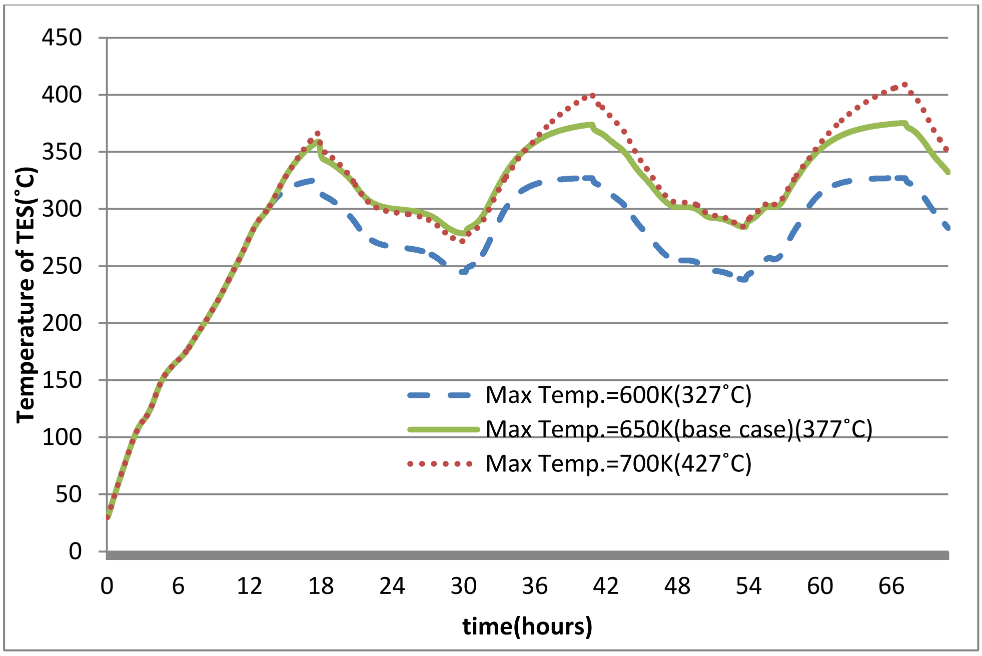

Figure 5-31 Effect of different maximum temperature of HTF on temperature of TES

When using higher maximum operational temperature of heat transfer fluid (700K), the heat exchange between the air and the heat transfer fluid did not stop until the temperature of the heat transfer fluid reaches 700K. This leads to a longer time of heat exchange between air and the heat transfer fluid which is seen more clearly in Figure 5-31 It is important to note that after 35 hours of operation, heat exchange actually stops when using maximum operating temperatures of 600K and 650K (only heat is extracted from the air by after-cooling) , while the heat exchange continues using maximum operational temperature of 700K (red curve). The result is illustrated Figure 5-32 and Figure 5-33 where there is a lower rate of temperature and hence a lower rate of pressure increase as well.

Table 5-7 Performance for using different maximum operating temperature of heat transfer fluid

Maximum operating Temperature of Oil (K)	**600**	**650(base case)**	**700**
Heat rate (MJ/kWh)	4070	4062	3930
Efficiency (%)	61.9	62	64
Combustion Energy (MWh)	4922	4638	4487

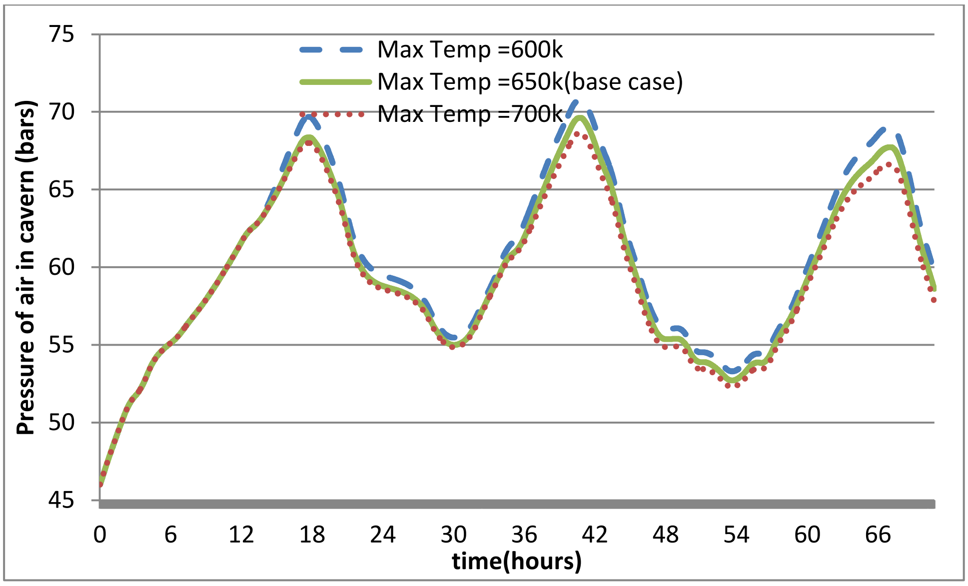

Figure 5-32 Effect of different maximum temperature of HTF on pressure of air in cavern

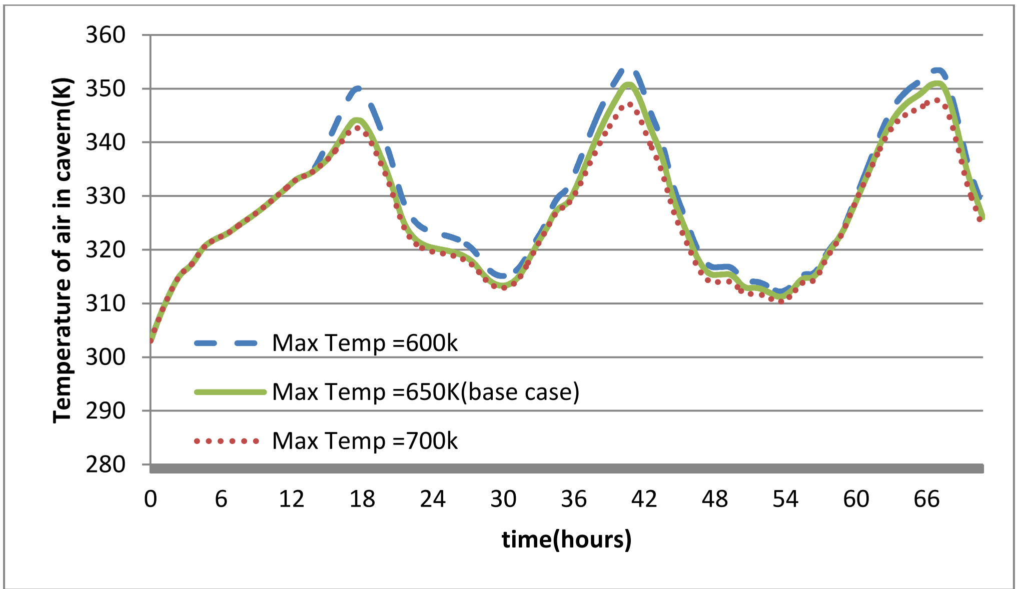

Figure 5-33 Effect of different maximum temperature of HTF on temperature of air in cavern

In addition, Figure 5-34 shows the effect of using different maximum operational oil temperature on the combustion power required for air before entering the turbine. This test shows clearly that the higher the maximum operational temperature of heat transfer fluid (oil), the higher the temperature of the thermal energy storage, the higher the gradient between the air coming out of the cavern and the heat transfer fluid outlet from the thermal energy storage, which will in turn result in a higher rate of increase of the air temperature before entering the turbine. Ultimately, this will result in lower combustion energy required and thus lowers the heat rate of the system and creates better performance. Again the combustion chamber curve does not show clearly the difference in results, but it can be identified in the case of a 600K simulation, more power is required. This is followed by the base case and then that of the 700K.

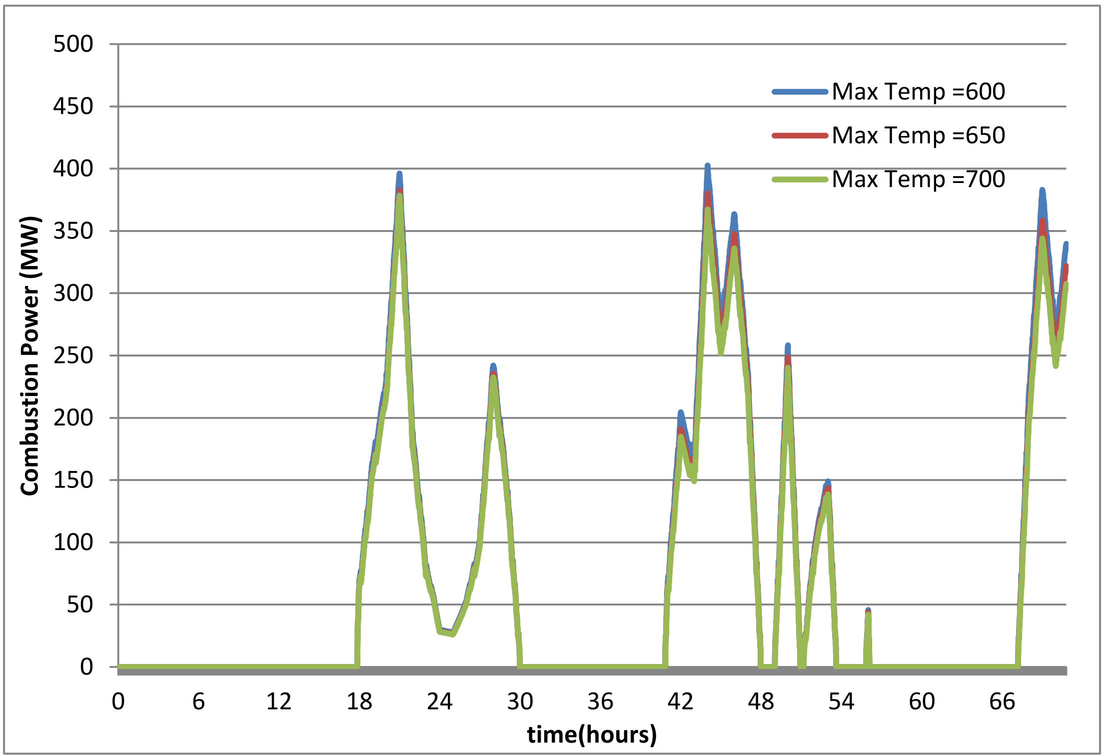

Figure 5-34 Effect of different maximum temperature of HTF on combustion power

Finally, Figure 5-35 shows the accumulative combustion energy required every 12 hours of operation using different maximum operating heat transfer fluid temperature.

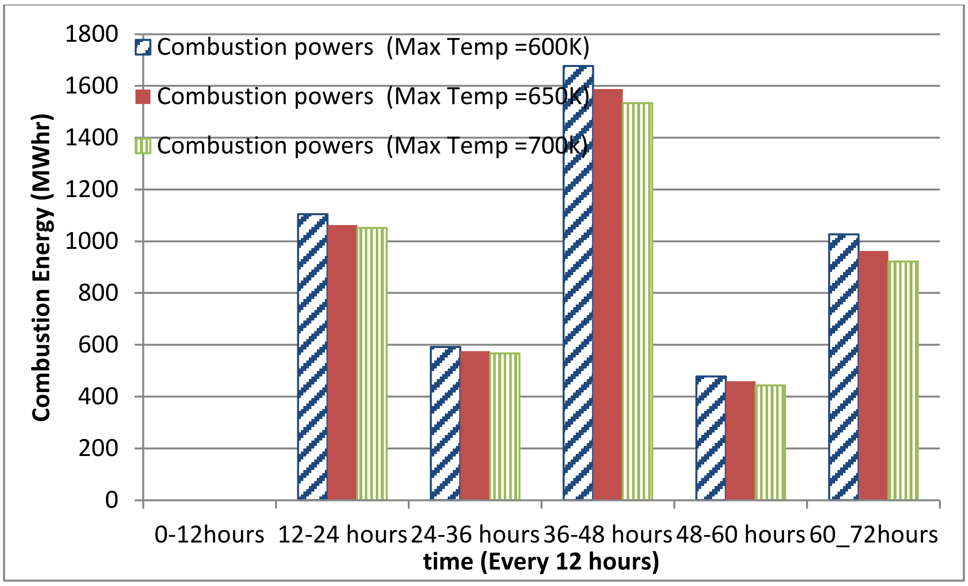

Figure 5-35 Combustion energy every 12 hours for different maximum operating oil temperature

It is also clear from this test that using a heat transfer fluid with higher operating temperature would always result in better system performance. It will allow the thermal energy storage to reach a higher temperature, hence allowing the temperature of the air to be higher before flowing to the turbine. This will result in less power from the combustion chamber and better performance of the system.

5.4.4.4 Operating pressure in cavern

In this sensitivity study, to find out the effect of this assumption on system performance, the maximum pressure varied from 75 bars to 80 bars, which is dependent on the geology of the location. The main effect of this study is on the temperature and pressure of air in the cavern. Since the maximum operating pressure in the cavern is changed, the design sizing of the cavern volume is changed as well. Table 5-8 shows the variation in the calculation of the parameters of the system for this sensitivity study.

Table 5-8 Performance for different range of operational pressure in cavern

	Base case	Pmax=80bars
Volume of cavern (m^3)	1,100,000	920,000
Heat rate (MJ/kWh)	4062	4035
Efficiency (%)	62	62.5

The calculation of the cavern volume is dependent on pressure range of operation in the cavern. Therefore the volume of cavern calculated decreases when the operation range of pressure increases. This results in a higher rate of pressure and a temperature increase in the cavern for a smaller volume of cavern.

Also, Figure 5–36shows the effect of using different operational pressure ranges for system sizing and the operation effect on the pressure of air. Since the volume of cavern is smaller using higher operational pressure range, the rate of increase of pressure of air in the cavern is higher compared to the base case.

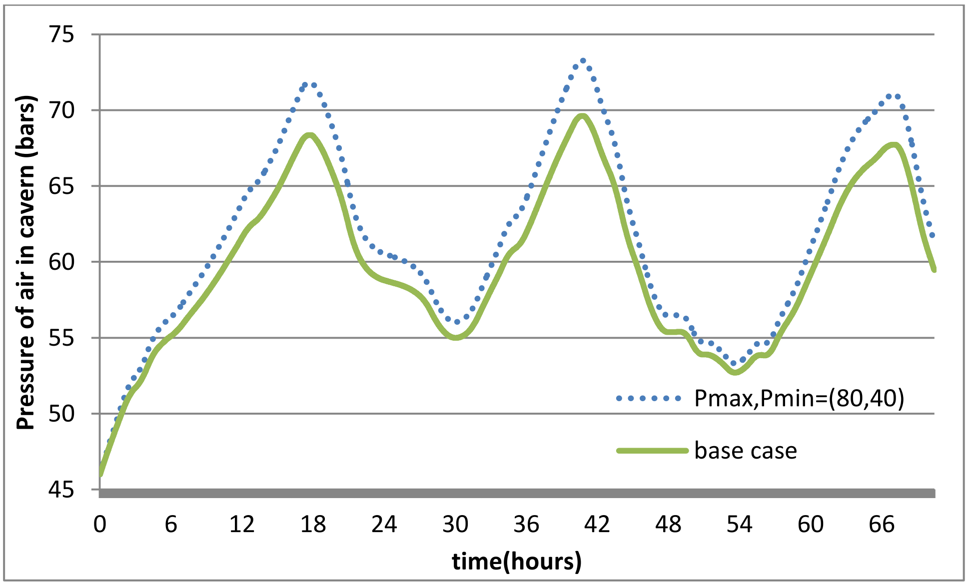

Figure 5-36 Effect of having different maximum and minimum operating pressure in cavern on pressure of air in cavern

In addition, Figure 5-37 shows the effect on the temperature of air in the cavern, which follows the same pattern as the air pressure. This is where using a bigger operational pressure range of air in the cavern results in a smaller sizing of the volume, which results in a higher rate of variation of temperature of air in the cavern.

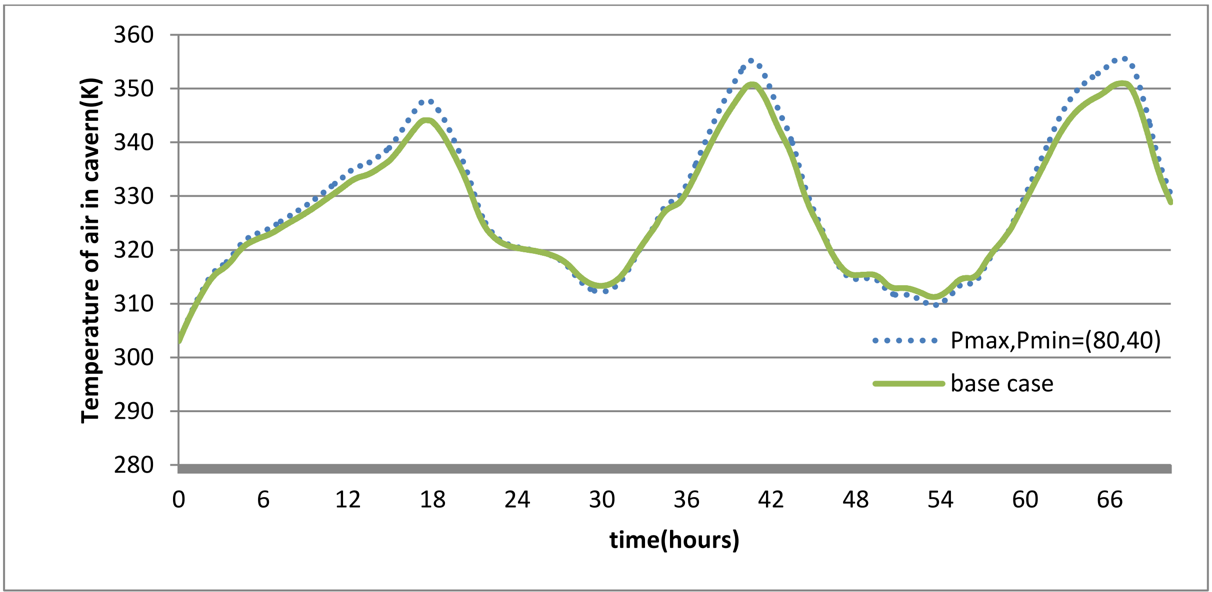

Figure 5-37 Effect of having different maximum and minimum operating pressure in cavern on temperature of air in cavern

It is thus clear that the effect of changing the maximum operating pressure of the cavern has a negligible impact on the thermal energy storage temperature. However there is a slightly more combustion power used in the base case as compared to the case of 80bars, which is due to the slightly lower temperature of air coming out of the cavern

Remarks on different operating pressure ranges

Whilst testing this assumption, it was demonstrated that having a higher operating maximum pressure of air in the cavern would result in a smaller sizing of the cavern, translating in a reduced cost of the system. The operation would be quite similar, but in the case of the higher operating pressure, the air in the cavern will have a higher temperature (closer to maximum operating temperature) and yet not reaching the maximum Therefore, having higher operating pressure would result in a lower cost of the system without affecting the performance of the system

5.4.5 Remarks on different sensitivity studies

The previous section presented the effect of varying different parameters on the operation of the CAES system. The performance indices of the CAES for each sensitivity study were presented using the heat rate and the efficiency of each system. Figure 5-38 shows the heat rate from the best performing case in each sensitivity study while Figure 5-39 shows the efficiency calculation. The results show that increasing the maximum operating temperature of the heat transfer fluid produced the lowest heat rate (best performance) while the conventional diabatic system produced the poorest performance (highest heat rate).

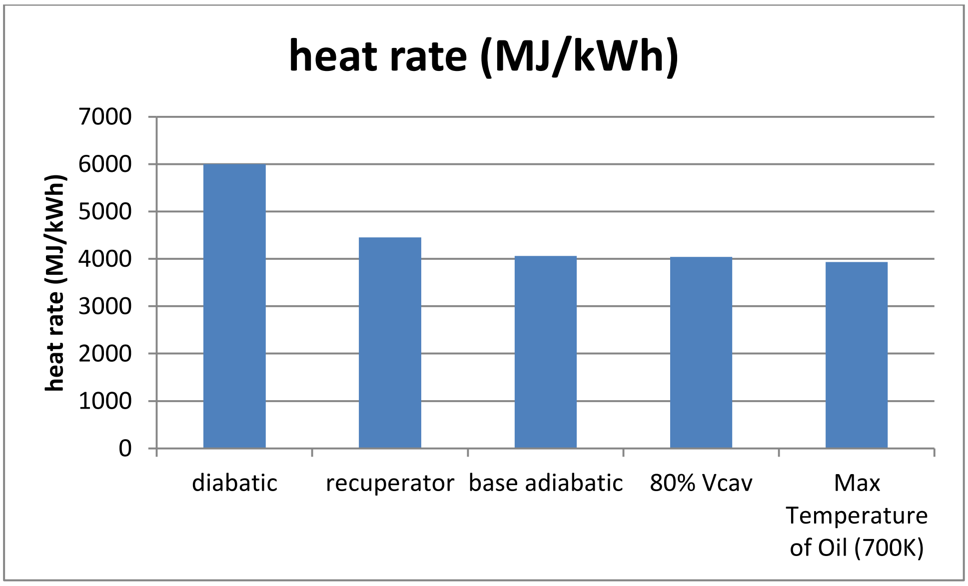

Figure 5-38 Heat rate for different performance parameters variation

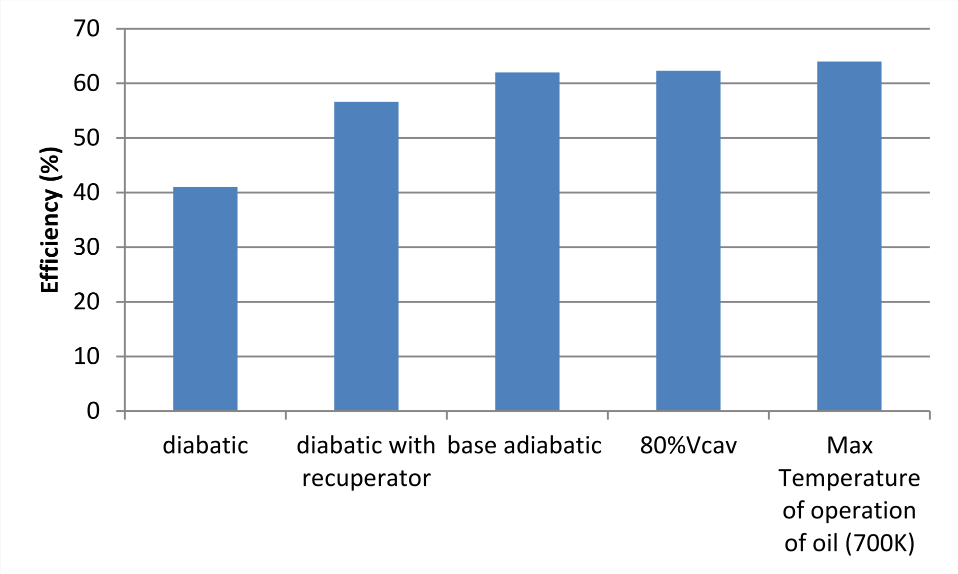

Figure 5-39 Efficiency for different systems configuration

5.5 Conclusions

This chapter discussed the MATLAB simulation of the Compressed Air Energy System for a case study of the SUEZ area in Egypt. A MATLAB model was developed to size and simulate the operation of the CAES system to illustrate the potential of the system in Suez. This allowed an examination of the results regarding the operation and behaviour of the air storage cavern, as well as the effect on the overall net power delivered to the load.

The model demonstrated the potential of adding a CAES system to an installed wind farm. The results show that the CAES system is able to store and supply the load at the time where wind power is lower than the load demand. Based on this finding, the CAES could play a large role in reducing the wind intermittency dilemma that may face the Egyptian grid due to the expected increase in wind power generation to 7.2 GW, or the supply of 12% of the Egyptian power demand. The model simulation was based on a load levelling principle. Based on the results obtained from the case study considered, it has been shown that CAES has a large potential as an efficient and environment friendly large-scale energy storage technique in Egypt. It could be one of the ways to solve the problem of wind energy intermittence and result in positive technical, economic and social impacts.

Also, a sensitivity analysis was carried out for the same case study of Suez. The sensitivity test was administrated for several variables. These include the cavern volume, the volume of the thermal energy storage, the maximum operational temperature of the heat transfer fluid, the load demand and the range of operational pressure of air in cavern. The operational results of the temperature and pressure of air in the cavern and the performance of the system modelled in the heat rate of the system, showed that the sizing techniques used in the MATLAB model for the volume of cavern as well as that of the thermal energy storage; gave the best performances when compared with different cases. It also showed that using a heat transfer fluid with higher operational maximum temperature improved the performance of the system. However the data used in our simulation for the heat transfer fluid was solely based on available commercial mineral oils available.

.

Chapter 6 Experimental testing of thermal energy storage

6.1 Scope of the work

Adiabatic Compressed Air Energy Storage System uses thermal energy storage to store the excess heat from the charging cycle (compression) and releases it for extraction by the air entering the turbine so as to improve the efficiency of the whole system. The thermal storage reduces the amount of energy that is needed by burning gas in the combustion chambers, hence improving the performance of the CAES system. The purpose of the experimental test is to inspect the thermal energy storage property of the CAES. In this case, concrete is used as the storage medium and heat transfer oil atonal 324 is used as the heat transfer fluid. The Concrete is used owing to its availability, relatively low cost compared to other thermal storage options, and its good heat transfer characteristics. Atonal 324 is a suitable heat transfer fluid because of its good heat transfer properties and safety, which complies well with the safety requirements. The system's efficiency and thermal storage capacity are tested and discussed under different conditions of flow rate and inlet temperatures of the heat transfer fluid. The lab results are also used to validate the CFD and the MATLAB computer models.

6.2 System description and working principle

A schematic description is given in Figure 6-1 showing the experimental arrangement. The system consists of two tanks- a hot tank (with immersion heater) and a cold tank, a pump, a flow meter and the TES system. The heat transfer fluid used is the heat transfer oil-atonal 324, the details of which are given in Table 6-1. The system runs two cycles: a heating cycle and a cooling cycle. In the heating cycle, the oil from the hot tank circulates, heating up the concrete block in a closed-loop system. In the cold cycle, the oil from the cold tank circulates within the system to absorb heat from the TES.

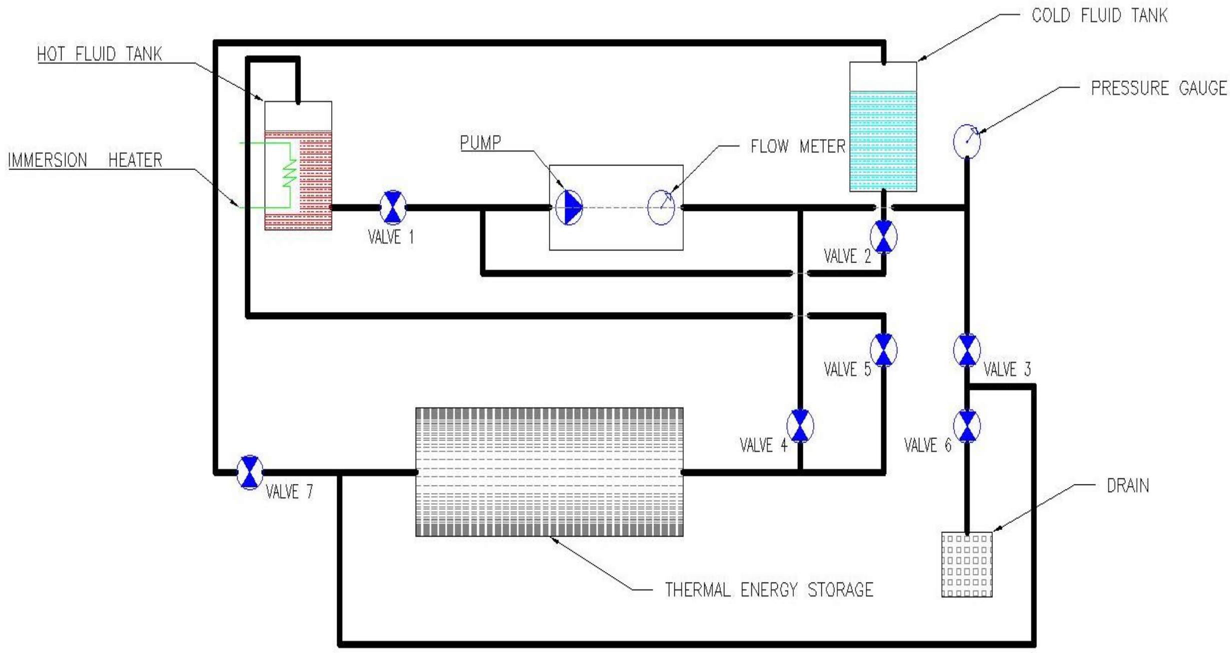

Figure 6-1 TES experimental test setup

6.3 Experimental Setup and System Components

The TES is made of a concrete cylinder block of 315mm diameter and 700mm long. 7 pipes, of a 22mm diameter each are assembled inside the concrete block, that are evenly distributed to improve the heat transfer to the entire block as shown in Figure 6-2. The concrete block's thermal conductivity is assumed at 0.9W/mK , with a specific heat capacity of 750J/kgK and a density of 2400kg/m^3. The block is also insulated with 5cm fiberglass with a thermal conductivity of 0.042W/mK.

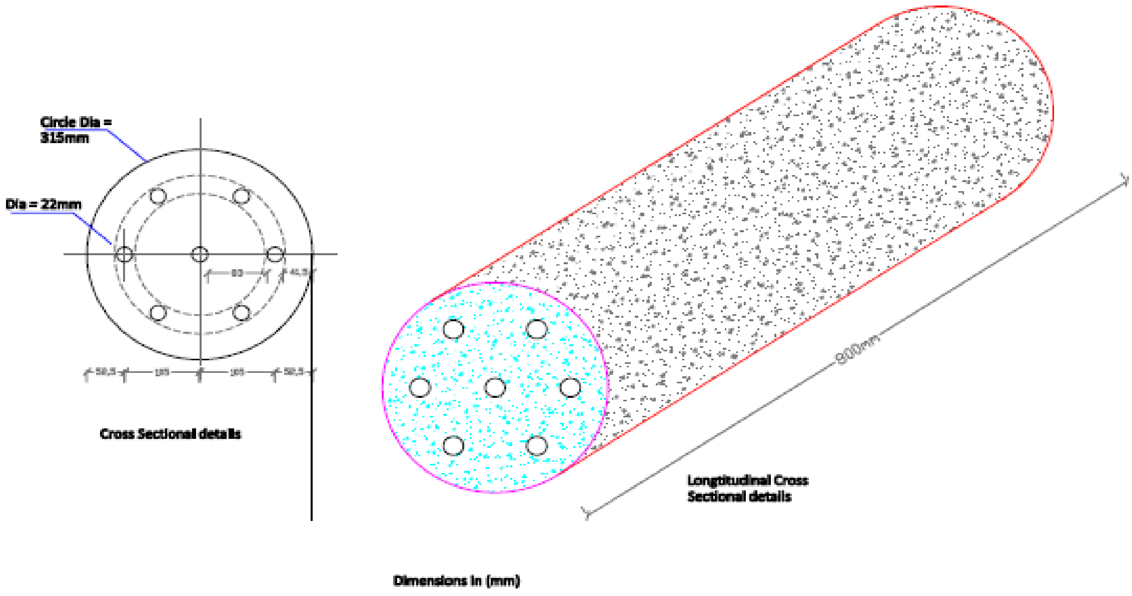

Figure 6-2 A schematic showing the details of the concrete block

The thermal conductivity of the oil is measured using *Iso-Therm device*. The tests were carried out at two different temperatures 20˚C and at 60˚C, yielding a thermal conductivity of $0.142W/mK$ and $0.141W/mK$ respectively. The density of oil here is around $870kg/m^3$, and its viscosity is 82cSt at 20˚C, 31cSt at 40˚C and 5.3cSt at 100˚C (Morris Lubricants technical data).

Table 6-1 Specifications of heat transfer fluid

Atonal 324	
Thermal conductivity (W/mK)	0.141
Density (kg/m^3)	870

A rectangular steel tank fitted with an immersion heater is used to heat the oil to the required temperature is shown in Figure 6-3. The heater has a built in thermostat that controls the temperature between 40 ˚C and 90 ˚C

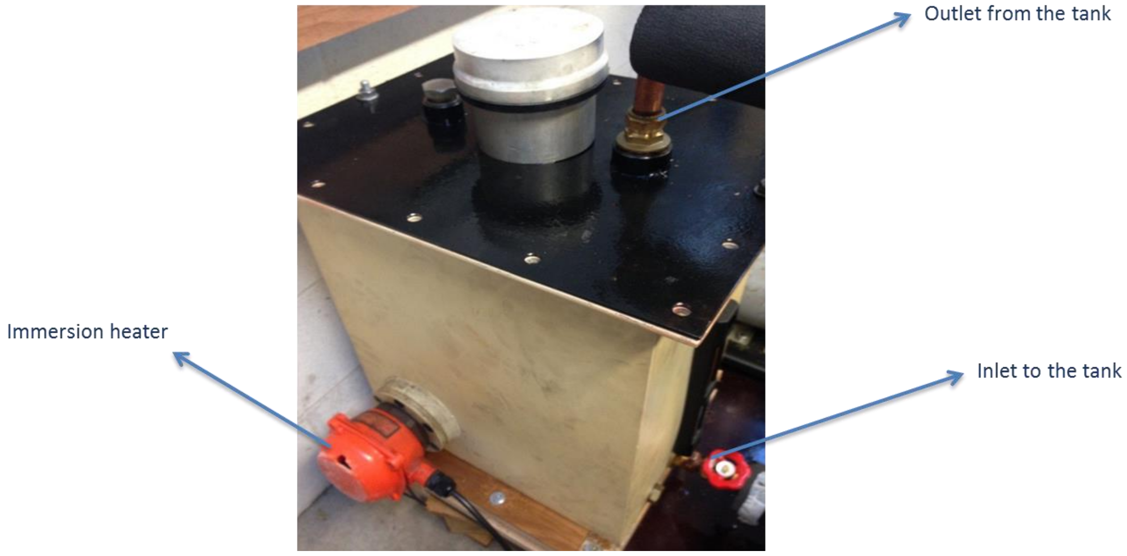

Figure 6-3 A photo of the tank with an immersion heater

A 25-litre cylindrical tank made of aluminium containing oil at room temperature is used as the cold tank.

An oil pump is used that produces a flow rate of 17.5$litres/minute$ when running at full capacity.

An oil flow meter is used to measure the flow rate during the heating and cooling operations

A pump speed regulator is used to regulate the pump flow rate. The regulator is connected to the pump electrically and can control the flow of the pump by choosing the percentage of capacity to operate at, hence inflicting control at all times.

In this system seven thermocouples were used to measure the temperature of the TES and the heat transfer fluid. Three were used in the concrete block at different positions, to assess the temperature distribution: 200mm from the inlet, 400 mm from the inlet (in the middle of the concrete block), and at 600 mm from the inlet (close to the outlet of the concrete) as shown in

Figure 6-4. Two thermocouples were used to measure the temperature of the oil at the inlet and another two measurements of the temperature of the oil at the outlet.

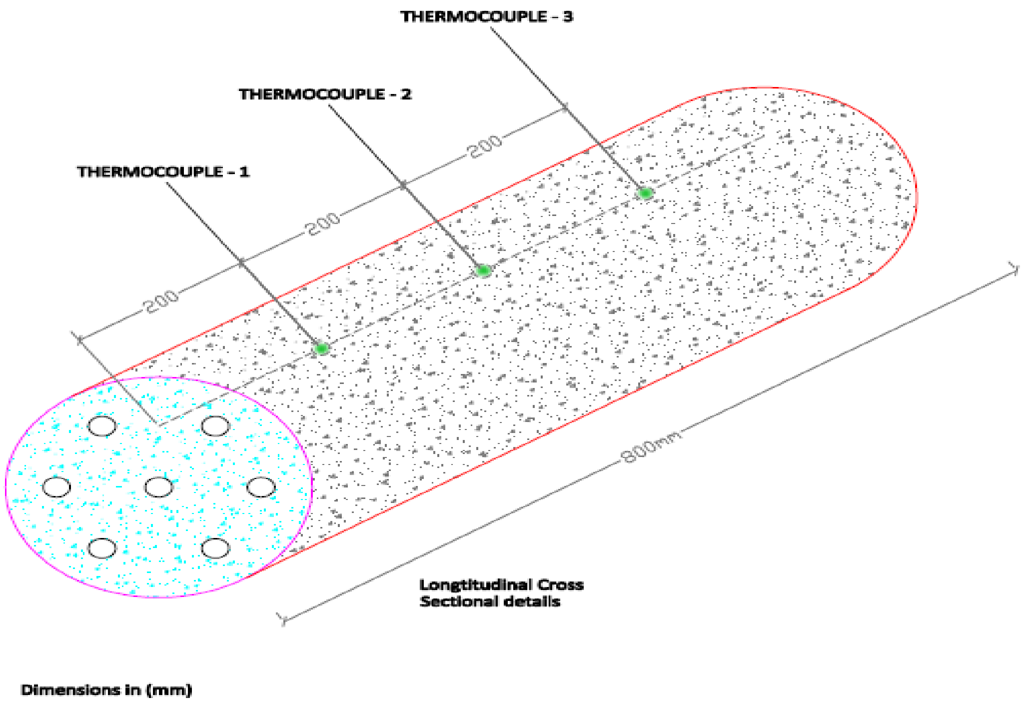

Figure 6-4 Thermocouple positions along the TES

A pressure gauge is used as a safety display to monitor the pressure of the system during the test This is so to ensure that there is an open flow of the oil and that the right valves are open throughout the different operation cycles of the system.

Some seven valves are used in the system to select the correct cycle of the oil flow for the four different cycles, as discussed in the next section.

A wooden barrier was erected bordering the whole system to block any oil spillage for safety reasons.

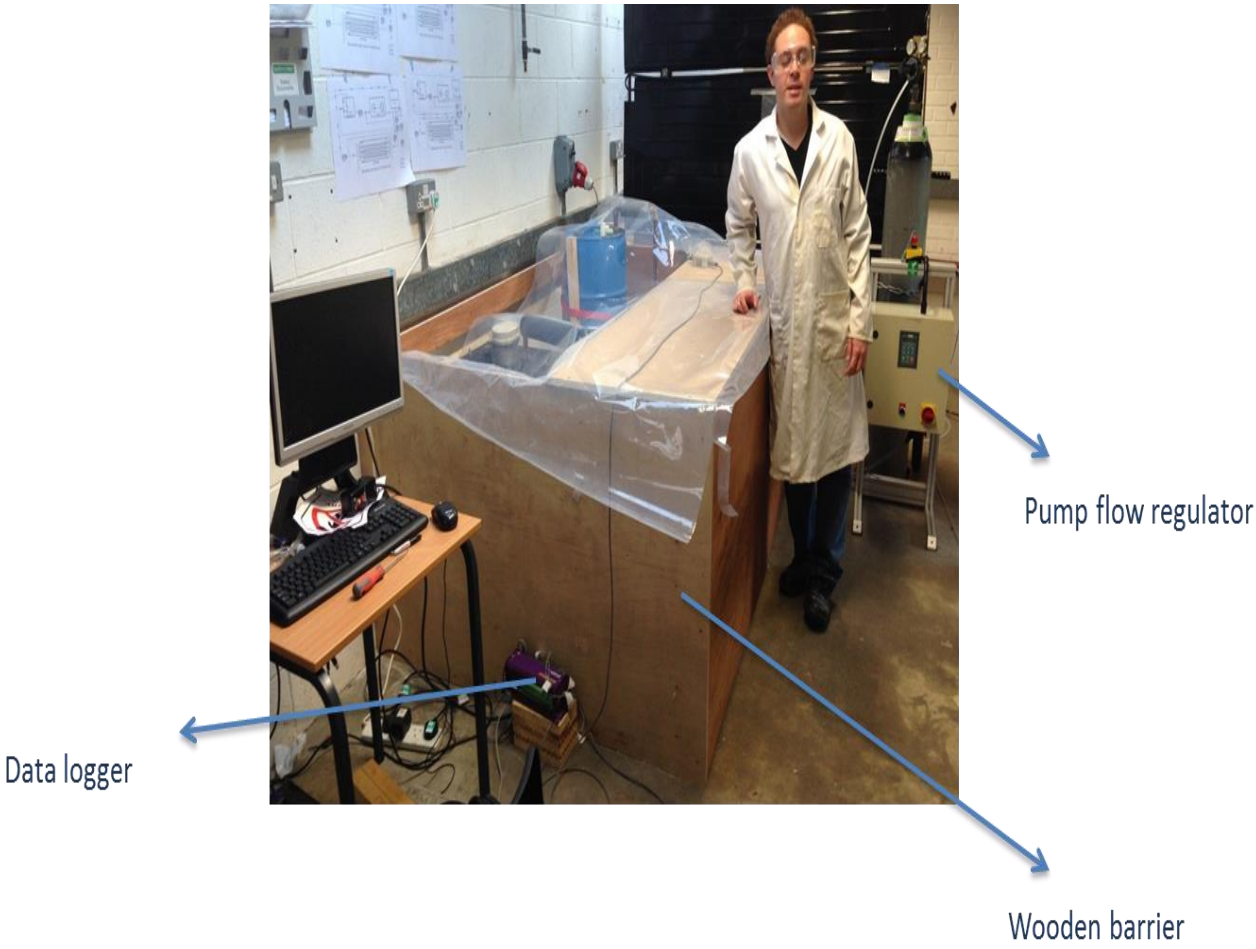

Figure 6-5 Safety wooden barrier and the data logger

A data logger was used to collect and record the data from the flow meter and the thermocouples throughout the test The data is logged into a computer using a data-logging program that is set to read the temperatures of the seven thermocouples and the oil flow rate from the flow meter during the test.

6.4 Testing procedure

The tests carried out were done for both charging and discharging cycles. The results of these tests were then compared to the CFD modelling results. These include:

1) Testing the thermal conductivity of atonal 324 using Iso-Therm (aforementioned)

2) Charging effect on different positions of concrete block

3) Effect of inlet flow rates for the charging cycle

4) Effect of inlet temperatures on the thermal storage for the charging cycle

5) Discharging cycle for different initial temperatures of the concrete storage

For each of these tests the temperatures of concrete, the hourly temperature rise and the hourly thermal energy stored are compared and discussed for each case.

There are 4 different cycles of operation of the experimental test. Two main operational cycles and two draining cycles were used to discharge the system.

a) Charging of the thermal storage

b) Discharging of the thermal storage

c) Draining of the hot tank

d) Draining of the cold tank

6.4.1 Charging Cycle

The oil is heated in the hot tank using an immersed electric heater and then pumped to the concrete block when the right temperature is achieved, heating the concrete for the charging cycle. This oil circulates back to the hot tank in a closed loop system. In this case valves 1, 3 and 5 are opened while the other valves are closed as shown in Figure 6-6. The arrows in the figure show the direction of oil flow in this cycle.

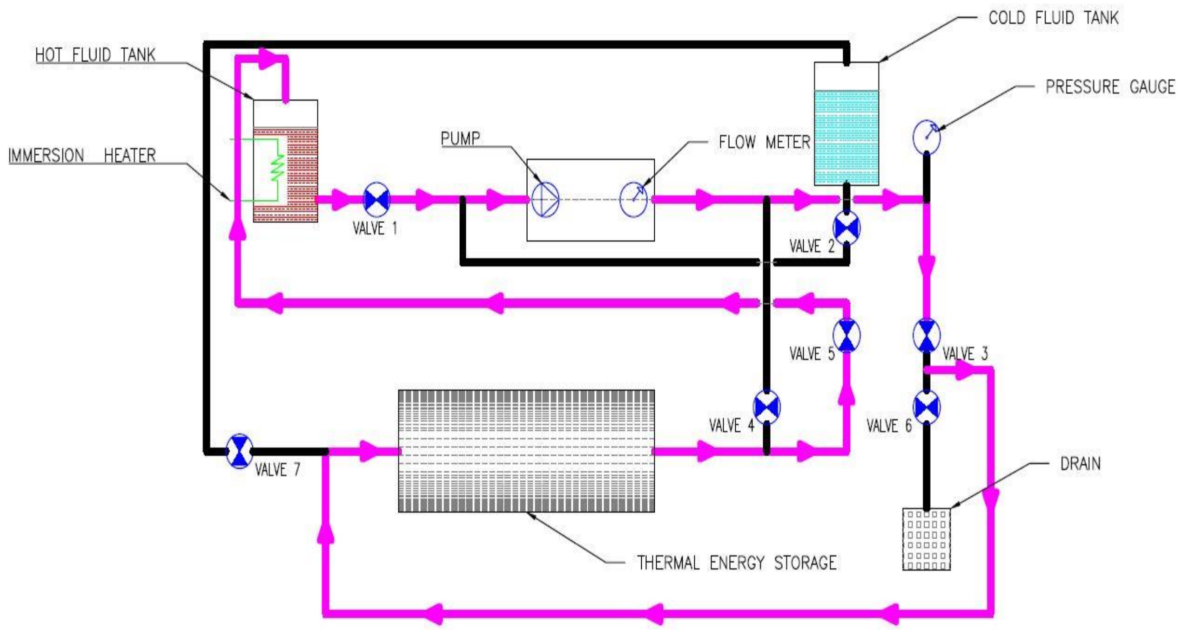

Figure 6-6 Charging cycle of the thermal energy storage

6.4.2 Discharging Cycle

For this cycle, the cold oil from the cold tank is pumped to the concrete block cooling the concrete for a number of hours. The oil circulates back to the cold tank in a closed loop system. In this case valves 2, 4 and 7 are opened while the other valves are closed as shown in Figure 6-7. The arrows in the figure show the direction of oil flow in this cycle.

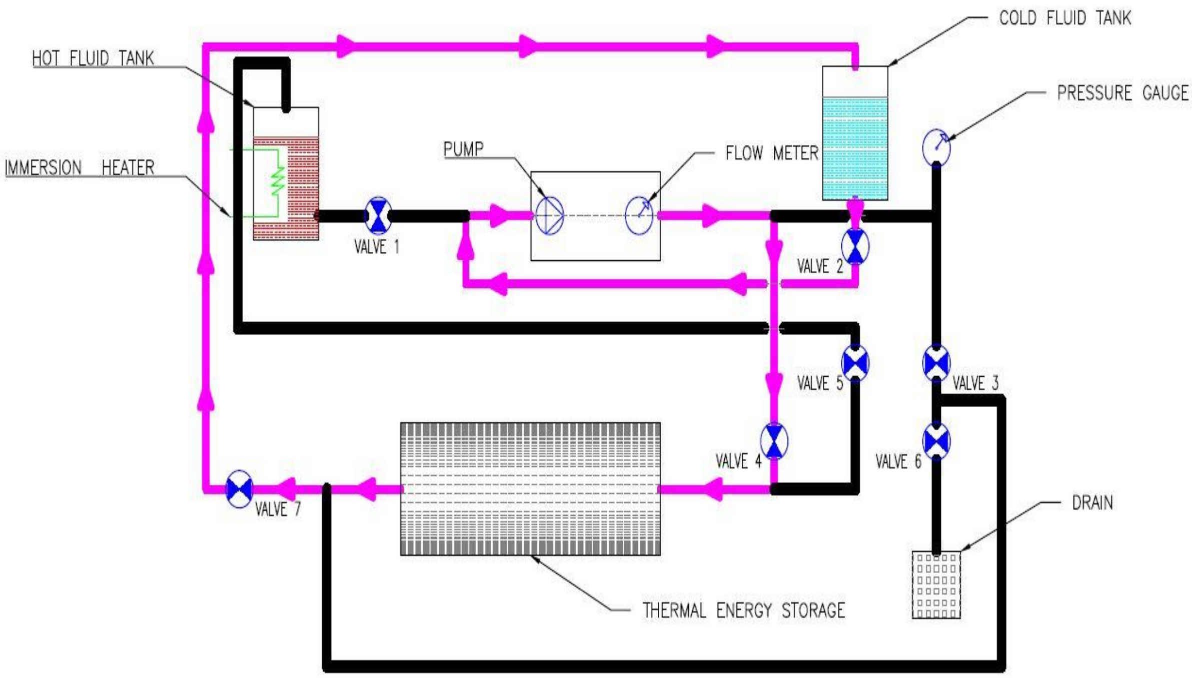

Figure 6-7 Discharge cycle

At the end of the charging test, the hot oil is pumped from the hot tank to the drain where the oil is collected into a reserve tank. Valves 1, 3 and 6 are open while the other valves are closed for this cycle. While at the end of the discharging cycle, the cold oil is drained from the cold tank by opening valves 2, 3 and 6 while closing the other valves.

6.5 Results and discussions

In this section, the results of the experimental tests carried out are discussed and compared.

To begin with the pump used has a capacity of $17 litres/minute$. For the design of the concrete used in the experiment, the velocity can be calculated as

$$Velocity\left(\frac{m}{\sec}\right) = \frac{Volume\ flow\ rate(\frac{litres}{minute})}{Area\ of\ pipes(m^2)\times conversion} \tag{6-1}$$

$$conversion = litres \rightarrow m^3 \times minute \rightarrow sec = 1000 \times 60 = 60000 \tag{6-2}$$

$r = 0.011 meters$

$$cross\ section\ of\ pipes = 7 \times pi \times r^2 = 2.7 \times 10^{-3} m^2 \qquad (6\text{-}3)$$

$$Mass\ Flowrate = Velocity \times cross\ section\ of\ pipes \times Density\ of\ Oil \qquad (6\text{-}4)$$

Therefore the maximum velocity of the pump is around 0.105 m/sec which is equivalent to 0.23 kg/sec.

6.5.1 Impact of charging on different positions in concrete (Test 2)

The first test of concrete was carried out to assess the temperature distribution in the thermal storage block. The thermocouples data used in this test are thermocouple 1 and thermocouple 3 as shown in Figure 6-4 Also, this test will show how long it takes the concrete to reach saturation with a specific inlet temperature and initial temperature of the concrete. For this test, the inlet temperature of the heat transfer oil was $72°C$. The heating in this case was applied specifically for six hours. Figure 6-8shows the temperature of concrete for the duration of the operation at two different positions of concrete (thermocouple 1 and thermocouple 3). Position 1 is thermocouple 1 and position 2 is thermocouple 3.

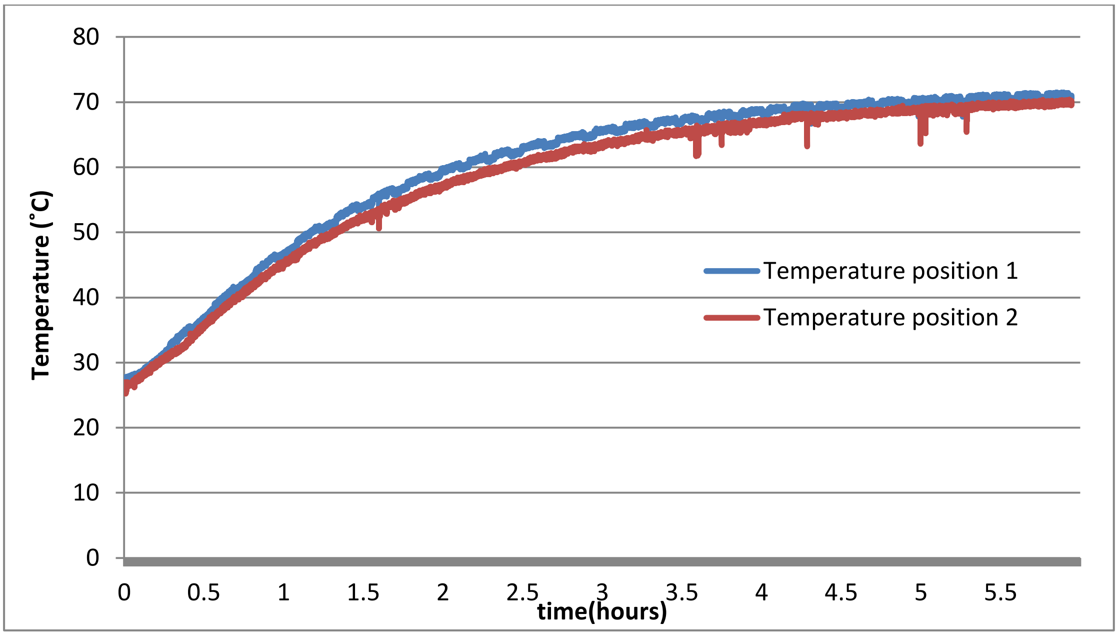

Figure 6-8 Variation of temperature of the concrete block for $70°C$ inlet temperature

Figure 6-9shows the concrete's temperature for two different positions (thermocouple 1 and 3). For position 1, the initial temperature for this test was around 28°C, reaching a maximum temperature of around 70.5°C after 6 hours of operation; keeping in mind that the initial inlet fluid temperature used was around 72°C. Figure 6-8 also shows that the concrete temperature almost became constant after six hours because the temperature of the concrete block became very close to that of the fluid inlet temperature.

As for position two, the initial temperature for this test was around 27°C, the temperature of the concrete block increases continuously until it reaches a maximum of around 70 °C, compared to the initial inlet fluid temperature of 72°C.

It is obvious that the temperature of concrete at position 1 is always higher; however the gradient between the two positions is reduced with the operation.

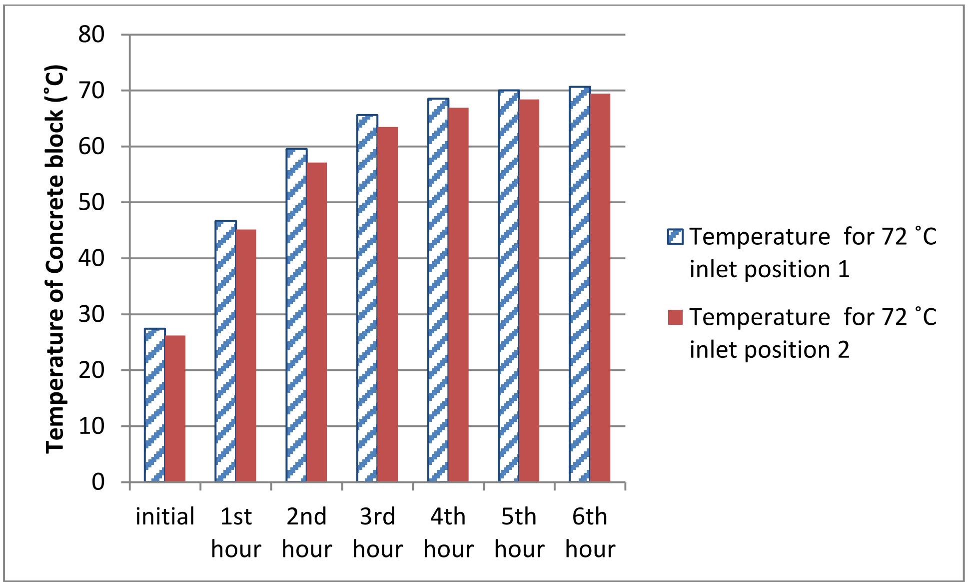

Figure 6-9 Hourly temperature profile of the concrete block for fluid inlet temperature of 72°C

Additionally, Figure 6-10shows the hourly temperature rise for the two positions in the concrete block. For position 1, the temperature rise was around 19°C for the first hour, going down to 13°C in the second hour. After that, the temperature gradient becomes increasingly lower as the temperature gradient between the inlet fluid and the concrete becomes smaller. This is illustrated clearly at the 6th hour, where the concrete temperature increases by less than $1°C$. This shows that after six hours of operation for a fluid inlet of around $72°C$, the concrete almost completely saturates and the heat transfer between the concrete and the inlet fluid becomes almost negligible.

As for position 2, the temperature rise was around $18.5°C$ in the first hour, going down to $12°C$ in the second hour and continuously decreasing. After that, the concrete temperature increase drops to less than $1°C$ during the sixth hour. This shows again similar results where after six hours of operation for a fluid inlet of around $72°C$, the concrete almost completely saturates as it approaches the fluid inlet temperature and the heat transfer becomes almost negligible.

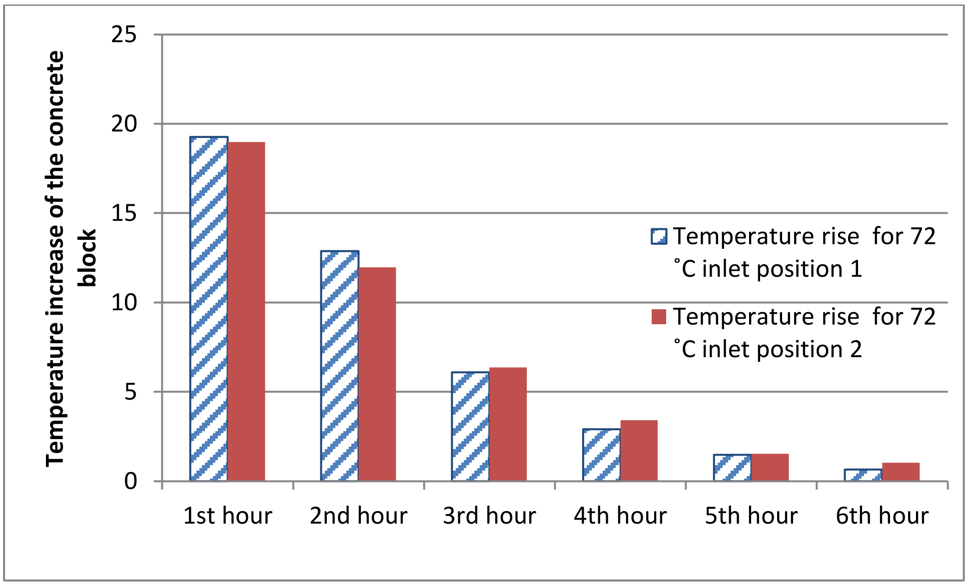

Figure 6-10 Hourly temperature rise for fluid inlet temperature of $72°C$

Figure 6-11 shows the hourly temperature gradient between the 2 concrete positions. During the first hour the difference was around $1.5°C$. It goes up to $2.4°C$ two hours later; yet after that the temperature gradient decreases, reaching $1.2\ °C$ by the end of the sixth hour.

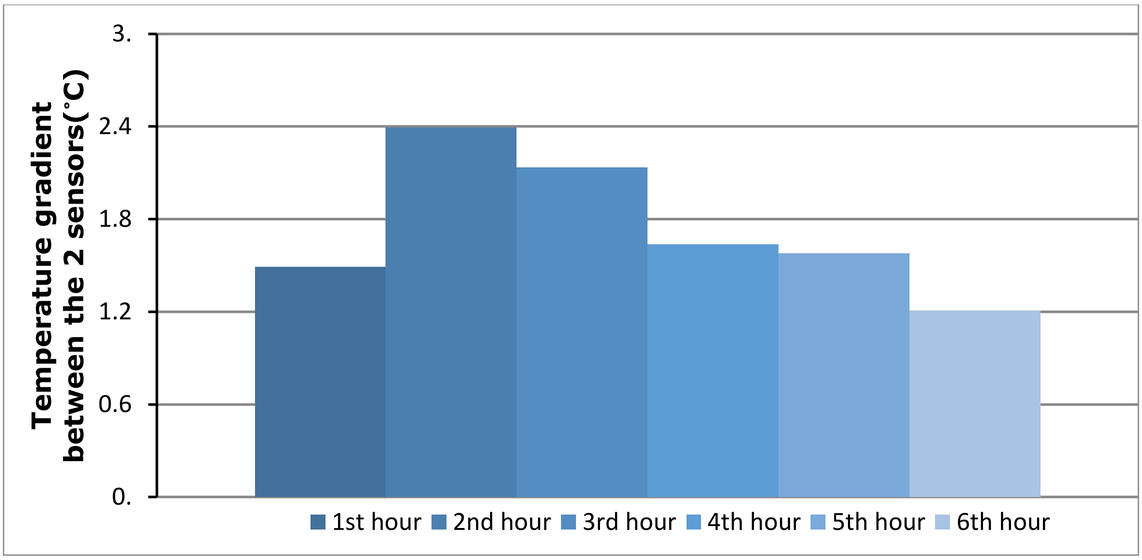

Figure 6-11 Temperature gradient between the 2 positions in concrete

The temperature gradient results can be explained by the fact that during the first couple of hours when the concrete temperature was at least 10 $°C$ lower than that of the fluid inlet, the heat transfer was high, especially at the position closest to the concrete inlet. This thus decreases the fluid temperature, causing the fluid temperature at the second position to be lower, hence resulting in less heat transfer. However, after a couple of hours when the concrete temperature increases to around 65 $°C$, the heat transfer decreases. Therefore the fluid temperature entering position 2 is still high and the temperature gradient between the fluid and concrete at position 2 is higher than that at position 1. As a result, higher heat transfer for concrete at position 2 causes the temperature gradient between the two positions of concrete to decrease in the following hours.

The following figures will now look at tests pertaining to energy storage in the system. The energy stored is governed by

$$Energy\ out\ oil = \dot{m} \times C_p \times (Toutlet - Tinlet) \qquad (6\text{-}5)$$

$$T_{concrete} = \frac{T_{sensor1} + T_{sensor2} + T_{sensor3}}{3} \qquad (6\text{-}6)$$

$$Energy\ stored\ concrete = Mass\ concrete \times C_p \times (Tfinal - Tinitial) \qquad (6\text{-}7)$$

Figure 6-12 shows the hourly energy stored for the 72°C inlet test. The energy stored in the first hour was around 0.61kWh, then the energy stored continuously decrease down to less than 20Wh in the final hour of testing. After 6 hours, the total energy stored was around 1.4kWh.

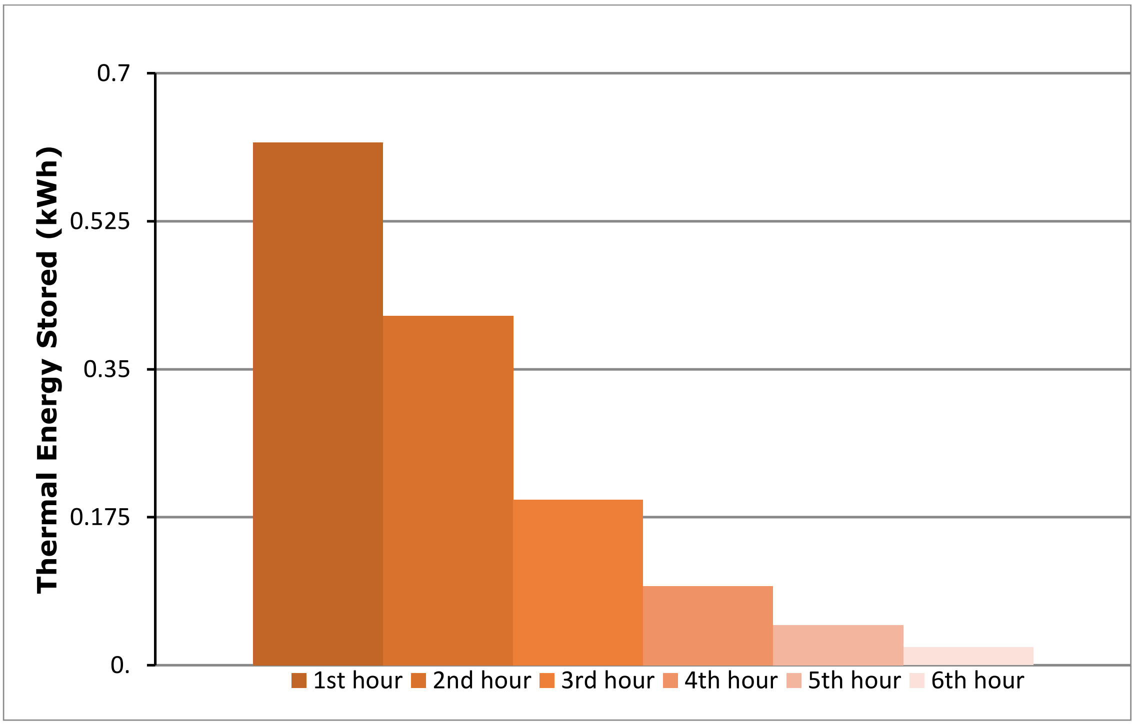

Figure 6-12 Hourly energy stored in the concrete block

Remarks on the heat transfer at different positions in the TES system

The previous test shows that for 70 ˚C inlet fluid temperature, the concrete almost completely saturates after six hours with the majority of heat transfer happening during the first two hours. After that the heat transfer becomes relatively small especially in the final two hours of operation. This test also shows that for the first two hours, the position closest to the inlet showed a higher temperature compared to that close to the outlet, due to the higher temperature of inlet fluid for the first position. After 2 hours when the heat transfer decreases between the fluid and the concrete, the heat transfer rate becomes higher for the concrete in the second position as the temperature gradient between the concrete and the fluid in that position is higher than the gradient for the position close to the inlet.

6.5.2 Effect of inlet velocities (Test 3)

The following set of results is based on tests pertaining to inlet velocities. The test was run under different inlet fluid flow rates using the speed regulator to control the pump flow. First, the difference in temperature along the operation is displayed for both of the flow rates tested, namely 0.15Kg/sec and 0.086 Kg/sec respectively.

Figure 6-13 shows the effect of different flow rates on the temperature of the TES. The higher the flow rate, the higher the heat transfer. After around two hours when the temperature of the concrete block starts to approach the inlet temperature of the fluid, the heat transfer becomes lower.

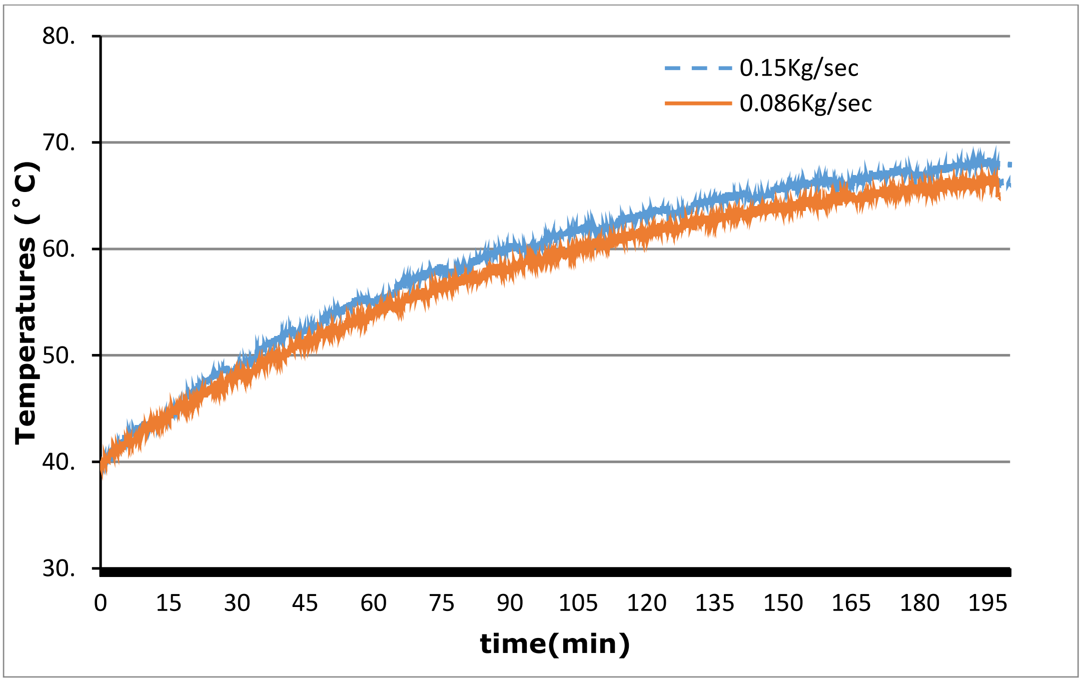

Figure 6-13 Effect of different inlet flow rates on concrete temperatures

Specifically, data for position 2 is used in this test for analysis for both flow rates. For a flow rate of 0.086kg/sec (0.04m/sec) and an initial temperature of 40$°C$, after one hour the temperature of the concrete block rises to around 54$°C$, and reaches 66$°C$ after three hours.

For the flow rate of 0.15kg/sec (0.07m/sec), the initial temperature was also around 40°C. After one hour, the temperature of concrete rises to 55°C, and reaching around 67°C after three hours as shown in Figure 6-14.

Results show clearly that the rate of heat transfer is higher at a higher flow rate during the full three hours of operation.

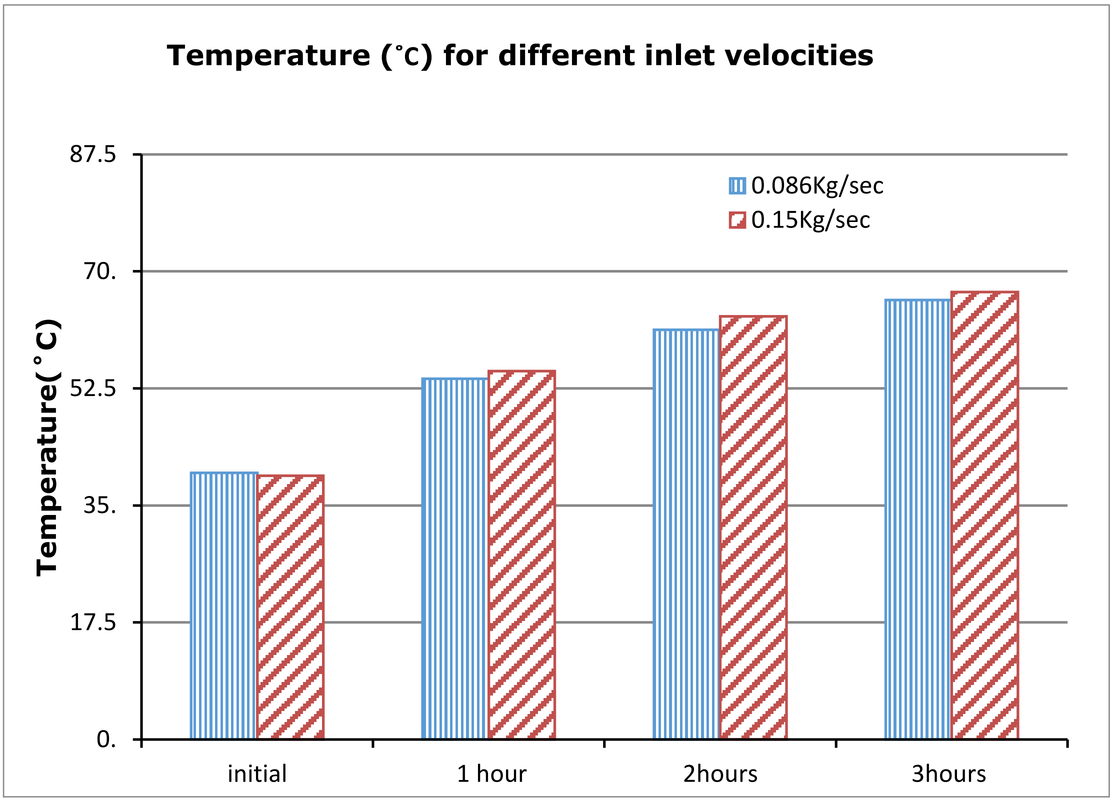

Figure 6-14 Effect of flow rates on the temperature of the TES

Figure 6-15shows the temperature gradient with time during the heating cycle for both inlet flow rates. For the inlet flow rate of 0.086 kg/sec, during the first hour the temperature rose by around 14°C, falling to a little over 4°C after the 3rd hour of operation. This can be explained by the fact that as the temperature of the concrete increases, the concrete temperature becomes closer to that of the inlet fluid; hence less heat transfer as the operation goes on.

Similarly, for the inlet flow rate of 0.15 kg/sec, during the first hour, the temperature rise was around 15°C, falling to less than 4°C in the 3rd hour.

Also in the first hour the temperature rise for the larger speed was higher, and the same happens in the second hour. Nevertheless, in the third hour, the temperature rise for the smaller speed is higher. The reason for this is that during the first two hours there was higher heat transfer due to higher flow rate of inlet oil. Yet since the temperature of concrete is higher using a higher inlet flow rate after a number of hours, the temperature gradient between the inlet fluid and the concrete becomes low. This results in a lower heat transfer, and thus a higher heat transfer occurs in the third hour for the 0.086kg/sec inlet fluid test compared to that of the 0.15kg/sec test.

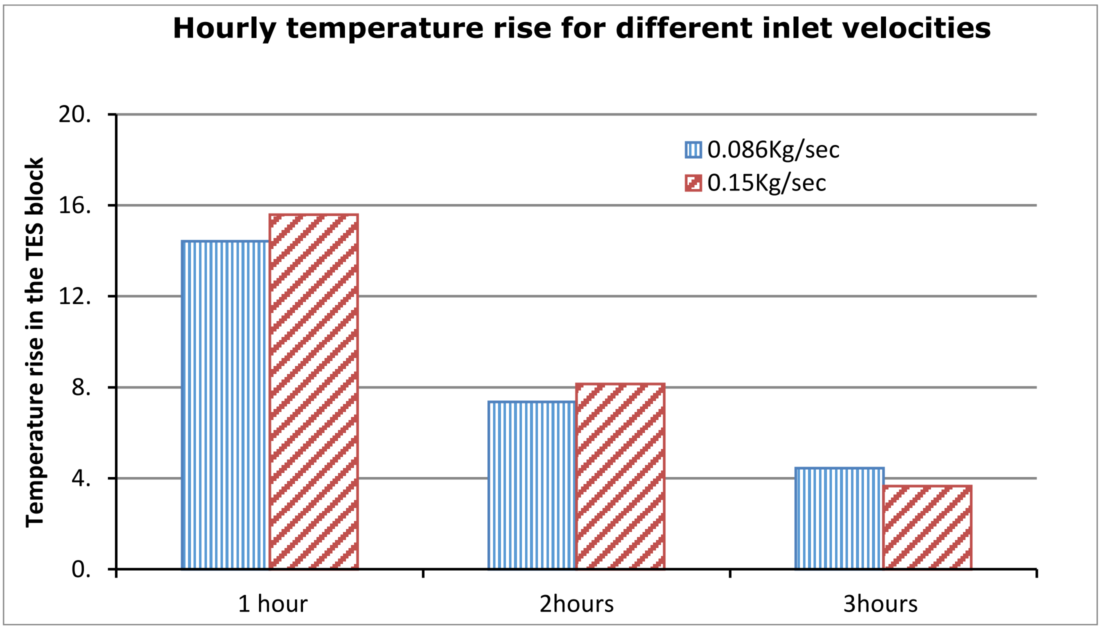

Figure 6-15 Effect of inlet flow rates on hourly temperature rise of the TES block

The hourly energy stored in the TES system is shown in Figure 6-16. For the inlet flow rate 0.086kg/sec, in the first hour the energy stored was around 0.46kWh, and this drops to 0.14kWh in the final hour of the charging.

For the flow rate of 0.15kg/sec, the energy stored was initially around 0.5kWh at the start, dropping to 0.12kWh in the final hour of testing.

Figure 6-16 thus shows exactly the same pattern as that of temperature gradient curves which also follows the same profile. After the end of the three hours, the total energy stored for the 0.086kg/sec test was 0.83kWh and 0.086kWh for the 0.15kg/sec test.

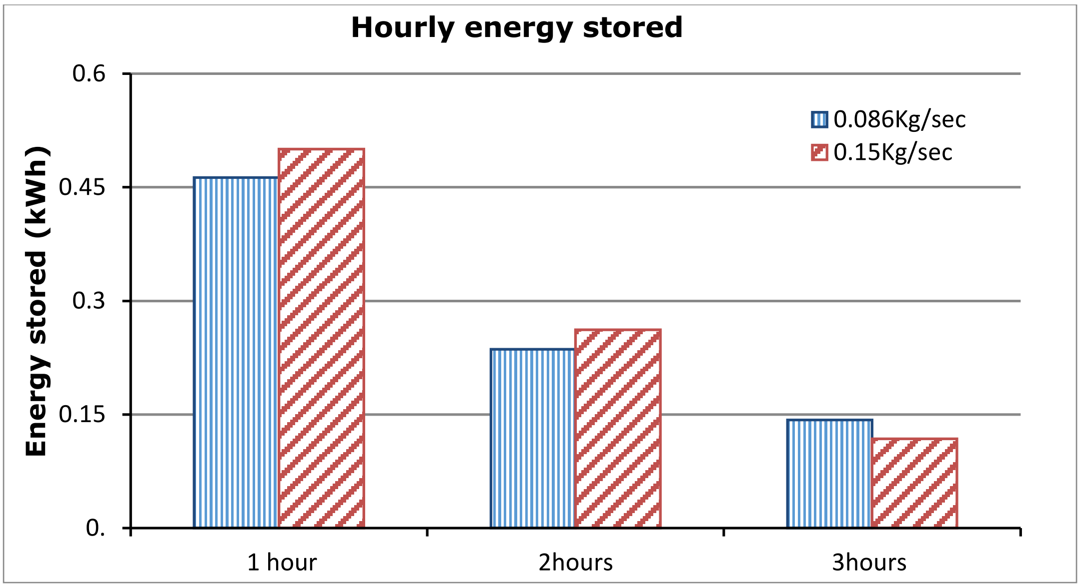

Figure 6-16 Hourly Energy stored at different inlet flow rates

Remarks on flow rates effect on heat transfer in the TES system

For these tests, the inlet fluid flow rate effect on the heating cycle of the thermal energy storage is compared. The results showed that for the first two hours of operation for a 70 ˚C inlet fluid temperature and an initial condition of 40 ˚C concrete temperatures, the heat transfer for the higher flow rate of inlet fluid is higher than that of the lower flow rate. However, as the charging operation continuous, the heat transfer rate becomes higher for the lower flow rate of heat transfer fluid.

The heat transfer is governed by:

$$E = \dot{m} C_p \Delta T$$

At the start of the operation, the flow rate is the dominant factor on the rate of heat transfer as the temperature of the concrete for the tests of both flow rates is similar. However, as the operation continues the temperature gradient factor has more effect than the flow rate effect. Therefore, depending on the application of the thermal energy storage and whether this application requires faster heating of the TES or slower, the optimized flow rate could be chosen.

6.5.3 Effect of inlet temperatures on the heat transfer rate (Test 4)

This test shows the effect of different inlet temperature on the heat transfer between the heat transfer fluid and the thermal storage media. For this test, three inlet temperatures are used: 60˚C, 70 ˚C and 80 ˚C.

Figure 6-17 shows the effect of inlet temperatures on the heat transfer rate. It demonstrates that the higher the inlet temperatures, the higher the heat transfer rate. As such, for the three inlet temperatures, the 80 ˚C inlet has the highest heat transfer rate while the 60 ˚C inlet has the lowest heat transfer rate.

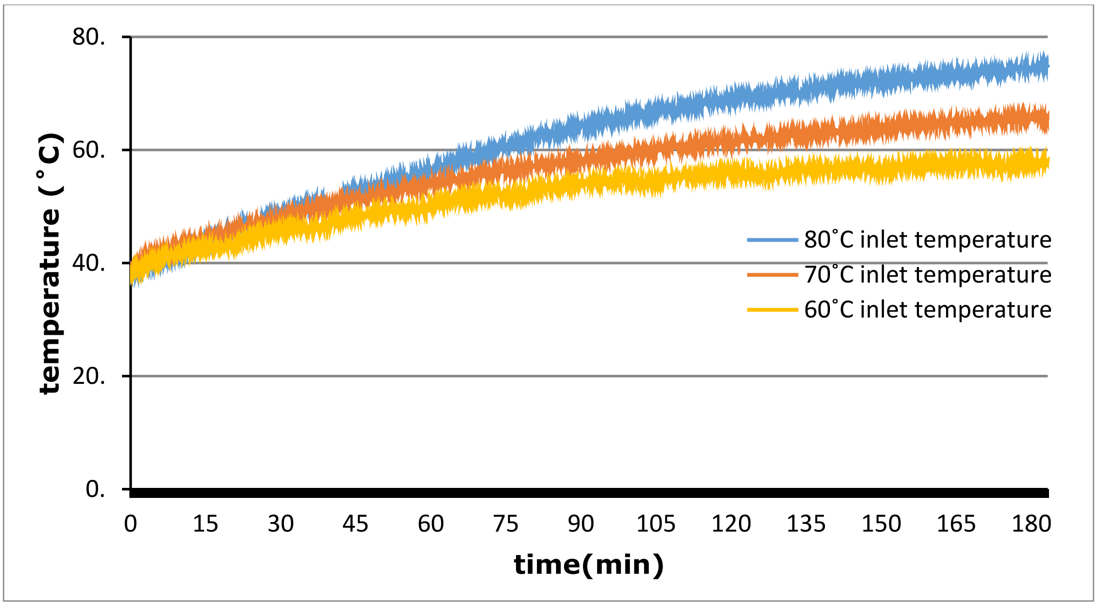

Figure 6-17 Effect of inlet temperatures on TES temperature

Figure 6-18 shows the concrete temperature during the charging operation for the test at 60 ˚C inlet heat transfer fluid temperature. The initial temperature was around 39 ˚C, rising 55 ˚C after 3 hours.

Secondly, for a 70 ˚C inlet fluid temperature, the initial temperature was around 39 ˚C, rising to around 54 ˚C after one hour and finally levels at 66 ˚C after three hours of charging operation.

Thirdly, for the 80˚C fluid inlet temperature, the initial temperature was again 39 ˚C, rising to 74 ˚C by the end of the 3rd hour of charging.

As demonstrated, the initial temperature used was almost the same around 39 ˚C and it becomes clear that the test with higher inlet temperature reaches higher temperature of TES due to the higher gradient between the fluid inlet and the concrete temperature and thus a higher rate of heat transfer.

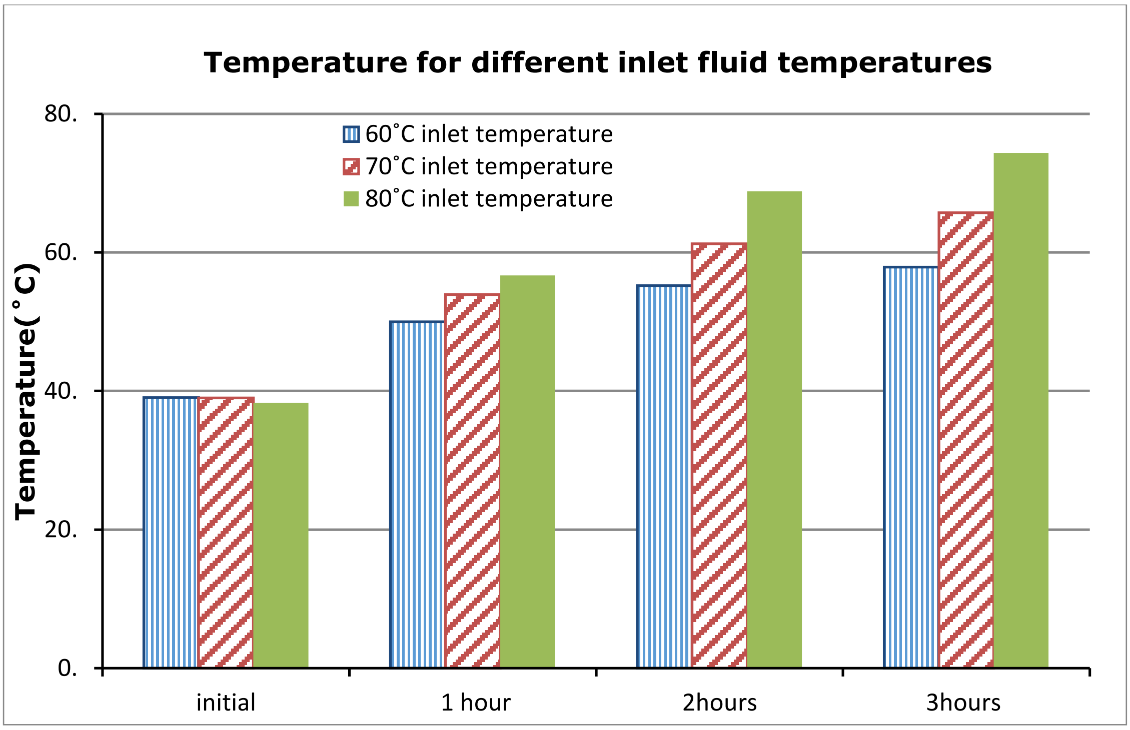

Figure 6-18 Concrete temperatures at different inlet flow rates

Figure 6-19 shows the hourly temperature rise comparison for the different inlet temperatures of the oil. Firstly for the 60 ˚C inlet test, the temperature rise was around 11 ˚C in the 1st hour, falling to 2.5˚C in the 3rd hour of charging.

Secondly, for a 70 ˚C fluid inlet temperature, the temperature rise was around 14 ˚C in the 1st hour, down to 4 ˚C in the final hour.

Finally, for an 80 ˚C fluid inlet temperature, the temperature rise was around 18 ˚C in the 1st hour, going down to 8.5 ˚C in the final hour of testing.

The results shown are expected as the temperature rise is always higher for the test using higher fluid inlet temperature, due to the higher gradient between the fluid temperature and that of the concrete storage.

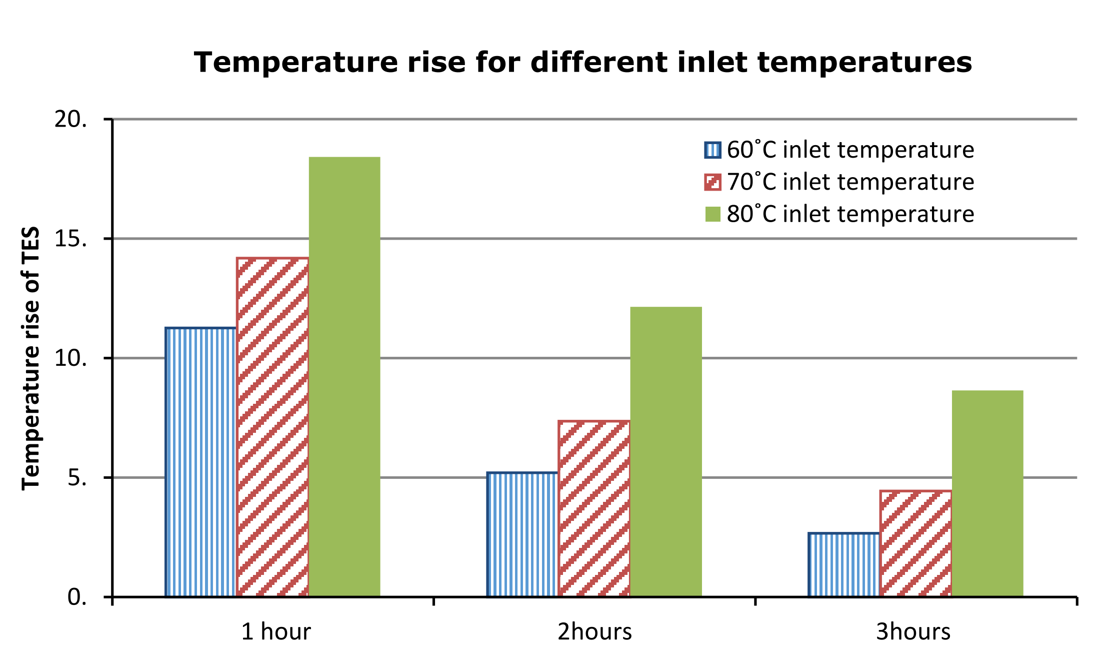

Figure 6-19 Hourly temperature rise for different inlet fluid temperatures

Figure 6-20 shows the hourly energy stored for different inlet fluid temperatures. Starting with the 60 ˚C inlet fluid temperature, the energy stored was around 0.36kWh in the 1st hour, decreasing to around 0.17kWh, and reaching 86Wh over the duration of the three hours. For the following 70 ˚C fluid inlet temperature, the energy stored was around 0.455kWh, going down to 0.24kWh, and reaching 0.1kWh for the final hour of testing.

Similarly, at a 80 ˚C temperature, the energy stored was around 0.59kWh, then 0.4kWh, followed by an additional reduction of 0.28kWh for the final hour of testing.

As a result after three hours of operation, the total energy stored was 0.6kWh for the initial temperature of 60 ˚C; 0.86kWh for that at 70 ˚C; and 1.16kWh for a temperature of 80 ˚C.

As illustrated by the test, the higher the inlet temperature, the higher the temperature gradient between the fluid inlet and concrete, the higher energy stored.

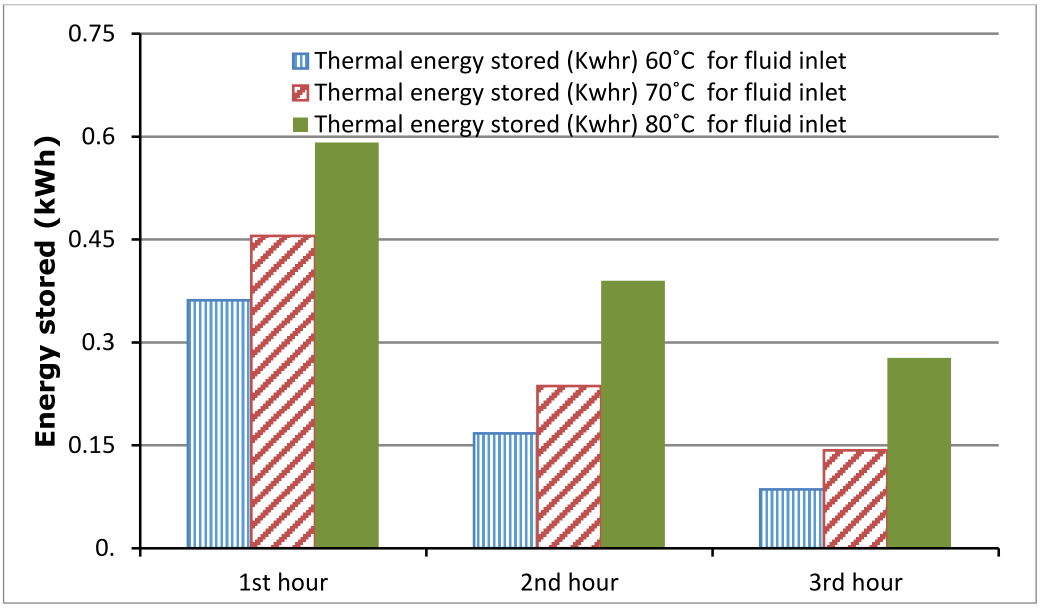

Figure 6-20 Hourly energy stored for different inlet temperatures

Remarks on effect of fluid inlet temperatures on heat transfer rate

Through the implementation of variable fluid inlet temperatures, it was simple to discern the effect of different inlet temperatures on the heat transfer of the thermal storage. It was clear that the temperature gradient between the heat transfer fluid and the concrete block is always higher using a higher inlet fluid temperature. Therefore at any point in the operation, the temperature gradient and the hourly energy stored will always be higher for the 80 ˚C fluid inlet test followed by the 70 ˚C followed by that of 60 ˚C.

6.5.4 Discharging Cycle (Test 5)

The subsequent tests are performed to address the effect of the same parameter during the cooling cycle of the TES system. Figure 6-21shows the cooling cycle for the different initial temperatures of concrete block. It illustrates that the slope for the concrete with an initial temperature of around 75 ˚C is higher than the other two tests where the initial temperature was 65 ˚C in one case and 55 ˚C in the third test. The reasoning behind this is a higher heat transfer due to the higher temperature gradient between the fluid and concrete.

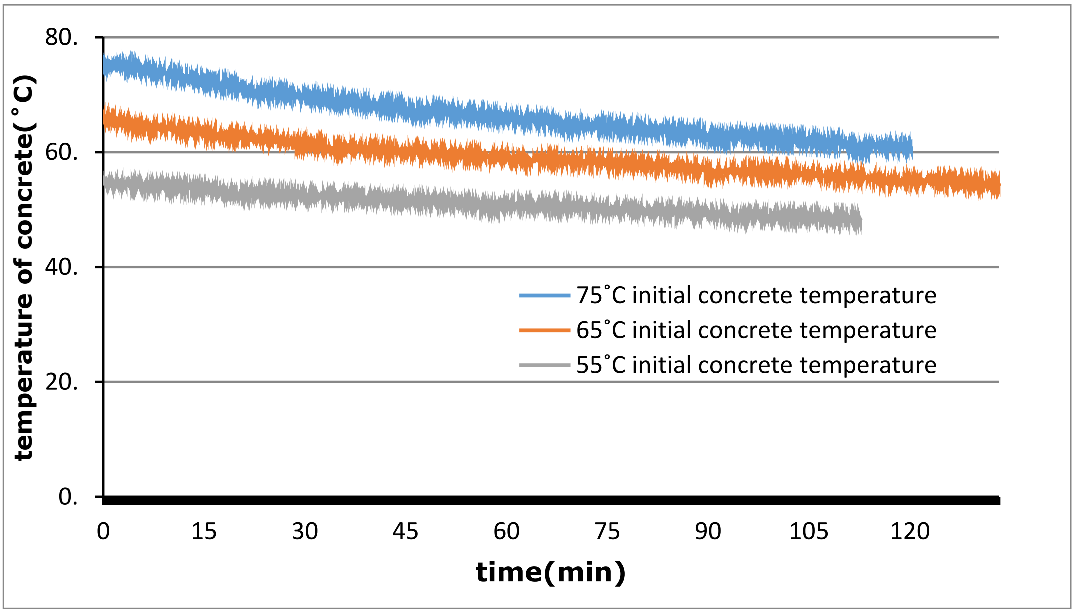

Figure 6-21 TES temperature during the cooling cycle for different initial temperatures of concrete

Figure 6-22 shows the temperatures of the concrete block for the cooling cycle at different initial temperatures of concrete. Taking the 55 ˚C as initial temperature of concrete, the cold inlet oil in this case is 42 ˚C during the operation. The initial temperature after the heating cycle ended was around 54.5 ˚C, which falls down to 49.5 ˚C after 1.5 hours of cooling.

As for a concrete temperature of 65 ˚C, the cold fluid inlet temperature was around 45 ˚C. The initial temperature was thus around 66 ˚C, which then decreases down to around 56.5 ˚C after 1.5 hours of cooling.

Finally for the initial temperature 75 ˚C, the cold fluid inlet temperature was around 47 ˚C. The initial temperature was again around 75 ˚C, decreasing to approximately 63 ˚C by the end of the cooling cycle.

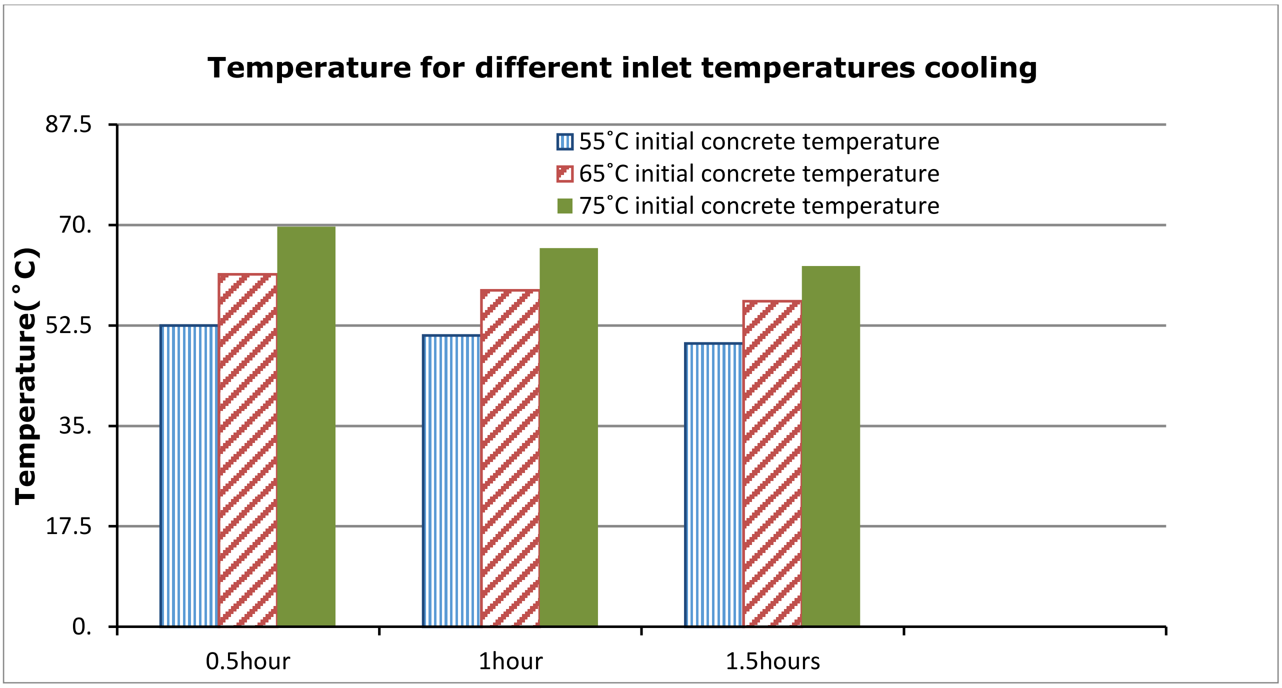

Figure 6-22 Concrete temperatures after cooling with different initial conditions

Similarly, Figure 6-23shows the hourly temperature decrease for the different initial temperatures of concrete block. Once more, for an initial temperature of 55 ˚C, the temperature decrease was around 2.23 ˚C in the first 30 minutes, falling to around 1.4 ˚C in the final 30 minutes.

Secondly, for the initial temperature of 65 ˚C of concrete storage, the temperature decrease was dropped to 1.9 ˚C in the final 30 minutes of discharging.

And thirdly, for a temperature of 75 ˚C, the temperature decrease started with 5.2 ˚C, dropping 3 ˚C in the final 30 minutes of cooling.

As a result, the temperature decrease is always higher for the test with higher initial temperature of concrete, since there is higher temperature gradient between the concrete and the inlet fluid.

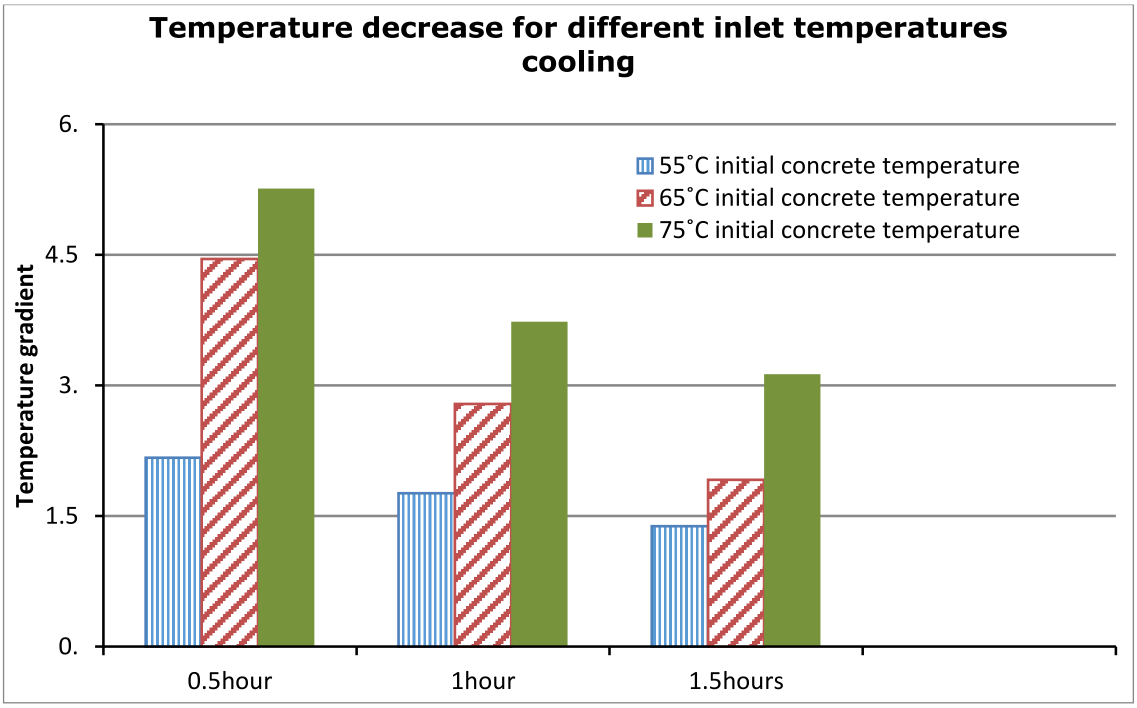

Figure 6-23 Temperature drop for different initial temperatures of concrete

Figure 6-24 shows the energy released from the concrete block for different initial temperatures of concrete. Starting with concrete at an initial temperature of 55 ˚C, the energy taken in the first 30 minutes was around 70Wh, followed by 56Wh and to almost 44Wh after 1.5 hours.

Similarly at 65 ˚C, the energy taken from concrete showed a progression over the 1.5 hours from about 143Wh, to 90Wh, to almost 62Wh.

While for an initial temperature of concrete of 75 ˚C, the energy taken in the first 30 minutes was around 170Wh, followed by 120Wh, then finally down to 100Wh.. In this way, after 1.5 hours, the total energy absorbed from concrete was 0.17 kWh for concrete with initial temperature of 55 ˚C, 0.29 kWh for that of 65 ˚C and 0.39kWh for 75˚C .

As a result, the energy taken from concrete is always higher for the test with higher initial temperature of concrete. Following a similar reasoning to other tests, this is due to the higher temperature gradient between the cold fluid and the hot concrete storage; hence a higher heat transfer.

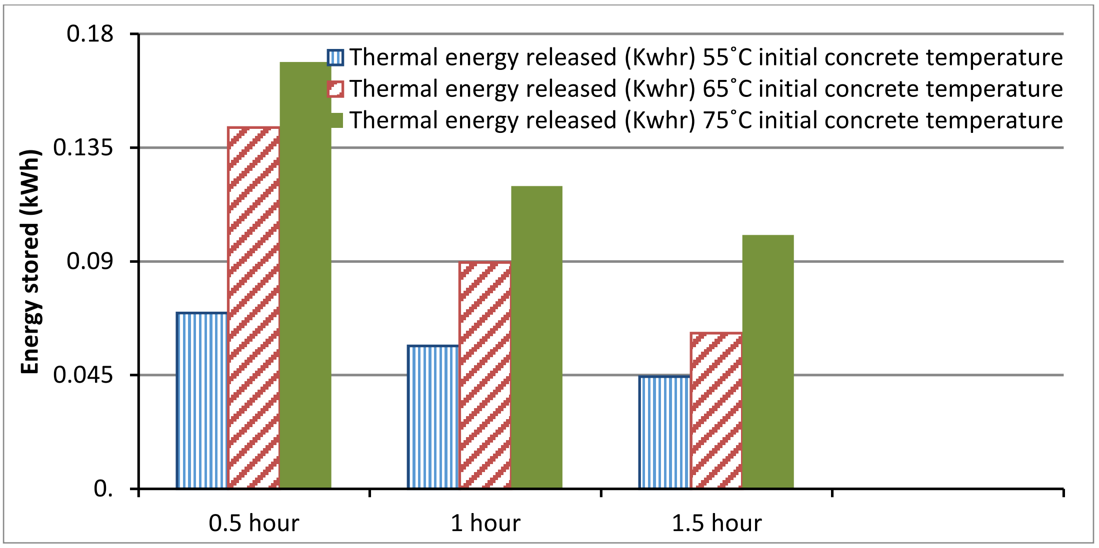

Figure 6-24 Energy released for different initial temperatures of concrete

Remarks on initial temperature of TES on heat transfer for cooling

Having gone through the aforementioned results, this test shows the cooling cycle with different initial conditions of concrete which follows the heating process for the test using different fluid inlet temperatures. For this case due to limitations with the amount of oil available, a closed loop system was used for the cooling cycle causing the cold fluid inlet in this case to vary. Thus in this case for the concrete with an initial condition of 55 ˚C, the cold fluid inlet was around 42 ˚C, 65 ˚C was equivalent to 45 ˚C, and with 75 ˚C, the cold fluid inlet was around 47 ˚C. However, this did not have much effect in the operation which was about two hours for the three tests.

To sum up, the higher the temperature gradient between the now hot concrete and the cold fluid inlet resulted in higher heat transfer and thus the half hourly temperature decrease and thermal energy storage is always higher for the test with highest initial concrete temperature

6.6 Experiment validation of the CFD model

The next section shows the previous results of the experimental testing compared with the CFD modelling that was done with the same initial conditions, the properties of heat transfer fluid and concrete; as well as similar operating conditions. These results are compared to show how accurate the experimental testing was. The accuracy for each case was calculated using

$$Discepancy = \left(100 - \frac{t_{exp} - t_{cfd}}{t_{exp}}\right) \times 100 \qquad (6\text{-}8)$$

a. Validation of 0.15Kg/sec flow and 70˚C inlet fluid temperature for position 1

To begin with, Figure 6-25 shows the CFD plot in comparison with the experimental plot of the temperature of the concrete block for the same position for the duration of the operation. The fluid inlet temperature for that case is 70 ˚C and the same inlet flow rate of the heat transfer fluid was used which is 0.15kg/sec.

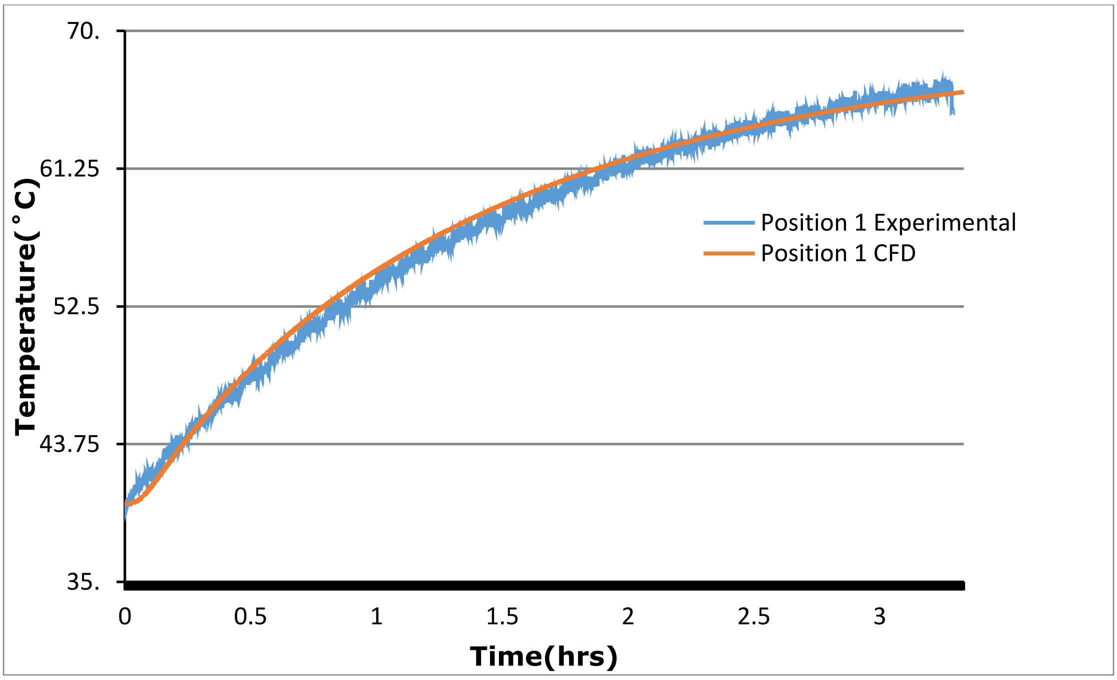

Figure 6-25 CFD and experimental results comparison for 0.15kg/sec flow rate

The discrepancy was calculated on a second by second basis and Figure 6-26 shows the discrepancy plot for the previous comparison of the experimental and the CFD plots. The discrepancy is almost always lower than 3.5 % at any point of the operation. The accuracy was relatively lower at the start of the operation but after one hour, the discrepancy was always lower than 2%.

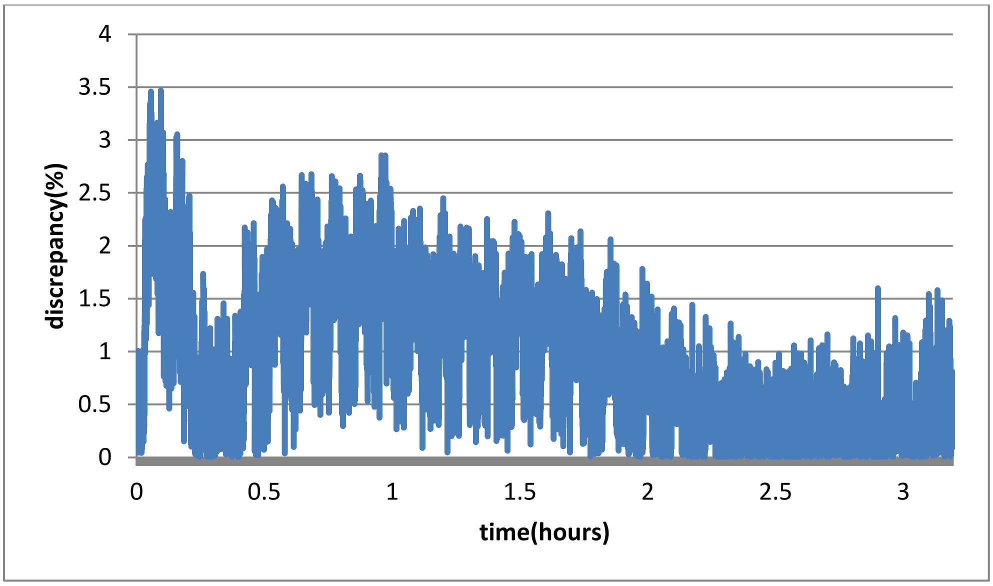

Figure 6-26 Discrepancy for 70˚C inlet and 0.15kg/sec flow rate

b. Validation of 0.15kg/sec flow and 70˚C inlet fluid temperature for position 2

Similarly, Figure 6-27 shows the comparison between the CFD and experimental testing for the same flow rate of 0.15kg/sec and 70 ˚C fluid inlet temperature, for position 2. The plots are almost identical which allows us to deduce that the experimental results were highly accurate. This discrepancy is calculated and the results are shown in Figure 6-28

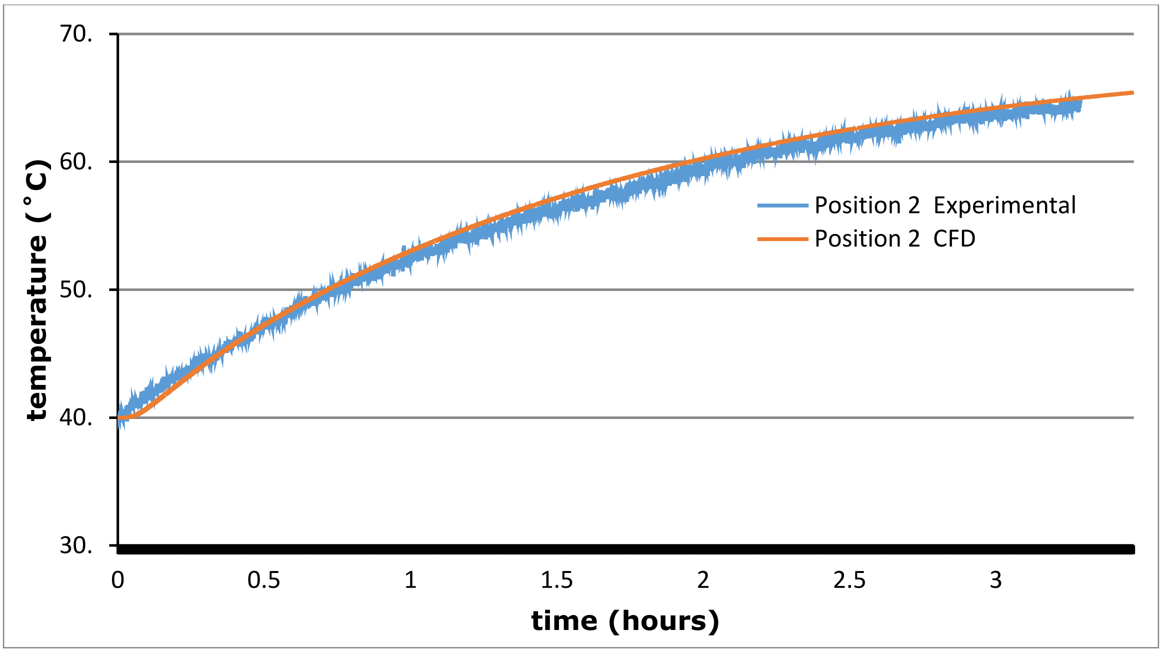

Figure 6-27 CFD and Experimental comparison for position 2 at 70 inlet and 0.15KG/sec flow

Figure 6-28 shows that the percentage of discrepancy does not exceed 4% at any time during the operation. The discrepancy is slightly higher at the start of the operation, but once more it is almost less than 2% for the rest of the operation.

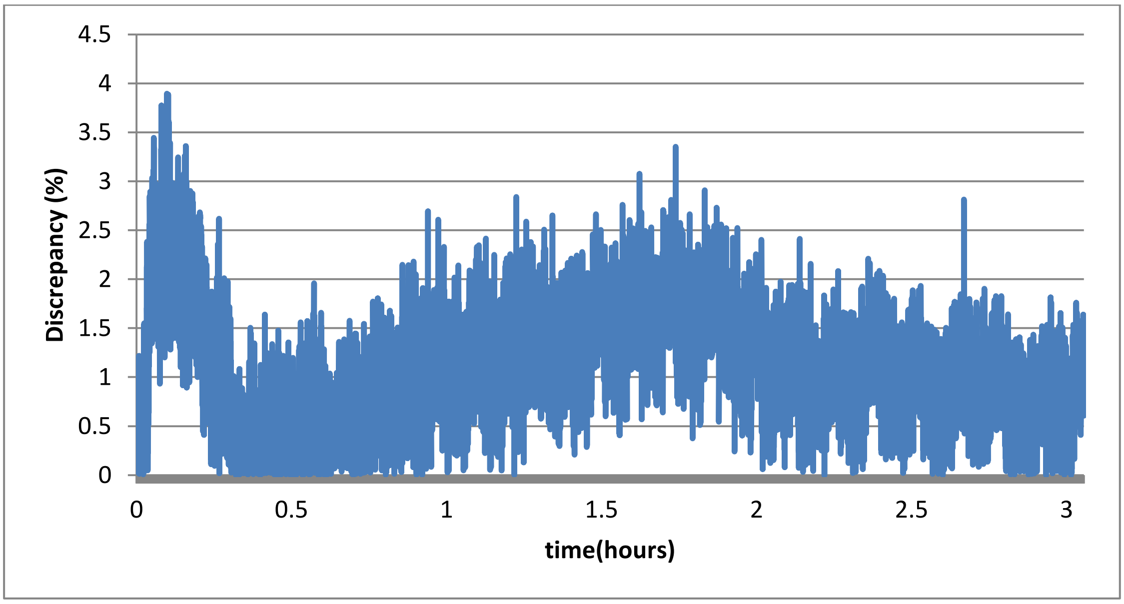

Figure 6-28 Discrepancy at position 2 for 0.15kg/sec flow test

c. Validation for 0.1kg/sec flow rate and 60 ˚C fluid inlet temperature

For this validation, the fluid inlet temperature chosen was 60 ˚C and the same inlet fluid flow rate of 0.1kg/sec was chosen. Figure 6-29 shows the CFD modelling and the experimental results for this test. The results are also very close which provides reason to regard the operation as on point and yields accurate results.

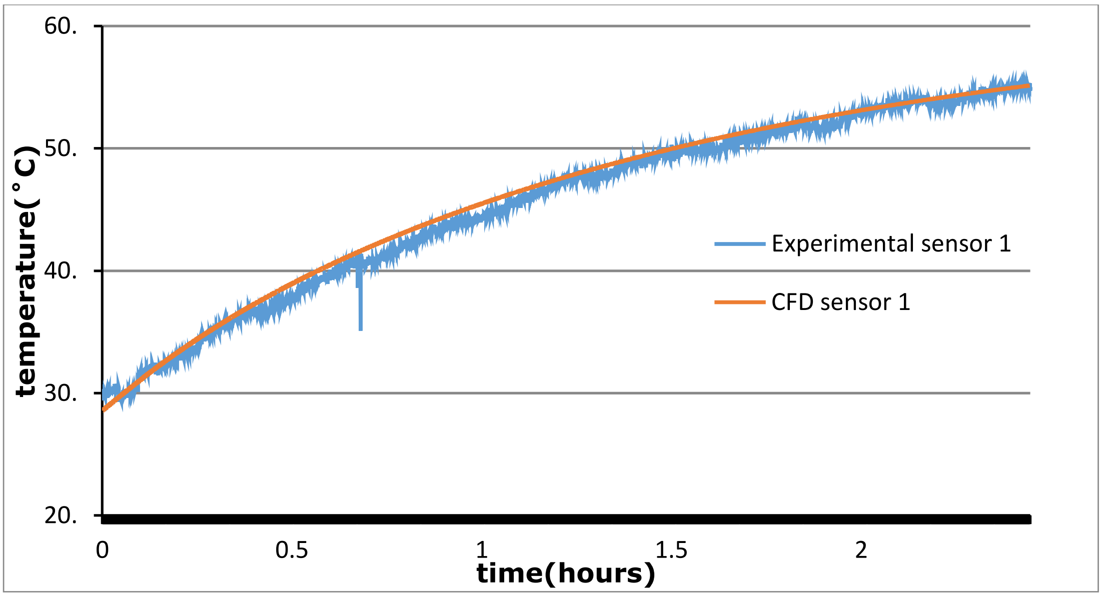

Figure 6-29 CFD and Experimental comparison for 60˚C inlet

Figure 6-30 shows the discrepancy for the 60 ˚C inlet heating for CFD and the experimental results. Here the highest point is around 4% and it averages around 2%. This still shows very accurate testing results compared to the modelling results achieved by using CFD for the same conditions.

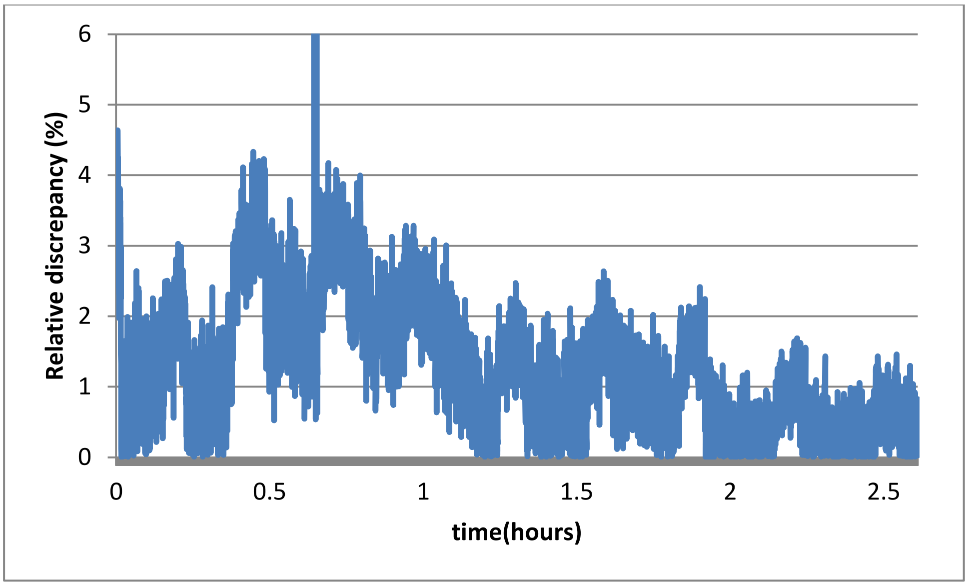

Figure 6-30 Discrepancy for 0.1kg/sec flow rate and 60˚C fluid inlet temperature

d. Validation of heating for 80 ˚C fluid inlet temperature and 0.1kg/sec flow

Similarly, Figure 6-31shows the heating cycle for the 80 ˚C inlet temperatures for both CFD and experimental results. The same flow rate of 0.1kg/sec was used as well and as illustrated in Figure 6-31, which again show similar results.

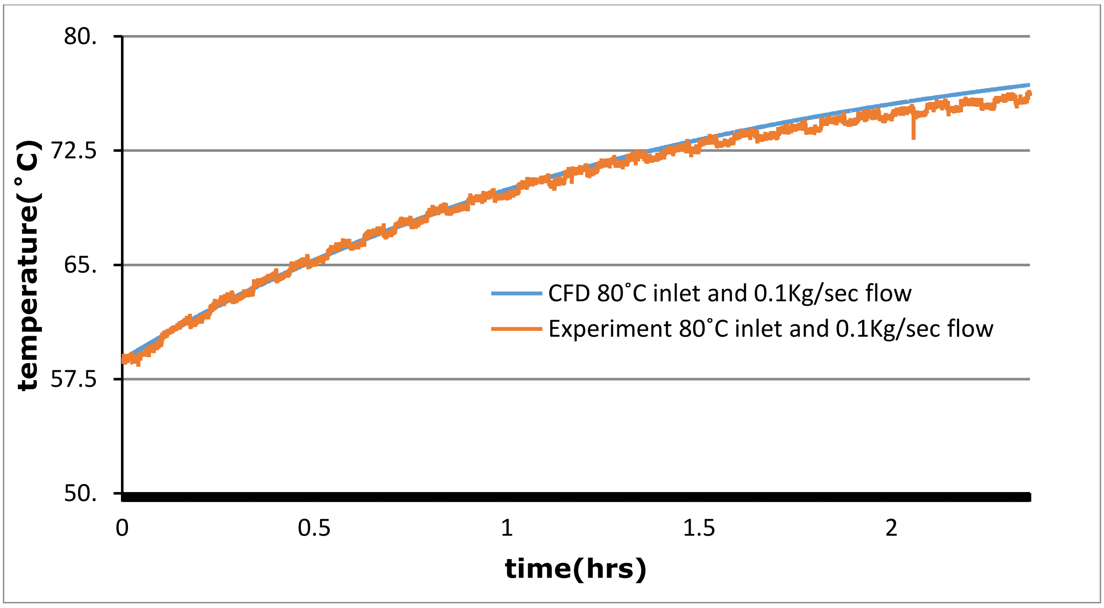

Figure 6-31 CFD and experiment analysis for 80˚C inlet temperature and 0.1kg/sec flow rate

Additionally, Figure 6-32 shows the relative discrepancy for the comparison between the CFD and the experimental results for the 80 ˚C inlet temperature of the hot fluid and using 0.1kg/sec flow rate. Once more, there is high accuracy as the levels of the relative discrepancy do not exceed 2% for most of the operation.

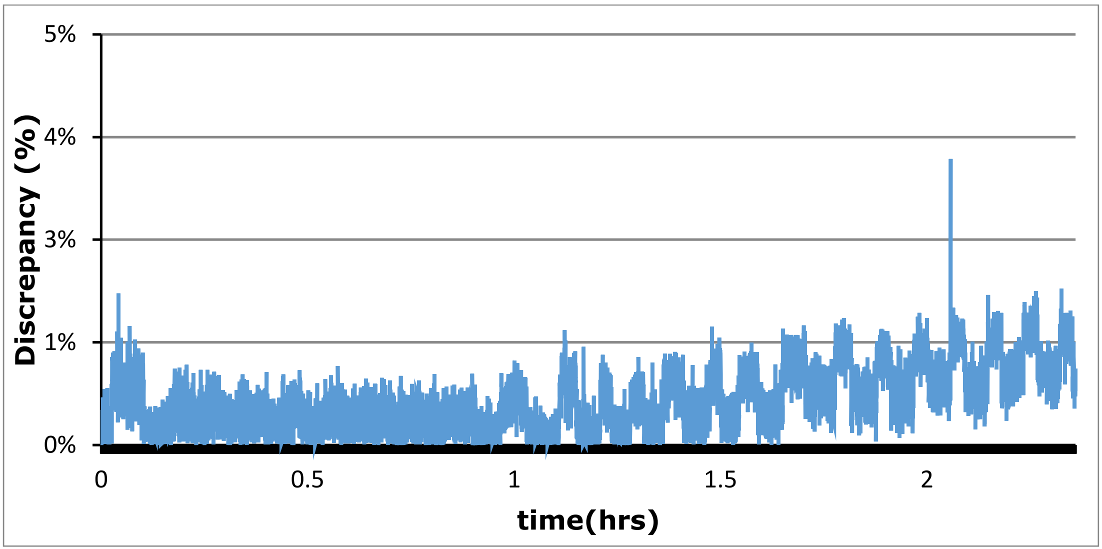

Figure 6-32 Relative discrepancy for 80˚C inlet temperature and 0.1kg/sec flow rate

e. Validation for Cooling Cycle for 65 ˚C initial temperature of concrete and 0.1 kg/sec of flow rate

i. Temperature profile at position 1

Figure 6-33 shows the comparison between the experimental testing and the CFD modelling for the cooling cycle. For this case the initial temperature of the concrete was around 65˚C. The same fluid inlet flow rate of 0.1kg/sec is used and the cold fluid inlet temperature of 45˚C was used in both the experimental testing and the CFD modelling.

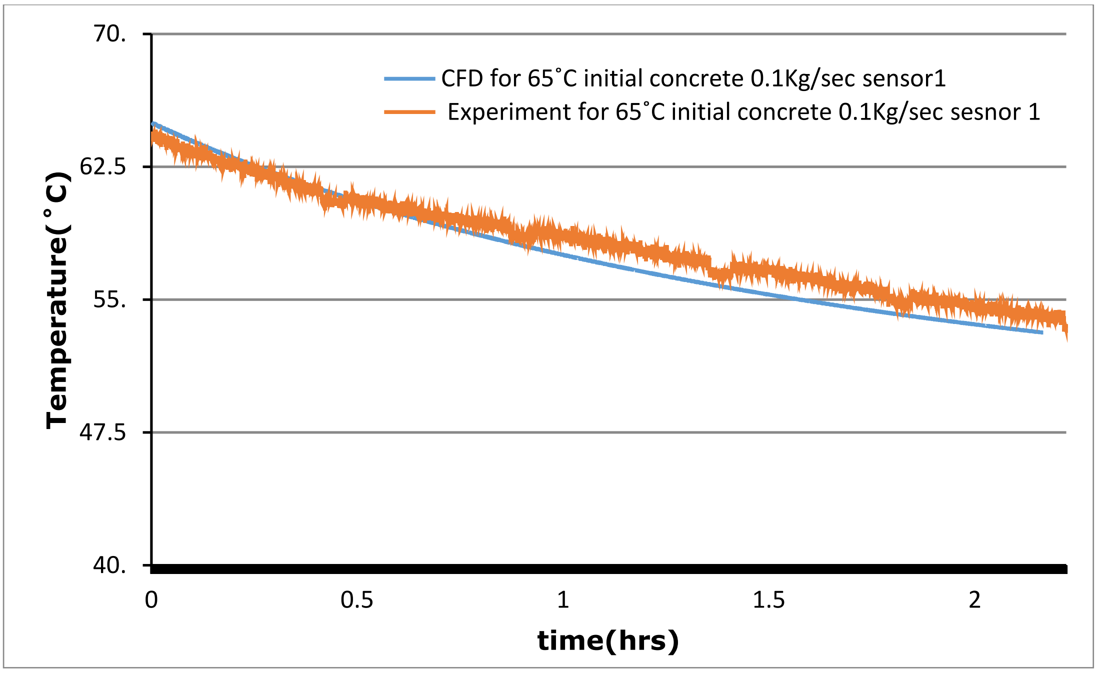

Figure 6-33 CFD and experimental results for cooling cycle for position 1

Figure 6-34 shows the relative discrepancy between the CFD modelling and experimental results. As seen from Figure 6-34, the margin of discrepancy at any point during the two hours of operation does not exceed 4%, and so the results show that the CFD modelling was accurate.

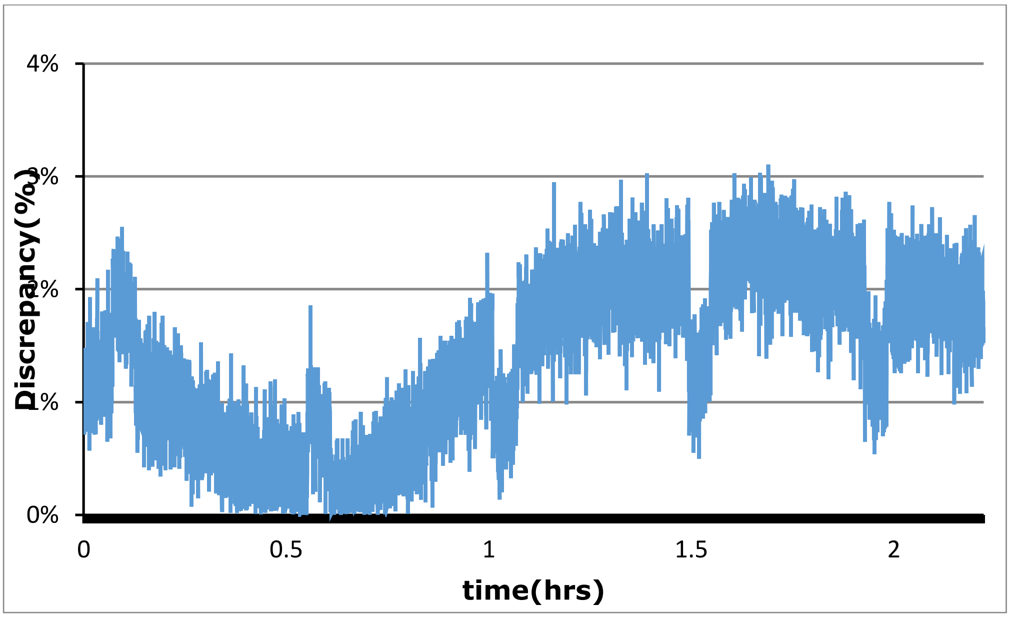

Figure 6-34 Relative discrepancy of CFD and experimental for position 1

ii. Temperature profile at position 2

Concerning position 2 in the concrete, Figure 6-35shows the comparison between the experimental testing and the CFD modelling for the cooling cycle in this case. Here the initial temperature of concrete was around 62˚C. While the same fluid inlet flow rate of 0.1kg/sec is used, as well as the cold fluid inlet temperature of 45˚C in both the experimental testing and the CFD modelling.

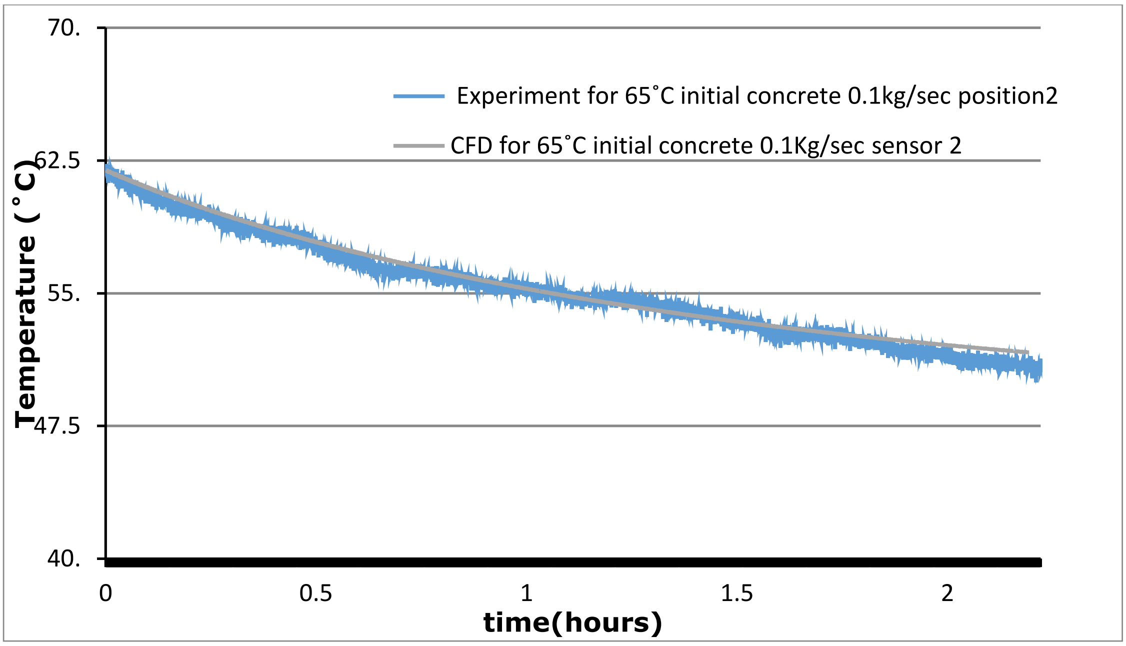

Figure 6-35 CFD and experimental results for cooling cycle for position 1

Figure 6-36 shows the relative discrepancy comparing the CFD modelling and experimental results. As seen from Figure 6-36 the discrepancy at any point during the two hours of operation did not exceed 3%, which points to the accuracy of the CFD modelling.

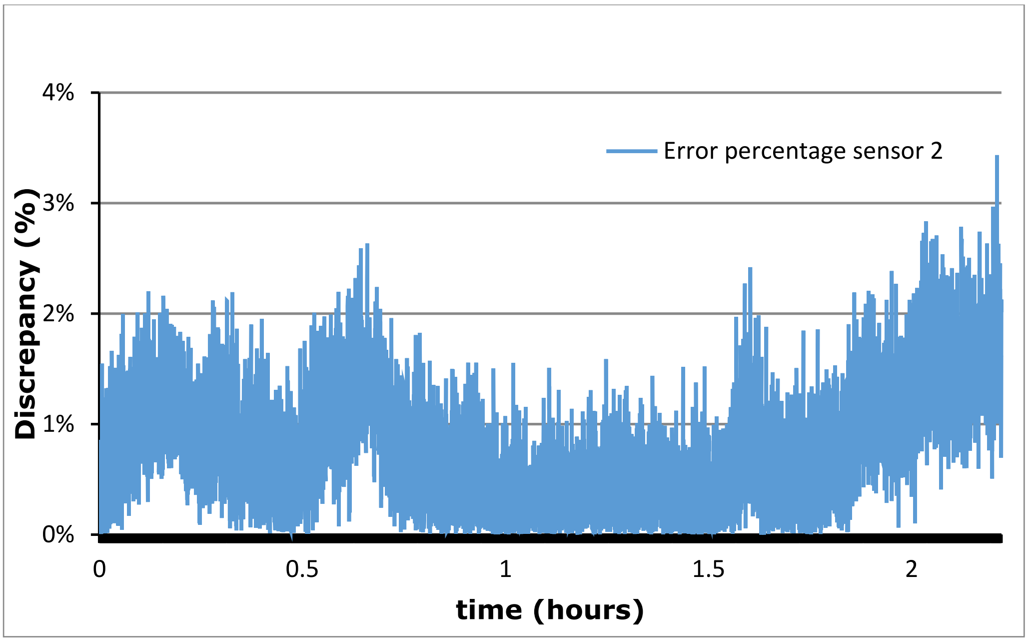

Figure 6-36 Relative discrepancy of CFD and experimental for position 2

6.7 Conclusions

Experimental tests were carried out to test the heat transfer for a concrete block using thermal oil as heat transfer fluid. The concrete block tested is similar to the one simulated in both the CFD and the MATLAB, but on a smaller scale. As such, the heat transfer was tested under different inputs including different fluid flow rates, and fluid inlet temperatures both for charging and discharging cycles. The experiment was limited in terms of size of concrete block, and a cap on the highest temperature for operation due to safety measurements.

The results showed that for a specific period of time:

1) For a concrete block of mass 144kg, and an inlet temperature of 70 ˚C, the heat transfer is high at the beginning of the charging cycle but decreases on a timely basis with an almost saturation after six hours.

2) It was clear that the higher the flow rate, the higher the heat transfer, and thus more energy stored for charging cycle, especially at the beginning of charging (during the first

two hours). However, after a number of hours, the lower flow rate overtakes in terms of temperature rise and energy stored.

3) Also, the higher the inlet temperature the higher the heat transfer, and ultimately the increase in energy stored.

Finally, the experimental test was performed with conditions similar to that of the CFD, and the CFD modelling results were validated with the experimental testing and showed high accuracy of CFD modelling for the different initial conditions with a range of discrepancy between 1% and 4%.

.

Chapter 7 Economic Study on CAES

This chapter assesses the economic value of adding a CAES plant to a renewable energy system and how this impacts the overall financial appeal of the system at hand. On technical grounds, CAES is widely recognized as an exceptionally viable solution for large-scale grid integrated renewable energy systems in terms of load levelling. The report herein focuses on how the inclusion of a CAES system can add value to renewable energy systems in financial terms as well.

7.1 Purpose of CAES

The CAES system can be used for load levelling, hence improving the power supply from intermittent energy systems (e.g. solar and wind). When there is an excess in renewable energy source, the surplus energy is stored and is released to the grid when power from the renewable energy source is deficient. CAES can also be used to improve the profitability of renewable energy systems by timing the sale. In this case, energy is stored in the CAES when selling prices are low, and supplied to the grid when spot prices are high. In the Egyptian grid case, it is particularly useful to use the CAES system for load levelling given the weakness of the grid and the frequent power outages, which currently surpass its value add economically.

7.2 Energy supply strategy with CAES

It is imperative to define a number of terms reiterated throughout this chapter relating to the trading of power between energy providers and the grid systems. Where the CAES system is used to improve economic benefits, the CAES is filled at times of minimum cost, and acts thereby as an energy store, whereas power is sold at times of highest market prices in which case the CAES functions as a trader of electricity. The spot market comprises day-ahead and intra-day trades. The day-ahead market is a forward market in which hourly contracts are traded, supporting the hourly operation of a CAES system. Alternatively, in intra-day markets, trades can be made on the same day, as shortly as 75 minutes before dispatch. Ancillary services products address short-term imbalances in electricity markets by dispatching resources within minutes or seconds of an impending unacceptable such gap. CAES can provide ancillary service to the grid by competing in minute reserve markets. Minute reserve markets can be positive or negative, where power has to be delivered within 15 minutes of trading. Positive reserve markets refer to providers supplying excess power to the grid while negative reserve markets comprise providers drawing and consuming power from the grid. CAES can use less compressor power for positive reserve cases and provide less power in negative reserve cases. CAES systems can compete in such markets owing to their ability to run up to full load in 10-15 minutes and at half load in less than 5 minutes.

7.3 Egyptian electricity market's path to liberalisation

Up until early 1990s, Egypt's ministry of electricity was in full control of all power generation, transmission and distribution activities. In 1996, the government issued a law allowing local and foreign investors to build, own, operate and later transfer (BOOT) generation stations to the state, which saw the establishment of 4 such private companies, selling mostly to the government as governed by long-term contracts dictating dollar-denominated pre-set prices, and based on subsidized natural gas supplied to those companies by the government. In 2001, the private sector was further allowed to supply power to particular consumers, like factories, at which time a handful of private electricity generation companies started up, and a number of factories established their own power plants as an emergency backup, but both could only sell electricity at modest prices set by the state, which was again feasible at that time with subsidized gas prices. This, however saw the government's Electricity Holding Company (mother company responsible for some 16 other state-owned enterprises) accumulate losses of EGP163m as of July, cost the government fifth of its public spending in subsidies, and shut out all private investors. Hence, to attract investments, it was necessary to liberate generation and distribution from the state's grip, and to hand these activities over to private companies with sustainable and profitable business models, creating a free market that is more viable for all parties. Therefore, earlier this year, the government issued the New Electricity Law that dictates the grid feed-in-tariff for renewable energy independent power producers (IPPs), with the tariff for electricity generated from conventional fuels set to follow shortly. It also completed the unbundling of generation, transmission, and distribution to unwind the single-buyer mechanism and pave the way for competition and free market operation, supported by direct bilateral agreements and third-party access to transmission and distribution networks. This was especially inevitable following the government's enforcement of a plan to phase out energy subsidies over the next 5 years, in another move to free the markets, lure investments and push for much-needed fiscal consolidation. As power suppliers compete for customers, service should improve, prices should stay low, pressure on the national grid be relieved, and more room be allowed for the Holding company to overhaul some 20-year old generation and distribution networks making up 40% of capacity. While the regulator would still intervene to prevent unreasonable price hikes and monopolies, the long-term target is to create a real open market for electricity, much like any other freely traded product (Business Monthly , 2015 ; MOEE 2014)

7.4 Methodology and Results

Computer programing is used to implement yearly simulation of the economic analysis of the system. The system's total annual revenues are calculated. Capital costs are also calculated, converted into yearly payments, and added to the system's total fixed and variable annual costs. The annual net profit/loss and the return on investment (ROI) was calculated accordingly, and used as a measure of economic feasibility. Two systems were simulated, the first being the implementation of a wind farm without CAES, and the second simulating the addition of a conventional CAES system. The analysis is performed using MATLAB. For each scenario, the system's annual net present value (NPV) and annual ROI are calculated. Additionally, a sensitivity analysis is carried out on some of the model's input parameters to gauge the effect of each on the NPV of the system and to gain a better sense of how these parameters can change the economic feasibility of the system.

It is worth mentioning that there are also a number of constraints that govern the CAES operations, whether used for load levelling or for economic optimization. These constraints have to do with cavern air. The minimum and the maximum pressure must be calculated at all times. Compression can only be made if the CAES cavern is not full (at maximum pressure), whilst expansion or selling electricity to the grid can only be done if the cavern is not empty (less than minimum pressure).

As previously mentioned, the economic analysis for this case study is carried out for the following two setups:

1) Wind farms with no energy storage
2) Wind farm with CAES

7.4.1 Wind power without CAES

The wind farm costs can be divided into (1) capital costs and (2) annual running costs, which include labour cost and operational maintenance cost.

1. Capital costs comprise:
    a. Wind turbines
    b. The foundation
    c. Grid connection

d. Planning

A breakdown of the capital cost is shown in Figure 7-1(Irena, 2013). The capital cost per unit power of wind varies significantly across countries. Denmark has the lowest capital cost per unit power of \$1634/KW, while Japan has one of the highest capital costs of \$3426/KW of installed capacity (International Energy Agency, 2013). The figures were adapted from the IEA wind report for 2012 installations, with the majority of the available data being for developed countries.

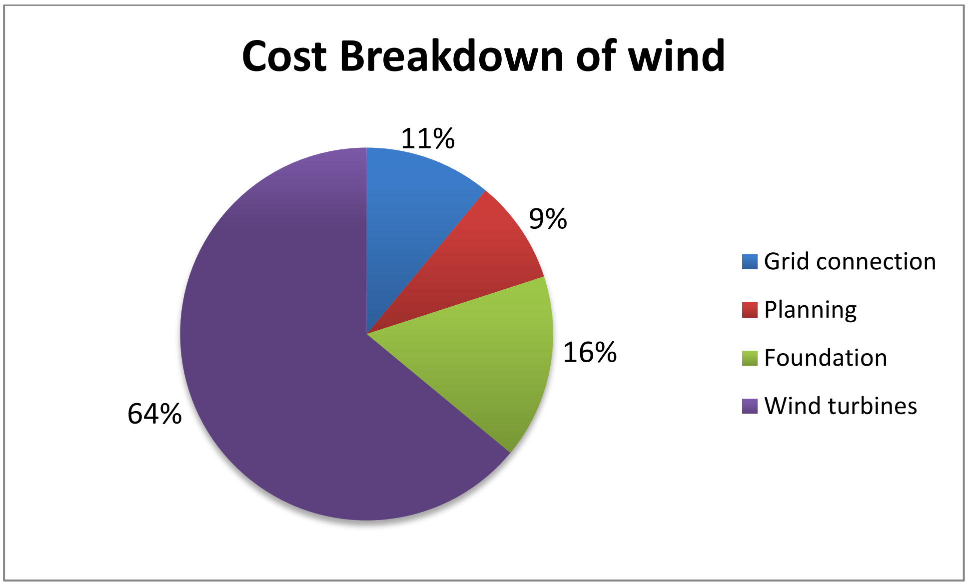

Figure 7-1 Cost breakdown of wind turbines (IRENA,2013)

2. Running costs comprise:
    a. Fixed costs, which normally include insurance, administration, fixed grid access fees and service contracts for scheduled maintenance.
    b. Variable O&M costs, which typically include scheduled and unscheduled maintenance not covered by fixed contracts, as well as replacement parts and materials, and other labour costs.

Fixed and variable operation and maintenance costs (O&M) vary across countries typically depending on the size of the installed capacity for each country. The O&M costs vary from

$10/MWh for the US to as high as $43/MWh in Switzerland, with the European countries tending to have higher O&M costs (Irena, 2013). An assumption is made that since the expertise in the wind turbines maintenance is lacking in Egypt, the relative O&M cost will be assumed to be on the higher end with $43/MWh used in our simulation.

The annual revenues from wind farms are calculated using Eq. (1)

$$R_w = \sum_{t=1}^{8760} P_w \times P_m \tag{7-1}$$

Where P_w is energy supplied from wind and P_m is the market price

The NPV of the system is calculated using Eq. (2)

$$NPV_w = -C_w + \sum_{t=1}^{T} \frac{(R_w - AC_w) \times e^{t-1}}{(i+1)^t} \tag{7-2}$$

Where C_w is the capital cost of building a wind farm, $AC_w$is the annual cost of the wind farm, e is the escalation factor and i is the interest rate.

The NPV is converted to average annual payments, A_w, using Eq. (3)

$$A_w = \left(\frac{(i \times (i+1)^t)}{(i+1)^t - 1}\right) \times \left(C_w + \sum_{t=1}^{T} \frac{(AC_w) \times e^{t-1}}{(i+1)^t}\right) \tag{7-3}$$

Electricity production cost for the wind farm is calculated using Eq. (4)

$$Prod_w = \frac{A_w}{\sum_{t=1}^{8760} P_w} \tag{7-4}$$

$$ROI = \frac{Annual\ profits}{(i+1)^t \times C_w} \tag{7-5}$$

7.4.1.1 Wind energy assumptions

Based on a number of contracts signed in Egypt in 2014 and 2015 for renewable projects, the investment cost averages $1.73m/MW for wind projects with capacities in the range of 100-220 MW. As for the economic life of the system, the average is around 25 years, consonant with that of the CAES system. According to the Egyptian government's newly announced feed-in tariffs, the grid will buy wind power for EGP0.68-0.82/kWh—equivalent to $89-108/MWh—depending on the number of annual operating hours of the wind farm. Running the numbers for the assumed number of hours of annual operation in our simulation gives a feed-in tariff of cent$9.57/kWh in the first 5 years, dropping to cent$8.93/ kWh during the remaining years of operation (MOEE annual report, 2014). An annual interest rate of 5% is assumed, which will be varied later in a sensitivity analysis.

Table 7-1 New wind feed-in tariffs (MOEE annual report 2014)

Number of operating hours	Energy purchase price (first 5 years of operation) (cent$/kWh)	Energy purchase price (remaining years of operation) (cent$/kWh)
2500	11.48	11.48
2600		10.56
2700		9.71
2800		8.93
2900		8.19
3000		7.51
3100	9.57	8.93
3200		8.33
3300		7.76
3400		7.23
3500		6.73
3600		6.26
3700		5.81
3800		5.39

To maximize revenues, a new mode of operation is elected in place of load levelling, where the wind will only produce power when its speed is close to the rated power, minimizing thereby the number of operating hours per year. This ensues from the arrangement that entails a decreasing purchase price as the number of annual operating hours increases, according to the new feed-in tariff law. Therefore, whenever the wind speed is lower than the rated speed (the extent of which is constantly gauged for profit maximization purposes), the wind turbines are shut down. Conversely, whenever the wind speed is close to the rated speed, the wind farm runs normally, selling the generated power to the grid. Using the available wind speed 3-day data for the said model, a wind production capacity factor of 0.35 is calculated, and an annual interest rate (i) of 5% is used in this base case simulation. The NPV and ROI values are shown next. Firstly, Figure 7-2 shows the mode of operation of the wind turbines, which is limited to the scenario of a power output that is 80% of the rated power ,the choice of which is implemented for highest economic benefit based on results obtained in Figure 7-5 where highest NPV ($207m) is achieved for 3100 hours of operation per annum; as otherwise the wind power is either dumped or delivered to CAES for storage, if a CAES system is available.

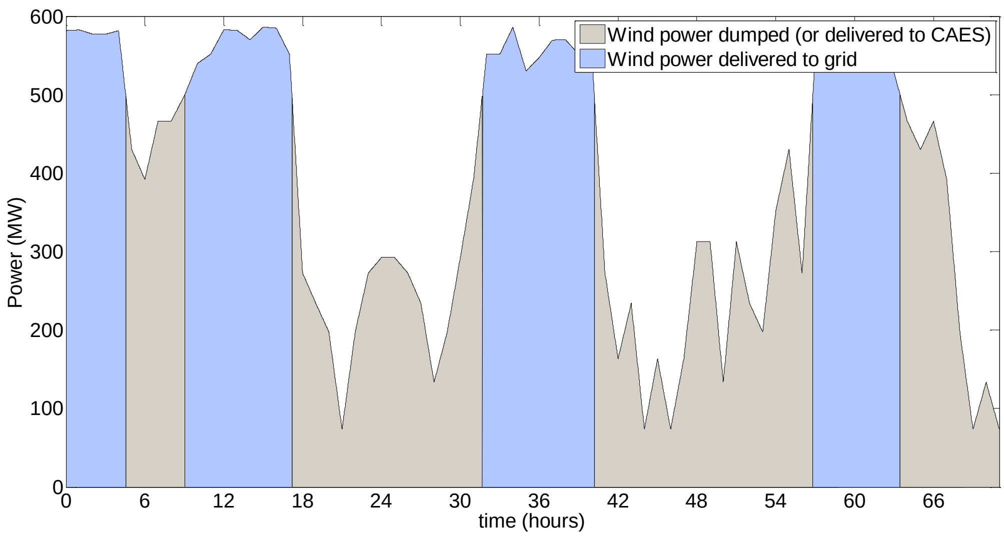

Figure 7-2 Wind power production for profit maximization

Table 7-2 (base case parameters for the wind system)

Wind without CAES (Egypt) base case parameters	
Selling price to grid	$95.7/MWh (first 5 years of operation) $89.3/MWh (remaining years of operation)
Interest rate (i)	5%
Annual fixed and variable O&M costs	$43/MWh
Capital cost	$1730/KW

7.4.1.2 Wind energy economic results

A graph plotting NPV overtime is shown in Figure 7-3, where the NPV value increases from -$1003m to $207m by the end of year 25 of operations, assuming a selling price of $95.7/MWh for the first 5 years and $89.3/MWh for the remaining years of operation, as set by the new Egyptian law for wind turbines newly integrated to the grid.

Table 7-3 (Calculated costs and revenues for a wind farm in Egypt's Suez governorate)

Wind without CAES (Egypt) – Suez example	
Capital cost ($m)	1003
Annual O&M costs ($m)	76

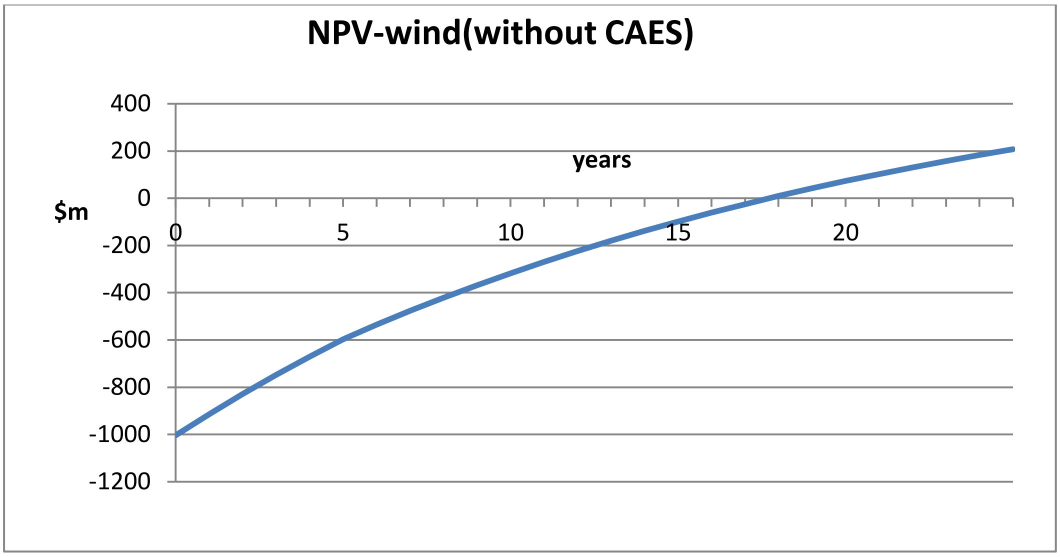

Figure 7-3 Cumulative discounted net cash flow of wind turbines

At year 0, a cash outflow of $1,003m occurs, representing the project's investment cost. In subsequent years, annual revenues exceeded annual costs, resulting in a build up of positive net cash flows against the initial investment cost until the system breaks even after around 17.5 years of operation, having accumulated enough positive cash flows to cover the initial outlay. Thereafter, project NPV turns positive and increases overtime. By the end of a 25-year base case simulation period, the system is estimated to have produced $207m in economic profits. It is worth noting, however, that the results factor in the earlier mentioned assumption that power is dumped whenever the wind speed is lower than the rated speed The ROI, on the other hand, starts at 9% and decreases overtime on the back of a longer discounting period of a fixed net cash flow, as annual fixed costs are assumed constant...

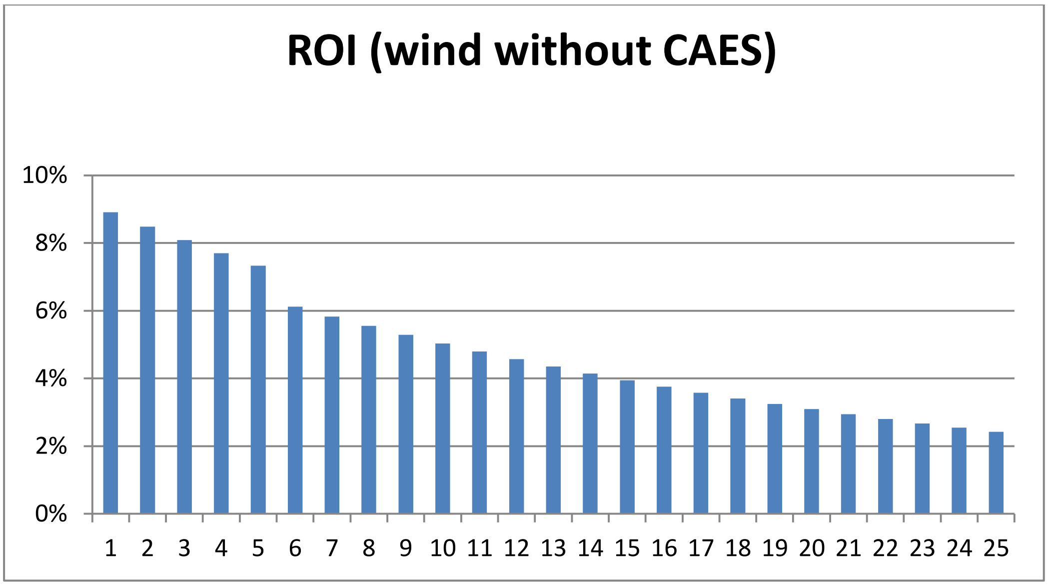

Figure 7-4 ROI for wind turbines

7.4.1.3 Sensitivity analysis for wind farms in the Suez area

The following parameters are varied in this analysis to test the effect of each on the NPV value of the wind power system:

A. Selling price to grid
B. Capital cost of the wind system
C. Annual costs of wind system
D. Annual interest rate (i)
E. Replacement cost of the wind system

A. Sensitivity to selling price

As mentioned previously, Egypt's newly set wind feed-in tariff varies with the number of operating hours of the wind farms. Therefore, in this sensitivity study, the selling price is varied in correspondence with the relevant assumed number of hours of wind operation, and the effect on the value creation of the wind farm measured accordingly.

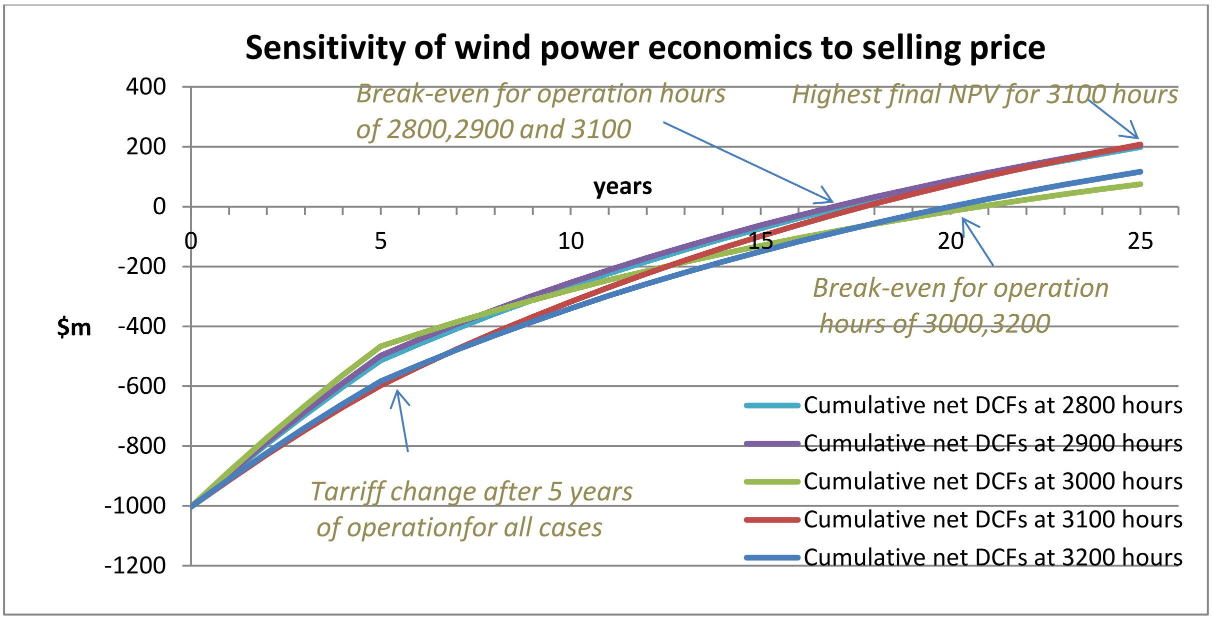

Figure 7-5 Cumulative discounted net cash flow scenarios reflecting different selling prices to the grid

The results show that profitability peaks at the optimal number of operating hours in the vicinity of 3100 hours per annum, where the system breaks even after 18 years and yields an NPV of $207m. The profitability of the 2800-hour and 2900-hour zones ranks next, with a break-even period of around 17 years and NPVs of $194m and $204m, respectively. The worst performers, amongst the tested operations, are the vicinities of the 3000-hour and the 3200-hour annual operations, with a break-even period of 20 years and NPVs of $75m and $116m, respectively.

B. Sensitivity to capital cost

As earlier mentioned, the capital cost estimate for the initial simulation was taken as $1730/KW, based on the data available from recent agreements for wind projects in Egypt (Sewedy and Gabal el Zeit). The figure is varied in the analysis herein across different points between the minimum and maximum capital cost in developed countries, i.e. in the range of $1600-3500/KW of installed capacity.

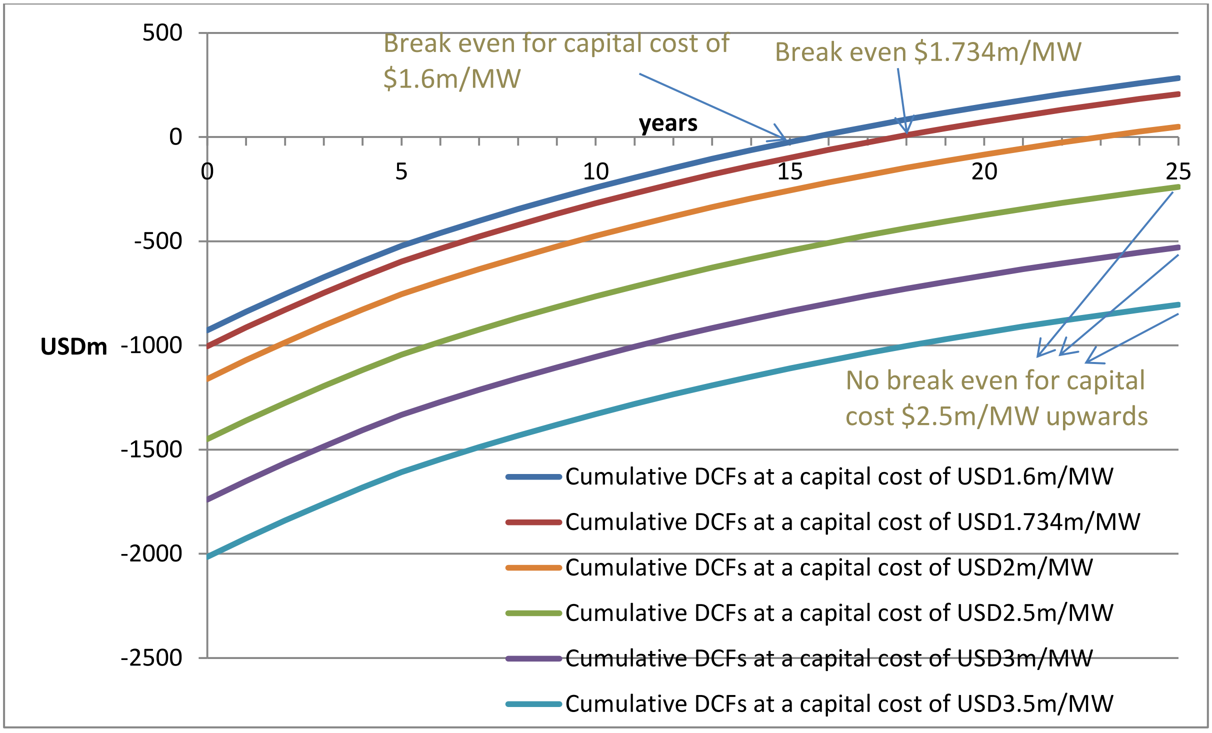

Figure 7-6 Cumulative discounted net cash flow scenarios reflecting different initial investment costs of wind turbines

The chart shows that at the minimum assumed capital cost (that of the Denmark), and assuming a base-case scenario of a selling price of $95.7/MWh in the initial years and $89.3/MWh afterwards (based on a 3100-hour operational year), the investment pays back the initial capital cost after 15.5 years of operation. The payback period increases to 23 years at a capital cost of $2000/KW. At higher capital costs, the investment falls short of a break-even during its useful life.

C. Sensitivity to annual costs

The fixed and variable costs are changed in unison from a minimum total O&M cost of $10/MWh, for a country like the U.S., to a maximum total O&M cost of $50/MWh. Figure 7-7 shows that at the minimum fixed and variable cost points (simulating the U.S. situation), the wind farm breaks even after nearly 8.5 years. The system achieves a break-even during its lifetime in all simulated O&M cost scenarios, with the worst-case scenario of a cost of $50/MWh showing a break-even period of 24 years.

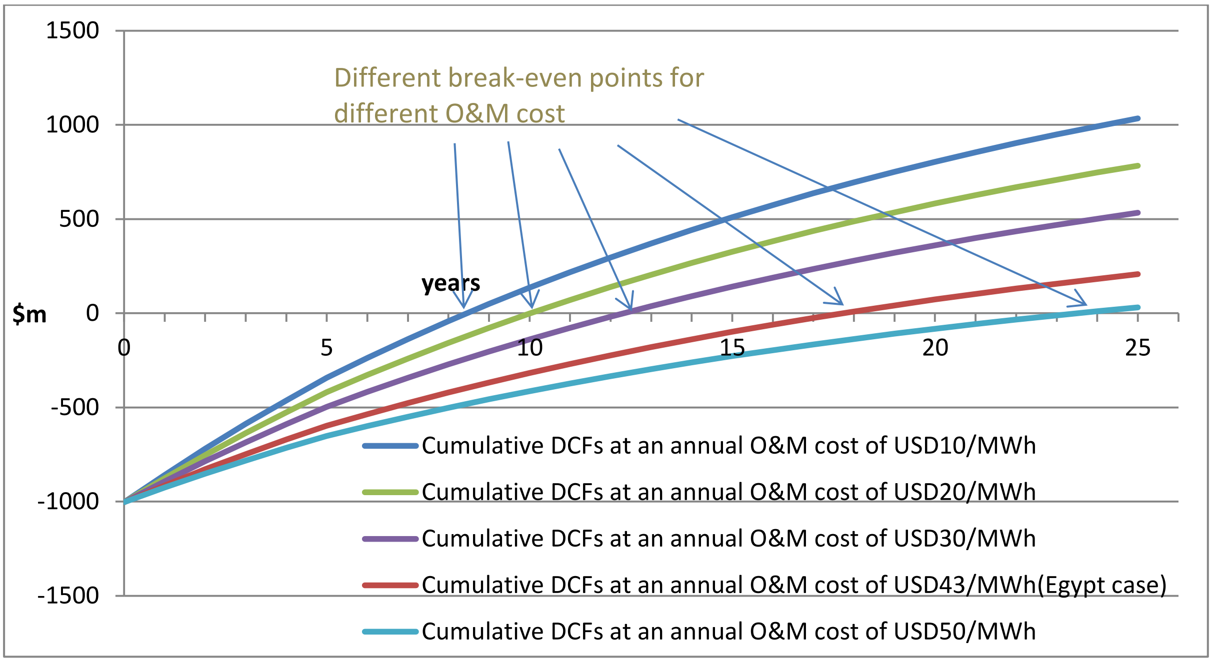

Figure 7-7 Cumulative discounted net cash flow scenarios reflecting different fixed and variable annual costs of wind turbines

D. Sensitivity to interest rates

To test its effect on the system's economic feasibility, the interest rate in the simulation is varied between 4% and 8%, with the base case set at 5%.

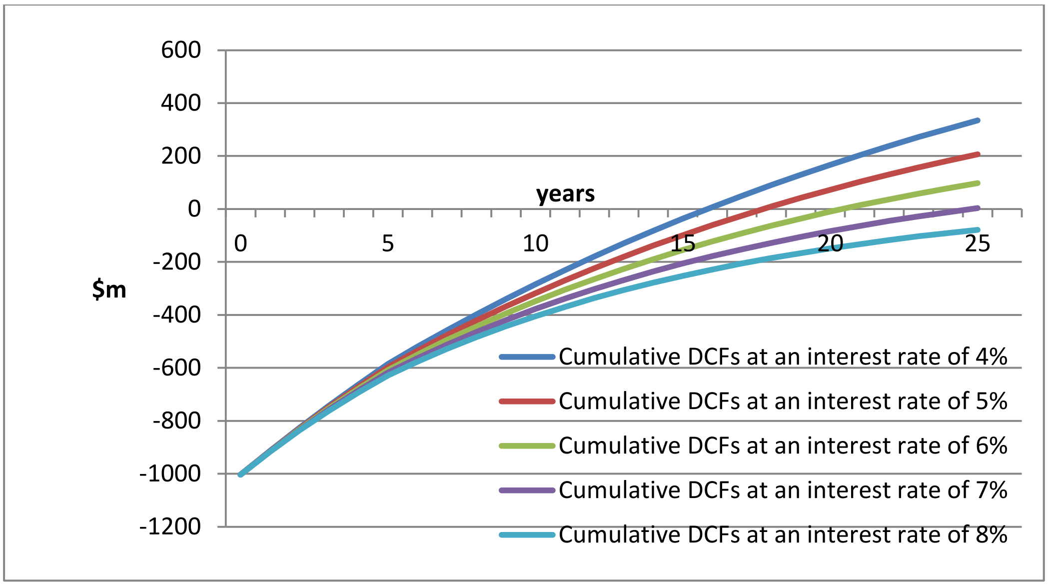

Figure 7-8 Cumulative discounted net cash flows reflecting different interest rates scenarios

The analysis reveals that the NPV of the system is exceptionally sensitive to the prevailing interest rate environment. At an annual rate of 4%, the base case system breaks even in 15 years. Increasing the interest rate results in a progressively decreasing NPV, and extends the break-even period from 15 years at a 4% interest rate to perpetuity (no break-even during the project's economic life) at an interest rate of 8%.

E. Sensitivity to replacement cost

The analysis simulates the need to replace 0-30% worth of the wind turbine cost, the main components which are subject to more wear and tear and hence are more likely to be replaced are rotor blades and the gear box of the wind turbines. The wind turbine cost represents around 64% of the total capital cost of wind, with the assumption being that some of its components will need replacement after 10 years of operation.

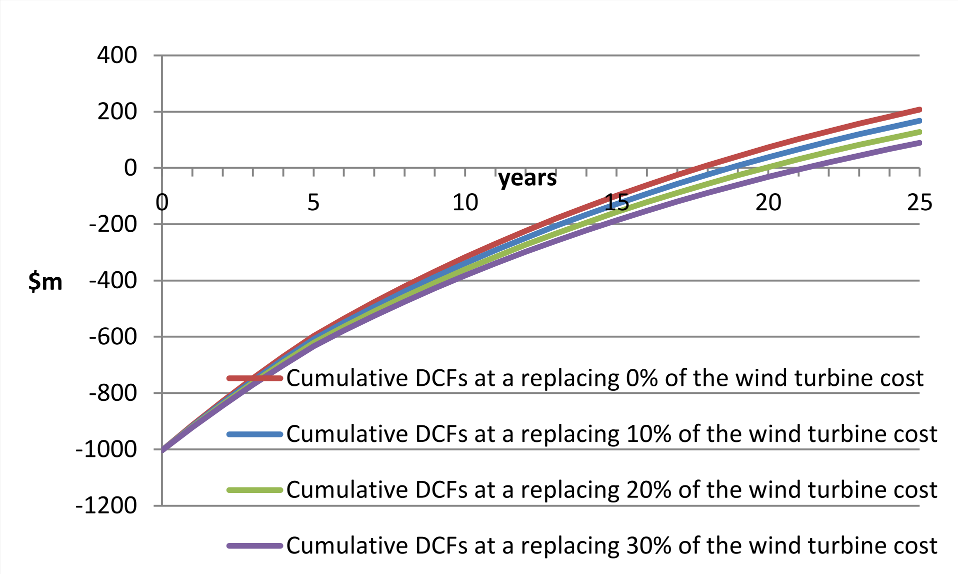

Figure 7-9 Cumulative discounted net cash flow scenarios reflecting different percentage replacement costs

7.4.1.4 Discussion of Sensitivity Analysis on Wind

All of the tested factors have proven to bear a significant effect on the wind system economics. In the paragraphs to follow, each will be discussed in more detail in comparison to other factors.

As the selling price to the grid was varied according to the number of annual operating hours of the wind farm, the NPV came in at $75m at the lowest and +$207m at the uppermost bound..

As the capital cost of wind was varied between $3500/kW (205%) and $1734/kW (100%), the resulting NPV increased by around 486% for the 105% range of variation.

As the annual cost of the system was varied from $10/MWh(25%) of O&M costs to $43/MWh(100%) of O&M costs, the NPV dropped by around 400% for the 75% range of variation of O&M cost

The NPV of the wind system dropped by 61% for the increase of interest rate from 5% to 8%

As replacement needs upon 10 years of operation were varied from 0% to 30% of wind turbine cost (or 64% of total capital cost), the NPV dropped by 57%, assuming 30% of the wind components need replacement after operating for 10 years.

The figures show that interest rate has the most significant effect on the case study results. This is followed, in order, the annual O&M costs of the system, the capital cost of the system and finally the replacement cost.

7.4.2 Adding a CAES plant

The economic feasibility of a CAES plant is examined using the same method, applying a discounted cash flow approach. First, the capital cost of the CAES plant is calculated, and then the fixed and variable costs are added. The total annual payments are then deducted from annual revenues to calculate net cash flows, which are discounted respectively.

7.4.2.1 Methodology

a) Capital cost of a CAES plant

The capital cost of a CAES plant includes

a) The cost of building an underground storage

b) Compressors cost

c) Turbines cost

d) Other costs, which include the cost of heat exchangers, pumps, transportation of components and installation costs (including pipe works).

The majority of studies primarily account for the cost of building a reservoir as well as the compressors and turbines cost. Other costs are added as well for other components of the system (Madlener et al, 2013).

The initial cost of the CAES system is calculated using the formula:

$$IC_{CAES} = c_{cons} + c_t P_t + c_c P_c + c_{cc} P_{cc} + other\ costs + Installationcost \qquad (7\text{-}6)$$

Where IC is the initial capital cost, c_{cons} is the construction cost per unit capacity of CAES ($/MW), c_t is the specific turbine cost ($/MW), P_t is the turbine power, c_c is the specific compressor cost ($/MW), and P_c is the compressor power.

The initial cost of the CAES system can be converted into annual payments using Eq. (7-7)

$$A_{ICAES} = IC_{CAES}\left(\frac{(i\times(i+1)^t)}{(i+1)^t-1}\right) \quad (7\text{-}7)$$

b) Running Costs

1. Fixed annual cost of a CAES plant

Fixed costs entail labour, maintenance and other fixed costs related to the operation of the CAES system. The fixed cost ($AFixed_{CAES}$) of the CAES plant is estimated as a factor of the initial capital cost of the CAES system. In contemporary studies (Madlener et al 2013; Mauch et al 2012; Zafirakis et al 2009; Greenblatt et al, 2007), the figure ranges between 2% and 3% of the total capital cost.

2. Variable annual cost of a CAES plant

The variable cost calculation of a CAES plant is more complex. It cannot be estimated as a factor of the total capital cost as several and inconstant factors affect the variable cost of a CAES system. These include the components replacement cost, and more importantly, the price of natural gas used in the expansion process (pre-heating the air before turbine stage).. The fuel price is variable and changes on a regular basis.

i) Replacement Costs

These entail the cost of changing some of the components of the system if their lifetime falls short of that of the CAES system. Normally, the system's key capital cost components (compressors, turbines) have a life span of more than 25 years and therefore need not be replaced during the operational life of CAES. Component parts whose replacement is worth consideration primarily include the heat exchangers and the pipe works. If the system has a component part that needs replacement after a given number of years, the following equation applies:

$$Rep_{cost\_NPV} = \frac{Price_{new\_comp}}{(i+1)^{nc}} \tag{7-8}$$

Where Rep_{cost_NPV} is the net present worth of the replacement cost, nc is the number of years until replacement, and $Price_{new\_comp}$ is the price of the new component.

ii) Natural gas cost

In the past 5 years, the natural gas price has varied considerably from $2/MMBTU to $6/MMBTU, averaging $3.7/MMBTU (EIA Natural Gas Spot Market Price).

1 MMBTU = 1055.87 MJ

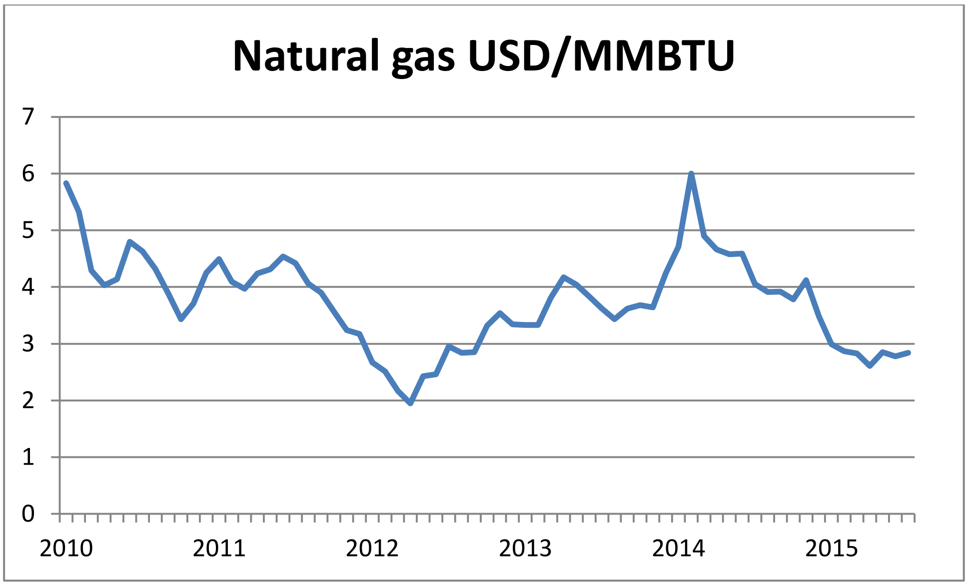

Figure 7-10 Variation of natural gas price in the past 5 years

The heat rate for CAES is an important factor in the calculation of the annual fuel costs. Table 7-4 below shows the heat rate for the aforementioned CAES plants. Employing thermal energy storage in the McIntosh CAES plant case, for every 1kWh of output, 1.17kWh of natural gas is used, giving a heat rate of 4.25MJ/kWh— equivalent to 4000BTU/ kWh; while the Huntorf plant in Germany has a higher heat rate of 5.9MJ/ kWh (5.6 BTU/kWh) because it is a diabetic system that utilizes no recuperation (no TES), thus the need for higher natural gas consumption.

Table 7-4 Heat rates of existing CAES plants

CAES Plant	Heat rate (MJ/ kWh)
Huntorf	5.9
McIntosh	4.25

The equation pertaining to the annual payments of natural gas is

$$N_f = \text{heat rate (MMBTU/kWh)} \times \text{naturalgas price (\$/MMBTU)} \quad (7\text{-}9)$$

Another way to calculate the variable costs as equal annual payments is to convert the variable annual payments to NPV and then annualize the payments

$$NPV_f = \sum_{t=1}^{T} \frac{N_f}{(i+1)^t} \quad (7\text{-}10)$$

$$AN_f = NPV_f \left(\frac{(i \times (i+1)^t)}{(i+1)^t - 1} \right) \quad (7\text{-}11)$$

c) Production cost of CAES and calculation of present worth of system

2 methods are explained in the next section for calculating the production cost of the system and the present worth.

1) Including capital cost as annualized payments
2) Net present values of annual revenues and payments, and discretely deducting initial capital cost in today's dollars

a) Annualized payments

In this method, total costs including the capital costs are annualized, and then present worth is calculated based on the annual revenues compared to production cost defined as annual costs including the capital cost.

The total cost of operating the CAES is calculated using Eq. (10)

$$AT_{CAES} = A_{ICAES} + AFixed_{CAES} + AN_f \tag{7-12}$$

If the CAES is not government-operated, meaning it buys its power from the wind farm to operate the compressors, then another term should be added to the annual operation cost of CAES. This term can be calculated as:

$$C_{w-CAES} = Energybought \times market\ price \tag{7-13}$$

In this case, the total annual cost of energy production using CAES becomes

$$AT_{CAES} = A_{ICAES} + AFixed_{CAES} + AN_f + C_{w-CAES} \tag{7-14}$$

The energy production per unit energy is calculated as:

$$AT_{CAES-KWh} = \frac{AT_{CAES}}{\sum_{y=1}^{n} CAESenergy} \tag{7-15}$$

Where $CAESenergy$ is the energy produced by CAES annually

If $AT_{CAES-KWh}$ is lower than the market price of selling electricity to the grid, then the CAES system is making annual profits, and vice versa.

b) NPV method

This is the method used in our calculations earlier, where annual revenues and costs are calculated excluding the initial capital cost. Revenues are a product of selling electricity to the grid, while the cost of operating the CAES is confined to the running costs: fixed and variable. Annual profits are netted out and discounted to compute annual system NPV and

ROI. Hence, the capital cost is omitted from annual cash flow calculations (Zafirakis et al, 2009) .

$$AT_{CAES2} = AFixed_{CAES} + AN_f \quad (7\text{-}16)$$

Where AN_f is the annualized fuel cost and $AFixed_{CAES}$ is the annualized CAES fixed costs

Energy production cost becomes:

$$AT_{CAES(2)-KWh} = \frac{AT_{CAES2}}{\sum_{y=1}^{n} CAESenergy} \quad (7\text{-}17)$$

CAES revenue is calculated as:

$$R_{CAES} = \sum_{t=1}^{t-turbin} CAESenergy \times selling\ price \quad (7\text{-}18)$$

Annual profit/loss is thus:

$$\frac{P}{L} = R_{CAES} - AT_{CAES2} \quad (7\text{-}19)$$

Where $R_{CAES}$and AT_{CAES2} are the annual revenues and the annual O&M costs of CAES respectively

Profit/Loss is measured in present value terms using the equation:

$$P/L_{NPV} = \sum_{t=1}^{t=n} \frac{P}{L} \Big/ (i+1)^n \quad (7\text{-}20)$$

Finally, system NPV is calculated by deducting the initial capital cost (IC_{CAES}).

The next section takes a closer look upon CAES revenues and how to maximize them. As mentioned earlier, CAES can operate either in the day-ahead market or minute reserve markets. Only the day-ahead spot market revenue is considered in this simulation. The calculation of both, however, is worth a mention. The total revenue attainable by a CAES system is given by the following equation (Madlener et al, 2013):

$$R_{CAES} = R_{sm} + R_{MR} \quad (7\text{-}21)$$

Where R_{sm} is the spot market revenue, used in Eq. (15) as the R_{CAES} value, and R_{MR} is the minute reserve revenue.

The minute reserve revenue, can be either positive, where CAES reduces compressor power use, or negative reserve where CAES can reduce expander power output (Madlener et al, 2013):.

$$R_{MR} = \sum_{t=1}^{t-turbine} Pout \times Price_{NR} + \sum_{t=1}^{t-comp} Pin \times Price_{PR} \quad (7\text{-}22)$$

It is worth mentioning that after the end of the useful life of the CAES plant (around 25 years), there remains an unused underground reservoir, representing a salvage value that can be added to the system, calculated as:

$$NPV_{sal} = \frac{Sal_f}{(i+1)^n} \quad (7\text{-}23)$$

Where Sal_f is the future salvage value.

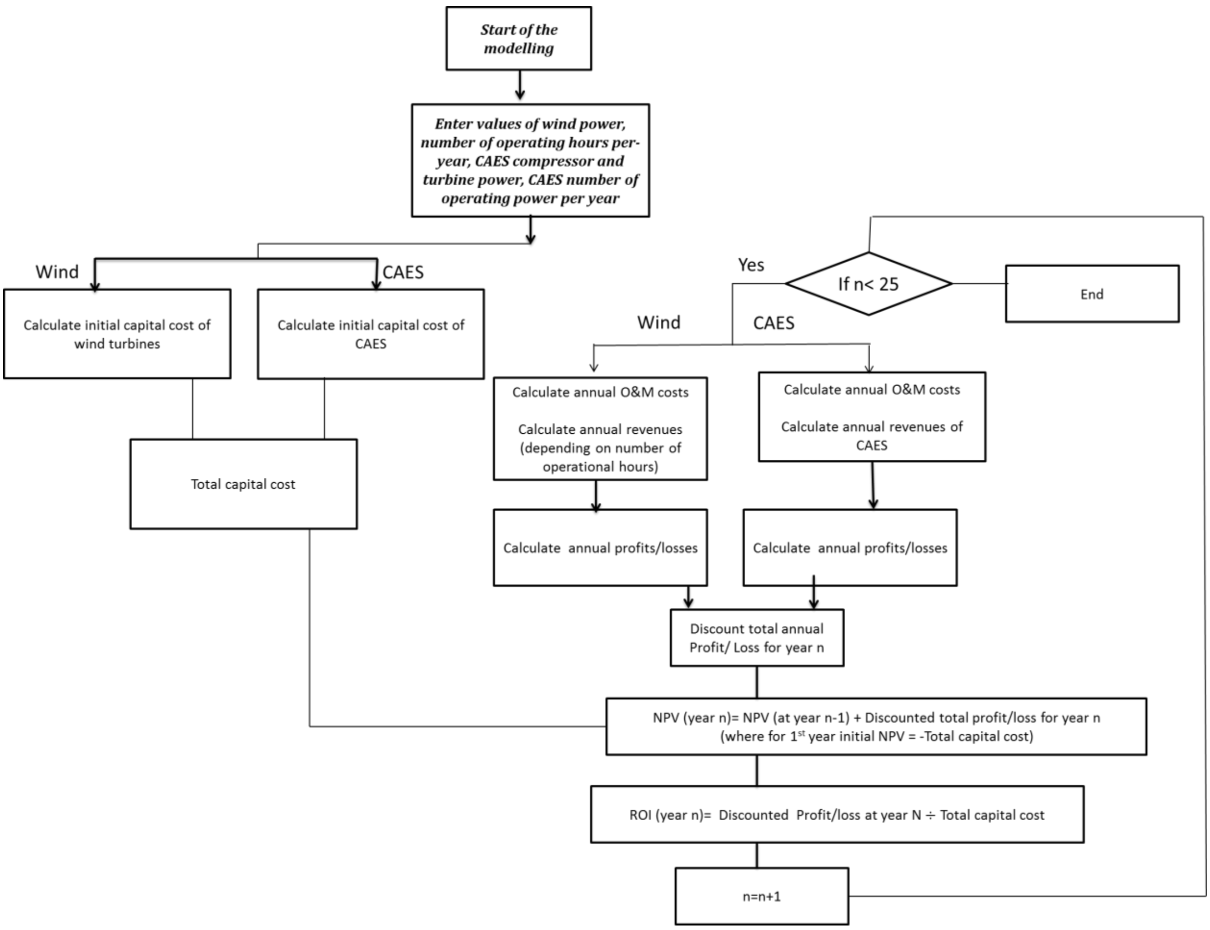

Figure 7-11 Flowchart of economic analysis for Wind+CAES

7.4.2.2 Assumptions

a) CAES capital cost

The Suez area neighbouring the site of the wind farms is formed of basement rocks. This type of geology is less favourable economically compared to molten salt, for instance, as rocks excavation could cost around $30/kWh compared to $1/kWh for salt caverns. The cost of initial installation for a 300MW CAES is around $135m for a salt dome cavern, which rises up to c$190m for the rock caverns (based on the cost assumption of $30/kWh of excavation) where initial costs include acquisition, space and installation costs. The lifetime of a CAES reservoir is around 25 years.

Other CAES system installation costs include heat exchangers, addition of pumps, pipe works and transport of system components. Based on a survey of a number of studies , the value of these other costs stands at around $350/KW.

b) Compressors

The compressor’s life span is around 100,000 hours of operation. This translates to around 27 years of operation, based on an estimated compressors operation runtime of around 10 hours/day. Compared against CAES’s estimated operational life of 25 years, the compressors life span is considered suitable, and eliminates the need for a replacement and the variable costs thereof.

Compressors cost ranges from $400/KW to $450/KW, based on a survey of various studies.

c) Turbines

The turbine expanders normally have a life span of around 100,000 hours, again, appropriate for the operational life of CAES of 25 years. The turbine cost, according to the surveyed studies, ranges between $440/MW and $500/MW.

Table 7-5 Case studies for economic analysis

	US (salt caverns)	Egypt (rock caverns)
Number of years	25	25
Construction cost ($/kWh)	1	30
Specific compressor cost ($/KW)	420	420
Specific turbine cost ($/KW)	475	475
Fuel market price ($/MMBTU)	4	4

Egypt case study

In this case study, the modelling technique is not based on load levelling as in Chapter 4 earlier. Instead, the CAES is specifically sized and operated such that it maximizes profit as implied by the new tariff program provisions. The new modelling technique assumes CAES absorbs the power when the wind farms are dumping their surplus production thereof. In the supposed profit-maximizing scenario, this shadows instances when the wind speed is lower than the rated speed, as explained in the previous section; unlike in the load-levelling scenario, where the CAES absorbs power when the output from wind is higher than the load. The CAES is hence set to provide power at the same time the wind system is selling power to the grid. Under this scenario, CAES is modelled to have a capacity of around 300MW with a cavern volume of 850,000m^3, which is lower than the volume of the cavern for the load levelling of Egypt's Suez project (Chapter 4), owing to the briefer operation time. In the simulation showcased, however, the system would produce on average 250MW for 8.5 hours/day. The heat rate of the system is calculated as 4060MJ/kWh (3866 BTU/kWh).

For the Egyptian case, the value of CAES lies in its use in load levelling as opposed to economic optimization, since the Egyptian grid is weak and daily power cuts are common in Egypt. Therefore, the importance of CAES owes primarily to its role in dealing with the intermittency of wind rather than improving the economic performance of the wind systems. This chapter yet sheds light on its marginal economic benefit. Carried out in this section is an economic analysis of adding a CAES system to future wind farms projects. The CAES system will be treated as a wind farm for the power trades, implying that the selling price for the CAES system will equal the selling price for wind. The system governing the Egyptian power trade market differs significantly from its European and American counterparts. The government recently issued a law dictating feed-in tariffs for power produced from wind. Under the newly formed system, the government will buy wind power at a fixed price, irrespective of the selling time (peak or not) to encourage the growth of the wind energy sector in Egypt. Figure 7-12and Figure 7-13 show the different operation modes runnable by CAES systems. The first, which was discussed in previous chapters, pertains to the use of CAES for load levelling, while the second entails the use of CAES to maximize profits, according to the new tariff system for wind power in Egypt.

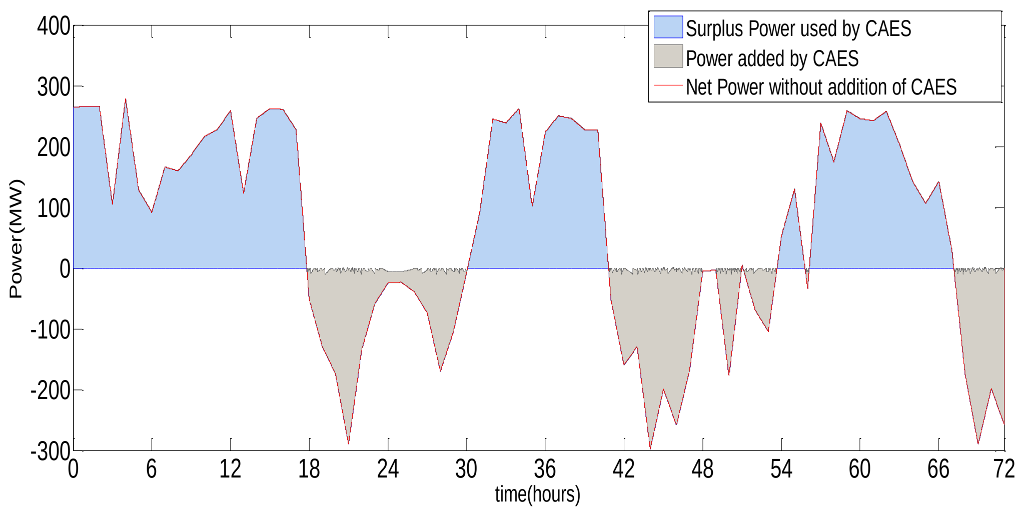

Figure 7-12 CAES operation mode for load levelling

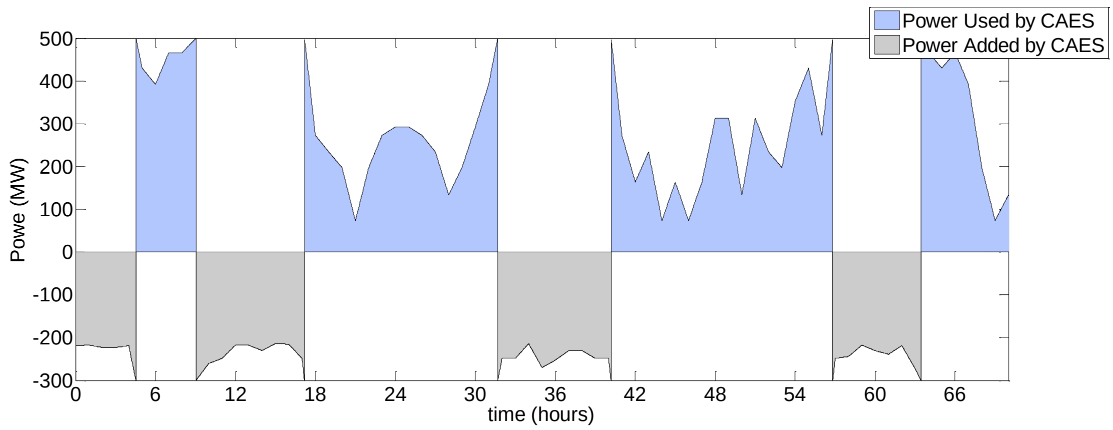

Figure 7-13 CAES operation mode for economic benefit

Figure 7-14 shows the output power that will be sold to the grid to best exploit the makeup of wind power prices in Egypt. As explained earlier, wind will only produce power when the output power of wind is 80% or more of the rated power, and the CAES system will produce power concurrently with the wind, so as to realize the best possible price offered in the wind power tariff program.

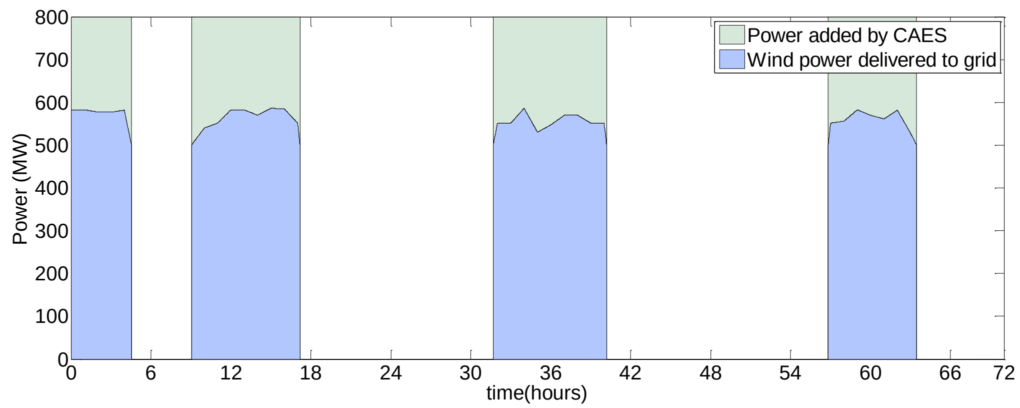

Figure 7-14 Output power from Wind+CAES system

In this scenario, the revenue from total power production will be considered, whether flowing from the wind farm to the grid or from the CAES system to the grid. The expected annual revenues are thus higher albeit with a higher capital cost.

Table 7-6 base case parameters for Wind+CAES for Suez case study

Wind with CAES (Egypt) base case parameters	
Selling price to grid	\$95.7/MWh (first 5 years of operation) \$89.3/MWh (remaining years of operation)
Interest rate (i)	5%
Fixed annual factor	2%

7.4.2.3 Results and discussion of Wind+CAES

Table 7-7 CAES costs for the Suez case study

CAES plant costs	
Construction cost (\$m)	180
Equipment cost (\$m)	350
Other costs (\$m)	105
Annual fixed cost (\$m)	12
Annual variable cost (\$m)	8

In this simulation, the initial investment is around \$1500m. By the end of the 25 years of operation, the Wind+CAES case is estimated to have produced \$306m in economic profits.

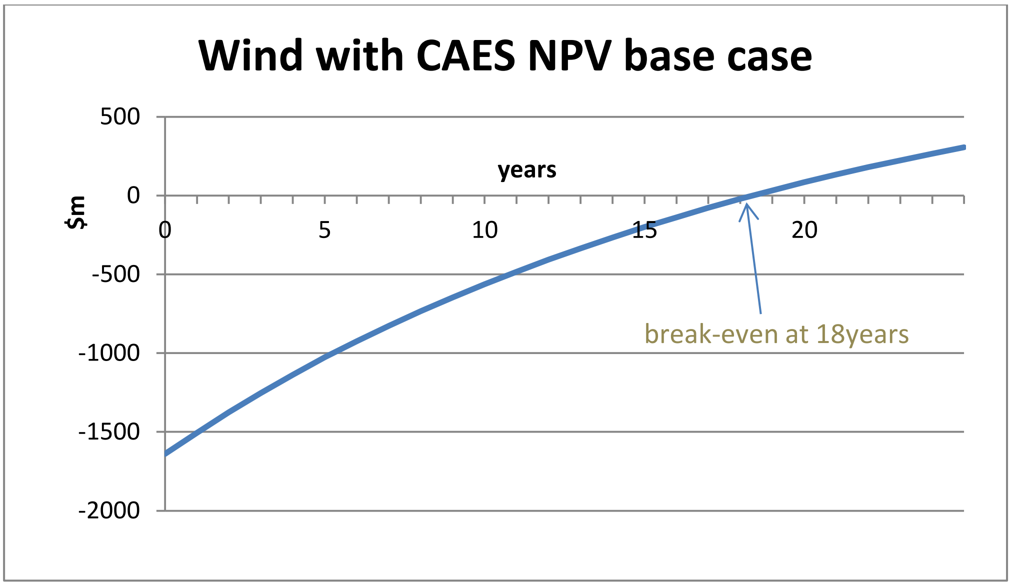

Figure 7-15 Cumulative discounted net cash flow of Wind+CAES system—base case scenario

The ROI starts at around 8% and gradually drops to around 2.5% by the end of the system's 25 years of operation.

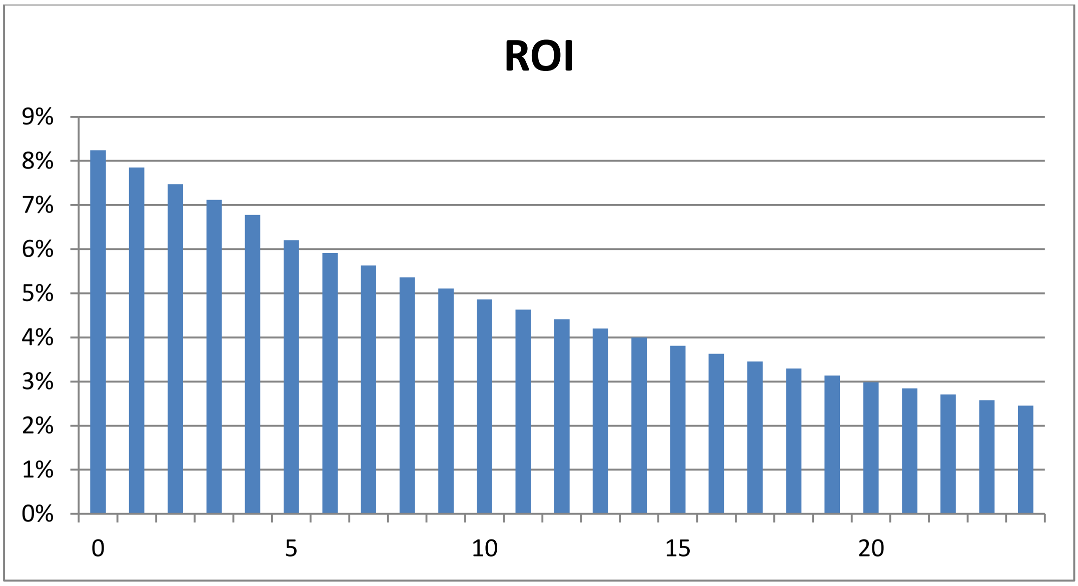

Figure 7-16 ROI of Wind+CAES system—base case scenario

7.4.2.4 Discussion of the effect of adding CAES to wind on the NPV of the system

In the base case scenarios of both wind alone and Wind+CAES, the NPV of the systems was above 0, meaning both systems more than economically break-even assuming base case values—observing, as mentioned earlier, the assumptions made. For wind alone, these assumptions are as follows:

a) The wind energy will be sold to the grid only when the wind speed is close to the rated speed (within 80%), to maximize profit
b) If the wind power is more than 20% lower than the rated wind power, it will be dumped (or wind turbines will be shut down)

For the Wind+CAES system, the assumptions are:

a) Instead of dumping the wind power, the surplus power is stored in CAES
b) The CAES delivers the stored power to the grid concurrently with the wind's power supply, and at the same purchase price

Under those assumptions, the wind only system broke even after 18 years with a NPV of $207m, while the Wind+CAES system broke even after roughly 18 years with a NPV of around $306m. This shows that adding CAES improves the system's economics when operated in a profit-maximizing mode. On the other hand, if CAES is operated for the purpose of load levelling, the addition of a CAES system will not be economically attractive. Nonetheless, CAES also has the ability to add value by providing ancillary services to the grid, but this is not yet applicable to the Egyptian market given its current stage of development and dynamics. In the future, however, CAES systems could provide higher economic returns if ancillary services are considered by the government.

7.4.2.5 Sensitivity analysis of Wind+CAES

A number of parameters were varied to test their effect on the net present value of the system. As the wind system sensitivity analysis results were discussed earlier, this section only looks at the sensitivity to the CAES parameters. These are:

a) Natural gas price

b) Initial capital cost of CAES

c) Initial capital cost of the whole system

d) Replacement cost of Wind+CAES

Even though CAES is not used in a load-levelling mode in this scenario, it still adds value to the grid by means of smoothing out the output power of wind. Figure 7-17 shows the results of adding a 5% incentive payment on the purchase price from Wind+CAES systems if the government decides to remunerate the said benefit and encourage the addition of such systems. Under this scenario, the system breaks even in 16 years with a NPV of $457m, owing to the incremental c$150m of revenues from incentive payments.

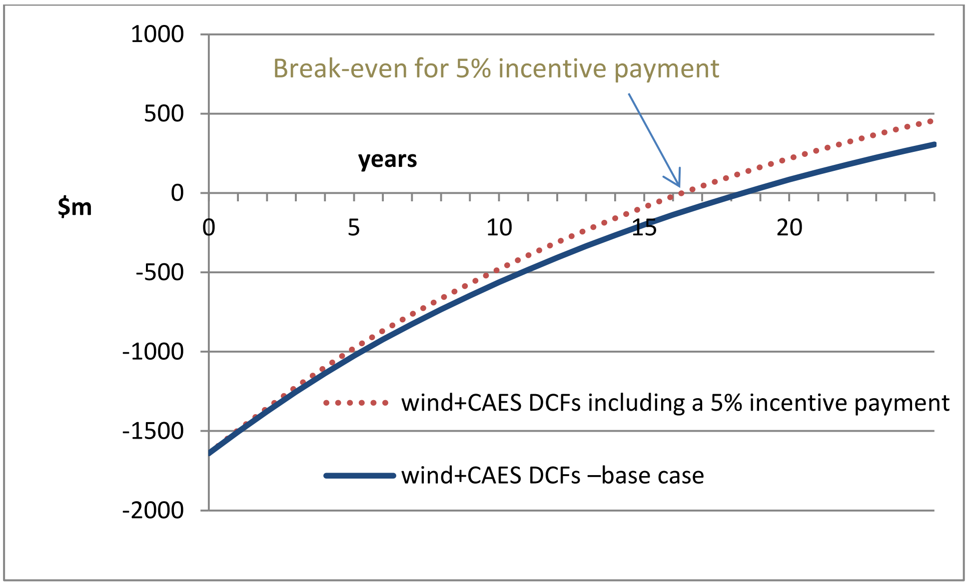

Figure 7-17 Cumulative discounted net cash flows showing base case and the addition of a 5% incentive payment

a) Natural gas price

Annual escalation rates of natural gas prices of -5%, 0%, 5% are simulated to test the sensitivity of the net present value of the system to natural gas cost. The results are shown in Figure 7-18.

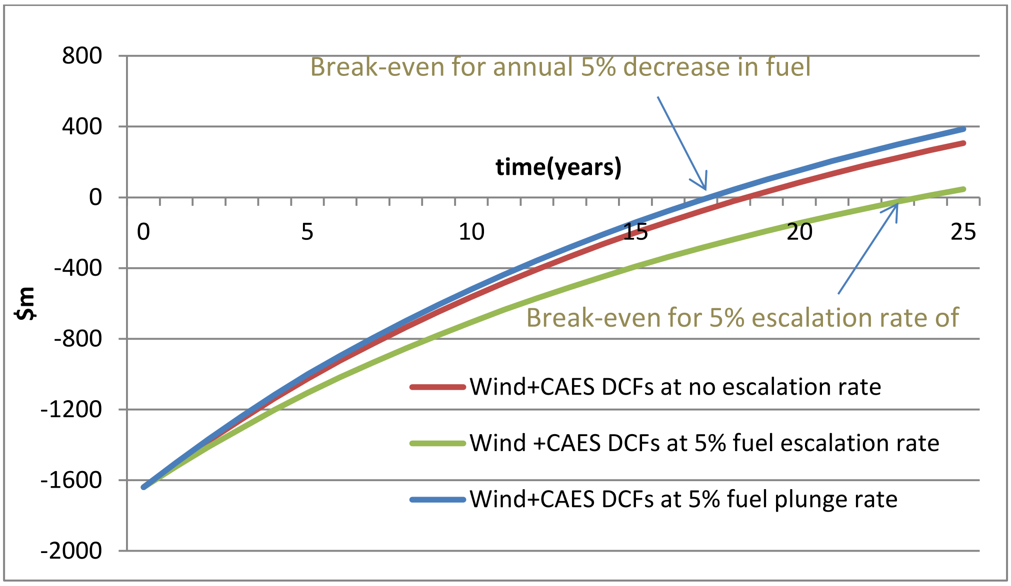

Figure 7-18 Cumulative discounted net cash flows for different annual fuel escalation rates

Figure 7-18 shows that an annual 5% drop in the price of fuel results in a system break-even at 17 years, compared to 18 years at a constant fuel price (0% escalation rate), while increasing the fuel escalation rate to an annual 5% results in the system only breaking even after 24 years of operation.

b) Initial capital cost of CAES

The total initial capital cost of CAES is varied between 80% and 110% of the base-case cost assumed based on a range of values from a number of studies, which includes construction, compressor, turbine and other costs. The 80% scenario suits the assumption of the government subsidizing the remaining 20% or a portion of it, or a lower capital cost owing to a decrease in the price of some of the components. The 110% scenario simulated suits the assumption of an increase in the price of components, or the construction cost of the reservoir for the CAES.

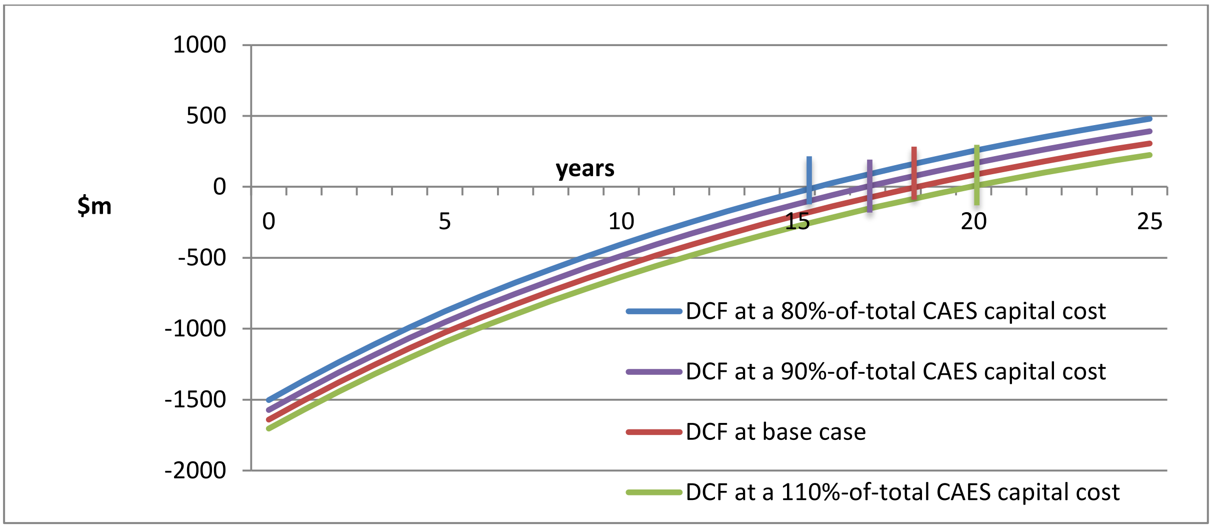

Figure 7-19 Cumulative discounted net cash flows for different initial capital costs of CAES

Changing the capital cost in 10% intervals has a minor effect on the whole system NPV as the capital cost of CAES only represents a fraction of the total capital cost of the system, hence, its lesser effect on the overall NPV of the system.

c) Initial capital cost of the Wind+CAES

In this sensitivity analysis, the whole system (Wind+CAES) capital cost is varied between 80% and 110%.

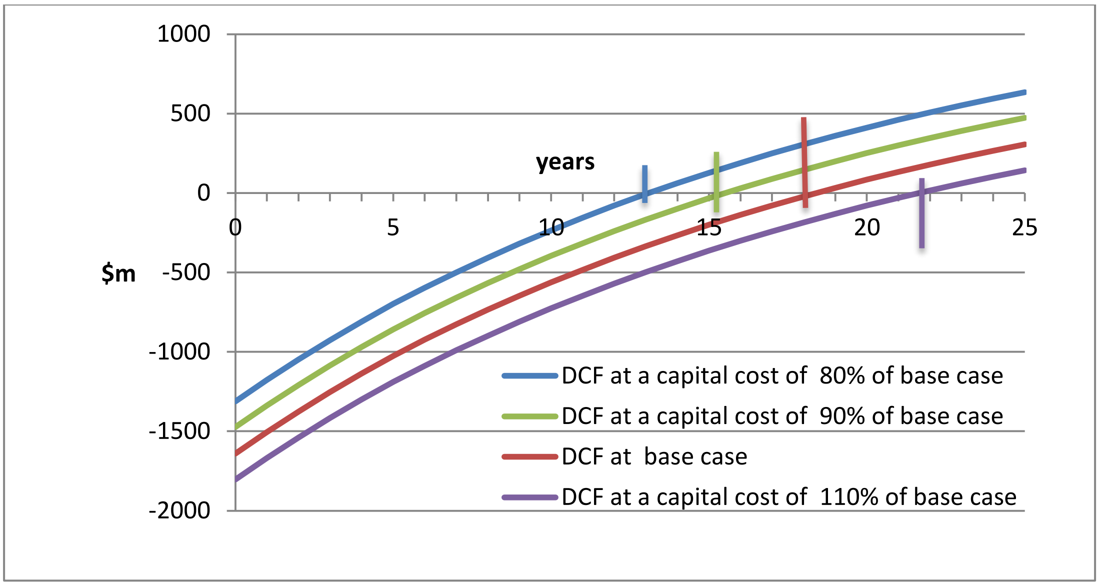

Figure 7-20 Cumulative discounted net cash flows for different total initial capital costs of Wind+CAES

Figure 7-20 shows the effect of changing the initial capital cost of the whole system. Expectedly, the effect is much more significant compared to variation in capital cost of solely the CAES system. In this case, the initial investment changes from $1302m to $1800m for the range applied, whilst the initial investment changed from $1503m to $1700m in the former scenario involving the variation of only the CAES capital cost.

d) Replacement cost of Wind+CAES

Because some of the system components may need replacement after a period of time, replacement cost is considered. The assumption is that a percentage of the components will need replacement following 10 years of operation. The sensitivity is varied between 0% and 30% of the wind and CAES components.

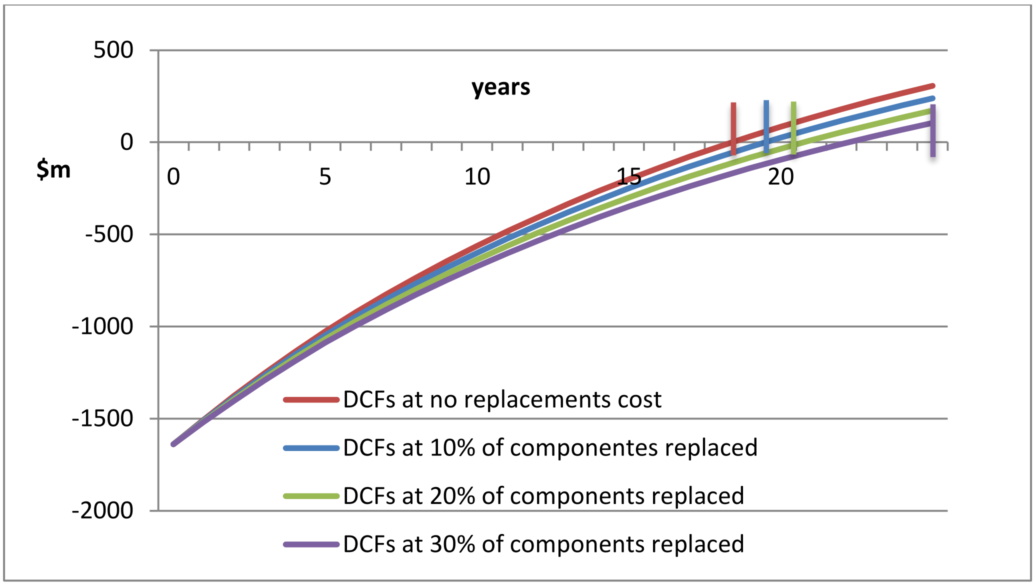

Figure 7-21 Cash flow for different replacement cost of Wind+CAES

As more components need replacement, the NPV drops, albeit staying positive across all scenarios, with the worst-case of 30% of the components needing replacement yielding an NPV of $104m.

Discussion of sensitivity analysis on Wind+CAES

The tested factors varied in their effect on the system's economics. Each is discussed in this section in more detail in comparison to the other factors.

a) Natural gas price was varied by annual escalation rates ranging from -5% to 5%, where NPV dropped by 85% for an increase of 5% from the base case while the NPV increased by 26% from the base case for an annual 5% plunge in fuel rate .
b) Initial capital cost of CAES was varied from 80% of CAES cost to 110% of CAES cost. A 20% reduction in CAES cost from the base case results in an NPV increase of 56%. While a 10% rise in CAES cost from the base case results in a drop in the NPV by 26%.
c) Initial capital cost of the whole system was similarly varied from 80% to 110%. A 20% reduction in whole system cost from the base case results in an NPV increase of

106%. While a 10% rise in CAES cost from the base case results in a 53% drop in the NPV.

d) Replacement cost was increased from 0 in the base case where none of the components need replacement to 30% of the components needing replacement after 10 years of operation. NPV for the said range dropped by 66%.

Table 7-8 Average final NPV variation for different varying parameters

Parameter sensitivity	Change in parameters (%)	Average NPV variation (%)
Natural gas	10	110
Initial capital cost of the system	10	53
Initial capital cost of CAES	10	27
Replacement cost	10	22

Out of the tested factors, and given the chosen range for each, NPV of the system proved most sensitive to changes in the natural gas price. The initial capital cost of the system comes next, followed by the initial capital cost of CAES alone, and at last the replacement cost of system components.

7.5 Conclusions

The results of the simulations carried out for the case study of the Suez area in Egypt indicate that wind installations with or without CAES, are economically profitable, assuming Egypt case parameters. Varying a number of parameter values to the upside shows that wind and Wind+CAES setups can, in many cases, become increasingly profitable as exemplified by the higher selling price to the grid and lower interest rate scenarios. The Egyptian government is eager to encourage the installation of new renewable energy systems, which is therefore expected to grow steadily in the coming years, inducing along the way adjustments to the market prices set forth by the newly issued law, based on which the economic analysis herein is performed. CAES was found to improve the economic feasibility of wind alone system, should the assumption that the extra power produced by wind is dumped hold. If the government provides for subsidies to implement renewable energy projects, the viability of the given system would increase as well, turning it to profitability and enabling it to break-even in 13 years in the case that 20% of the estimated capital cost is borne by the government compared to break-even in 18 years without subsidies. This brings us to the effect of interest rates, which is again related to the government. If the government incentivizes loans for renewable energy projects through lower interest rates, the Wind+CAES system could prove highly profitable as well.

Chapter 8 Conclusions and Recommendations for future work

8.1 General Conclusions

This chapter recaps the research and work done in this thesis, and discusses their limitations and some recommendations for future work.

The market for renewable energy technologies is growing worldwide, with plenteous research being carried out for the different renewable energy technologies, principally solar and wind. This uptrend in the renewable energy industry is expected to continue into the next decade or so. The performance of renewable energy systems is expected to improve significantly, which can only make them more attractive technically and economically. In general, renewable energy systems come with limitations. Their major shortcoming is their intermittency, which will always be an inhibiting factor to the growth of this industry. On the upside, however, energy storage systems could play a major role in containing this problem, and help with the integration of renewables to the central grid or even to isolated grid systems.

Energy storage systems vary in scale and performance. This thesis focuses on large-scale renewable energy systems, mainly pumped hydro and CAES systems, which are particularly well suited for renewable energy applications. CAES could play a big role in shaping the future of renewable energy systems. Not only can CAES bring load levelling to the system, but it can also add substantial value by providing ancillary services to the grid, owing to its fast response, including voltage and frequency support to the grid as well as power reserve provision. CAES has been tested before with two operating plants for more than 20 years with great reliability. CAES systems have also been the subject of extensive research lately, with plenty of upcoming projects currently underway. The two main limitations of CAES are the prerequisite of a suitable geology, and the safety hazard ensuing from the high pressure and temperature operating conditions.

This thesis focuses on adiabatic CAES, which tries to minimize the use of natural gas by using recuperators and thermal energy storage systems, where the heat from the air during the compression stages is extracted with a heat transfer fluid, stored, and then supplied back during the expansion process.

The main aim of this project was to explore the potential benefit of CAES system, both technically and economically.

The work carried out in this study involves dynamic MATLAB modelling of a novel configuration of CAES systems that uses parallel chains of compressors and turbines in an attempt to accomplish an operational efficiency very close to that rated for both compressors and turbines, leading into the ability to cater for low power during the stages of compression and expansion. Adequate heat storage was also added in the simulation for the purpose of testing the adiabatic CAES system. The performance results of this system were compared to the results of the currently operating CAES plants (McIntosh and Huntorf). The proposed system scored a marked improvement to the operational efficiency of the existing CAES plants, albeit the system is not a completely adiabatic system due to the need for some combustion power to raise the temperature of air to that required at the turbine inlet.

Further research was made on the thermal energy storage system using ANSYS CFD and experimental testing. The objectives of these tests were to establish the optimized design sizing of the thermal storage in an adiabatic CAES system, evaluate the suitability of different conditions and parameters for the operation of the thermal storage system.

Finally, an economic study was carried out to test the feasibility of adding a Wind+CAES system as well as a standalone CAES system to the studied case of the Egyptian grid. The results showed that at the current tariffs offered by the government, Wind+CAES is economically feasible. Its economic benefit could also be further enhanced in the future if the government elects to price the ancillary services that a CAES system can provide.

In general, the work carried out in this research was able to develop a model that is capable of optimizing various components of the CAES system and predict its long term performance using MATLAB. The CFD modelling was able to optimize the thermal energy storage system for adiabatic CAES system and was validated by experimental testing. The results showed the ability of CAES to improve the performance of renewable energy systems both from a technical perspective (load levelling) and from an economic perspective as presented for the case study of the Egyptian grid.

8.2 Limitations of the research

The main limitations of this research relate to the economic study of the CAES system. The Egyptian government has recently set tariffs for renewable energy sources, which are subject to change in the future as more renewable energy projects penetrate to the grid. A significant such move could render the conclusions herein inapplicable. Another concern has to do with the ancillary services that can be provided by CAES. These were neglected in the study, as no market for those services exists thus far in Egypt. Likewise, however, this is expected to change as the infant market develops and deepens along the lines of mature markets in a number of developed countries. In brief, the results of the case study are short-sighted, being narrowly focused on the current phase of the Egyptian market’s life cycle, the reason why sensitivity analyses were provided complementarily.

Other limitations to the research pertain to the built model’s components. Concrete was used as the sensible heat storage, chosen on merits of its reliability and availability, though it may not be the best performing heat storage medium. In future, considering latent heat storage for adiabatic CAES system could result in superior performance. Moreover, the experimental testing was constrained to fairly low temperatures compared to those of the real-life application, owing to the safety hazard of replicating the high operational temperatures of an adiabatic CAES system's thermal storage inside the lab. That said, the temperature was limited to a maximum of 90˚C. If accessible facilities allow testing the performance of the thermal storage under higher temperatures, the accuracy of the results would certainly be improved.

In the MATLAB modelling of the system, a number of the assumptions made—including the temperature of the cavern surroundings, the effectiveness of the heat exchangers, and the polytropic efficiencies of compressors and turbines—were based on other researches. These assumptions should be very close to reality, but if actual figures for these parameters can be obtained, the model reliability would definitely be enhanced.

8.3 Future work recommendations

The following recommendations for improving endeavoured future work and research on CAES systems are warranted. Researching and testing the use of latent heat storage can serve to improve the performance of the thermal storage systems. Encapsulating the sensible heat storage mediums with latent heat storage is another idea that could mark a new standard for thermal storage implementation in adiabatic CAES. As for improving modelling practices, heat losses in the pipes during the operation of CAES, which were neglected in this study due to their relative minuteness compared to other losses, should be considered if a more realistic performance is to be replicated. Also, evidently, the use of real-life parameter figures, as opposed to assumptions and proxies (as with the surrounding temperature of the underground cavern, for instance) would always improve model reliability.

8.4 Concluding Remarks

The work backing this research has shown that energy storage, in general, and CAES systems, in particular, can play a considerable role in the future especially given the anticipated steadfast growth in renewable energy technologies. For the Egyptian case study, particularly, the remarkably ambitious plans to increase the renewable energy contribution to the country's power mix strongly encourage the research and implementation of various energy storage systems, from small-scale schemes like batteries for household PV systems to large-scale structures like CAES for large-scale PV and wind farms. The proliferating renewable energy penetration levels can have a major toll on the grid upon their integration, and CAES systems can immensely help improve the performance of these renewable systems by means of load levelling, as well as by providing ancillary services to the grid, besides the associated economic benefit. Therefore, CAES implementation is highly recommended for the Egyptian grid system.

.

References

World Energy Outlook Executive Summary, IEA. 2014. Printed in France by CORLET

Haines A, Kovats RS, Campbell-Lendrum D, Corvalan C. Climate change and human health: impacts, vulnerability and public health. Public Health 2006;120:585–96

Renewables 2015 Global Status Report-Key findings, Ren21.2015. ISBN 978-3-9815934-7-1

Jacobson MZ. Review of solutions to global warming, air pollution, and energy security. Energy & Environmental Science 2009;**2**:148-173

Shedroff N (2009), "*Nuclear Energy: Pros and Cons*, Triple Pundit". [Online] Available:http://www.triplepundit.com/2009/02/nuclear-energy-pros-and-cons/

El Wakil MM. Power plant technology. McGraw Hill; 1984

Ackermann T, Söder L. An overview of wind energy-status 2002. Renewable and Sustainable Energy Reviews. 2002;**6**:67–128

Blaabjerg F, Teodorescu R, Chen Z, Liserre M. Power converters and control of renewable energy systems. In: Proceedings of 6th International Conference on Power Electronics, Busan, Korea. 2004

Manwell, J. F., J. G. McGowan, et al. (2002). Wind Energy Explained: Theory, Design, and Application. West Sussex, England, John Wiley & Sons Ltd

Lantz E, Wiser R, Hand M. IEA Wind Task 26:The Past And Future Cost Of Wind Energy, Work Package 2.Technical Report. National Renewable Energy Laboratory ,IEA .2012

Sherwani A, Usmani J, Varun. Life cycle assessment of solar PV based electricity generation systems: A review. Renewable and Sustainable Energy Reviews.2010;**14**:540-544

Goswami D, Vijayaraghavan S, Lu S, Tamm G. New and emerging developments in solar energy. Solar Energy. 2004;**76**:33-43

Panwar N, Kaushik S, Kothari S. Role of renewable energy sources in environmental protection: A review. Renewable and Sustainable Energy Reviews. 2011;**15**:1513-1524

Solar Energy Perspectives, IEA. Imprimerie Centrale. 2011. ISBN 978-92-6412-457-8

Akhil A, Huff G, Currier A, Kaun B, Rastler D, Chen S, Cotter A, Bradshaw D, Gauntlett W. DOE/EPRI 2013 Electricity Storage Handbook in Collaboration with NRECA.2013

Electric Energy Storage Technology Options: A White Paper Primer on Applications, Costs, and Benefits. EPRI, Palo Alto, CA, 2010. 1020676

Del Rosso A, Eckroad S. Energy Storage for Relief of Transmission Congestion. IEEE TRANSACTIONS ON SMART GRID.2014;**5**:1138-1146

Taylor P, Bolton R, Stone D, Upham B. Developing pathways for energy storage in the UK using a coevolutionary framework. Energy Policy. 2013; **63**: 230-243

IEC. Grid integration of large-capacity renewable energy sources and use of large-capacity electrical energy storage, Tech report; 2012

Beaudin M, Zareipour H , Schellenberglabe A, Rosehart W . Energy storage for mitigating the variability of renewable electricity sources: An updated review. Energy for Sustainable Development. 2010; **14**: 302-314

Moore T, Douglas J. Energy storage, big opportunities on a smaller scale. EPRI J 2006; Spring Issue, 16–23

Drury, E., Denholm, P., Sioshansi, R. The value of compressed air energy storage in energy and reserve markets. Energy. 2011; **36**, 4959–4973

Chen H, Cong Y, Yang W, Tan C, Li Y, Ding Y. Progress in electrical energy storage system: a critical review. Progress in Natural Science. 2009;**19**(3):291–312

McDowall JA. High power batteries for utilities – the world's most powerful battery and other developments, In: Power engineering society general meeting, IEEE. 2004; 2034–2037

Kemet corporations. Sodium Sulphur batteries and super capacitors. 2013

Albright G, Edie J, Hallaj S. A Comparison of Lead Acid to Lithium-ion in Stationary Storage Applications. All Cell Technologies LLC. 2012

Connolly D. An investigation into the energy storage technologies available, for the integration of alternative generation techniques. University of Limerick. 2007

Zhao H, Wu Q, Hu S, Xu H, Rasmussen C. Review of energy storage system for wind power integration support. 2015;**137**: 545-553

Hadjipaschalis I, Poullikkas A, Efthimiou V. Overview of current and future energy storage technologies for electric power applications. Renewable Sustainable Energy Reviews. 2009;**13**:1513–1522

Lipman T, Ramos R, Kammen D. An assessment of battery and hydrogen energy storage systems integrated with wind energy resources in California. Technical Report by University of California, Berkley; 2005

Ibrahim H, Ilinca A, Perron J. Energy storage systems characteristics and comparisons. Renewable Sustainable Energy Rev. 2008;**12**:1221–1250

Ter-Gazarian A (1994)," Energy Storage for Power Systems", Peter Peregrinus Ltd, ISBN 0 863412645

Sorensen B (2007), "Renewable Energy Conversion, Transmission and Storage", copyright © 2007 Elsevier Inc., ISBN: 978-0-12-374262-9

Denholm P, Kulcinski GL. Life cycle energy requirements and greenhouse gas emissions from large scale energy storage systems Energy Conversion and Management. 2004; **45:2153**–2172

Schoenung SM. 2001. Characteristics and Technologies for Long vs. Short-Term Energy Storage: A Study by the DOE ESSs Program. SAND2001-0765, Sandia National Laboratories, Albuquerque, New Mexico

Ribeiro P, Johnson B, Crow M, Arsoy A, Liu Y. Energy Storage Systems for Advanced Power Applications. Proceedings of the IEEE.2006: **89**:1744-1756

Beacon Power. Energy Storage Association. http://energystorage.org/energy-storage/technologies/flywheels, Last accessed (February 2016)

Van der Linden S. Bulk energy storage potential in the USA, current developments and future prospects. Energy 2006;**31**:3446–3457

Succar S, Williams R. Compressed air energy storage: theory, resources, and applications for wind power. Tech.rep. Princeton Environmental Institute; 2008

Cavallo A. Controllable and affordable utility-scale electricity from intermittent wind resources and compressed air energy storage (CAES). Energy. 2007;**32**:120–127

Zafirakis D, Kaldellis J. Autonomous dual-mode CAES systems for maximum wind energy contribution in remote island networks. Energy Conversion and Management. 2010;**51**: 2150-2161

Kere A, Goetz V, Olives R, Sadiki N, Mercier E. Dynamic behavior of a sensible-heat based thermal energy storage. Energy Procedia. 2015.;**69**:957-957

IEC. Electrical energy storage white paper. Tech report; 2011

Schainker R. Executive overview: energy storage options for a sustainable energy future. Proceedings of Power Engineering Society General Meeting. IEEE. 2004; **2**:2309–2314

Wang S, Yu J. Optimal sizing of the CAES system in a power system with high wind penetration. International Journal of Electrical Power & Energy Systems.2012;**37**. 117-125

D. J. Swider. Compressed air energy storage in an electricity system with significant wind power generation. IEEE Transactions on Energy Conversion.2007; **22**: 95-102

Study of Compressed Air Energy Storage with Grid and Photovoltaic Energy Generation. Arizona Research institute for solar energy. 2010

Taylor, P.,Johnson, L., Reichart, K., DiPietro, P., Philip, P., Butler, J. A Summary of the State of the Art in SMES, FES and CAES Systems. Sandia National Laboratories

Report . 1999

Lux KH. Design of salt caverns for the storage of natural gas, crude oil and compressed air: geomechanical aspects of construction, operation and abandonment, underground gas storage: worldwide experiences and future development in the UK and Europe. 2010

Kim H, Rutqvist J, Ryu D, Choi B , Sunwoo C, Song W. Exploring the concept of compressed air energy storage (CAES) in lined rock caverns at shallow depth: A modelling study of air tightness and energy balance. Applied Energy. 2012;**92**:653-667

Funk J. FirstEnergy postpones project to generate elecricity with compressed air.2013. Last accessed (June 2014)

Crotogino F, Mohmeyer K-U, Scharf R. Huntorf CAES: More than 20 years of successful operation. 2001 Orlando, Florida

Meyer F (Ed.) .Compressed air energy storage power plants. BINE Projekt-Info, FIZ Karlsruhe GmbH, Bonn, Germany. 2007

Schulte R, Critelli N, Holst K, Huff G. Lessons from Iowa: Development of a 270 Megawatt Compressed Air Energy Storage Project in Midwest Independent System Operator.2012

Doetsch C,Wolf D. Bewertung und Charakterisierung von netzintegrierten druckluftbasierten Energiespeicherkonzepten. Fraunhofer Institut Umwelt.2009

Ibrahim H, Belmokhtar K, Ghandour M. Investigation of Usage of Compressed Air Energy Storage for Power Generation System Improving - Application in a Microgrid Integrating Wind Energy. Energy Procedia. 2015;**73**: 305-316

Alotto P, Guarnieri M, Moro F. Redox flow batteries for the storage of renewable energy: A review. Renewable and Sustainable Energy Reviews. 2014: **29**;325–335

A. Rogers, A. Henderson, X. Wang and M. Negnevitsk,. Compressed Air Energy Storage: Thermodynamic and Economic Review.IEEE. 2014. Published in PES General Meeting | Conference & Exposition, 2014 IEEE

SustainX Begins Startup of World's First Grid-Scale Isothermal Compressed Air Energy Storage System. Sustain X. 2013. http://www.sustainx.com/e9c13ca1-134c-49e9-9031-036592c1b37a/about-us-news-events-detail.htm.(lastaccessed, June 2015)

McBride T, Bell A, Kepshire D. ICAES INNOVATION: FOAM-BASED HEAT EXCHANGE. Sustain X. 2103

Nakhamkin M, Schainker R, Marean J. Second Generation of CAES Technology-Performance, Operations, Economics, Renewable Load Management, Green Energy. 2009. POWER-GEN International, Las Vegas

Nakhamkin M, Chiruvolu M, Daniel. Available Compressed Air Energy Storage (CAES) Plant Concepts. 2007.In: Power-Gen International, Minnestota

Kondoh J, Ishii I, Yamaguchi H, Murata A, Ontai K, Sakuta K, et al. Electrical energy storage systems for energy networks. Energy Conversion and Management 2000; **41**:1863-1874

Pieper C, Rubel H. Electricity Storage – Making large-scale adoption of wind and solar energies a reality. The Boston Consulting Group. 2010

Kim YM, Favrat D. Energy and exergy analysis of a micro compressed air energy storage and air cycle heating and cooling system. Energy. 2010;**35**: 213-220

Kim YM, Chin D, Favrat D. Operating characteristics of constant-pressure compressed air energy storage (CAES) system combined with pumped hydro storage based on energy and exergy analysis. 2011;**36**: 6220-6233

Meherwan P.Boyce (2012), " Gas Turbines Engineering Handbook, Fourth Edition ", Elsevier Inc. 2012

Zunft S, Jakiel C, Koller M , Bullough C . Adiabatic Compressed Air Energy Storage for the Grid Integration of Wind Power. 2006. Sixth international workshop for wind output large-scale integration, Delft, Netherlands

Hartmann N, O. Vöhringer, C. Kruck, L. Eltrop . Simulation and analysis of different adiabatic Compressed Air Energy Storage plant configurations. Applied Energy. 2012; **93**: 541-548

Barnes F, Levine J. Large Energy Storage System Handbook. ISBN :9781420086003 1420086006 . 2011

ESC Energy Solutions Center (2012), http://www.energysolutionscenter.org/gas_solutions/regenerators_and_recuperators.aspx(Last accessed June, 2014)

EPRI-DOE Handbook of Energy Storage for Transmission &Distribution Applications, EPRI, Palo Alto, CA, and the U.S. Department of Energy, Washington, DC: 2003. 1001834

Greenblatt J, Succar S, Denkenberger D, Williams R, Socolow R. Baseload wind energy: modeling the competition between gas turbines and compressed air energy storage for supplemental generation. Energy policy.2007;**35**: 1474-1492

Jubeh N, Najjar Y. Power augmentation with CAES (compressed air energy storage) by air injection or supercharging makes environment greener.Energy.2012:38:228-235

Wolf D, Budt M . LTA-CAES – A low-temperature approach to Adiabatic Compressed Air Energy Storage. Applied Energy.2014; **125**: 158-164

Jubeh N, Najjar Y. Green solution for power generation by adoption of adiabatic CAES system. Applied thermal engineering. 2012;**44**:85-89

Rutqvist J, Kim H, Ryu D, Synn J, Song W. Modeling of coupled thermodynamic and geomechanical performance of underground compressed air energy storage in lined rock caverns. International Journal of Rock Mechanics & Mining Sciences. 2012; **52**:71-81

Zhao P, Dai Y, Wang J. Design and thermodynamic analysis of a hybrid energy storage system based on A-CAES (adiabatic compressed air energy storage) and FESS (flywheel energy storage system) for wind power application.Energy.2014;**70**:674:68

Grazzini G, Milazzo A. Thermodynaamic Analysis of CAES/TES systems for renewable energy plants. Renewable Energy. 2008; **33**: 1998-2006

Barbour E, Mignard D, Ding Y, Li Y. Adiabatic Compressed Air Energy storage with packed bed thermal energy storage. Applied Energy . 2015; **155**:804-815

Zhang Y, Yang K, Li X, Xu J. The thermodynamic effect of thermal energy storage on compressed air energy storage system. Renewable Energy. 2013;**50**:227-235

Garvey S. The dynamics of integrated compressed air renewable energy systems. Renewable energy. 2012;**39**:271-292

Li Y, Wang X, Li D, Ding Y. A tri-generation system based on compressed air and thermal energy storage. Applied Energy. 2012;**99**:316-323

Pehnt M, Oeser M, Swider D. Consequential environmental system analysis of expected offshore wind electricity production in Germany.Energy.2008; **33**: 747-759

Denholm P, Sioshansi R. The value of compressed air energy storage with wind in transmission constrained electric power systems. Energy Policy. 2009;**37**:3149-3158

Mauch B, Carvalho P, Apt J. Can a wind farm with CAES survive in the day-ahead market?. Energy Policy.2012;**48**:584-593

Madlener R, Latz. Economics of centralized and decentralized compressed air energy storage for enhanced grid integration of wind power. Applied Energy.2013;**101**:299-309

Zafirakis D, Kaldellis J. Economic evaluation of the dual mode CAES solution for increased wind energy contribution in autonomous island networks. Energy Policy. 2009; **37**: 1958-1969

Safaei H, Keith D. Compressed air energy storage with waste heat export: An Alberta case study. Energy Conversion and Management. 2014;**78**:114-124

Lund H, Salgi G. The role of compressed air energy storage (CAES) in future sustainable energy systems. Energy Conversion and Management. 2009; **50**: 1172-1179

Lund H, Salgi G. Optimal operation strategies of compressed air energy storage (CAES) on electricity spot markets with fluctuating prices. Applied Thermal Engineering. 2009;**29**:799-806

Marano V, Rizzo G, Tiano F. Application of dynamic programming to the optimal management of a hybrid power plant with wind turbines, photovoltaic panels and compressed air energy storage. Applied Energy. 2012;**97**:849-859

Abbaspour M, Satkin M, Ivatloo B, Lotfi F, Noorollahi Y. Optimal operation scheduling of wind power integrated with compressed air energy storage (CAES). Renewable Energy. 2013; **51**: 53-59

Mason J, Archer C. Baseload electricity from wind via compressed air energy storage (CAES). Renewable and Sustainable Energy Reviews. 2012;**16**:1099-1109

Yang Z. Wang Z, Ran P, Li Z, Ni W. Thermodynamic analysis of a hybrid thermal-compressed air energy storage system for the integration of wind power. Applied Thermal Engineering. 2014;**66**:519-527

Zhang Y, Yang K, Li X, Xu J. Thermodynamic analysis of energy conversion and transfer in hybrid system consisting of wind turbine and advanced adiabatic compressed air energy storage. Energy.2014;**77**:460-477

Yang K , Zhang Y, , Li X, Xu J. Theoretical evaluation on the impact of heat exchanger in Advanced Adiabatic Compressed Air Energy Storage system. Energy. 2014;**86**:1031-1044

De Boer HS, Grond L, Moll H, Benders R. The application of power-to-gas, pumped hydro storage and compressed air energy storage in an electricity system at different wind power penetration levels. Energy. 2014;**72**:360-370

Maton J, Zhao L, Brouwer J. Dynamic Modelling of compressed gas energy storage to complement renewable wind power intermittency. International Journal of Hydrogen Energy. 2013; **38**:7867–7880

Raju M, Khaitan S. Modelling and simulation of compressed air storage in caverns: A case study of the Huntorf plant.Applied Energy.2012; **89**: 474–481

Wu C. Intelligent computer based engineering thermodynamics and Cycle analysis. New York: Nova Science Publishing; 2002

NREA Annual Report 2010/2011. Available on website of New and Renewable Energy Authority(NREA). Accessed on (October 2013)

MOEE Annual Report 2009/2010. Available on website of MOEE, Egypt. Accessed on (October 2013)

Kushnir R, Dayan A, Ullmann A. Temperature and pressure variations within compressed air energy storage caverns. International Journal of Heat and Mass Transfer 2012; **55**: 5616–5630

Rabeh T. Structural set-up of Southern Sinai and Gulf of Suez areas indicated by geophysical data. Annals of Geophysics, 2003; **46**: 1325-1337

VESTAS V-90 3MW manual. Accessed on (September 2014)

Tatro SB. Thermal Properties. In: Lamond JF, Pielert JH (eds.). Significance of tests and properties of concrete and concrete-making materials. Bridgeport, NJ:ASTM International;2006: 226-237

Kuravi S, Trahan J, Goswami Y, Rahman M, Stefanakos E. Thermal energy storage technologies and systems for concentrating solar power plants. Progress in Energy and Combustion Science. 2013; **39**: 285-319

Glatzmaier G. Summary report for concentrating solar power thermal storage workshop. NREL; 2011

Herrmann U, Kearney DW. Survey of thermal energy storage for parabolic trough power plants. Journal of Solar Energy Engineering. 2002;**124**: 145-152

Schaube F, Worner A, Tamme R. High temperature thermochemical heat storage for concentrated solar power using gas solid reactions. Journal of Solar Energy Engineering 2011;**133**

Bhatt V, Gohil K, Mishra A. Thermal Energy Storage Capacity of some phase changing Materials and Ionic Liquids. International Journal of ChemTech Research.2010;**2**:1771-1779

Kenisarin M. High temperature phase change materials for thermal energy storage. Renewable and sustainable energy reviews. 2010;**14**:955-970

Zalba B, Marin JM, Cabeza LF, Mehling H. Review on thermal energy storage with phase change: materials, heat transfer analysis and applications. Applied Thermal Engineering 2003;**23**:251-283

Fan L, Khodadadi JM. Thermal conductivity enhancement of phase change materials for thermal energy storage: a review. Renewable and Sustainable Energy Reviews 2011;**15**:24-46

Jegadheeswaran S, Pohekar SD. Performance enhancement in latent heat thermal storage system: a review. Renewable and Sustainable Energy Reviews 2009;**13**:2225-2244

Laing D, Bahl C, Bauer T, Lehmann D, Steinmann WD. Thermal energy storage for direct steam generation. Solar Energy. 2011;**85**: 627-633

Laing D, Steinmann WD, Tamme R, Richter C. Solid media thermal storage for parabolic trough power plants. Solar Energy 2006;**80**:1283-1289

Gil A, Medrano M, Martorell I, Lazaro A, Dolado P, Zalba B, Cabeza L. State of the art on high temperature thermal energy storage for power generation. Part 1—Concepts, materials and modellization." Renewable and Sustainable Energy Reviews. 2010;**14**: 31-55

Pomianowski M, Heiselberg P,Zhang Y. Review of thermal energy storage technologies based on PCM application in buildings. Energy and Buildings.2013; **67**: 56-69

Wu M, Li M, Xu C, He Y, Tao W.The impact of concrete structure on the thermal performance of the dual-media thermocline thermal storage tank using concrete as the solid medium. Applied Energy.2014; **113**: 1363-1371

Shin A, Kodide U. Thermal conductivity of ternary mixtures for concrete pavements. Cement and Concrete Composites.2012; **34**:575-582

Islam MR, Tarefder R. Determining thermal properties of asphalt concrete using field data and laboratory testing. Construction and Building Materials.2014; **67:**297-306

TT Boilers Thermal fluid data. http://www.ttboilers.com/Termisk_Olie_Tabel.pdf. (Last accessed February 2013)

EIA , US Energy Information Administration, Henry Hub Natural gas Spot Price. http://www.eia.gov/dnav/ng/hist/rngwhhdM.htm (Data Last accessed July 2015)

International Renewable Energy Agency. RENEWABLE ENERGY TECHNOLOGIES: COST ANALYSIS SERIES, Power Sector, Wind Power. 2012; Volume 1

International Energy Agency . IEA Wind 2012 Annual Report. 2013 http://www.technicalreviewmiddleeast.com/power-a-water/renewables/el-sewedy-electric-to-complete-gebel-el-zeit-project-in-egypt (data last accessed July 2015)

http://www.evwind.es/2012/11/25/wind-power-plant-to-be-set-up-in-gabel-el-zeit-egypt/26347(data last accessed July 2015)

MOEE Annual Report 2014. Available on website of MOEE, Egypt. Accessed on (August 2015)

Hafez T. Power to the free market. The journal of American chamber of commerce in Egypt.2015

http://www.amcham.org.eg/resources_publications/publications/business_monthly/issue.asp?sec=4&subsec=Energy%20&im=6&iy=2015 (date last accessed July 2015)

A. Appendix

Simulink blocks developed initially for modelling

Simulink blocks were developed to illustrate the process followed in developing the MATLAB computer model. In this section, Simulink block presentation is used instead of the update MATLAB modelling because the MATLAB modelling code was quite large to add this thesis.

Figure A-1 shows the initial configuration used for the Simulink programming including compressor block, cavern block, turbine block and the TES block.

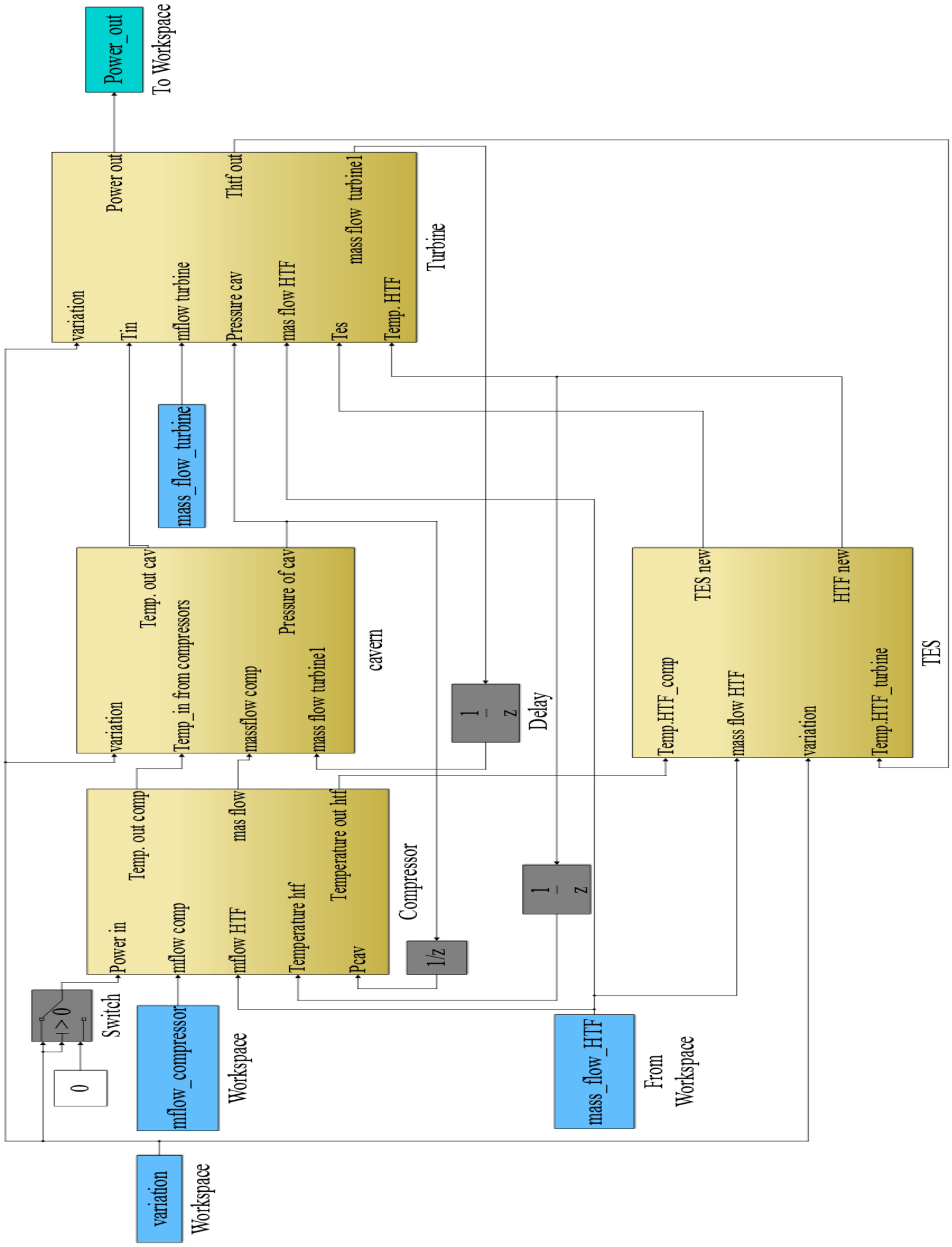

Figure A-1 System design using Simulink

Figure A-2 shows the blocks associated with the compression stage developed in the Simulink initial modelling

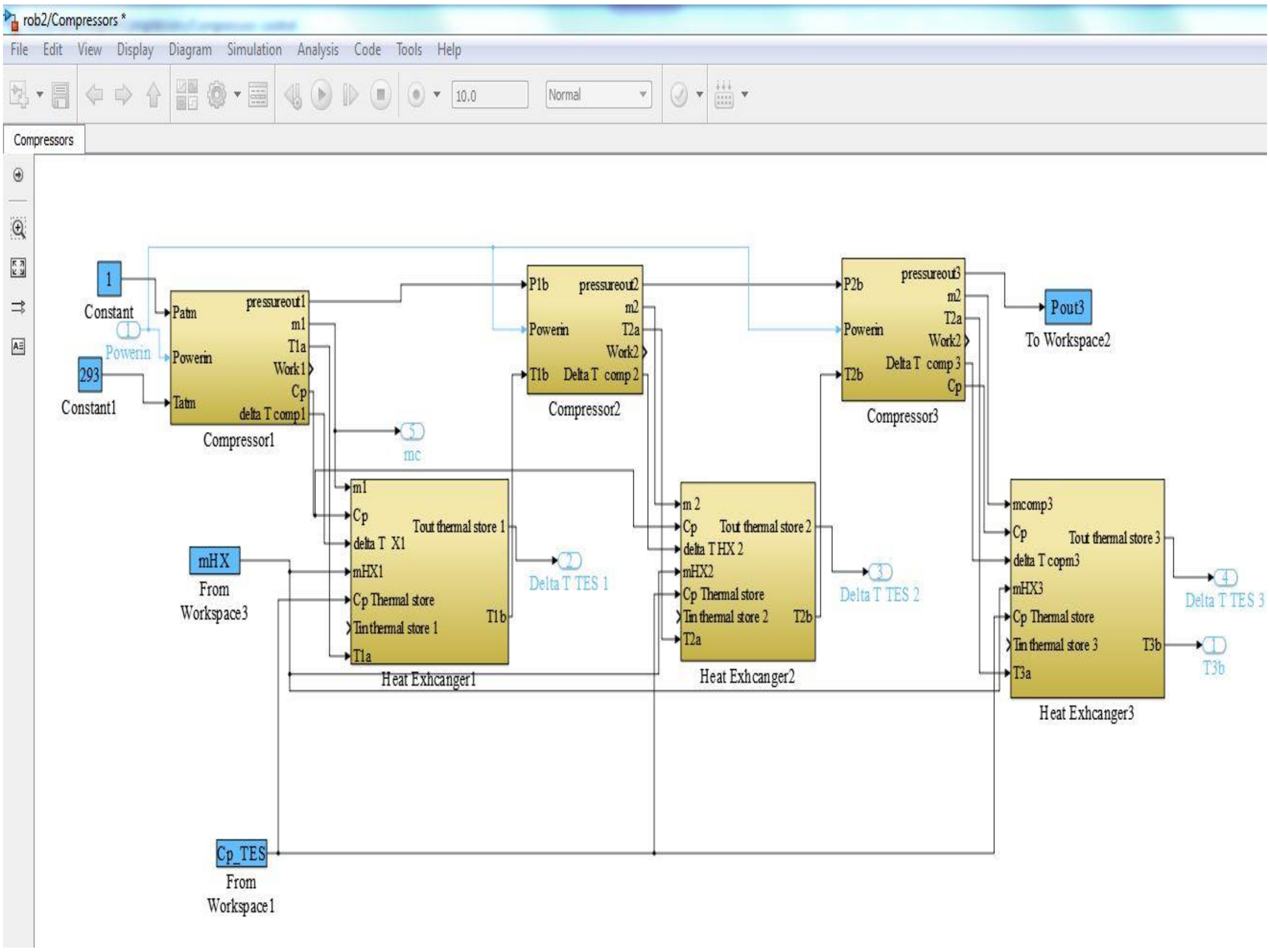

Figure A-2 Compression stage

Figure A-3 shows the cavern block developed in the initial modelling using Simulink. Some of the numerical modelling initially used in the cavern simulation was altered to achieve more accurate results of the temperature and pressure variations of air in the cavern.

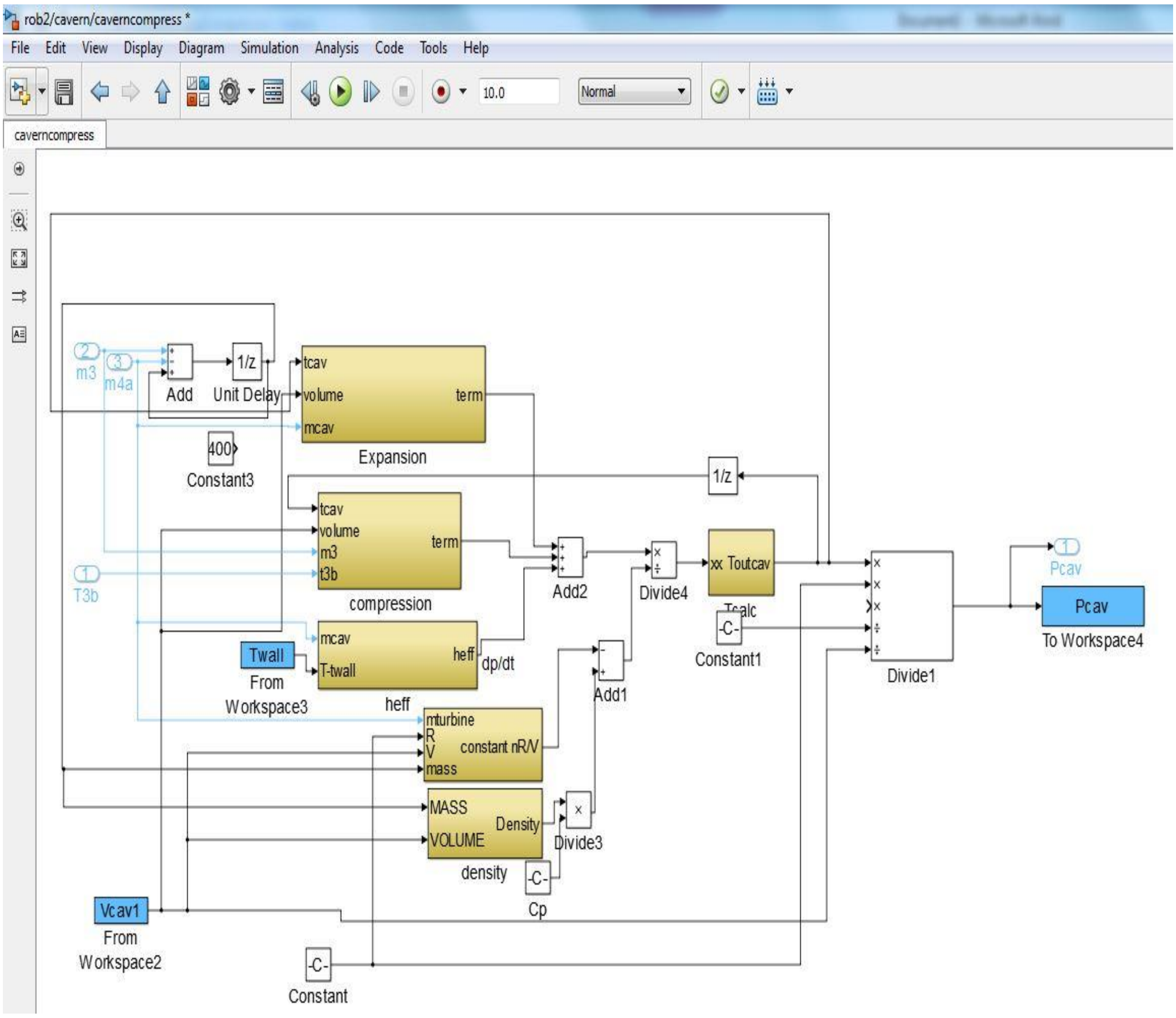

Figure A-3 Cavern block

Figure A-4 shows the 1st high pressure expander of the turbine stage with heat exchanger before it to utilize the heat of the heat transfer fluid.

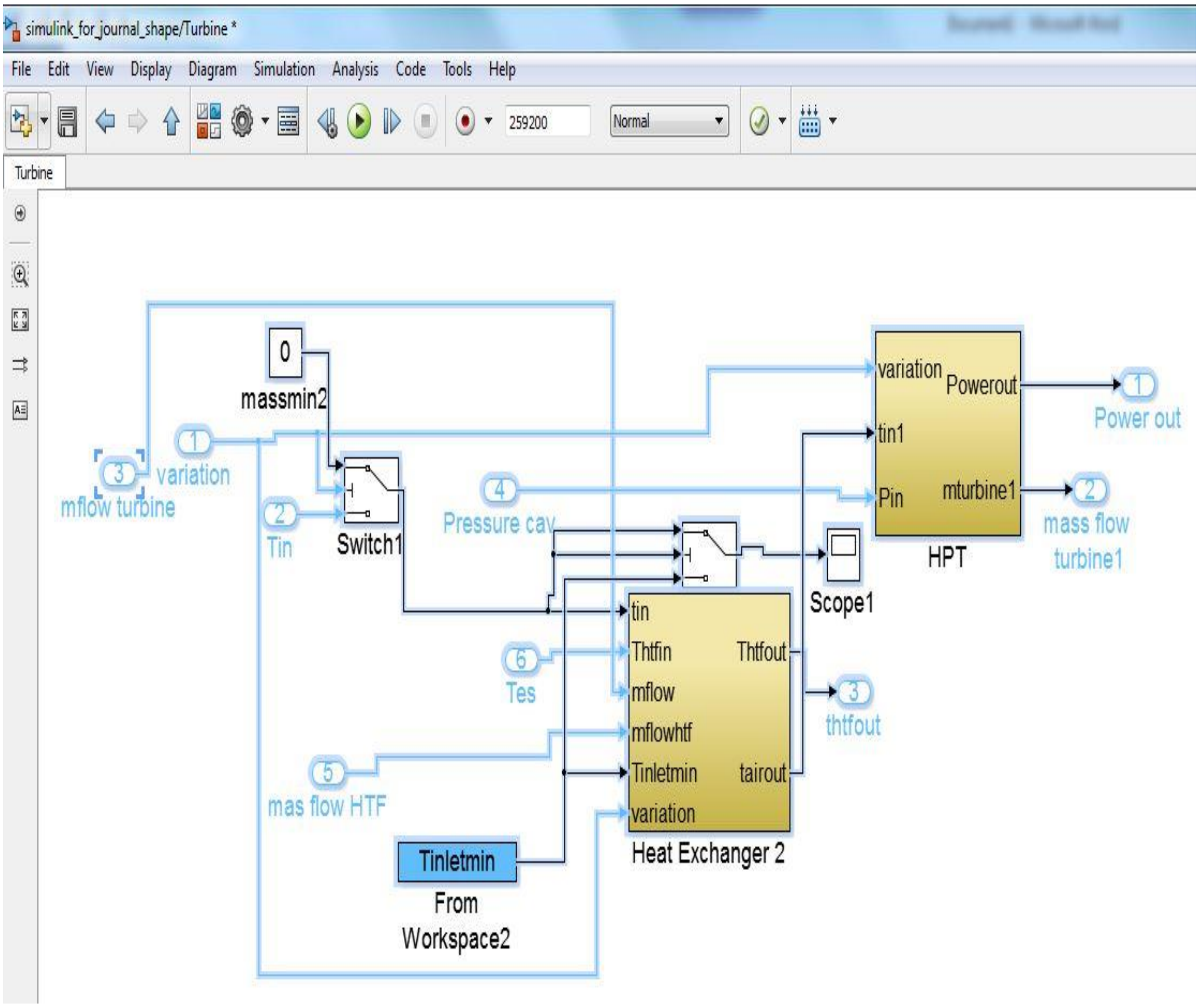

Figure A-4 1st stage if turbine block in Simulink

Initial modelling of the cavern

Initial testing of the cavern was performed for different inlet parameters for different flow rates in the compression stage. Again some of the numerical methodology implemented in these test was altered for improved accuracy of operation which was later used in the developing results achieved in Chapter 5. Some of the results of these tests are discussed next; first the results for just the compression stage for sizing of the cavern for 22 hours of compression. Then results are shown for the complete operation with compression then expansion according to the input available for variable initial conditions for 24 hours of operation.

Compression stage Operation

Results for the modelling are shown for random inputs which were implemented before acquiring real data from the case study location. The input chosen were full day compression for values between 40MW to 60MW power available. For this configuration 2 runs of the model are done for 2 different initial values

1) Starting with cavern mass half full
2) The cavern mass is ¾ of the maximum mass available
3) The cavern mass is 25% full
4) The cavern mass is 60% full

3 important factors decide when to stop the operation of the system:

a) The mass flow is higher than maximum allowed
b) The temperature is higher than maximum
c) The pressure in the cavern exceeds maximum

The parameters results from the operation include:

1) Mass in cavern
2) Pressure in cavern
3) Temperature in the cavern
4) Mass flow from the compressors

Figure A-5 shows the different figures for different initial conditions of the cavern mass. As obvious from the figure, during the compression stage the mass inside of the cavern increases due to the incoming flow from the compressors of high pressured air. In the 75% the mass flow reaches a level which is higher than the other runs then stops. This means that at some point the compressors stop working which means that a stop condition is applied which in this case the air in the cavern has reached maximum pressure which is obvious in the pressure graphs. Therefore in this case the final mass in the cavern can be different depending on the initial condition.

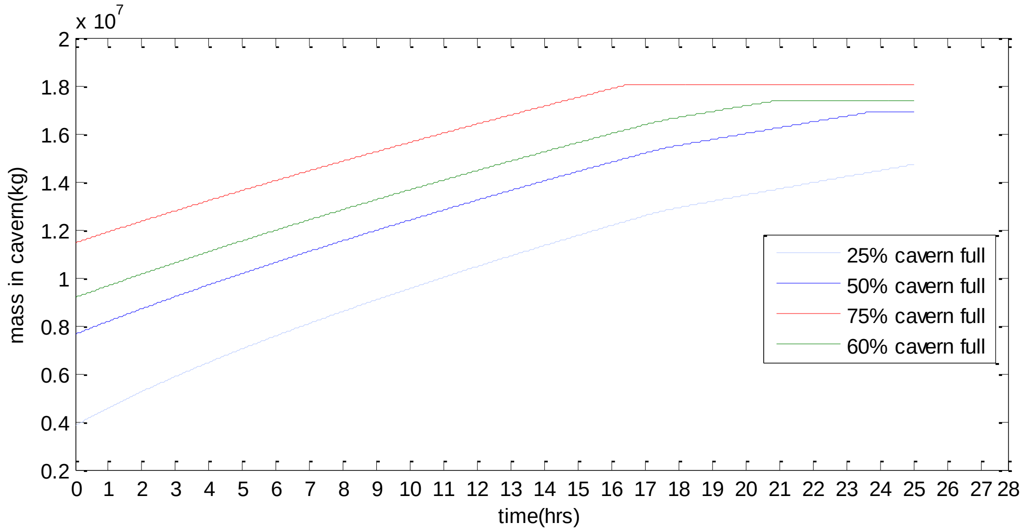

Figure A-5 Mass of air in cavern for different initial conditions

Figure A-6 shows the pressure variation in the cavern for different simulations. In this case a maximum pressure allowable of 65 bars is assumed. As shown in the figure different initial values of pressure are shown according to the initial mass in the cavern when the operation starts. When the maximum pressure of 65 bars is reached the compression stops.

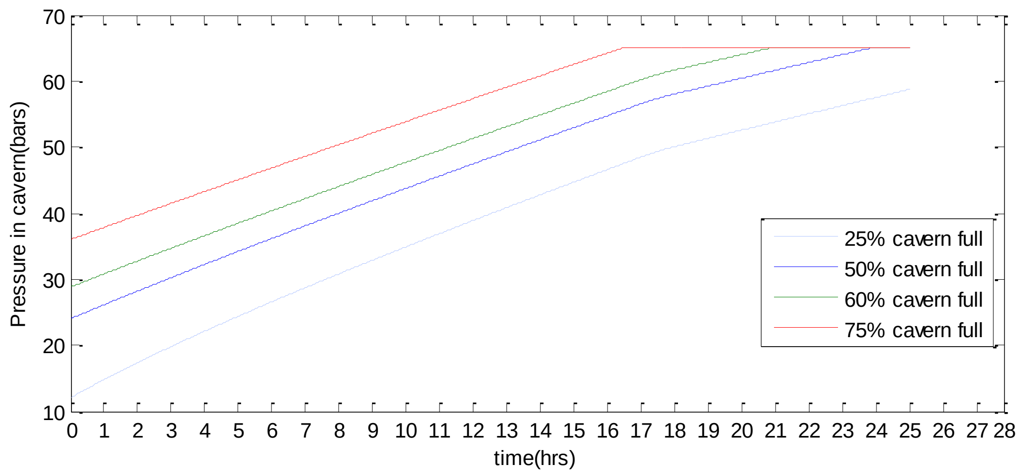

Figure A-6 Pressure of air in cavern for different initial mass of air in cavern

Figure A-7 shows the temperature variation in the cavern. I this case a initial temperature of 273 kelvin is assumed for all simulations. Since it is assumed that intercooler manage to keep a constant input temperature to the cavern; these results show a higher rate of increase in temperature for the 25% cavern initial since there is higher flow rate from the compressors with the same temperature as other runs which causes higher increase in the temperature compared to the other different initial conditions of operation

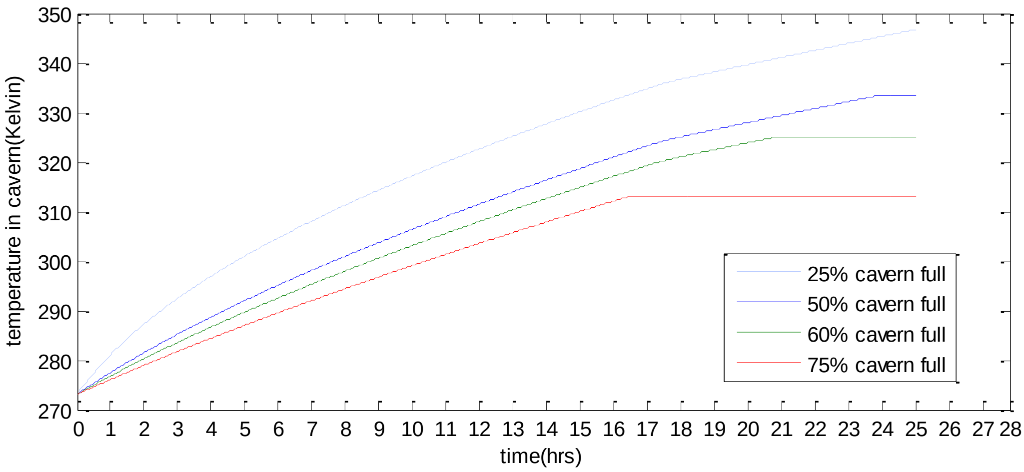

Figure A-7 Temperature of air in cavern for different initial mass of air in caven

Effect of different surplus/ Deficiency in Power

Two simulations were performed under 2 different incoming inputs from the grid. Figure A-8 shows the 2 different runs which affect the performance of the operation and sizing of the system. The volume of the cavern used was 250000 m^3 with maximum allowable pressure of 65 bars in the cavern. As mentioned before these 2 parameters depend on the geology of the location, therefore is input to the model. For the 2simulations of input shown in Figure A-8, the operation output is shown in the following figures.

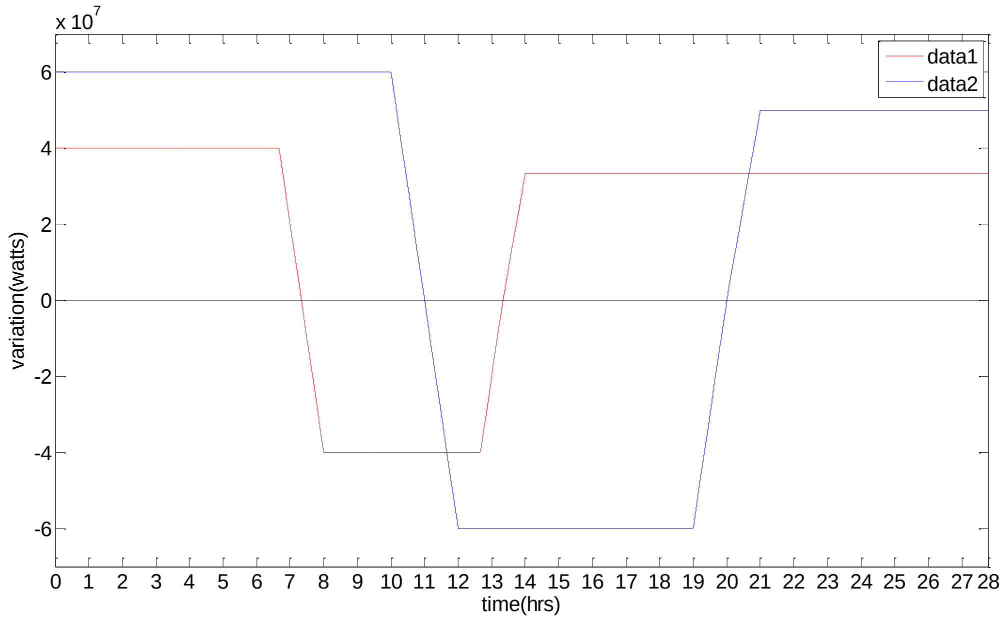

Figure A-8 Different Surplus/ Deficiency in Power

Figure A-9 shows the difference in mass flow rates for the compressors in the different runs. As expected simulation 2 shows higher flow rates required as higher power is injected to the compressors. In both simulations when the variation value reaches zero, the compression stops and flow rate is 0. Compression starts again when the variation becomes bigger than 0 which means the grid has excess power to deliver to the compressors.

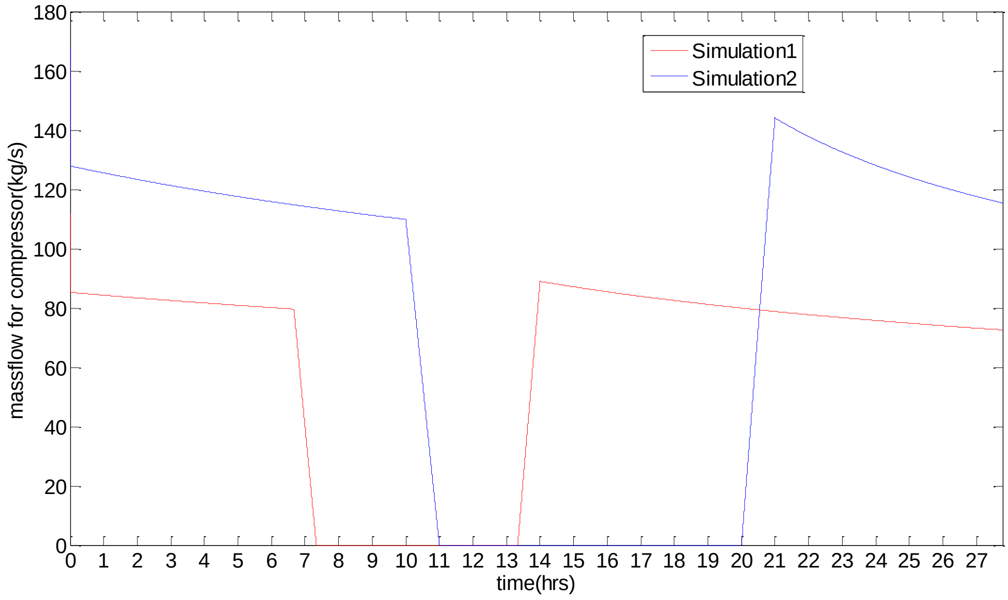

Figure A-9 Effect of Surplus power on flow rates of compressors

Figure A-10 shows the mass flow rate to the turbine. The values of the turbine level are assumed to be the same for a fixed power output by the turbine of 60MW. Therefore, the starting flow rate is the same for the turbines which is 400kg/sec. However, when the pressure in the cavern decrease due to the expansion process till it becomes lower than a specific operational pressure value which in this case is set to 35 bars, the flow rate in the turbines decreases gradually till it completely stops when the grid does not need any more power from the turbine.

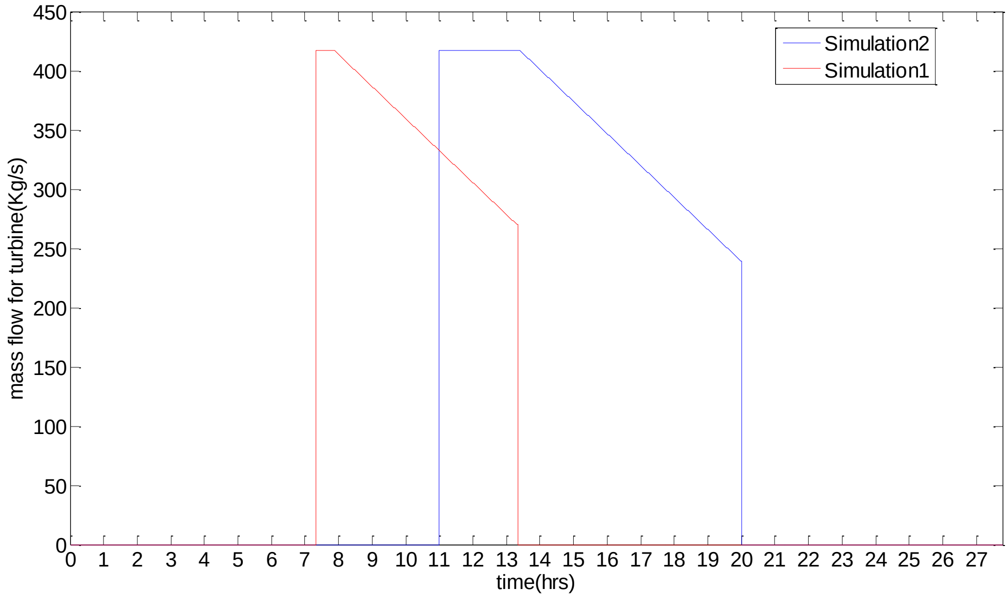

Figure A-10 Different flow rates of turbines for different Surplus/ Deficiency in Power

Figure A-11 shows the mass inside the cavern which is basically a reorientation of the last 2 figures for compression and expansion. The mass in the cavern increase during compression then reduces during expansion process.

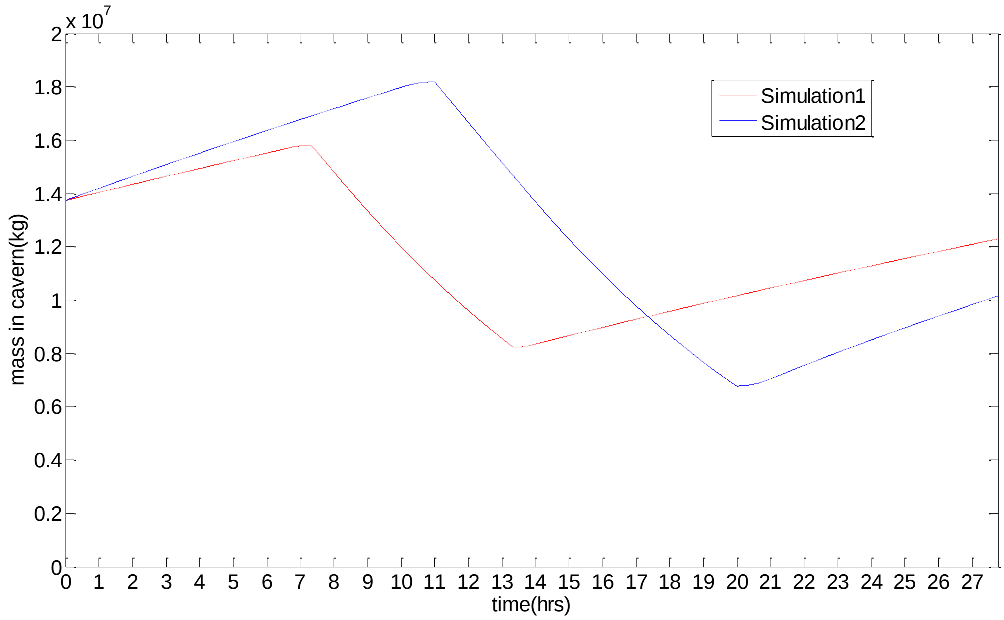

Figure A-11 Effect of different Surplus/ Deficiency in Power on mass of air in cavern

Figure A-12 shows the variation of temperature inside the cavern during the operation process for the 2 simulations. Generally for both the temperature inside the cavern increases during compression reduces during expansion then increases again when compression starts again.

Same initial condition is used for both simulations. However the rates of increase in temperature in simulation 2 where the input power available to the compressors are higher. Although the same value of inlet temperature to the cavern is output (effectivity=1), higher masses going into the cavern in simulation 2 compared to simulation causing the higher rate of temperature rise during compression. During the expansion process, the previous temperature of the cavern after compression as well as the mass inside the cavern at the time cause the variable effect on the rate of decrease during expansion between the 2 simulations. For the final compression part, for both simulations the rate of increase in temperature is higher compared to the first compression. This happens because the mass in the cavern the 2nd phase of compression stars is much lower than the first stage of compression with higher flow rates incoming, which causes higher rates of temperature rise in the second stage of compression.

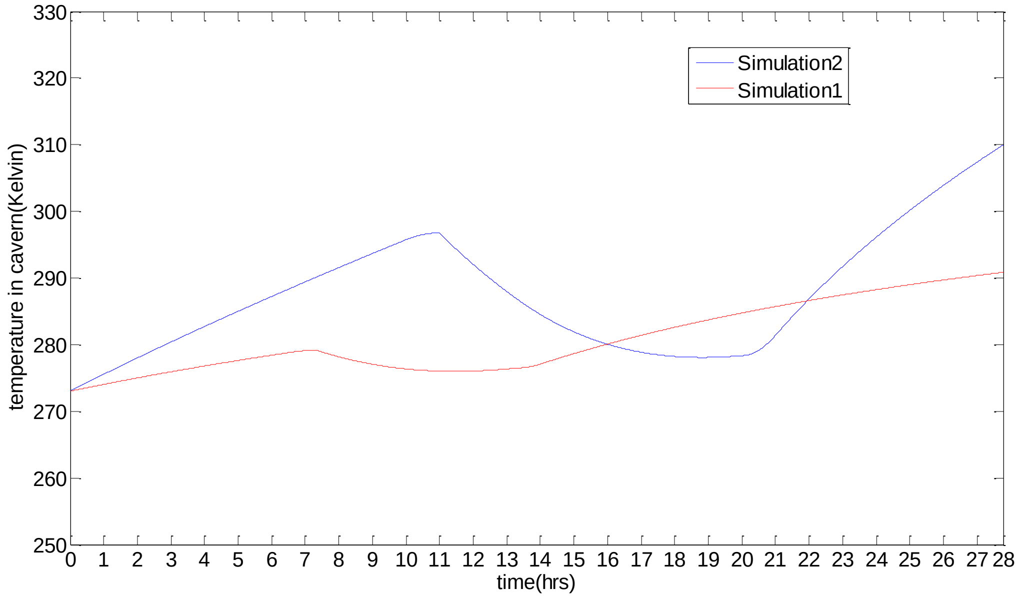

Figure A-12 Effect of Surplus/ Deficiency in power on temperature of air in cavern

Figure A-13 shows the pressure variation during the operation process, which increases during compression and decreases during expansion which is quite obvious in the figure. Since pressure is calculated using 6. It depends on the mass in the cavern as well as the temperature. The pressure reaches higher levels in simulation 2 as the mass in the cavern as well as the temperature are quite higher than simulation 1 which was explained earlier.

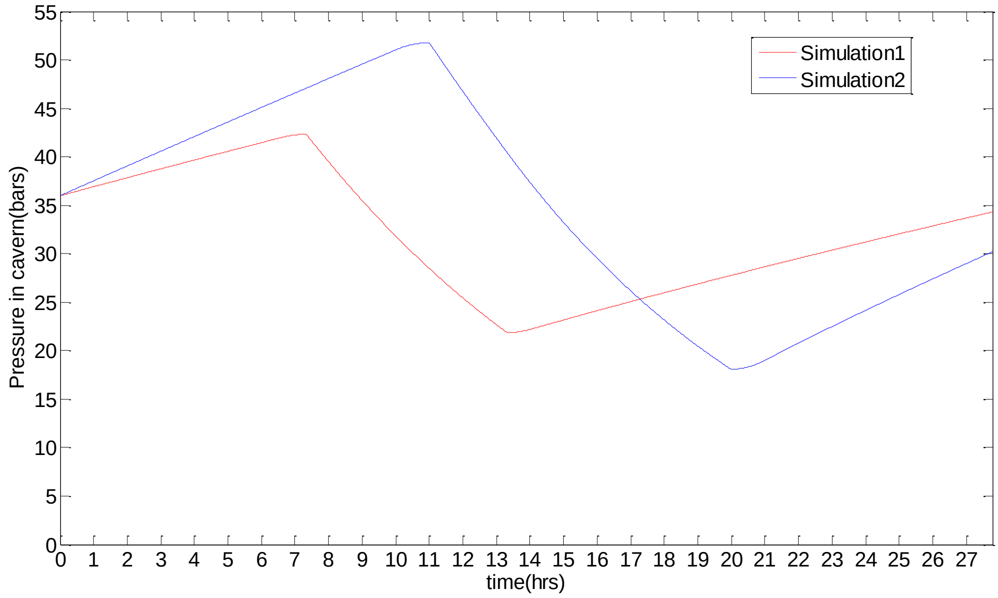

Figure A-13 Effect of Surplus/ Deficiency in power on pressure of air in cavern

CFD temperature contours during charging process of the thermal energy storage

The temperature contours of the heat transfer fluid and thermal energy storage are presented after 3 hours of operation in Figure A-14 . The temperature of the heat transfer fluid at positions near the pipes could be from 544K to 561Kand it is in the range from 561K to 531K for outer wall of the thermal energy storage which is the coldest part for the whole TES.

Positions of monitors placed every 100 mm from inlet have been created to generate the temperature contours as presented in Figure A-15, which shows the evenly distribution in temperatures, however near the edges of the thermal energy storage the temperature is less evenly distributed (cooler than the rest of the TES). Also, Figure A-15 shows that the further away from the inlet, the colder the temperature of the TES is.

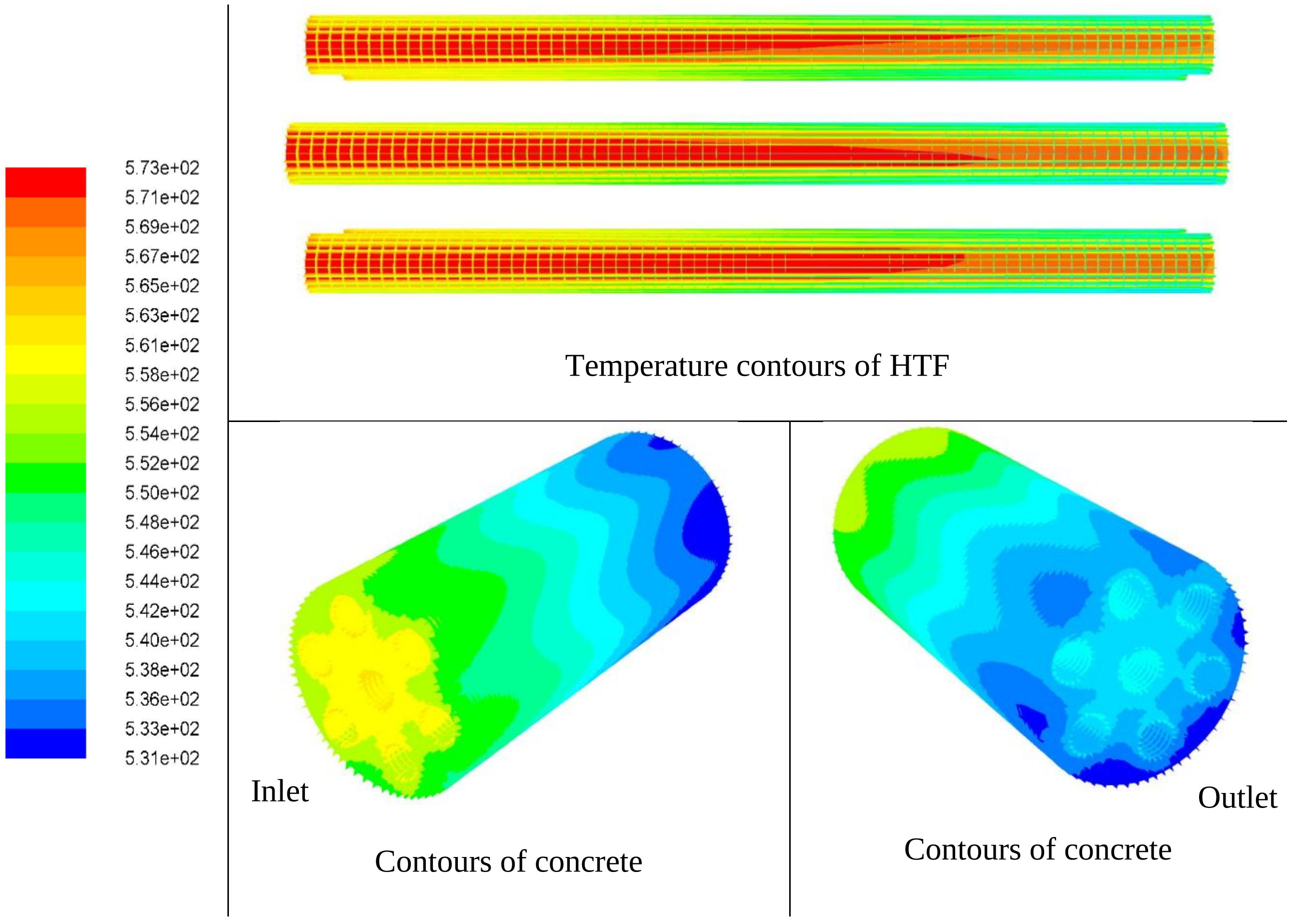

Figure A-14Charging temperature contours after 3 hours

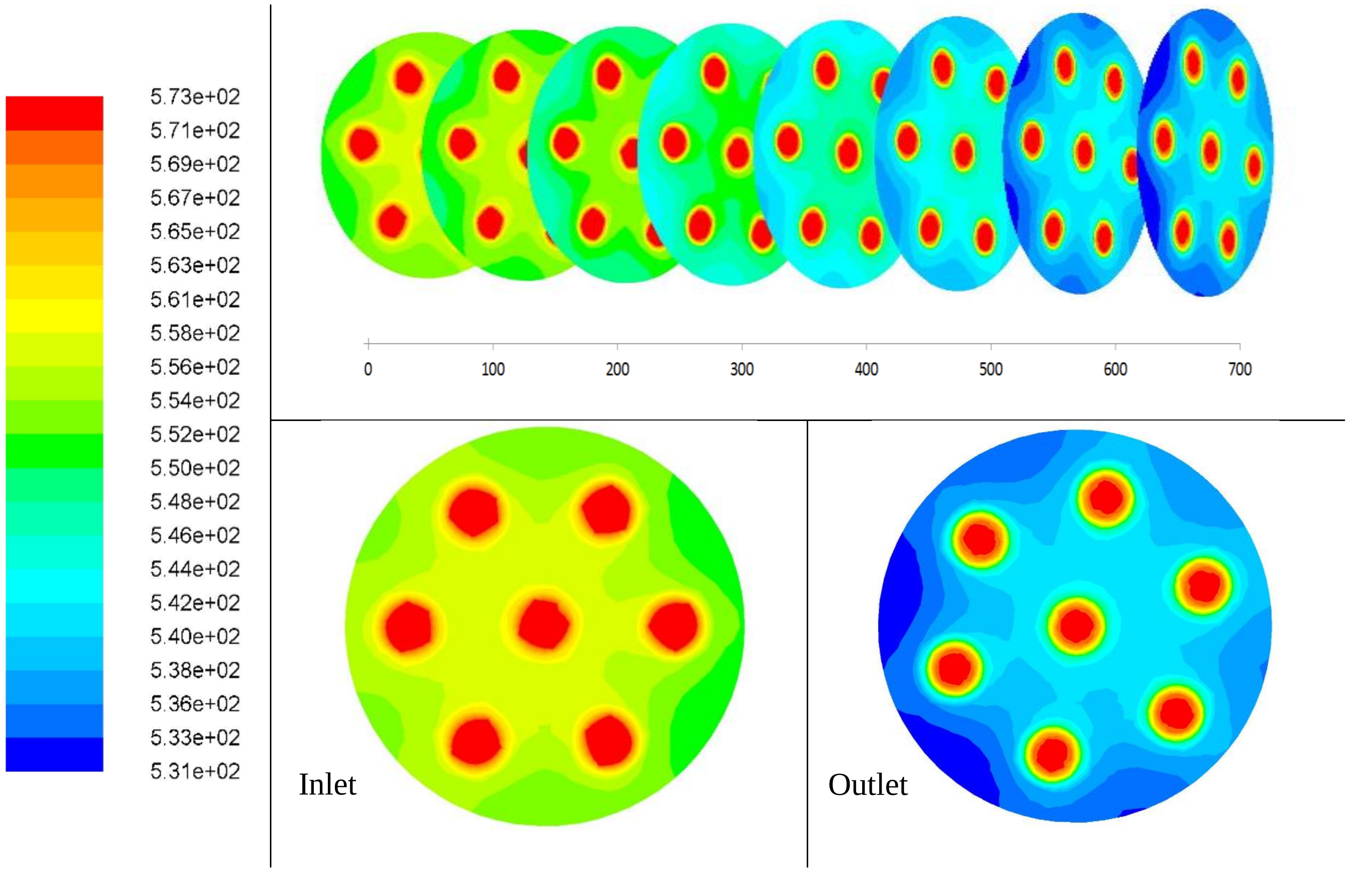

Figure A-15 Temperature contours at different positions of charging